

**Braided rivers: an exploratory study combining
flume experiments and the analysis of
remotely-sensed data**

Grecia Alejandra Garcia Lugo

A thesis submitted for the degree of Doctor of Philosophy
School of Geography, Queen Mary University of London

2014

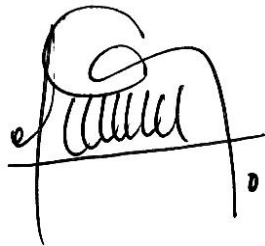
I, Grecia Alejandra Garcia Lugo, confirm that the research included within this thesis is my own work or that where it has been carried out in collaboration with, or supported by others, that this is duly acknowledged below and my contribution indicated. Previously published material is also acknowledged below.

I attest that I have exercised reasonable care to ensure that the work is original, and does not to the best of my knowledge break any UK law, infringe any third party's copyright or other Intellectual Property Right, or contain any confidential material.

I accept that the College has the right to use plagiarism detection software to check the electronic version of the thesis.

I confirm that this thesis has not been previously submitted for the award of a degree by this or any other university.

The copyright of this thesis rests with the author and no quotation from it or information derived from it may be published without the prior written consent of the author.

A handwritten signature in black ink, appearing to read 'Grecia Alejandra Garcia Lugo', written over a horizontal line.

Signature:

Date: 11th of September, 2014

Details of collaboration and publications:



Erasmus Mundus
Joint Doctorate Programme

SMART - Science for Management of Rivers and their Tidal systems

PhD in River Science

Research for this thesis was conducted within the framework of SMART (Science for Management of Rivers and their Tidal systems), which is an Erasmus Mundus Joint Doctoral Programme (EMJD).

EMJDs aim to foster cooperation between higher education institutions and academic staff in Europe and third countries with a view to creating centres of excellence and providing a highly skilled 21st century workforce enabled to lead social, cultural and economic developments. All EMJDs involve mandatory mobility between the universities in the consortia and lead to the award of recognised joint, double or multiple degrees.

The SMART programme represents a collaboration among The University of Trento, Queen Mary University of London, and Freie University Berlin. Each doctoral student within the SMART programme has conformed to the following during their 3 years of study:

- (i) Supervision by a minimum of two supervisors in two institutions (their primary and secondary institutions).
- (ii) Study for a minimum period of 6 months at their secondary institution.
- (iii) Successful completion of a minimum of 30 ecus of taught courses.
- (iv) Collaboration with an associate partner to develop a particular component / application of their research that is of mutual interest.
- (v) Submission of a thesis within 3 years of commencing the programme.

Abstract

Braided rivers exhibit extremely complex and dynamic morphologies as their multiple channels are constantly re-worked. The research reported in this thesis explored a number of properties of braided river form and dynamics and some controlling factors through three individual but complementary research elements.

The first research element was concerned with some of the controls on the transition between single thread and multi-thread channel patterns. Twenty-seven different flume experiments were conducted, supported by fourteen replicates. In these experiments, channel confinement (maximum possible channel width) and formative discharge were varied in a 25 x 2.9 m flume of constant slope (1%) and bed material ($D_{50} = 1\text{ mm}$) with sediment supply constrained to match sediment output. As the maximum potential channel width increased, the channel pattern changed from a single channel with alternate bars, to the formation of mid-channel bars, and finally to a multi-thread braided pattern. Bed elevation frequency distributions showed distinct changes in their median, standard deviation, skewness and kurtosis as channel width and discharge increased, indicating the consequences of confining braided channels and regulating discharge on their bed elevation and morphology.

The second and third parts of the research use remotely sensed data sets to explore (i) the degree to which a real river shows similar characteristics to those generated in the flume experiments and (ii) the variety in braiding patterns that are found in association with different boundary conditions of slope, width, discharge, and riparian vegetation.

For the second research element, a Lidar survey of a 36 km reach of the lower Tagliamento river, Italy, was investigated. Within this reach, the river shows only small variations in slope and bed material size and is subject to the same flood flows. Analysis focused on thirty-six 1 km sub-reaches and demonstrated clear associations among the median, standard deviation, kurtosis and skewness of the bed and also clear downstream trends. Measures of vegetation cover showed statistically-significant associations with the median, standard deviation, kurtosis and skewness of the bed, particularly when only the 32 truly braided reaches were analysed. The measures of vegetation cover also showed downstream trends that corresponded with the trends in bed morphology.

Overall, variations in bed morphology showed similar characteristics to those observed in the laboratory flume, but also they showed correspondence with riparian vegetation cover, indicating a topographic signature of vegetation on the bed morphology. The downstream trends appear to be associated with the changing vigour of the riparian vegetation and possibly variations in river baseflow characteristics associated with varying groundwater levels in the alluvial aquifer. The most mature patches of vegetation within the braid plain of the most downstream part of the 36 km reach appear to occur on remnants of braid plain isolated by river bed incision.

The third and final research element considered the morphology of six European braided rivers of different slope, width, discharge and riparian vegetation type. Information extracted from Google Earth and other aerial imagery, and gauged river flow data supported an analysis of changes in braided river characteristics through time, and among the six European river sites. Four traditional planform indices were used to characterise the braiding pattern (B_i – braiding index, A_i and A_{i2} –anastomosing indices; S_i – main channel sinuosity) were combined with measures of stream power and its component variables (width, Q_{10} , and slope). Robust data for bed material calibre was not available. Statistical analysis of the entire data set revealed a potential influence of riparian vegetation type on the relationship between unit stream power and braid channel width; and a trend of increasing B_i , A_i , A_{i2} , and S_i with decreasing unit stream power. However, a larger and more complete data set is needed to confirm these general trends and to fully explore transitional rivers.

This research has illustrated the morphological consequences of confining braided rivers and the dependence of the braiding pattern on stream power. It has also illustrated the role of vegetation in contributing to the morphological complexity of braided rivers and the potential role of riparian vegetation in constraining the relationship between stream power and braided river width.

Acknowledgements

First, thanks must go to my supervisor Professor Angela Gurnell, without whom this thesis wouldn't have been possible. I've learned so much from you and it has been a privilege to work with you. To my second supervisors, Dr. Alex Henshaw, and Dr. Walter Bertoldi, without your comments, tutoring, endless discussions, corrections and suggestions in each of these chapters, this simply couldn't have been done.

Thanks to the European Union, through the Erasmus Mundus fellowships and the SMART consortium, for the opportunity to better myself through learning and research in a multi-cultural and interdisciplinary environment.

To the laboratory staff at University of Trento who helped with the intensive laboratory work of my project, especially Martino Salvaro, Lorenzo Forti, Andrea Bampi, and Matilde Welber.

My work has included a wide variety of data collection in a range of forms, management, display, analysis techniques and visualization. I am very grateful to Judy England and Lucy Shuker from the Environment Agency in the UK for the provided data, suggestions, as well as the opportunity to have done my associate partnership with them. For guidance in processing data: Simone Zen, Francesca Pilotto, Bob Grabowski, Alex Henshaw, and Walter Bertoldi, thank you for helping me solve the mysteries of ArcGIS, R, Excel, MatLab, and Fusion.

To my family your support, cheering, hours of long distance conversations, I wouldn't be who I am today without you.

Fellow SMART and postgraduate students in London, Italy and Berlin who have been there to support me and offer help and advice when most needed. You all have been my adopted traveling family for the last three years. Thank you.

Special thanks to Isabel Ávalos, Wen Penderson and PG for their invaluable help editing and layout assistance of the final publication draft.

To the secretaries –past and present- of the SMART programme: Marina Rogato, Marta Timoncini, Laura Martuscelli, and Claudia Fraizingher, without you this programme wouldn't be the same.

God, for always being my best friend and having my back.

Table of Contents

Abstract	4
Acknowledgements.....	6
Table of Contents.....	8
List of Figures.....	12
List of Tables	19
Chapter 1 Introduction	22
Chapter 2 Developing a Process-based Understanding of Alluvial River	
Channel Styles: A Brief Introduction to the Braid-meander Transition.....	24
2.1 INTRODUCTION.....	24
2.2 THE DESCRIPTIVE ERA.....	24
2.3 INCORPORATING PROCESS UNDERSTANDING: DISCHARGE, SEDIMENT AND GRADIENT CONTROLS	25
2.4 THE ROLE OF RIPARIAN VEGETATION.....	38
2.5 CONCLUSIONS	41
2.6 RESEARCH QUESTIONS	42
Chapter 3 Flume Experiments to Investigate Braided Channel	
Development Under Controlled Conditions.....	44
3.1 INTRODUCTION.....	44
3.1.1 Definitions of “Braiding”	45
3.1.2 Quantifying Properties of Braided Channel Form	45
3.1.3 Controls on Braiding and Braided Channel Morphology.....	47
3.1.4 Research Questions	51
3.2 METHODS	52
3.2.1 Flume Experiments.....	52
3.2.2 Data Analysis	56
i) <i>Data preparation for DEM construction and description</i>	56
ii) <i>DEM construction</i>	57
iii) <i>Estimation of dimensionless stream power</i>	58
3.3 RESULTS	59

3.3.1 Descriptive Statistics	59
3.3.2 Digital Elevation Models	63
3.3.3 Elevation Frequency Distributions	69
3.3.4 Associations Among Processes and Channel Size and Form	71
i) <i>Dynamic equilibrium in sediment transport</i>	71
ii) <i>Wetted and active widths</i>	72
iii) <i>Changes in channel form in response to changes in stream power and flume width</i>	75
iv) <i>Channel morphology and the emergence of mid-channel bars</i>	78
v) <i>Repetition runs</i>	79
3.4 DISCUSSION AND CONCLUSIONS	83
3.4.1 Research Question 1: To what extent does bed morphology vary between experiments conducted with the same formative discharge and fixed maximum channel width?	83
3.4.2 Research Question 2: To what extent does bed morphology change in response to different fixed formative discharges / stream powers within the constraints of a fixed maximum channel width?	83
3.4.3 Research Question 3: To what extent does bed morphology change in response to a fixed formative discharge / discharge within the constraints of different fixed maximum channel widths?	83
3.4.4 Research Question 4: To what extent does bed morphology change in response to different fixed, formative discharges within the constraints of different fixed maximum channel widths?	84
3.4.5 Comparison of the Experimental Results with Observations and Predictions From Previous Work	85
3.4.6 Concluding Remarks	87
Chapter 4 Interactions Between Vegetation and Channel Morphology on a Braided River: The Lower Tagliamento River, Italy	89
4.1 INTRODUCTION	89
4.2 THE STUDY SITE	91

4.3 METHODS	92
4.3.1 Extraction and Analysis of a Digital Elevation Model of the River Bed	92
4.3.2 Extraction and Analysis of a Vegetation Canopy Surface Model.....	94
4.4 RESULTS	96
4.4.1 Description of the Detrended DEM Data for the 36 1km Reaches	96
4.4.2 Relationships Among Bed Morphological Properties Across the 1 km Reaches.....	107
4.4.3 Relationships Between Vegetation and Bed Morphological Properties Across the 1 km Reaches	109
4.5 DISCUSSION AND CONCLUSIONS	123
4.5.1 River Bed Topography	123
4.5.2 Associations Between Bed Topography and Vegetation.....	125
4.5.3 Outlier Reaches	127
Chapter 5 Braiding, Anastomosing and Sinuosity Indices: a Comparison Among Reaches of Six European Braided Rivers.....	128
5.1 INTRODUCTION.....	128
5.2 MATERIALS AND METHODS.....	129
5.2.1 Selection of Rivers and Images.....	129
5.2.2 Extraction of Information From Images	130
5.2.3 Discharge, Bed Material and Stream Power	136
5.2.4 Data Analysis	141
5.3 RESULTS	141
5.3.1 Options 1 and 2	141
5.3.2 Selecting Informative Variables.....	142
5.3.3 Associations Among Variables within a Single River	144
5.3.4 Associations Among Planform, Channel Dimension and Stream Power Variables Across Six European Braided Rivers	147
5.4 DISCUSSION AND CONCLUSIONS	154
Chapter 6 Summary, Implications, Future Research, and Conclusions.....	159
6.1 INTRODUCTION.....	159

6.2 SUMMARY OF RESEARCH FINDINGS	159
6.2.1 Research Question 1: What are the influences of variations in discharge and river confinement on river style and bed morphology?	159
6.2.2 Research Question 2: What is the influence of vegetation on braided and transitional river morphology?.....	162
6.2.3 Research Question 3: Does the type and extent of vegetation influence / co-vary with braided river planform?.....	166
6.3 FUTURE RESEARCH.....	168
6.4 RELEVANCE OF RESEARCH TO RIVER MANAGEMENT.....	170
References	174

List of Figures

Figure 2.1	Combinations of slope and bankfull discharge observed for natural channels, and a line separating braiding and meandering channels (from Leopold and Wolman, 1957).....	27
Figure 2.2	Association between river planform style, discharge and slope showing the threshold between meandering and braiding defined by Leopold and Wolman, 1957 (data sources: Leopold and Wolman, 1957, Ferguson, 1987, Knighton and Nanson, 1993, Beechie et al., 2006). (from Gurnell et al., 2009).	28
Figure 2.3	Association between river planform style, discharge, slope and bed sediment calibre (data sources as for Fig. 2.2, thresholds between styles from Church 2002). (from Gurnell et al., 2009).	29
Figure 2.4	Channel styles associated with different modes and calibres of sediment transport, stream power, sediment calibre and sediment load (after Schumm, 1985).....	33
Figure 2.5	Channel styles differentiated according to stream power, amount and size of bedload, width-depth ratio and channel instability (after Ferguson 1987 in Kleinmans, 2010).	33
Figure 2.6	Association of alluvial river channel form with the principal governing factors (from Church 2006, after Church 1992, based on the concept of Mollard 1973 and Schumm 1985). Shading indicates sediment character and vegetation cover.	34
Figure 2.7	Approximate distribution of specific stream power, bed and bank sediment calibre, lateral migration rate, vertical accretion rate, channel sinuosity and island length/channel width ratio for eight types / subtypes of anabranching river (from Nanson and Knighton, 1996).....	35
Figure 2.8	Q-S plot locating six types of anabranching river in relation to the meander-braid threshold of Leopold & Wolman (1957) (from Nanson and Knighton, 1996).....	35
Figure 2.9	Patterns of equilibrium alluvial rivers. (A) Data subdivided by bar pattern; (B) Data subdivided by sinuosity.....	37

Figure 2.10	Channel pattern discriminant functions expressed as a function of slope, discharge and relative bank strength (from Eaton et al., 2010).....	38
Figure 2.11	Conceptual model of associations between tree growth performance, flood magnitude/frequency and channel style. Sediment supply is assumed to be sufficient to support the different channel styles. Three trajectories of riparian tree growth (solid lines) from seedling / sapling, through shrub, young and mature tree stages (dashed lines) according to different growing conditions are compared with the range in the maximum time period between floods capable of uprooting trees across the three trajectories (thin grey arrows) to prevent transitions between the given river planform styles (<i>italic text</i>) (from Gurnell et al., 2009).	40
Figure 3.1	The flume used in the experiments. A) Volumetric sand feeder, parallel camera to the flume bed, carriage and lap top controller. B) Example of an experimental configuration showing the plastic cover used in all the runs, configured to a width of 0.30 m at “low flow”. C) Laser profiler, D) Chute and submerged sediment tank.....	53
Figure 3.2	Transporting, non-transporting and dry areas of the flume bed. Measures of a) Dry, b) Wetted, and c) Active widths where obtained by measuring along 20 transects, spaced 0.50 m apart. These measurements were made (“by hand”) while running an experiment and also from photographic record.....	56
Figure 3.3	Relationship between wetted widths (in m) measured from photographs (horizontal axis) and by hand (vertical axis).....	59
Figure 3.4	Wetted and active channel widths observed at different flume widths (the three discharges are shown for each width using the same symbol).....	60
Figure 3.5	Relationship between ω (calculated for flume, wetted and active width for three formative discharges) and flume width.....	62
Figure 3.6	Mean sediment transport rate (left) and dimensionless sediment transport rate (right) in relation to discharge across all flume widths (key).....	62

Figure 3.7	DTMs produced by a discharge of 1.5 l/s applied to different flume widths.	65
Figure 3.8	DTMs produced by a discharge of 2.0 l/s applied to different flume widths.	66
Figure 3.9	DTMs produced by a discharge of 2.5 l/s applied to different flume widths.	67
Figure 3.10	Bed elevation frequency distributions generated by different combinations of discharge (vertical) and channel width (horizontal). Each frequency distribution is labelled by run number (1 to 27) and employs an equal bin size of 0.5 on the horizontal axis with values ranging from -9 to +9. The vertical axis expresses density with a minimum value of 0 and a maximum of 1 for all of the runs.	68
Figure 3.11	Conceptual sketches of the impact of different bed elevation kurtosis and skewness on the appearance of the cross profile of a braided river.	69
Figure 3.12	Variations in the A. median; B. standard deviation; C. kurtosis; D. skewness of the bed elevation with flume width and formative discharge.	70
Figure 3.13	Scatter plots with indicative regression trend lines illustrating a decline in A. mean sediment transport rate (Q_s in g/s) and B. dimensionless sediment transport rate (q_s) with increasing wetted channel width. The different symbols indicate the presence (triangular markers) or absence (circular markers) of mid-channel bars, and the colours indicate different flume widths.	72
Figure 3.14	Scatter plots with indicative trend lines illustrating relationships between ω (flume width) and A. mean sediment transport rate (Q_s in g/s) and B. dimensionless sediment transport rate (q_s) defined across the 27 experimental runs.	73
Figure 3.15	Scatter plots illustrating A) Changes in the ratio of active to wetted width as flume width with increasing ω (with trend line). B) Changes in wetted channel width with increasing discharge. C) Changes in active channel width with increasing discharge.	74

Figure 3.16	Scatter plots illustrating relationships between stream power (ω related to flume, wetted and active widths) and properties of the channel morphology (median, standard deviation, skewness and kurtosis of the elevation frequency distribution). The key explains the symbols used for runs with different flume widths).....	76
Figure 3.17	Variations in median, standard deviation, kurtosis and skewness of the bed elevation frequency distribution with changes in discharge. The key explains the symbols used for the different widths.	78
Figure 3.18	Presence of mid-channel bars in relation to the four parameters of the elevation frequency distribution (black dots are channels without mid-channel bars; white dots are channels with mid-channel bars).....	79
Figure 3.19	Frequency distributions of the differences in elevation between the original runs (A) and their repetition (B) organized vertically by discharge and horizontally by flume width. Each of the distributions is labelled according to the original run number with C to indicate the distribution relates to the difference in elevation between runs A and B. The individual horizontal axis for all of the figures is equally distributed in bins with a 0.5 size, with a range value from -9 to +9, while the vertical axis indicates density with a minimum value of 0 and a maximum value of 1.	82
Figure 4.1	Detrended DEMs for 1 km reaches 1 to 19. Note that length scales vary slightly between the three images.....	97
Figure 4.2	Detrended DEMs for 1 km reaches 20 to 36. Note that length scales vary slightly between the three images.....	98
Figure 4.3	Relative elevation frequency distributions for 1 km reaches 1 to 9.	99
Figure 4.4	Relative elevation frequency distributions for 1 km reaches 10 to 18.	99
Figure 4.5	Relative elevation frequency distributions for 1 km reaches 19 to 27.	100

Figure 4.6	Relative elevation frequency distributions for 1 km reaches 28 to 36.	100
Figure 4.7	Changes in a: standard deviation (m), b: elevation range (m), c: skewness and d: kurtosis from reach 1 downstream to reach 36. The dashed line denotes the downstream limit of the braided reaches (reach 1 to reach 32). The arrows indicate reaches 23, 28, 29, 30, 31, 32, which are discussed later in section 4.4.2.	106
Figure 4.8	Scatter plots of skewness of the bed elevation frequency distribution against the median (m), standard deviation (m), and kurtosis. Left: scatter plots include all 1 km reaches; Right: scatter plots for braided reaches only, with outlier reaches indicated by their reach number.	108
Figure 4.9	Scatter plots of vegetation cover variables (unvegetated, %vegetation > 1m, %vegetation > 5m, % vegetation > 10m) against the standard deviation (a to d) and the median (e to h) of the bed elevation frequency distribution for all 1 km reaches. ...	112
Figure 4.10	Scatter plots of vegetation cover variables (unvegetated, %vegetation > 1m, %vegetation > 5m, % vegetation > 10m) against the standard deviation (a to d) and the median (e to h) of the bed elevation frequency distribution for braided reaches only.	113
Figure 4.11	Scatter plots of vegetation cover variables (unvegetated, %vegetation > 1m, %vegetation > 5m, % vegetation > 10m) against the kurtosis (a to d) and the skewness (e to h) of the bed elevation frequency distribution for all 1 km reaches.....	114
Figure 4.12	Scatter plots of vegetation cover variables (% unvegetated, %vegetation > 1m, %vegetation > 5m, % vegetation > 10m) against the kurtosis (a to d) and skewness (e to h) of the bed elevation frequency distribution for braided reaches only.....	115
Figure 4.13	Changes in the cover of vegetation across the braid plain (a: % unvegetated, b: % vegetated, c: % with vegetation taller than 5 m; d: % with vegetation taller than 10 m) from reach 1 downstream to reach 36. The dashed lines denotes the downstream limit of the braided reaches (reach 1 to reach 32). The arrows indicate reaches 23, 28, 29, 30, 31, 32.....	117

Figure 4.14	DTM and vegetation cover maps for nine of the 1 km reaches upstream of reach 23.....	118
Figure 4.15	DTM and vegetation cover maps for nine of the 1 km reaches downstream of reach 22.	119
Figure 4.16	DTM and cross profiles for reaches 23, 28 and 29 (note differences in the scales of the cross-sectional profiles).....	121
Figure 4.17	DTM and cross profiles for reaches 30, 31 and 32 (note differences in the scales of the cross-sectional profiles).....	122
Figure 4.18	Scatter plots for the 36 Tagliamento reaches (left) and the 27 flume experiments (right) illustrating relationships between skewness and the median, standard deviation and kurtosis of the bed elevation frequency distribution.	124
Figure 5.1	Reach 2 of the Feshie River near Feshiebridge, a) shows a first interpretation of the active channel, b) shows a second possible interpretation of the active channel, referred to as “option 2”, and c) shows the difference between the two interpretations of the active channel.	131
Figure 5.2	In order to illustrate the process followed to determine vegetated islands when measuring the Anabranching index (A_i) the Tagliamento river section 9 is shown a) Island consist of a closed canopy vegetation b) Islands consists of a combination of closed canopy vegetation plus some adjacent discreet sparse vegetation areas.	132
Figure 5.3	Four indices of planform (A. B_i ; B. S_i ; C. A_i ; D. A_i^2) and unit stream power for Q_2 (E) and Q_{10} (F) plotted against active channel width for the Tagliamento middle reaches. Each symbol represents a different reach, with all image dates marked using the same symbol for the reach.	145
Figure 5.4	Four indices of planform (A. B_i ; B. S_i ; C. A_i ; D. A_i^2) plotted against active channel width for the river Feshie reaches. Each symbol represents a different reach, with all image dates marked using the same symbol for the reach.	146
Figure 5.5	Time series plots of B_i , S_i , A_i , A_i^2 for one reach of the river Feshie.	147

Figure 5.6	Scatter plots of A. unit stream power; B. B_i ; C S_i ; D A_i ; E A_i^2 plotted against active channel width (the colours of the symbols represent woodland vegetation with vigorous growth (black), other woodland vegetation (grey), vegetation with few trees (white)).....	148
Figure 5.7	Scatter plots of A. B_i ; B. S_i ; C. A_i ; D. A_i^2 plotted against active channel width (the colours of the symbols represent woodland vegetation with vigorous growth (black), other woodland vegetation (grey), vegetation with few trees (white)).....	150
Figure 5.8	(Left graphs) Scatter plots showing reach scores on the first two PCs of three different PCAs. (Right graphs) Vectors illustrating the loadings of the variables included in the PCA on the first two PCs.	153
Figure 6.1	Schematic changes in the bed cross profile, associated with shifts in skewness and kurtosis, as discharge and unit stream power decrease and flume width increases.	162
Figure 6.2	Schematic downstream changes in the bed cross profile, indicated by skewness and kurtosis of the bed elevation frequency distribution, along the 36km length of the Tagliamento River.	164
Figure 6.3	Distinct elevated areas (red polygons) within reaches 23, 28-32 that are represented as bumps and secondary peaks on the bed elevation frequency distribution, support mature riparian vegetation and may represent areas of the braid plain isolated by bed incision.....	165

List of Tables

Table 2.1	Characteristics of suspended, mixed and bedload dominated alluvial channels (after Schumm 1963).	30
Table 2.2	Characteristics of alluvial channels according to the mode of sediment transport (developed from Schumm (1963a) by Church (2006)).	31
Table 2.3	Role of vegetation in 7 of the 8 anabranching (sub)types identified by Nanson and Knighton (from Gurnell et al., 2009).	39
Table 3.1	Channel width, slope and discharge utilised in each experiment, the run time for the initial experiment (8T), and for any repetition runs (RT).	54
Table 3.2	Summary information on wetted, dry and active channel widths and related stream power, sediment transport rate and bed elevation frequency distribution of the 27 experimental runs.	61
Table 3.3	Summary information on run length (hr), discharge (Q in l/s), and the parameters (median, standard deviation, kurtosis, skewness) of the bed elevation frequency distribution for runs A and B and of the frequency distribution of the difference in elevation between A and B, which is labelled C.	81
Table 3.4	¹ Observed BI, and estimated bar types, bar mode (m) and BI based upon ² Colombini, Seminara and Tubino (1987) and ³ Crosato and Mosselman (2009) for values of their parameter b of 10 (recommended for gravel bed rivers) and 5. (M=meandering, T = transitional, B = braided).	86
Table 4.1	Description of the shape of the frequency histograms in Figures 4.3 to 4.6 according to five types (where specified, L and R refer to the location of the ‘bump’ or secondary peak on the left or right side of the histogram).	101
Table 4.2	Descriptive statistics of the bed morphology of thirty-six 1 km reaches of the Tagliamento river based on the analysis of lidar data from early spring 2001.	104
Table 4.2	Table 4.2 continued.....	105

Table 4.3	Product moment correlations among channel width and properties of the bed elevation frequency distribution (median elevation, standard deviation, skewness, kurtosis, and elevation range) across the 36 1km reaches and the 34 braided reaches (emboldened correlations are statistically significant ($p < 0.05$), italicised correlations are not statistically significant).....	107
Table 4.4	Product moment correlation coefficients between channel bed morphological and vegetation variables for all reaches and only braided reaches (emboldened correlations are statistically significant ($p < 0.05$), italicised correlations are not statistically significant).....	110
Table 5.1	The six rivers selected for study, their location, the number of reaches selected and the number of years for which data were available for analysis.....	129
Table 5.2	Information extracted from satellite and aerial images for the study rivers, river reaches and dates.	133
Table 5.2	Table 5.2 continued.....	134
Table 5.2	Table 5.2 continued.....	135
Table 5.3	Discharge, d_{50} and stream power estimates for the studied reaches.....	138
Table 5.3	Table 5.3 continued.....	139
Table 5.3	Table 5.3 continued.....	140
Table 5.4	Planform indices and active channel widths derived from applying options 1 and 2 to five river reaches.....	142
Table 5.5	Correlations among different stream power indices (ω^* is total stream power, ω^{**} is unit stream power, and ω^{***} is dimensionless stream power; Q_2 , Q_5 , and Q_{10} refer to the discharges for which the three different stream power indices are estimated).....	143
Table 5.6	Eigenvalues, variability explained and variable loadings on the first four PCs of a PCA on B_i , S_i , A_i , A_{i2} , slope, and channel width (all loadings > 0.7 are emboldened).....	151
Table 5.7	Eigenvalues, variability explained and variable loadings on the first four PCs of a PCA on B_i , S_i , A_i , A_{i2} , slope, and channel width and Q_{10} (all loadings > 0.7 are emboldened).	151

Table 5.8	Eigenvalues, variability explained and variable loadings on the first four PCs of a PCA on Bi, Si, Ai, Ai2, slope, and channel width and Q ₁₀ (all loadings >0.7 are emboldened).....	152
-----------	--	-----

Chapter 1

Introduction

This thesis is concerned with braided rivers, the controls on their morphology and their transition to single-thread forms. The research commences by investigating the three-dimensional morphology of braided and transitional rivers and the degree to which this is influenced by channel confinement and discharge. The association between riparian vegetation and the three-dimensional morphology of braided and transitional reaches of a single river are then investigated to develop understanding of the ‘topographic signature of vegetation’. Finally, a sample of braided and transitional rivers with different width, slope, discharge and riparian vegetation are investigated to assess the degree to which the influence of vegetation can be identified as other factors controlling river morphology also vary.

Chapter 2 provides a brief review of the literature on alluvial river channel styles and the braid-meander transition. It sets the scene for proposing the three research questions that are investigated in the thesis (section 2.5). Each of these three research questions is investigated in a separate Chapter (Chapters 3, 4 and 5). Each of these Chapters is written as a free-standing piece of research. As a result, the relevant detailed literature is reviewed within each of Chapters 3, 4 and 5, and Chapter 2 serves as a broad and relatively brief context for the research rather than an exhaustive review of the relevant literature.

The thesis uses a combination of research methods to address the three research questions. Experiments are conducted in a laboratory flume. Different remotely-sensed data sets are then analysed to investigate the characteristics of real braided and transitional rivers. Airborne lidar, colour and panchromatic air photographs, and satellite images are all analysed using both image processing and GIS software. In addition, statistical analyses are applied to several of the derived data sets. These methods provide the focus for each of chapters 3, 4 and 5, with laboratory flume research presented in Chapter 3; the analysis of airborne lidar data presented in Chapter 4; and the analysis of other remotely sensed data types presented in Chapter 5.

The research results combine to provide new scientific insights into several aspects of braided and transitional rivers. These results are of both scientific and management interest, but, as explained in Chapter 6, further research is needed to transform these new insights into quantitative tools that can be directly applied in river restoration and management contexts.

Chapter 2

Developing a Process-based Understanding of Alluvial River Channel Styles: A Brief Introduction to the Braid-meander Transition

2.1 INTRODUCTION

The research reported in this thesis focuses on braided rivers, including both their characteristics and how these differ from narrower transitional river forms. Each of the following three research chapters (Chapters 3, 4 and 5) reviews relevant literature and so this chapter provides a brief overview of braided rivers in the context of the continuum of river types that have been identified. In doing this, some of the key controls on braided and transitional rivers are outlined, providing support for the research questions that are posed at the end of the chapter (section 2.6).

To provide a brief context for the following research, this chapter outlines the historical development of research concerning alluvial channel styles with a particular emphasis on the transition between single thread (meandering) and multi-thread (braiding) styles, and the apparent controls on this transition. Research on this theme has passed through three main historical phases from early descriptive approaches to approaches that incorporate controls and processes in an increasingly quantitative way. Here, these phases are called: (i) the descriptive era (section 2.2); (ii) incorporating process understanding: discharge, sediment and gradient controls (section 2.3); and (iii) the role of riparian vegetation (section 2.4).

2.2 THE DESCRIPTIVE ERA

Until the 1950s, descriptive classifications of rivers were prevalent. The following three pieces of work are influential in different ways.

In relation to terminology, Jackson (1834) provided one of the earliest examples of the application of a classificatory approach to river planforms when he applied, for the first time, the term “anastomosing” to describe a river channel that separates into more than

a single channel at one point and re-joins further downstream (Carling et al., 2013), formally discriminating between single-thread and multi-thread planforms.

Probably the best known early classification of rivers was proposed by Davies (1899), who defined three adaptation stages in river style development (youthful, mature, old age). These were linked to phases of landscape development or denudation and so were inherently linked to land surface gradient and bed sediment calibre. When the stages were applied as an upstream to downstream sequence, they were also linked inherently to river discharge.

Alabayan and Chalov (1998) describe research that was published at about the same time as Davies' work but has received far less attention. Lokhtin (1897) anticipated the more quantitative, process-based approaches that emerged in the 20th century. Well ahead of other researchers, Lokhtin suggested that there were three main independent factors that controlled river forms: the discharge regime, the slope or gradient (influenced by the relief of the area crossed by the river), and the erodibility of the river bed (which varies according to the sediment properties). He proposed a 'channel development criterion', the ratio of stream power (discharge combined with gradient) and bed erodibility represented by bed material grain size, where low values of the criterion corresponded to stable meandering streams and high values to unstable braided streams. These factors form the basis of developments during the period of increased process understanding (section 2.3).

2.3 INCORPORATING PROCESS UNDERSTANDING: DISCHARGE, SEDIMENT AND GRADIENT CONTROLS

Although much of the early work suggested possible process controls on river style, the first quantitative links between fluvial processes and forms were proposed in the mid 1950s. Two pieces of research by Lane (1957) and Leopold and Wolman (1957) were particularly influential.

Lane (1957) suggested a qualitative relation that represented the governing conditions responsible for the different morphologies of alluvial channels (braided, intermediate and meandering):

$$Q_s/Q \sim S/D$$

where Q represents discharge of water, Q_s represents discharge of sediment, D is sediment calibre, and S is the slope. Thus the equation links river discharge, sediment size and load (availability), and topographic gradient.

In a similar analysis, Leopold and Wolman (1957) provided a quantitative definition of an apparent threshold between meandering and braided planforms. Although Leopold and Wolman (1957) suggested that rivers should be conceptualized as a continuum of different patterns, they subdivided rivers into three main planform styles (straight; meandering; braided) and they quantified the transition between meandering and braided patterns as a relationship between discharge (Q) and channel slope (S) (Figure 2.1):

$$S=0.012Q^{-0.44}$$

In both of these examples, the selection of an appropriate value for Q is open to debate but Leopold and Wolman (1957) selected the 'bankfull discharge' for the graph depicted in Figure 2.1. They also suggested six variables as the main controls on channel pattern in natural environments (i.e. discharge, slope, width, depth, velocity, and roughness), later adding sediment load and sediment size to the list (Leopold et al., 1964). Although subsequent research has shown that all of these variables are associated with river channel style, they are not independent of one another.

Between 1960 and 2000, researchers built on the above work, progressively incorporating greater detail concerning fluvial processes into the discrimination of channel styles, and incorporating quantitative analyses based upon the aggregation of field data from as many sites as possible. The properties of fluvial sediments (calibre, supply) were given particular attention.

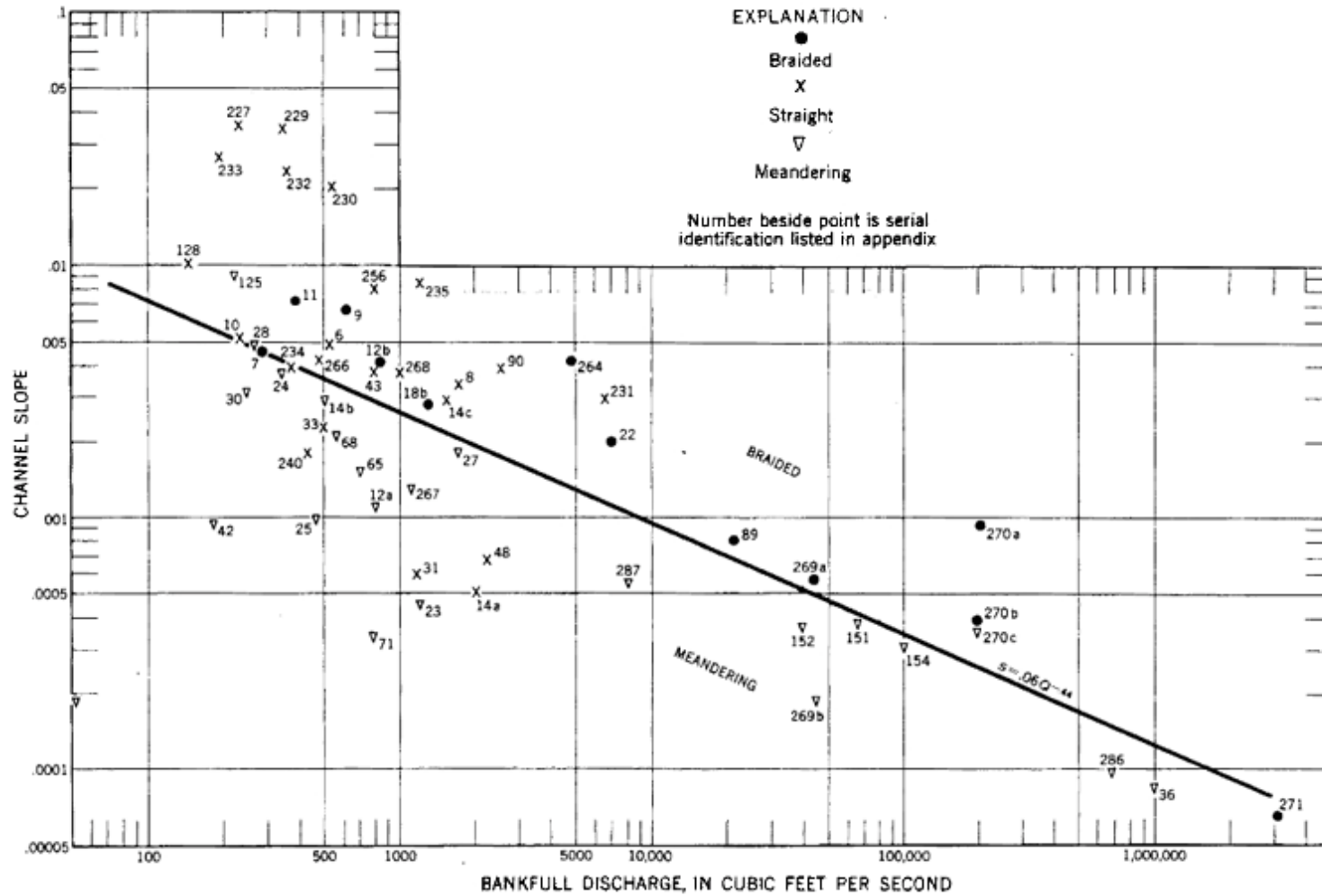


Figure 2.1 Combinations of slope and bankfull discharge observed for natural channels, and a line separating braiding and meandering channels (from Leopold and Wolman, 1957).

Researchers working in different river environments further developed the relationship proposed by Leopold and Wolman (1957, Figure 2.1) by estimating different slope-discharge threshold conditions based on bankfull or mean annual flood discharge to represent Q and channel or valley slope to represent S . They showed that sediment size was an additional crucial factor in discriminating meandering – braiding threshold conditions (e.g. Osterkamp, 1978; Begin, 1981; Bray 1973, 1982; Carson, 1984a and b; Ferguson, 1987; van den Berg, 1995), and developed these relationships using larger data sets (e.g. Ferguson, 1987, Knighton and Nanson, 1993, Beechie et al., 2006) to define new thresholds (e.g. Church 2002) within the data space shown in Figure 2.1. The addition of new data revealed that sites show a gradual transition across the plot according to bed material calibre, with predominantly gravel bed, braided and wandering streams plotting above the Leopold and Wolman (1957) transition line and streams with predominantly sand and finer bed sediment plotting below the line (Figure 2.2). In this analysis, ‘wandering’ is defined as a transitional, gravel-bed channel style described by Desloges and Church (1989, p360) as ‘irregularly sinuous channels, sometimes split about channel islands and in some places braided’. Following a deeper analysis, Church (2002) proposed different channel style thresholds depending on bed sediment calibre (gravel or sand, Figure 2.3).

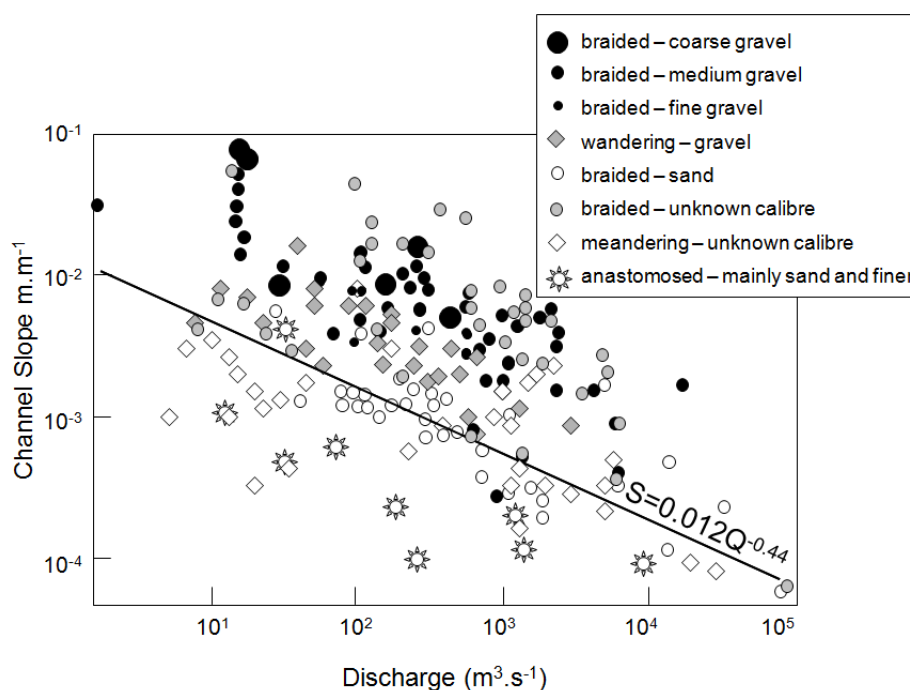


Figure 2.2 Association between river planform style, discharge and slope showing the threshold between meandering and braiding defined by Leopold and Wolman, 1957 (data sources: Leopold and Wolman, 1957, Ferguson, 1987, Knighton and Nanson, 1993, Beechie et al., 2006). (from Gurnell et al., 2009)

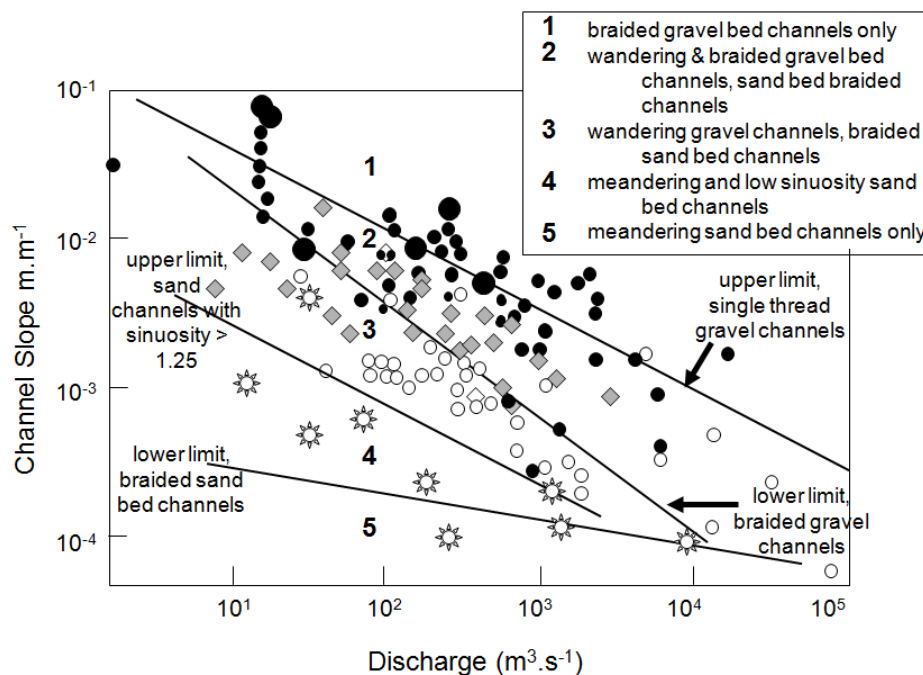


Figure 2.3 Association between river planform style, discharge, slope and bed sediment calibre (data sources as for Fig. 2.2, thresholds between styles from Church 2002). (from Gurnell et al., 2009).

Whilst this simple graphical approach incorporated bed sediment calibre, the incorporation of sediment supply required a slightly different approach, which was initiated by Schumm during the 1960s to 80s.

Schumm (1963) subdivided rivers according to their alluvial sediment calibre and thus the predominant mode by which they transported sediment (suspended, mixed, bedload channels), assigning ranges of channel gradient, width to depth ratio, and sinuosity to each mode and describing the way in which channels associated with each transport mode adjusted to erosion or deposition (Table 2.1).

Table 2.1 Characteristics of suspended, mixed and bedload dominated alluvial channels (after Schumm 1963).

	Stable	Depositing	Eroding	Suspended Load (%)	Bedload (%)
Suspended load channels	w/d < 7 sinuosity > 2.1 Gradient gentle	Major deposition on banks leads to narrowing	Dominant bed erosion Widening minor	85	15
Mixed load channels	w/d 7-25 sinuosity 1.5-2.1 Gradient moderate	Initial major deposition on banks followed by deposition on bed	Initial bed erosion followed by channel widening	65	35
Bedload channels	w/d > 25 sinuosity < 1.5 Gradient moderate	Bed deposition and bar and island formation	Widening dominant Little bed erosion	30	70

Schumm's subdivision of suspended, mixed and bedload alluvial channel types was further subdivided and extended into boulder-bed and silt-clay channels by Church (2002, 2006), providing a more detailed association between sediment transport mode and calibre, channel style, and channel geomorphological features (Table 2.2).

Table 2.2 Characteristics of alluvial channels according to the mode of sediment transport (developed from Schumm (1963a) by Church (2006)).

River Type / Characteristic Shields number	Sediment type	Sediment transport regime	Channel morphology	Channel stability
Jammed channel 0.04+	Cobble or boulder-gravel	Bed load dominated; low total transport but subject to debris flow.	Tep-pools or boulder cascades; width typically a low multiple of largest boulder size; $S > 3^\circ$.	Stable for long periods with throughput of bed load finer than structure-forming clasts; subject to catastrophic destabilisation in debris flows.
Threshold channel 0.04+	Cobble-gravel	Bed load dominated; low total transport in partial transport regime; bedload may actually be less than 10% total load.	Cobble-gravel channel bed; single thread or wandering; highly structured bed; relatively steep; $w/d > 20$ except in headwater boulder channels.	Relatively stable for extended periods, but subject to major floods causing lateral channel instability and avulsion; may exhibit serially reoccupied secondary channels
Threshold channel up to 0.15	Sandy-gravel to cobble-gravel	Bed load dominated, but possibly high suspension load; partial transport to full mobility; bed load typically 1%–10% of total load	Gravel to sandy-gravel; single thread to braided; limited, local bed structure; complex bar development by lateral accretion; moderately steep; low sinuosity; w/d very high (>40)	Subject to avulsion and frequent channel shifting; braid-form channels may be highly unstable, both laterally and vertically; single-thread channels subject to chute cutoffs at bends; deep scour possible at sharp bends
Transitional channel 0.15–1.0	Sand to fine-gravel	Mixed load; high proportion moves in suspension; full mobility with sandy bedforms	Mainly single-thread, irregularly sinuous to meandered; lateral/point bar development by lateral and vertical accretion; levees present; moderate gradient; sinuosity <2 ; $w/d < 40$	Single-thread channels, irregular lateral instability or progressive meanders; braided channels laterally unstable; degrading channels exhibit both scour and channel widening
Labile channel >1.0	Sandy channel bed, fine-sand to silt banks	Suspension dominated with sandy bedforms, but possibly significant bedload moving in the bedforms	Single thread, meandered with point bar development; significant levees; low gradient; sinuosity >1.5 ; $w/d < 20$; serpentine meanders with cutoffs	Single-thread, highly sinuous channel; loop progression and extension with cutoffs; anastomosis possible, islands are defended by vegetation; vertical accretion in the floodplain; vertical degradation in channel
Labile channel up to 10	Silt to sandy channel bed, silty to clay-silt banks	Suspension dominated; minor bedform development; minor bed load	Single-thread or anastomosed channels; prominent levees; very low gradient; sinuosity > 1.5 ; $w/d < 15$ in individual channels	Single-thread or anastomosed channels; common in deltas and inland basins; extensive wetlands and floodplain lakes; vertical accretion in floodplain; slow or no lateral movement of individual channels

Schumm (1985) used the three modes of sediment transport from Table 2.1 to produce a qualitative classification of river styles (Figure 2.4), which formed the basis of subsequent, more complex classifications. For example, Ferguson (1987) produced the modified diagram shown in Figure 2.5, concluding that at lower slopes and similar discharge, sand-bed rivers braid more easily than gravel-bed ones, and that the bank erosion needed for braiding requires a greater gradient than a meandering pattern at a given discharge. The diagram also recognizes the potential importance of bank vegetation for bank strength; identifying that inactively meandering (and anastomosing) channels possess strong banks that are hard to erode (Figure 2.5).

Schumm's (1985) diagram (Figure 2.4) was also revisited by Church (1992, 2006), who incorporated channel descriptions from Mollard (1973) to introduce a wider range of channel styles (Figure 2.6).

In Figure 2.6 only three commonly-recognised multi thread river styles are identified: wandering, braiding and anastomosing. However, some researchers have given the classification of multithread rivers particular attention. For example, Nanson & Knighton's (1996) identified eight (sub)types of anabranching (multi-thread) channel systems according to stream power, sediment calibre, vertical and lateral stability and morphological characteristics (sinuosity, island size and shape, Figure 2.7) and located them on the Leopold and Wolman (1957) Q-S plot (Figure 2.8).

The classification proposed by Rosgen (1994), which is widely applied by stream managers across the United States, is based heavily on the above work. Rosgen justifies his approach by stating that:

'Stream pattern morphology is directly influenced by eight major variables including channel width, depth, velocity, discharge, channel slope, roughness of channel materials, sediment load, and sediment size (Leopold et al., 1964). A change in any one of these variables sets up a series of channel adjustments which lead to a change in the others, resulting in channel pattern alteration. Because stream morphology is the product of this integrative process, the variables that are measurable should be used as stream classification criteria' (Rosgen, 1994, p171).

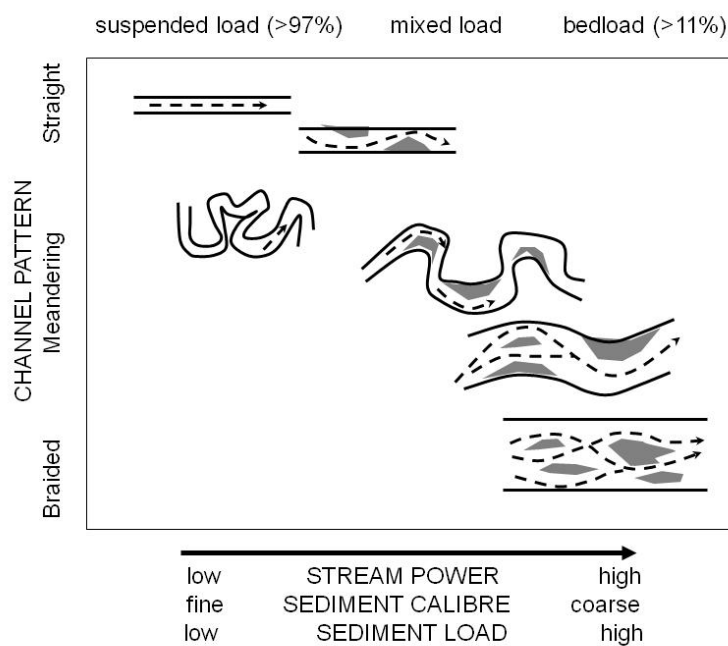


Figure 2.4 Channel styles associated with different modes and calibres of sediment transport, stream power, sediment calibre and sediment load (after Schumm, 1985).

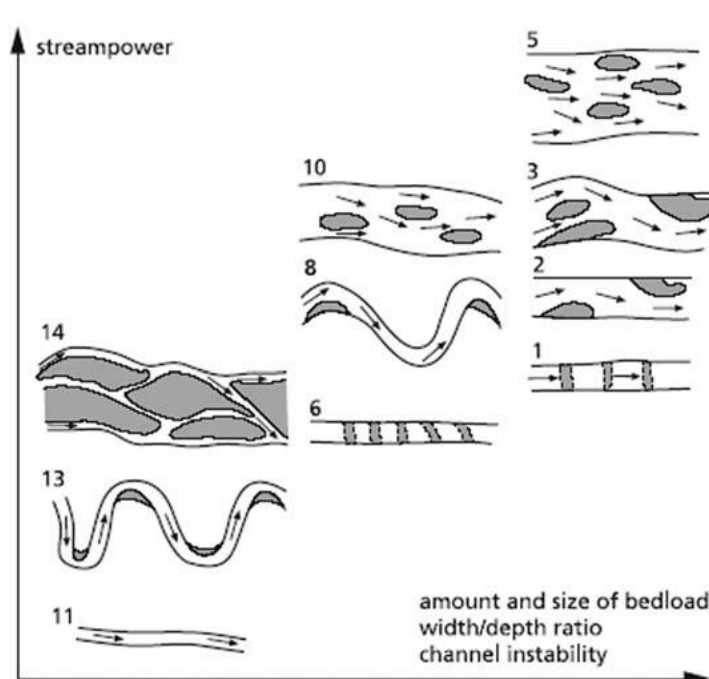


Figure 2.5 Channel styles differentiated according to stream power, amount and size of bedload, width-depth ratio and channel instability (after Ferguson 1987 in Kleinhans, 2010).

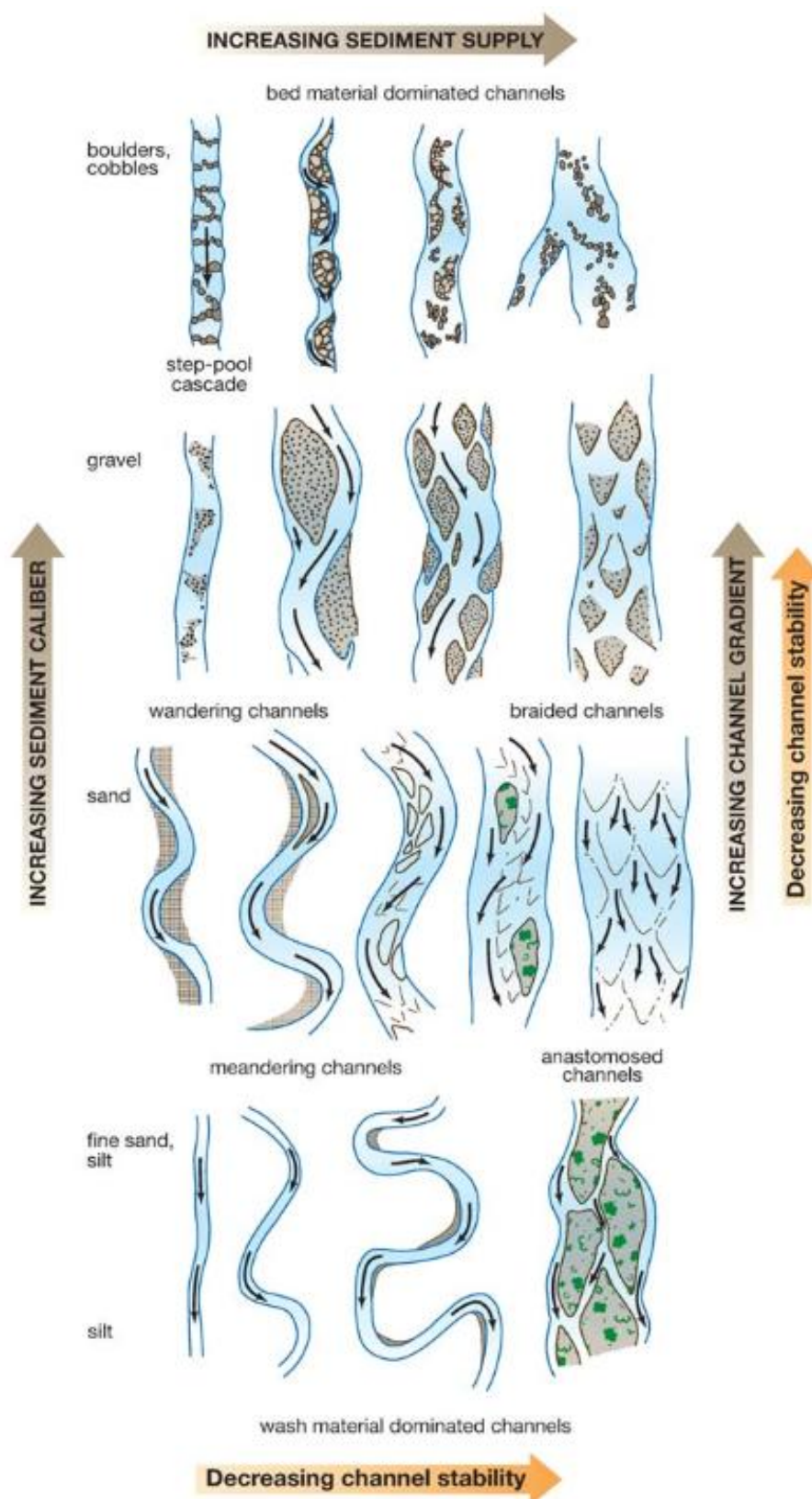


Figure 2.6 Association of alluvial river channel form with the principal governing factors (from Church 2006, after Church 1992, based on the concept of Mollard 1973 and Schumm 1985). Shading indicates sediment character and vegetation cover.

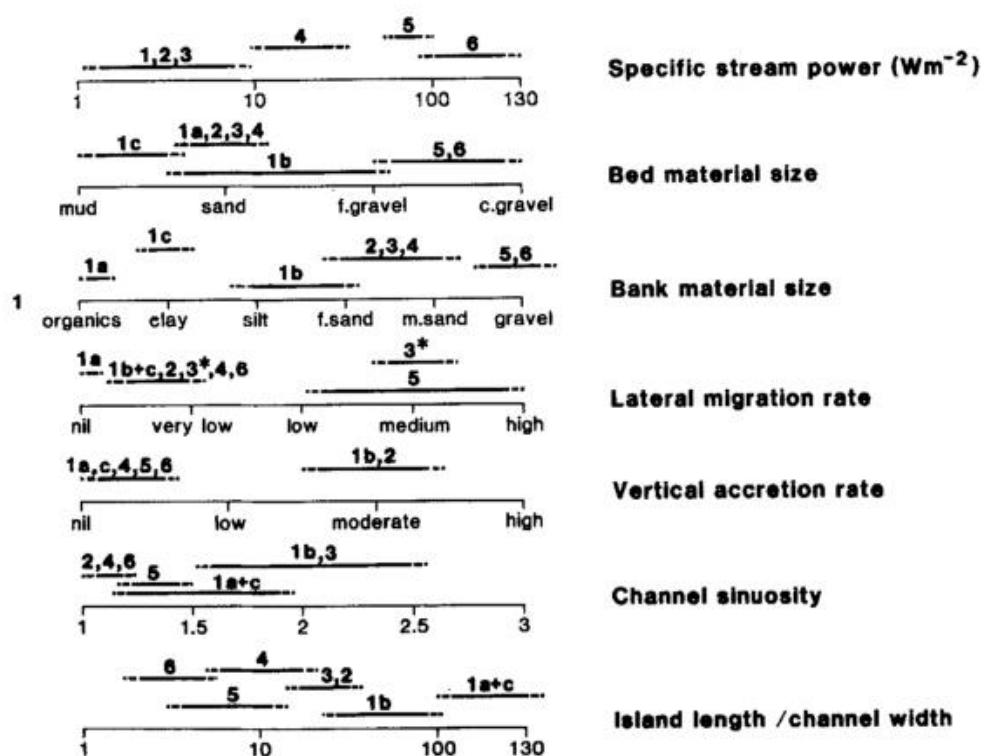


Figure 2.7 Approximate distribution of specific stream power, bed and bank sediment calibre, lateral migration rate, vertical accretion rate, channel sinuosity and island length/channel width ratio for eight types / subtypes of anabranching river (from Nanson and Knighton, 1996).

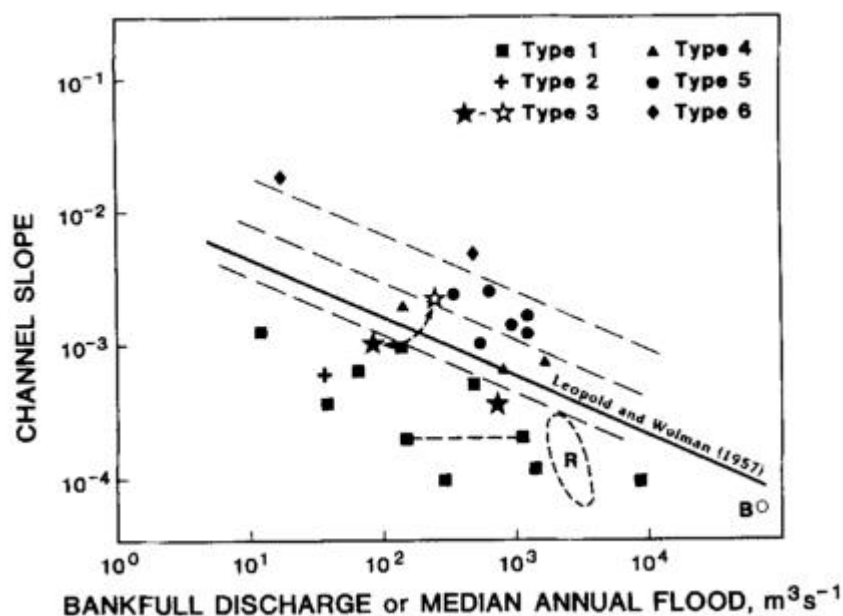


Figure 2.8 Q-S plot locating six types of anabranching river in relation to the meander-braid threshold of Leopold & Wolman (1957) (from Nanson and Knighton, 1996).

Thus, Rosgen's scheme, although based on a multi-level hierarchy of four inventories (geomorphic characterisation, morphological description, condition, verification) and developed from 'field observation of hundreds of rivers of various sizes in all the climatic regions of North America, experience in stream restoration, extensive teaching, and practical applications of the classification system by many hydrologists, geomorphologists, fisheries experts, and plant ecologists' (Rosgen, 1994, p173), essentially defines river type at level 1 (i.e. geomorphic characterisation) by slope, cross section (entrenchment ratio, width : depth ratio), plan view (sinuosity / single-/multi-thread) and dominant bed material.

In the last decade, considerable advances have been made in classifying channels based on both empirical and physics-based theoretical analyses of bar development. Since channel patterns (e.g. meandering, braided) and their subdivisions are closely related to the nature of the bars that are present, the nature of bars provides a new addition to the factors that can be used to distinguish channel types. Kleinhans and van den Berg (2011) provide a recent review of this topic, in which they described the bar regimes / bar modes developed theoretically by Parker (1976); Struiksma et al., 1985; Mosselman et al., 2006, and Crosato and Mosselman (2009). They classified 'natural' channel patterns from Google Earth images (available at: <https://www.google.com/earth/>) using the active braiding index and the presence of scroll bars, chute bars and scrolled point bars. Single-thread river patterns were subdivided into meandering with chute bars, meandering with scroll bars, and stable straight or sinuous rivers. Braiding intensity was quantified by the braiding index, defined as the average cross sectional number of active, unvegetated or barely vegetated braids. They illustrated a new empirical prediction of these bar and channel patterns on a plot of 'potential specific stream power' against median bed material grain size (D_{50}) (Figure 2.9). 'Potential specific stream power' is similar to specific stream power but it corresponds to a straight channel (sinuosity=1) and thus incorporates valley slope rather than channel slope; channel-forming discharge; a reference channel width which is independent of actual (pattern-dependent) channel width and is estimated from bed material size and channel-forming discharge. This development of classification based on bar properties is a very active area of current research, which, nevertheless, has roots in the work of Leopold and Wolman (1957) and will undoubtedly lead to further refinement of channel classification.

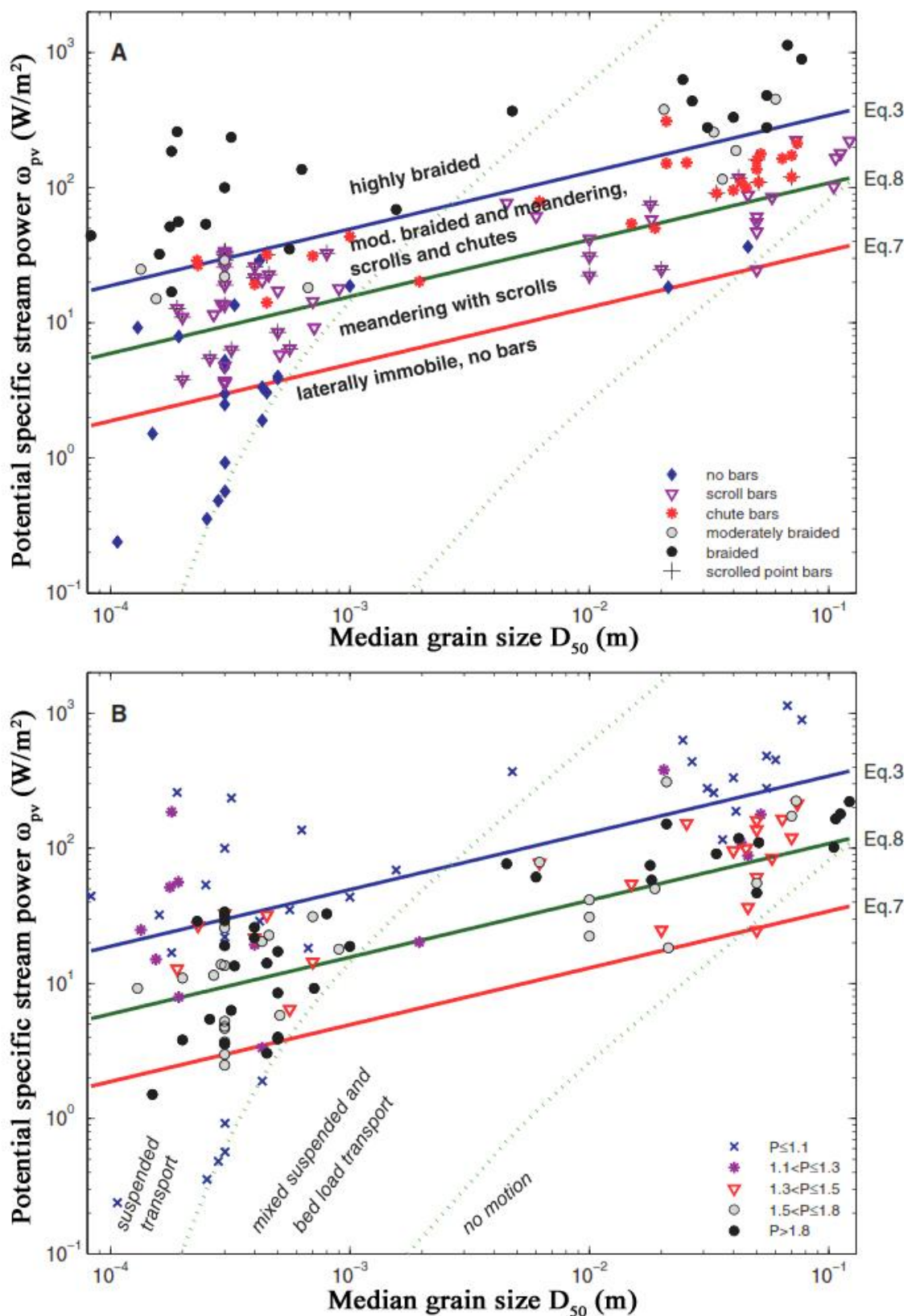


Figure 2.9 Patterns of equilibrium alluvial rivers. (A) Data subdivided by bar pattern; (B) Data subdivided by sinuosity.

Recently, Eaton et al. (2010) have also incorporated anabranching channels into the Leopold and Wolman Q-S plot by adding a third axis describing bank strength (Figure 2.10). This, to some extent, reflects the role of riparian vegetation and so leads this review to consider the specific role of riparian vegetation in controlling channel planform.

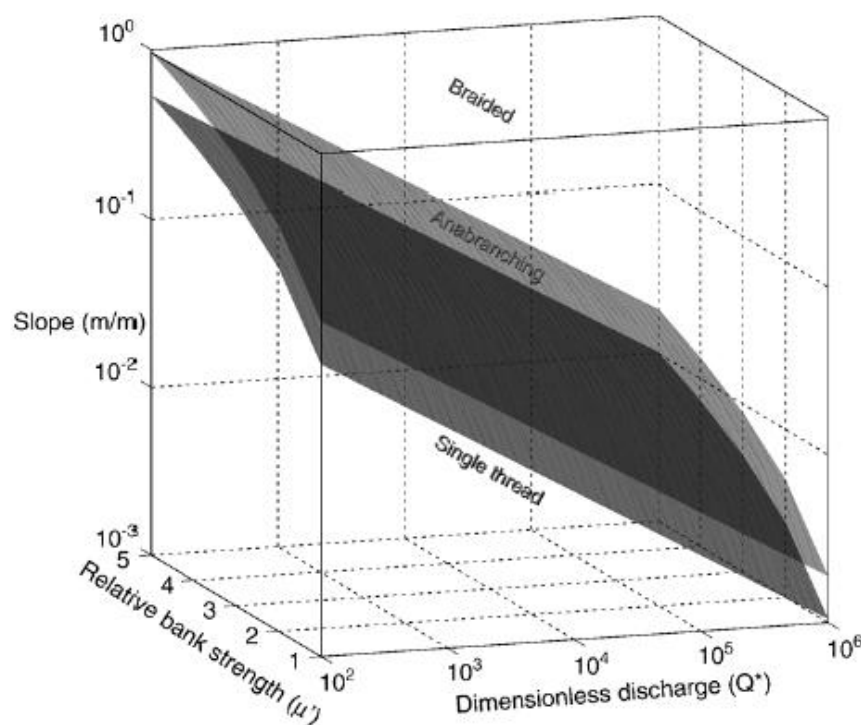


Figure 2.10 Channel pattern discriminant functions expressed as a function of slope, discharge and relative bank strength (from Eaton et al., 2010).

2.4 THE ROLE OF RIPARIAN VEGETATION

At an early stage, Leopold and Wolman (1957) mentioned vegetation in association with river style, but they did not recognise it as a control on style only as a passive feature of areas where fluvial disturbance was relatively low.

Many researchers have indicated the potential importance of vegetation for river style and dynamics. For example, through an empirical analysis of relationships among bankfull discharge and channel dimensions of gravel-bed streams in the UK, Hey and Thorne (1986) showed that bank vegetation provided an important explanatory variable, providing an early indicator of a link between vegetation and channel form / dimensions. Smith et al (1991) provided quantitative underpinning of the importance of vegetation when they showed that river banks covered by short alpine vegetation had a 20,000 times greater resistance to erosion than unvegetated river banks. Smith (2004)

and Griffin and Smith (2004) observed ‘floodplain unravelling’ (river transformation from a single to multi-thread channel pattern) as a result of extreme flood events following heavy grazing of floodplain woody vegetation, which suggested a role of woody vegetation in controlling the threshold between single thread and multi thread channel patterns. Also Beechie et al (2006) inferred that tree rooting depth was an important control on channel lateral migration from their analysis of channel style and vegetation patch age and diversity across straight – meandering - island braided - bar braided rivers. Moreover, Nanson and Knighton’s (1996) classification of anabranching river systems, although explicitly discriminated using physical properties, implicitly identified vegetation properties as discriminators of 7 of the 8 anabranching (sub)types (Table 2.3). Finally, based on field observations of riparian tree growth performance, Gurnell et al. (2009) conceptualised how the rate of riparian tree establishment and growth might affect the threshold stream energy at which planform pattern might change (Figure 2.11).

Table 2.3 Role of vegetation in 7 of the 8 anabranching (sub)types identified by Nanson and Knighton (from Gurnell et al., 2009).

Type Number	Type Name	Stated role of vegetation (page in Nanson and Knighton, 1996)
Low Energy Group		
Type 1 subtype a	Organic Systems	‘aggradation of bedload and the concomitant <i>growth of aquatic vegetation</i> constricts channel flow inducing periodic avulsion’ (224)
Type 1 subtype b	Organo-Clastic Systems	‘resistant, <i>well-vegetated banks</i> protect swampy, levee-banked islands’ (224)
Type 2	Sand- Dominated, Island-Forming	‘requires the combination of <i>stabilizing bank vegetation</i> and low stream energy to prevent the channel from braiding or meandering’ (224-5)
Higher Energy Group		
Type 4	Sand- Dominated Ridge-Forming	‘these ridges commonly form in wide sandy channels <i>as the result of within-channel tree growth</i> acting as an obstruction to flow’ (227)
Type 5	Gravel- Dominated, Laterally-Active	‘anabranching sections .. appear to be initiated by enhanced bed-sediment input ... the periodic formation of <i>log</i> or ice jams may augment this process’ (229), ‘Avulsion channels incise into existing floodplains, but in some cases islands grow vertically to floodplain height from large bars <i>stabilized by vegetation</i> within the channel’ (230)
Type 6	Gravel- Dominated, Stable	‘the means by which anabranches are formed appears to be similar to type 5’ (231)

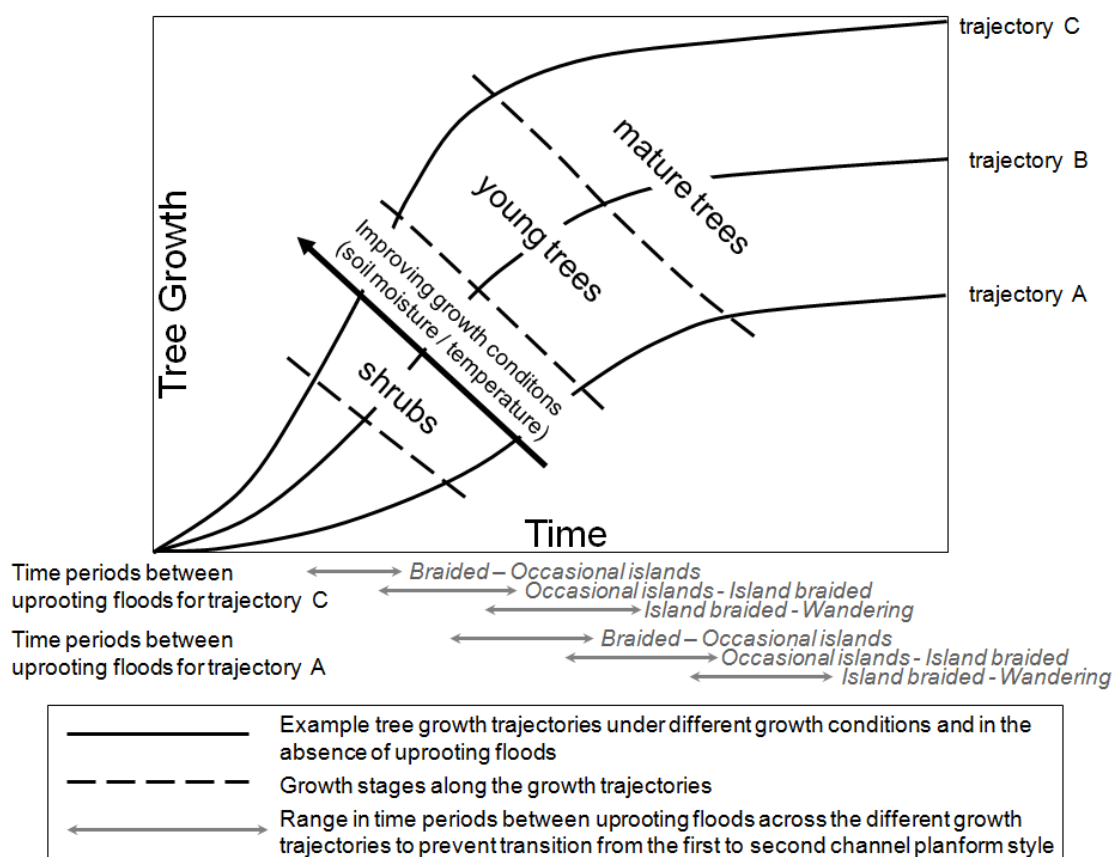


Figure 2.11 Conceptual model of associations between tree growth performance, flood magnitude/frequency and channel style. Sediment supply is assumed to be sufficient to support the different channel styles. Three trajectories of riparian tree growth (solid lines) from seedling / sapling, through shrub, young and mature tree stages (dashed lines) according to different growing conditions are compared with the range in the maximum time period between floods capable of uprooting trees across the three trajectories (thin grey arrows) to prevent transitions between the given river planform styles (italic text) (from Gurnell et al., 2009).

The importance of vegetation growth and establishment for braided river morphology has been demonstrated empirically by Bertoldi et al. (2011a), who through the analysis of properties of the vegetation cover and the bed elevation distribution of 21 reaches of the Tagliamento River, Italy, identified a ‘topographic signature of vegetation development’.

Building on field observations, laboratory flume experiments have investigated many aspects of the influence of vegetation on channel form and dynamics and have confirmed relationships observed in the field (e.g. Gran and Paola, 2001, Tal and Paola, 2007). In parallel, quantitative relationships linking vegetation to channel style have

focussed on bank stability. Particularly notable was the research by Millar (2000), who developed an improved theoretical meandering-braiding transition criterion incorporating the influence of riparian vegetation on bank stability. This has been developed in subsequent research by Eaton et al. (2010), where it has been incorporated into a number of useful graphics including the Leopold and Wolman (1957) Q-S plot (Figure 2.9) mentioned previously.

An important aspect of the role of vegetation as a control on channel style is that vegetation growth performance is itself dependent upon hydrological processes, particularly the river flow regime, and in some cases also the water retentive characteristics of riparian soils. This suggests that extremely complex interactions between vegetation growth, river discharge / moisture availability and sediment dynamics may govern variations in river channel style across space and time. This is a topic that has received remarkably little research attention, although Gurnell (2014) provides a recent review.

2.5 CONCLUSIONS

More than a century of research has revealed the importance of four main groups of factors in influencing channel style: discharge, gradient, sediment and vegetation. However, the precise nature of these controls is complex and includes many potential interactions and feedbacks. As a result, there are numerous questions that remain unanswered and thus many potentially-fruitful research paths to pursue. For example, Kleinhans (2010) recently listed the following 9 questions relevant to channel styles that require further research:

1. What is the role of flow strength and variation in flooding magnitude and frequency on the pattern?
2. What is the effect of the nature, magnitude, and variation of upstream sediment feed on patterns?
3. Is added bank strength due to sorting of fines and bed sediment a sufficient condition for meandering, and is vegetation also a sufficient condition? What extra interactions and feedbacks on channel pattern would arise if both occur?
4. What is the role of bar pattern and sorting at the bar scale? Is the emergence of fixed alternate (complex) gravel bars a sufficient condition for meandering in

gravel-bed rivers? To what extent do small-scale sorting processes cause large scale sorting patterns relevant for channel pattern?

5. In what parameter space of vegetation, fine sediment deposition (density, size, thickness) and flooding (magnitude, and frequency) do transitions between river patterns take place?
6. In what manner, to what extent and why do channel patterns and their causes in small rivers (1 m width) differ from those in large rivers (10 km width)?
7. What are the necessary conditions and time-scales for transitions between river patterns in response to changes in forcings?
8. How do channel patterns develop when the initial condition is another channel pattern rather than a hypothetical plane valley?
9. Are there hard thresholds (rather than transitions) that the system can cross during changing forcings due to extreme events? Can such threshold crossings lead to hysteretic or irreversible change due to vegetation or inherited floodplain structure?

2.6 RESEARCH QUESTIONS

The present research is concerned with braided rivers and their transition to single-thread forms. Based on the above review, and particularly developing from section 2.4, the research aims to investigate the impact of confinement imposed by unerodible (valley width) or cohesive (sediment, vegetation) banks on braided and transitional rivers through the following research questions:

1. **What are the influences of variations in discharge and river confinement on river style and bed morphology?** These two factors are explored experimentally in Chapter 3 where they allow consideration of the impact of natural (valley or cohesive bank) or human-induced (embanking and bed reinforcement) confinement on the transition from single-thread to braided channel patterns and the degree to which these are influenced by variations in (fixed) formative discharge.
2. **What is the influence of vegetation on braided and transitional river morphology?** This is explored in chapter 4 across 36 1km reaches of a natural river that are subject to similar peak discharges, slope and bed material but display differences in vegetation cover.

-
3. **Does the type and extent of vegetation influence / co-vary with braided river planform?** This question is explored in Chapter 5 across a selection of European braided rivers that display different amounts and types of vegetation but also different discharge regimes, slope and bed material. Google Earth images from different dates allow variations in river planform and vegetation extent to be compared through time, whereas comparisons among a sample of different rivers allow a qualitative comparison of vegetation and braiding characteristics.

Chapter 3

Flume Experiments to Investigate Braided Channel Development Under Controlled Conditions

3.1 INTRODUCTION

Although humans have long had an interest in different channel morphologies, significant progress in understanding the variety of morphologies that may occur and potential controlling processes commenced during the second half of the 20th century (see Chapter 2). Over the last 70 years, much research has focused on quantifying the properties of individual rivers, characterising the recurring properties of geomorphological features such as pools, riffles, bars, islands and associated bifurcations, and understanding the controls on the development of rivers of different type and their specific geomorphological features.

This chapter aims to contribute to this field of study by manipulating several potential controls on channel morphology and observing the morphological response to those manipulations within a laboratory flume. The focus of these experiments is to investigate the conditions under which multi-thread braided patterns develop as discharge and channel width change under a constant slope and grain size and a sediment supply that, through recirculation, matches the sediment transport rate. These experiments form a first phase in the research reported in this thesis, which investigates braided river morphologies in the laboratory and in field situations, gradually increasing the range and complexity of the potential controlling factors.

To provide a context for the laboratory experiments, this introductory section defines braided rivers (section 3.1.1); and briefly reviews how researchers have described and quantified braided river morphology (3.1.2), and the controls on braiding that have been identified (3.1.3). The section ends by listing the research questions that are investigated in the laboratory experiments (3.1.4).

3.1.1 Definitions of “Braiding”

Braided rivers develop in non-cohesive sediments composed predominantly of cobble, gravel, and / or sand grain sizes and are characterised by flows of water and sediment in multiple channels that diverge and converge at points that are called nodes (Lane, 1957, Bertoldi et al., 2009b). The individual channel threads vary greatly in size through time and space, and are separated by bars which may vary widely in their stability but are mainly unvegetated (Ashmore, 2009, Bertoldi et al., 2009b). However, where bars remain stable for a sufficient time, vegetated islands may form, giving rise to an island-braided morphology. The multiple threads of braided rivers are highly dynamic and complex (Brierley and Fryirs, 2008, Ashmore, 1990). Their planform and altimetry change rapidly during flood flows as a result of widespread sediment erosion and deposition, generating channel avulsions and inducing the formation and destruction of bars (Ashmore, 1982, Charlton, 2007, Chew and Ashmore, 2001, Jerolmack and Mohrig, 2007, Miall, 1977, Ashmore, 2013). These dynamics provide a wide diversity of physical and hydraulic habitats, frequent habitat turnover and, particularly in the case of island braided rivers, a very complex and rich habitat mosaic that supports extremely high biodiversity (Tockner et al., 2003, 2006).

3.1.2 Quantifying Properties of Braided Channel Form

As braiding is highly complex and also dynamic, this river planform presents considerable challenges to those attempting to quantify channel properties and their variations between rivers and also through time on the same river. Quantification of braiding properties has traditionally been based on three groups of measures:

- (a) The average number of channels across the river cross section or braid plane (Ashmore, 1990, Chew and Ashmore, 2001, Friend and Sinha, 1993, Howard et al., 1970, L.B. and Davies, 1979),
- (b) The total channel length within a given length of the river course or braid plane (Ashmore, 1990, Hong and Davies, 1979, Mosley, 1982, Richards, 1982, Robertson-Rintoul and Richards, 1993, Smith et al., 1996),
- (c) Bar dimensions and frequencies (Brice, 1960, Brice, 1964, Germanoski and Schumm, 1993, Rust, 1977).

All of these approaches represent means of counting and measuring the complexity of the braiding pattern. Of these broad approaches, channel counts (approach a) are

probably the most widely used. It produces a measure of braiding intensity or a 'braiding index'. In addition, measures of sinuosity of the individual channels are also widely used. These methods have been applied to assess changes in braiding pattern over time and its response to external controls. Many different methods have evolved to produce channel counts, with each producing potentially different results and inter-calibration between methods is difficult (Egozi and Ashmore, 2008). Therefore, it is crucial to use a single method and apply it consistently.

A development of the measurement of braiding intensity relates to whether the braid channels are active (i.e. actively transporting bed material) or not, leading to the discrimination of active braiding intensity and total braiding intensity. The difference between these two measures reflects the fact that, because the flow is separated into different channels the sediment transport is also divided, with some channels having insufficient energy to transport bed material (Ashmore, 1990, Bertoldi et al., 2009b, Egozi and Ashmore, 2009).

Although measures using approach (a) (and related ones using approach (b)) have been widely used, measures extracted using approach (c) can be complemented by predict from theoretical work that quantifies bar development (Toffolon and Crosato, 2007) and stability (e.g. Hansen, 1967; Callander, 1969; Seminara and Tubino, 1989). Furthermore, since the development of bars modifies channel planform (Olesen, 1984), approaches focusing on bar development and stability are particularly relevant to river channel management and restoration design (Malavoi et al., 2002). While direct measurements are informative, predictions of bar development using theoretical and numerical methods (e.g. Seminara and Tubino, 1989, Crosato and Mosselman, 2009) are potentially particularly valuable. For example, Crosato and Mosselman (2009) have proposed a physics-based but quite simple approach to determining what they call the bar mode:

$$m^2 = 0.17g \frac{b - 3}{\sqrt{\Delta D_{50}}} \frac{B^3 i}{C Q_w}$$

Where:

m = the bar mode

g = acceleration due to gravity (m.s^{-2})

b = degree of nonlinearity of sediment transport versus depth-averaged flow velocity (dimensionless).

B = river width (m)

Δ = relative sediment density under water (dimensionless)

D_{50} = median sediment grain size (m)

C = Chézy coefficient

Q_w = water discharge ($\text{m}^3 \cdot \text{s}^{-1}$)

The bar mode discriminates between the river types that are likely to develop with values of ≤ 1.5 indicating a meandering planform, values of ≥ 2.5 indicating a braided planform and intermediate values (> 1.5 and < 2.5) indicating a transitional planform. The method has been shown to produce quite reliable predictions for rivers with a width-to-depth ratio below 100. However, as the method incorporates channel width, discrimination between single thread and braided channel planforms might be already implied, since the braided rivers tend to have wider channels than meandering ones, providing space for a larger number of bars.

With the recent development of methods to rapidly measure the three-dimensional morphology of river channels, notably ground-based and airborne LiDAR, it has become possible to explore the third dimension of river channel form in detail and to develop new synthetic measures of braid channel morphology. For example, Bertoldi et al. (2011a) extracted elevation frequency distributions for the braid plain from which they were able to extract summary morphological indices such as the skewness and kurtosis of the braid plain form.

In this chapter, a selection of the above measures of braid channel form are used to compare the morphologies created during different experimental runs in a laboratory flume and also to assess the effectiveness of some theoretical predictions.

3.1.3 Controls on Braiding and Braided Channel Morphology

The determination of the main controlling variables on braiding as well as the analysis of the morphological responses to changes in these variables has been a contentious subject in the last 60 years. Much of this contention originates from questioning of the consistency / accuracy of measurements, the nature of the relevant variables, and the dynamics and disequilibrium of some of these variables over short timescales, such as the influence of sediment overloading during floods (Ferguson, 1987, Lewin and Brewer, 2001, Millar, 2005). As a result, even though there was early research that

attempted to understand the dominant variables that cause morphological changes in braided rivers, only in the last 25 years have technological advances allowed sufficiently precise measurements to deepen insights into the influences of various controls on channel planform development.

Despite the continuous debate, there is a core set of key variables that are acknowledged to influence braiding. This set was suggested by Lane (1955), who considered that interactions between discharge, channel or valley gradient, and sediment transport were the main causes of different channel patterns. Ashmore (1991) identified discharge, channel or valley gradient, and sediment particle size as the main variables, to which bank erosion resistance was later added, including the influence of bank sediments and riparian vegetation on this channel property (Eaton et al., 2010, Gurnell et al., 2009, Millar, 2000, Tal et al., 2004). Both field and laboratory investigations have contributed to developing understanding of the impact of these controls on braiding morphology and characteristics.

The flume experiments detailed in this chapter focus explicitly on the influence of discharge on channel morphology under different channel confinement conditions. Discharge combined with slope, determines the unit stream power (rate of energy dissipation) that acts on the bed and banks of a river and so dictates the potential for, and rate of, sediment transport. In order to restore and improve the ecological conditions of a river and avoid incision, unit stream power is calculated to determine the amount of energy the river possesses to move sediment in either bed load or suspended load per unit channel width. Thus, channel width is an important variable as its manipulation could be expected to lead to increased efficiency of sediment transport and channel bed incision (narrower widths) or less efficient transport of sediment and the deposition of bars (wider widths) if discharge and sediment supply remain constant.

While river discharge is acknowledged to be a control on braided channel morphology, it is difficult to specify how the two are linked unless it is in experimental situations where the discharge can be precisely measured (Begin, 1981, Bridge, 1993, Carson, 1984, Kellerhals et al., 1976, Mosley, 1982, Rust, 1977, Surian, 1999, van der Nat et al., 2002). For example, recent flume experiments have identified relationships between braiding intensity and discharge or stream power, revealing connections between the mechanics of braiding at the scales of the multi-thread network of channels and the

individual channels of which the network is composed (Ashmore, 2013). A gradual increase of the total braiding index to a relatively stable value exhibiting small fluctuations, has been observed in laboratory experiments starting from a single straight channel with a constant discharge and slope. Similar runs have shown a similar pattern, but values of instantaneous braiding intensity are variable. (Ashmore, 2009, Egozi and Ashmore, 2009). Once approximate equilibrium in the braiding intensity is reached, an additional increase in discharge for a particular sediment size causes braiding intensity to increase further. Other research based on measurements of braiding patterns from aerial photographs shows that the braiding intensity is proportional to stream power and inversely proportional to the bed material grain size (Bertoldi et al., 2009b, Egozi and Ashmore, 2009). Furthermore, both the active and total braiding intensity and the ratio of the number of active to total channels adjust in response to the imposed formative discharge and stream power (Ashmore, 2013).

Research has also demonstrated the influence of the formative discharge on the total river width (the sum of the wetted width of all channels in a cross-section) and the mean depth of the channel. This relationship has been revealed through a compilation of river cross-section data by Van den Berg (1995), who concluded that for a given formative discharge and compared to single thread rivers, braided rivers are wider and shallower making their width to depth ratio higher than that of single thread channels. However, this relationship is subject to considerable variability. This has been illustrated by flume experiments using the same discharge, which have shown a width variation of over 30% which may have been caused by different bedload conditions across the runs (Warburton, 1996). These results show a similar level of width variability to natural rivers analysed in New Zealand by Mosley (1983). The suggestion that width and discharge are linearly related, albeit with considerable noise, has been explored by Bertoldi et al. (2009a). They found variations in bedload flux under a constant discharge per unit width, suggesting that flux might be more dependent on river width than flow depth, unit discharge, or shear stress.

Discharge variability has also been considered to be an important influence on braiding. However, research incorporating non-cohesive sediment and a constant discharge in laboratory experiments have shown that a braided planform is a common occurrence regardless of the absence of discharge variability (Ashmore, 1982, Hong and Davies, 1979, Murray and Paola, 1994, Ashmore, 1990, Ferguson, 1993). Nevertheless,

frequency and duration of channel forming discharges or large flows that exceed a certain threshold may be important for maintaining a braided planform (Piégay et al., 2009) and discharge variability may also be an important component of bar evolution mechanisms (Lane, 2006)

In addition to discharge, the amount of sediment that is supplied to the river is also important because if it exceeds the energy available to move the sediment, different morphological structures develop. In single thread channels, bar structures characteristic of transitional rivers develop, and if the excess of sediment supply continues, additional sediment accumulation leads to the development of a braided channel. As a consequence, the ratio between discharge and sediment supply has been proposed as the principal control of both river and valley slope in alluvial sedimentary basins (Paola, 2001).

Sediment grain size is also important for river morphology since larger particles increase the threshold stream power required for braiding (Carson, 1984, Dade, 2000, Ferguson, 1984, Ferguson, 1987, Henderson, 1963, Kellerhals, 1982, Millar, 2000, Robertson-Rintoul and Richards, 1993, Van den Berg, 1995). This effect is particularly evident when sand and gravel bed rivers are compared (Ferguson, 1987, Kellerhals, 1982, Van den Berg, 1995, Bledsoe and Watson, 2001, Kleinhans and van den Berg, 2011). Bed material is also often considered to have a unique size, and so equal mobility of particles is assumed. While this may provide a reasonable approximation for some streams (Andrews, 1983, Andrews and Erman, 1986, Kuhnle, 1992, Parker and Klingeman, 1982), in others finer sediments are selected for transport over the coarser particles (Komar, 1987, Ashworth and Ferguson, 1989). Lisle (1995) compared bed load and bed material in 13 sampled natural rivers and concluded that the average size of the bedload was finer than the average size of the bed material.

Bed load transport is an important factor that helps maintain the variability and complexity of the braided network. The typical characteristics for braiding are a high bedload supply rate and high stream power and where erosion of bed and bank materials is low relative to stream energy (Osterkamp, 1978, Ferguson, 1987). As braiding develops in non-cohesive sediment and in bedload-dominated situations, it requires a combination of discharge and slope (stream power) that is sufficiently large to move the bed material (Leopold et al., 1957, Osterkamp, 1978, Dade, 2000, Ferguson, 1987, Van

den Berg, 1995). However, understanding and predicting bedload flux in braided rivers remains a significant problem because of the high transverse variability in the hydraulic parameters that control sediment flux across the braid plain (Bertoldi et al., 2009a) that are affected by, for example, the complex river morphology and variability in grain size (Carson and Griffiths, 1987). Dade (2000) assumed that the grain size of the transported sediment is correlated and in equilibrium with the size of the bed material, but this is difficult to verify. Particle tracing is beginning to yield information on how bed load movements are related to controlling factors such as bed morphology and properties of particular flow events but further experiments are needed to more comprehensively explore how bed material moves within braided systems (Martin and Church, 1995, McLean et al., 1999, Habersack, 2001, Martin and Ham, 2005).

A final factor that is influential with regard to braiding is bank erosion resistance. The resistance of river banks to erosion is dependent upon the cohesion of the bank sediments, which depends upon their silt and clay content, and the added flow resistance and cohesion provided by bank vegetation. The vegetation canopy traps sediment and its roots enhance the cohesion of the sediment, thus limiting the susceptibility of the banks to erosion (Millar, 2000; Tal et al., 2004; Gurnell et al., 2009; Eaton et al., 2010). In general, high bank erosion resistance restricts the potential for channel braiding and forces a higher threshold of stream power or slope above which braiding may develop (Eaton et al., 2010, Ferguson, 1987, Millar, 2000, Millar, 2005, Osterkamp, 1978, Schumm, 1963, Crosato and Saleh, 2011). Different flume experiments and field observations have illustrated that significant vegetation development can induce a transition from a braided to a single thread channel, and vegetation removal from the floodplain can induce the opposite (Gran and Paola, 2001, Gurnell et al., 2001, Tal et al., 2004, Tal and Paola, 2007, Zanoni et al., 2008, Jang et al., 2003).

3.1.4 Research Questions

Sections 3.1.2 and 3.1.3 have briefly summarised the methods used for measuring properties of braided channels and current knowledge of the controls on braiding. This chapter builds on this knowledge by reporting a series of laboratory experiments conducted in a flume of constant slope and constant bed material size. The experiments were conducted to investigate the impact of different constant formative discharges and different channel widths on channel morphology under a condition where sediment supply matches sediment yield from the flume through recirculation.

The experiments were designed to answer the following research questions:

1. To what extent does bed morphology vary between experiments conducted with the same formative discharge and fixed maximum channel width?
2. To what extent does bed morphology change in response to different fixed, formative discharges within the constraints of a fixed maximum channel width?
3. To what extent does bed morphology change in response to a fixed, formative discharge within the constraints of different fixed maximum channel widths?
4. To what extent does bed morphology change in response to different fixed, formative discharges within the constraints of different fixed maximum channel widths?

In relation to these experiments, the impact on morphology was assessed with respect to a range of the different measures of morphology described in section 3.1.2 and with particular reference to transitions between single thread and multi-thread planforms.

3.2 METHODS

3.2.1 Flume Experiments

Twenty-seven experiments were carried out in a large flume (25 m long, 2.9 m wide) located at the University of Trento, Italy (Figure 3.1) to answer the research questions listed in section 3.1.4. The flume was already filled with well-sorted sand with a typical grain size (d_s) of 1mm and had a fixed gradient of 0.010. This choice was made in order to represent a typical gravel-bed braided river, providing a compromise between a grain size that is large enough for grains to move independently (i.e. not cohesive) while being sufficiently small to be mobile at relatively low stream power and thus small discharges. Furthermore, as the amount of sand required to fill the flume is large (over 30 m³) and is moved manually, there was no realistic way to change the grain size between the experiments.

Each experiment was conducted within a fixed width channel, which varied among the experiments (Table 3.1). The nine different channel widths were achieved by excavating channels in the sand contained in the flume with the required dimensions. The channel edges were lined with a blue non-reflective plastic sheet to fix the width (Figure 3.1 B). The plastic had a small roughness to ameliorate any sharp velocity increment that might

arise if the plastic became exposed to flowing water. The experimental channel bed was composed of sand and was self-formed as most of the experimental runs commenced with a narrow straight central channel and flat bed cut into the middle of the area defined by the fixed width. However, repetitions for some of the widths and discharges used the previously formed morphology as a starting point in order to analyse the bed evolution pattern (Table 3.1).

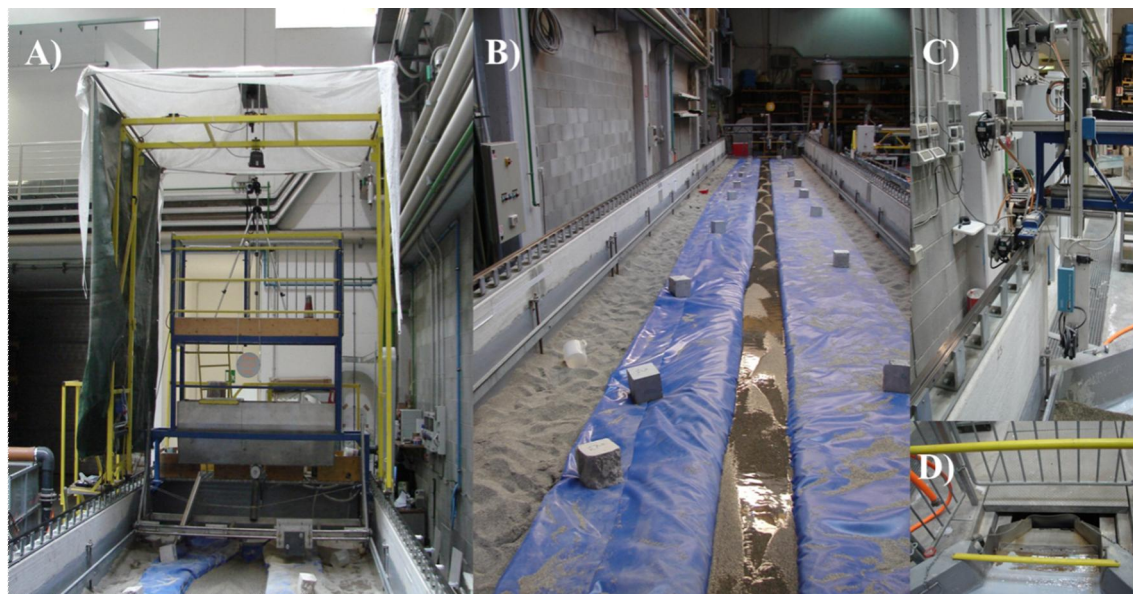


Figure 3.1 The flume used in the experiments. A) Volumetric sand feeder, parallel camera to the flume bed, carriage and lap top controller. B) Example of an experimental configuration showing the plastic cover used in all the runs, configured to a width of 0.30 m at “low flow”. C) Laser profiler, D) Chute and submerged sediment tank.

In order to design the duration of experimental runs, a time scale was calculated referring to the conservation of sediment mass equation (the Exner equation):

$$\frac{\partial \eta}{\partial t} = - \frac{1}{1-p} \frac{\partial q_s}{\partial x}$$

where η is bed elevation, p is sediment porosity, q_s is sediment flux per unit width, t is time and x is space. Performing a dimensional analysis on this equation, scaling η with flow depth D and x with channel width w , it is possible to quantify a temporal scale (T) of morphological evolution as:

$$T = \frac{D \cdot w}{Q_s/w}$$

As a result, T can be seen as the time needed to observe a bed change of the order of one depth on a longitudinal spatial scale of one channel width. At constant discharge, bed morphology is expected to reach a dynamic equilibrium in a few increments of T . Each experiment was run for a time of $8T$ to ensure a dynamic equilibrium between the sediment transport and sediment output from the channel and the bed morphology, and to collect the necessary data for the processing phase following completion of the experiments. Where second runs occurred, they were initiated on the preformed bed and were run for 40% of the original calculated time of ' T ' from Exner's equation (Table 3.1).

Table 3.1 Channel width, slope and discharge utilised in each experiment, the run time for the initial experiment ($8T$), and for any repetition runs (RT).

Run No.	Width (m)	Slope	Discharge (l/s)	Time (Min)	$8T$ (Hr)	RT (Min)
1		0.01	1.5	9.01	1.2	-
2	0.15	0.01	2.0	5.62	0.7	-
3		0.01	2.5	5.95	0.8	-
4		0.01	1.5	13.12	1.7	-
5	0.20	0.01	2.0	10.83	1.4	-
6		0.01	2.5	9.02	1.2	-
7		0.01	1.5	26.24	3.5	10
8	0.30	0.01	2.0	20.85	2.8	8
9		0.01	2.5	16.47	2.2	-
10		0.01	1.5	63.46	8.5	25
11	0.40	0.01	2.0	39.64	5.3	16
12		0.01	2.5	29.83	4.0	-
13		0.01	1.5	133.24	17.8	53
14	0.60	0.01	2.0	82.70	11.0	33
15		0.01	2.5	55.46	7.4	-
16		0.01	1.5	175.23	23.4	70
17	0.80	0.01	2.0	124.80	16.6	50
18		0.01	2.5	78.30	10.4	-
19		0.01	1.5	372.91	49.7	149
20	1.00	0.01	2.0	248.77	33.2	100
21		0.01	2.5	175.46	23.4	-
22		0.01	1.5	586.71	78.2	235
23	1.25	0.01	2.0	408.38	54.5	163
24		0.01	2.5	267.37	35.6	-
25		0.01	1.5	752.98	100.4	301
26	1.50	0.01	2.0	413.04	55.1	165
27		0.01	2.5	358.34	47.8	-

The flume's hydraulic system allowed a discharge range from 0.5 to 20 litres per second. Sand was fed into the upstream part of the channel from a volumetric sand feeder (Figure 3.1 A). At the downstream end of the flume (Figure 3.1 D), a chute conveyed the solid and liquid flux (i.e. transported sediment and water) to a submerged tank where the sediment transport (Q_s) was measured by sampling the cumulative weight every minute, allowing the same quantity of sediment to be fed into the upstream end of the channel. In this way, the sediment supply was adjusted to match the sediment transported out of the flume.

Following each experimental run, a digital elevation model (DEM) of the bed topography was obtained using a laser profiler (Figure 3.1 C). The profiler was supported on a bridge mounted on a rail positioned on the top of the concrete walls of the flume. Bed elevation was measured at 5mm intervals across the flume and at 5 cm intervals along the flume to capture the entire width of the experiment and a further 4 cm beyond each of the banks. This provided a detailed DEM describing the channel form from 5 m to 20 m along the length of the flume and thus excluding areas subject to entrance and outflow effects.

Once a dynamic equilibrium in sediment transport had been achieved in each experiment, the mean sediment transport rate (Q_s) for the experiment was calculated from the remaining sediment transport measurements. A dimensionless mean sediment transport rate (q_s) was then calculated using the following formula:

$$q_s = \frac{Q_s}{w \cdot \rho_s \cdot \sqrt{g \left(\frac{\rho_s - \rho_w}{\rho_w} \right) d_{50}^3}}$$

Where Q_s is the sediment transport, w is the flume width, g is gravitational acceleration, ρ_s is the sediment density, ρ_w is water density, and d_{50} is the median grain size.

Once the dynamic equilibrium of sediment transport had been achieved, the transporting, non-transporting, and dry areas in the cross-section (Figure 3.2) were mapped manually using a metric tape at 0.5 m intervals from 8 m to 18 m along the length of the flume. When the runs exceeded 15 h length, these measurements were obtained twice, and then averaged.

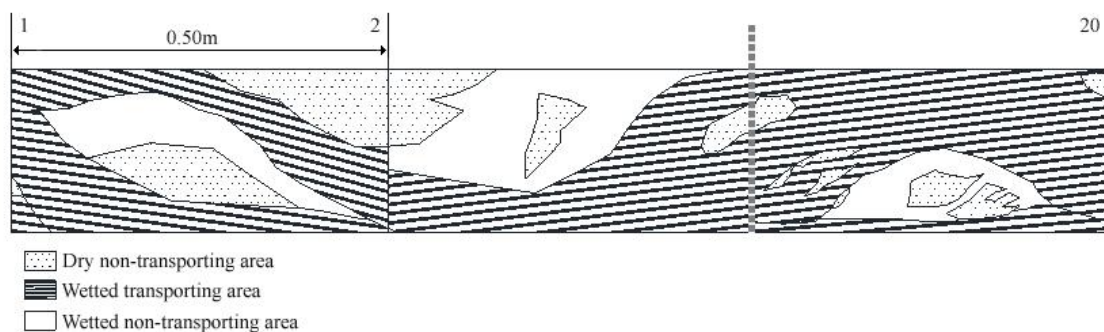


Figure 3.2 Transporting, non-transporting and dry areas of the flume bed. Measures of a) Dry, b) Wetted, and c) Active widths were obtained by measuring along 20 transects, spaced 0.50 m apart. These measurements were made (“by hand”) while running each experiment and also from the photographic record.

A ‘high flow’ photographic survey was carried out during each run when the full experimental discharge was flowing through the channel. The survey was conducted using a Nikon D3100 mounted on a hand-moveable carriage approximately 4 m above and parallel to the flume bed and was controlled through a lap top computer. In the minute following the cessation of each run, a second set of pictures were taken to represent ‘low flow’ (i.e. water was still present, mostly in scours and some deep channels).

3.2.2 Data Analysis

(i) Data preparation for DEM construction and description

In order to clean the “.txt” files produced by the laser, all the matrices were imported into Excel, and at least 8 cross sections were graphed including the first, middle and last cross sections in order to determine the bank locations. The columns containing the bank points were then removed and a second set of graphs were produced to check that all the bank points had been successfully removed. The file was then saved in a “.csv” format.

The statistical programme ‘R’ was used to analyse the cleaned matrices of 300 cross sections produced by the laser profiler for each of the runs. First, all values > 10.0 and < -10.0 were recoded as non-available (NA) since these values are used to indicate points that are outside the range of the profiler. Second, the matrix was de-trended by subtracting the mean elevation of each row (channel cross section) from each of the row

values, and then saved as a “.csv” file. Finally, the matrix was reorganized as a vector in order to compute the detrended elevation frequency distribution and calculate summary statistics describing its form (mean, median, standard deviation, upper and lower quartiles, skewness and kurtosis). The elevation frequency distribution was calculated using a bin size of 0.5, and percentage frequencies to allow visual comparison between experimental runs.

(ii) DEM construction

Each DEM was then processed for input to Arc GIS. Each of the rows of the original (i.e. including the banks and not de-trended) matrix was replicated 9 times using a Fortran programme to produce 3000 row ASCII files and thus the square cells required for analysis within a GIS. The ASCII files were imported and converted to raster using the Arc tool box in ArcGIS 10 with the values in a ‘float’ type to preserve the whole range of values. The slope of each map was calculated using the ‘focal statistics’ option to calculate the mean in a moving square window equivalent to the flume width of each run. The produced map was then subtracted from the original raster file in order to produce a de-trended map for each of the runs using the ‘raster calculator’. From the de-trended maps the banks and some parts close to the banks with missing information were clipped using the spatial analyst tool ‘extract by rectangle’. For the runs with a repetition, the slope was also calculated and subtracted from the runs, and then, using the georeferencing tool ‘add control points’, both rasters (of the repeated runs) were aligned using their banks as a reference. After this, using the raster calculator the repetition run was subtracted from the first run producing a raster map with the morphological changes, and then the banks were clipped off. This raster was exported as an ASCII using the conversion tools, and then imported into Excel and cleaned of the 999 values assigned by ARC GIS to the previously clipped columns.

A second ‘R’ code was written to analyse the matrices produced by the difference between the first run and its repetition. This code substitutes the values > 10.0 and < -10.0 for non-available (NA) and then organizes the cleaned de-trended matrix into a vector to calculate the elevation frequency distribution and the same descriptive statistics that were estimated for each of the individual runs.

Following the above data processing, a colour scheme was selected to display the de-trended channel maps from all of the experimental runs in a way that highlighted the

distribution of bars and channels. From these colour images, it was possible to separate runs that generated one of two different channel styles: a) predominantly single thread channels with alternate side bars, and b) predominantly multi-thread channels showing mid-channel bar development.

(iii) Estimation of dimensionless stream power

The photographic surveys of each of the experiments provided a total of 16 individual pictures for both the “high flow” and “low flow” surveys of each experimental run. These pictures were resized individually using the program ‘Image Converter’ and then stitched together using ‘Photo Stitch 3.1’. The “high flow” pictures were imported into ArcGIS 10 and georectified to fit each of the DEM’s using the banks as reference. A minimum of 8 control points were identified along the banks in each photograph for use in georectification.

Following georectification, a total of 20 cross sections spaced at 0.5 m intervals and commencing 5 metres from the upstream end of each DEM were inspected to measure dry and wetted areas within each cross section (Figure 3.2). It was not possible to measure areas transporting sediment due to the reflection of the water surface in the pictures.

The wet and dry areas were summed for each cross section and then averaged by run in order to compare with the surveys carried out by hand during each of the experiments (Figure 3.3). In this way the hand surveys were validated, giving confidence in the use of the hand measurements of the transporting areas to replace the measurements that could not be extracted from the photographs.

Different estimates of dimensionless stream power (ω) were then calculated for each of the averaged widths, namely: a) “Flume width”, the original configuration width selected for each run. b) “Wetted width”, the averaged submerged width at ‘high flow’, and c) “Active width”, the averaged transporting width in the channel at ‘high flow’. This was accomplished by using the following formula:

$$\omega = \frac{Q \cdot S}{w \cdot \sqrt{g \left(\frac{\rho_s - \rho_w}{\rho_w} \right) d_{50}^3}}$$

Where Q is the water discharge, w is the width (flume width, wetted width or active width), g is gravity, ρ_s is the sediment density, ρ_w is the water density, and d_{50} is the median grain size.

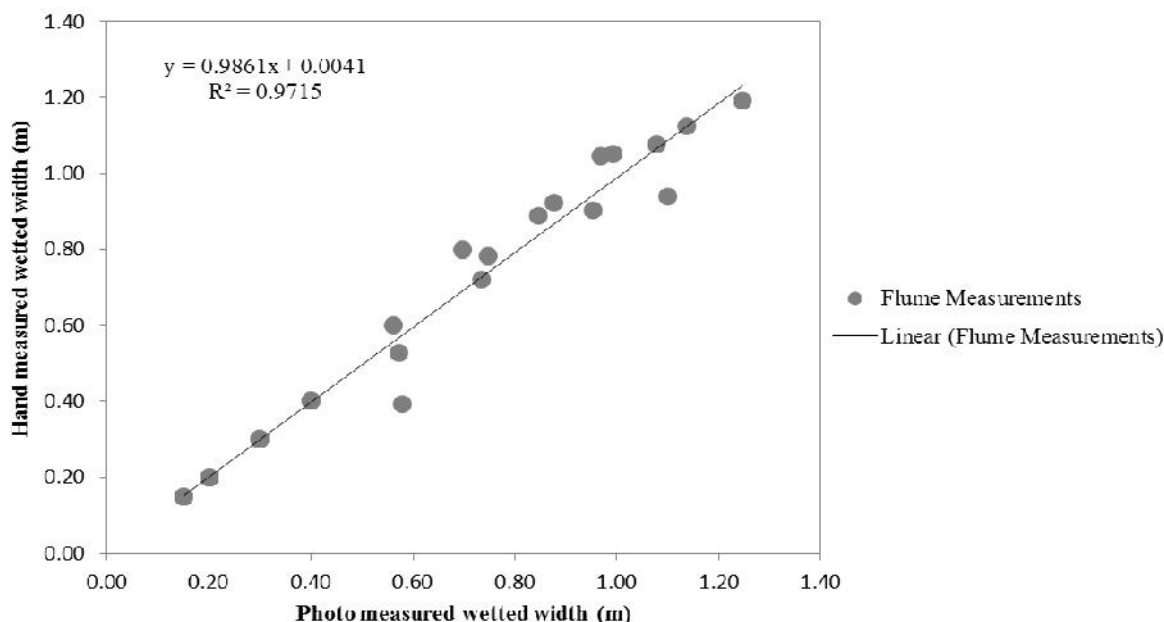


Figure 3.3 Relationship between wetted widths (in m) measured from photographs (horizontal axis) and by hand (vertical axis).

3.3 RESULTS.

3.3.1 Descriptive Statistics

Table 3.2 presents summary statistics describing the boundary conditions and process-form responses associated with all of the experimental runs. The Table is organised vertically to show the 27 runs with the three discharges nested within the nine flume widths. This section describes the broad trends observable from Table 3.2 in the order followed by the columns of the Table, but excluding the last three columns, which are described in detail in section 3.3.2.

At small channel widths, no differences are observed between the flume, wetted and active widths, with water actively moving sediment across the complete flume width at all experimental discharges. However, as the flume width increases, the wetted and active widths do not continue to occupy the entire flume width and the ratio between the active and the wetted width follows a decreasing trend with increasing channel width for each of the three experimental discharges (Figure 3.4). However, there are some

small deviations from this decreasing trend in the active to wetted width ratio at channel widths greater than 0.8 m.

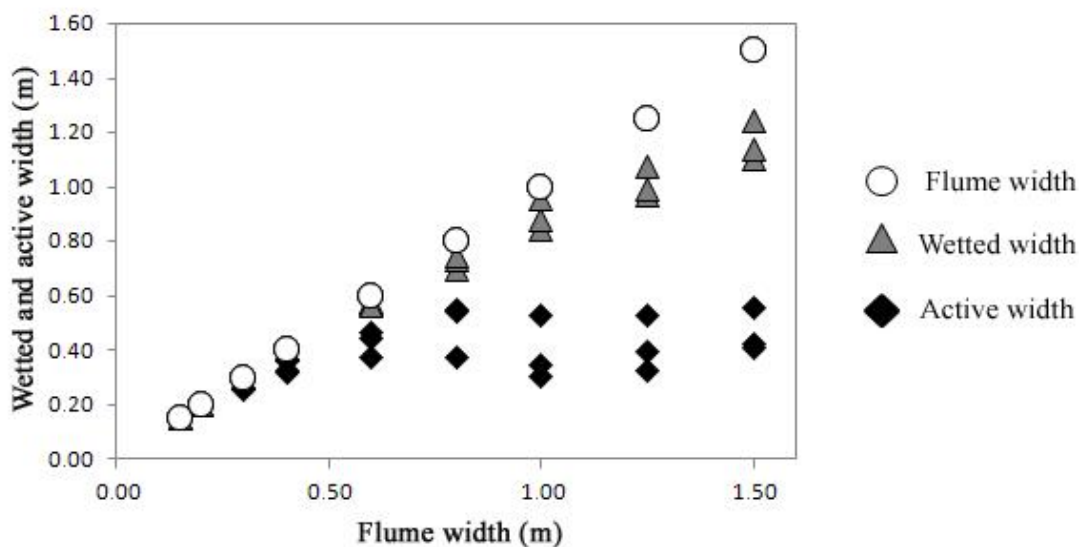


Figure 3.4 Wetted and active channel widths observed at different flume widths (the three discharges are shown for each width using the same symbol).

When discharge is converted to stream power and rendered dimensionless (ω) with respect to the three different widths (flume, wetted and active widths), as would be expected, the three estimates of ω show increasing values from channel through wetted to active width for each discharge and flume width combination (Figure 3.5). Each of the three estimates of ω also shows a decrease as the channel width increases (Figure 3.5), although there are slight deviations from this trend, notably in relation to ω estimates for active channel widths greater than 0.8 m (Figure 3.5).

Table 3.2 Summary information on wetted, dry and active channel widths and related stream power, sediment transport rate and bed elevation frequency distribution of the 27 experimental runs.

Run No.	Run length (hr)	Discharge Q (l/s)	Flume width (m)	Mean wetted width (m)	Mean dry width (m)	Mean active width (m)	Ratio Active/wetted width	ω (Flume width)	ω (Wetted width)	ω (Active width)	Mean sediment transport rate Qs (g/s)	Dimensionless sediment transport (qs)	Bed Elevation			
													Median (cms)	St. Dev. (cms)	Kurtosis	Skewness
1	1.2	1.5	0.15	0.15	0.00	0.15	1.0	0.731	0.731	0.731	3.552	0.065	0.005	0.164	0.434	-0.210
2	0.7	2.0	0.15	0.15	0.00	0.15	1.0	0.974	0.974	0.974	6.88	0.126	-0.002	0.136	0.575	-0.084
3	0.8	2.5	0.15	0.15	0.00	0.15	1.0	1.218	1.218	1.218	7.52	0.138	-0.008	0.143	0.410	0.128
4	1.7	1.5	0.20	0.20	0.00	0.20	1.0	0.548	0.548	0.548	3.536	0.049	0.036	0.260	1.010	-0.747
5	1.4	2.0	0.20	0.20	0.00	0.20	1.0	0.731	0.731	0.731	5.152	0.071	0.006	0.185	-0.043	-0.204
6	1.2	2.5	0.20	0.20	0.00	0.20	1.0	0.913	0.913	0.913	7.104	0.098	0.006	0.199	0.148	-0.219
7	3.5	1.5	0.30	0.30	0.00	0.30	1.0	0.365	0.365	0.365	3.056	0.028	0.122	0.559	1.735	-1.162
8	2.8	2.0	0.30	0.30	0.00	0.30	1.0	0.487	0.487	0.487	4.56	0.042	0.087	0.431	3.263	-1.468
9	2.2	2.5	0.30	0.30	0.00	0.254	0.845	0.609	0.609	0.720	6.64	0.061	0.039	0.305	1.455	-0.908
10	8.5	1.5	0.40	0.40	0.00	0.317	0.793	0.274	0.274	0.346	1.872	0.013	0.146	0.595	2.606	-1.446
11	5.3	2.0	0.40	0.40	0.00	0.360	0.899	0.365	0.365	0.406	3.568	0.025	0.174	0.693	0.826	-1.051
12	4	2.5	0.40	0.40	0.00	0.329	0.823	0.457	0.457	0.555	5.408	0.037	0.169	0.648	2.484	-1.450
13	17.8	1.5	0.60	0.57	0.03	0.445	0.777	0.183	0.191	0.246	1.568	0.007	0.123	0.613	1.616	-1.103
14	11	2.0	0.60	0.58	0.02	0.469	0.809	0.244	0.252	0.312	2.992	0.014	0.194	0.744	1.763	-1.285
15	7.4	2.5	0.60	0.56	0.04	0.378	0.674	0.304	0.326	0.483	5.088	0.023	0.134	0.751	1.883	-1.211
16	23.4	1.5	0.80	0.70	0.10	0.374	0.535	0.137	0.157	0.293	1.792	0.006	0.108	0.618	1.184	-0.962
17	16.6	2.0	0.80	0.74	0.07	0.551	0.750	0.183	0.199	0.265	2.976	0.01	0.142	0.711	1.393	-1.032
18	10.4	2.5	0.80	0.75	0.05	0.542	0.725	0.228	0.244	0.337	5.392	0.019	0.199	0.787	3.084	-1.460
19	49.7	1.5	1.00	0.85	0.15	0.305	0.360	0.110	0.129	0.360	1.158	0.003	0.124	0.599	2.900	-1.296
20	33.2	2.0	1.00	0.88	0.12	0.344	0.392	0.146	0.167	0.425	2.042	0.006	0.184	0.701	1.305	-1.137
21	23.4	2.5	1.00	0.95	0.05	0.530	0.555	0.183	0.191	0.345	3.298	0.009	0.132	0.691	0.902	-0.940
22	78.2	1.5	1.25	0.97	0.28	0.327	0.337	0.088	0.113	0.335	1.008	0.002	0.113	0.628	1.072	-0.921
23	54.5	2.0	1.25	0.99	0.26	0.399	0.402	0.117	0.147	0.366	1.706	0.004	0.132	0.691	0.902	-0.940
24	35.6	2.5	1.25	1.08	0.17	0.531	0.493	0.146	0.169	0.344	2.968	0.007	0.160	0.775	2.387	-1.224
25	100.4	1.5	1.50	1.10	0.40	0.420	0.382	0.073	0.100	0.261	1.018	0.002	0.106	0.555	2.568	-1.172
26	55.1	2.0	1.50	1.14	0.36	0.411	0.361	0.097	0.129	0.356	2.184	0.004	0.118	0.629	1.295	-1.019
27	47.8	2.5	1.50	1.25	0.25	0.554	0.444	0.122	0.147	0.330	2.864	0.005	0.147	0.703	2.149	-1.241

* Flume width is equal to the complete width measured inside the plastic cover.

** Mean wetted width is equal to the average of all the water submerged areas in the cross section.

***Mean dry width is equal to the average area of all the areas exposed above the water level in the cross section.

****Mean active width is equal to the average area in the cross section that is submerged and transporting sediment.

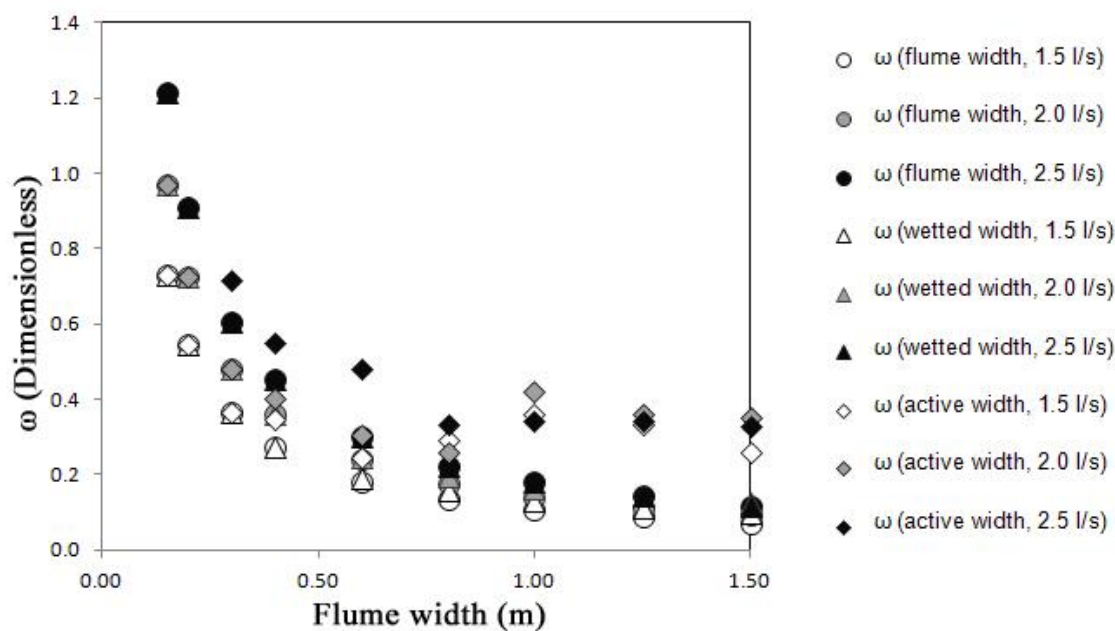


Figure 3.5 Relationship between ω (calculated for flume, wetted and active width for three formative discharges) and flume width.

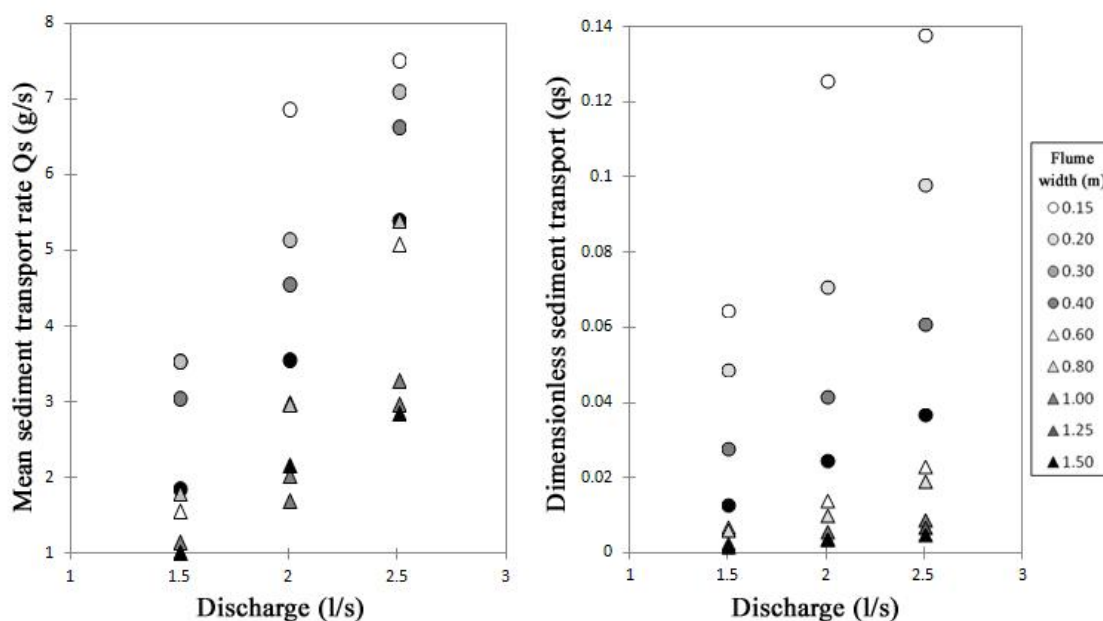


Figure 3.6 Mean sediment transport rate (left) and dimensionless sediment transport rate (right) in relation to discharge across all flume widths (key).

The sediment transport rate (Q_s in g/s) and the dimensionless sediment transport rate (q_s) both appear to vary according to both the flume width and the discharge that is transporting the sediment (Figure 3.6). In general, larger amounts of sediment are transported by higher discharges within the same flume width and less sediment is

transported in wider channels by the same discharge. Thus, Q_s and q_s appear to vary according to the combination of discharge and width.

3.3.2 Digital Elevation Models

Figures 3.7 to 3.9 illustrate the DEMs produced by each of the experimental runs associated with $Q=1.5$ l/s, $Q=2.0$ l/s, $Q=2.5$ l/s, respectively. In each Figure the colour scales from dark orange in the highest elevation areas to pale yellow in the lowest areas, the extreme elevation values, and the median elevation for each run are shown on the scale associated with each DEM.

For $Q=1.5$ l/s (Figure 3.7), the elevation range of the DTM generally increases with increasing channel width, although the ranges at 0.6 m and 1.25 m show slightly lower values than adjacent channel widths. A regular and symmetrical distribution of alternate bars can be observed up to a 0.30 m channel width. At 0.40 m width, the alternate bars remain regular but they elongate and start to exhibit a longitudinally asymmetrical shape and higher surface elevation. At 0.6 m width, mid-channel bars start to appear in addition to alternate bars. Above 0.6 m width, channel complexity increases. In general, a main channel can be observed in these wider channels following a sinuous course with an increasing wavelength accompanying increases in width. The number of smaller channels and chutes also increase so that highly complex braided forms emerge at 1.25 and 1.5 m widths.

For $Q=2$ l/s (Figure 3.8), the elevation range is greater than for the $Q=1.5$ l/s runs for the 0.15 and 0.2 m widths. Thereafter, the ranges tend to be smaller than were observed for $Q=1.5$ l/s. A regular and symmetrical distribution of alternate bars can be observed up to a 0.40 m channel width, with bar length progressively increasing as channel width increases. At 0.60 m width, mid-channel bars started to appear, but they only become clear at 0.80 m width. Larger channel widths show increasingly complex multi-channel forms. At 1.0 and 1.5 m widths, the main channel exhibits a sinuous course but this is less marked than was observed in the channels formed by $Q=1.5$ l/s (Figure 3.7). In addition, the contrast between main and secondary channels is less noticeable than in Figure 3.6, so that several sinuous threads appear to overlay one another.

For $Q=2.5$ l/s (Figure 3.9), the elevation ranges are similar to those for $Q=2$ l/s for narrow channel widths (e.g. 0.15 and 0.2 m), but thereafter they tend to be larger with

some exceptions (e.g. 0.6 m). Well-defined, evenly-spaced alternate bars are observed up to 0.4 m width, with bar lengths increasing and bars taking an increasingly asymmetrical plan shape as width increases. At 0.60 m width the bars start to lose their regular shape and to develop a form more akin to mid-channel bars. For channels of 0.80 m width and wider, mid-channel bars and a multi-thread planform are apparent, and the main channel adopts a sinuous planform of increasing wavelength with increasing channel width. As was observed for $Q=2.0$ l/s, the secondary channels and chutes also display sinuous planforms that show different amplitudes and wavelengths from the main channel.

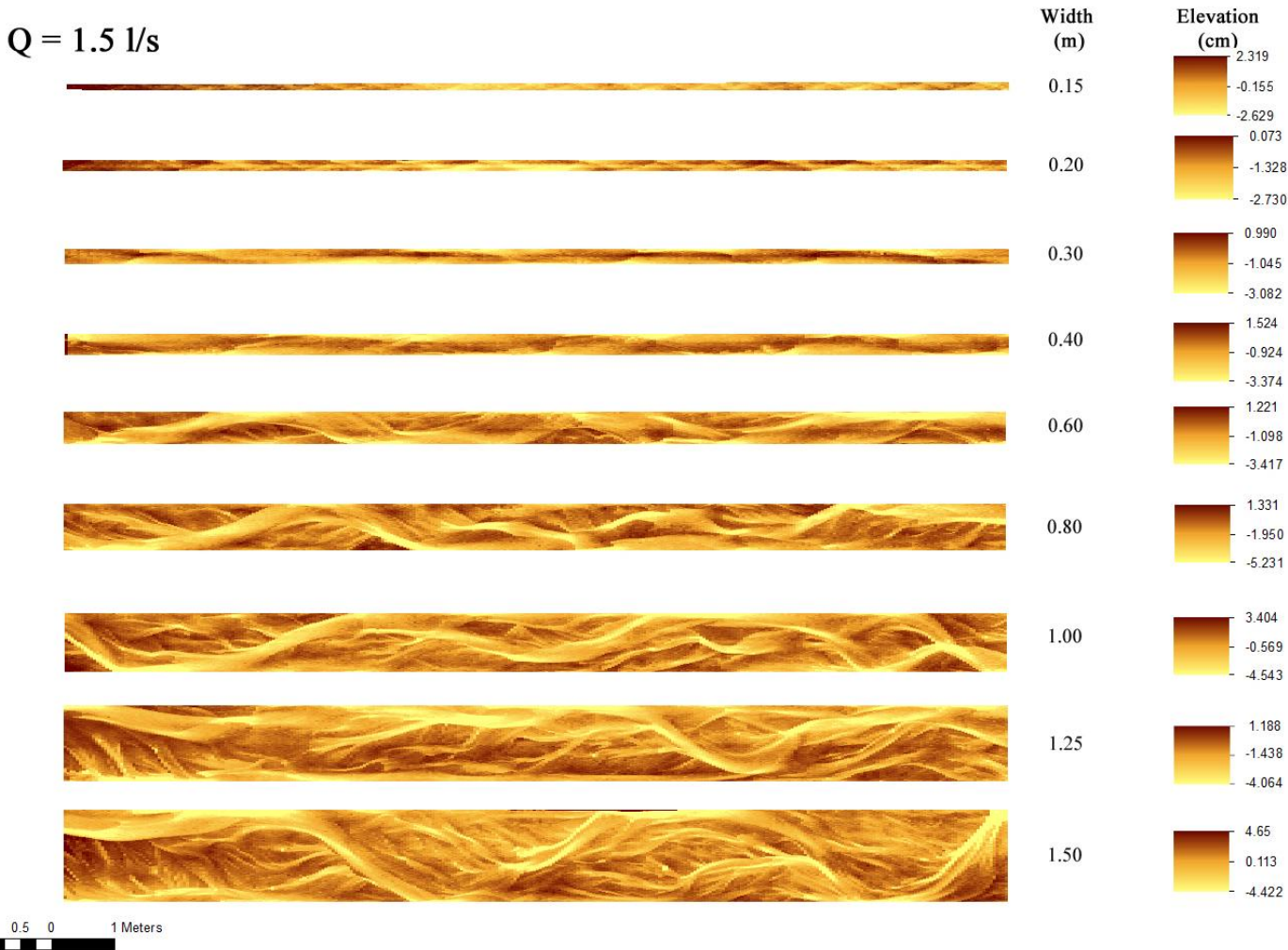


Figure 3.7 DTMs produced by a discharge of 1.5 l/s applied to different flume widths.

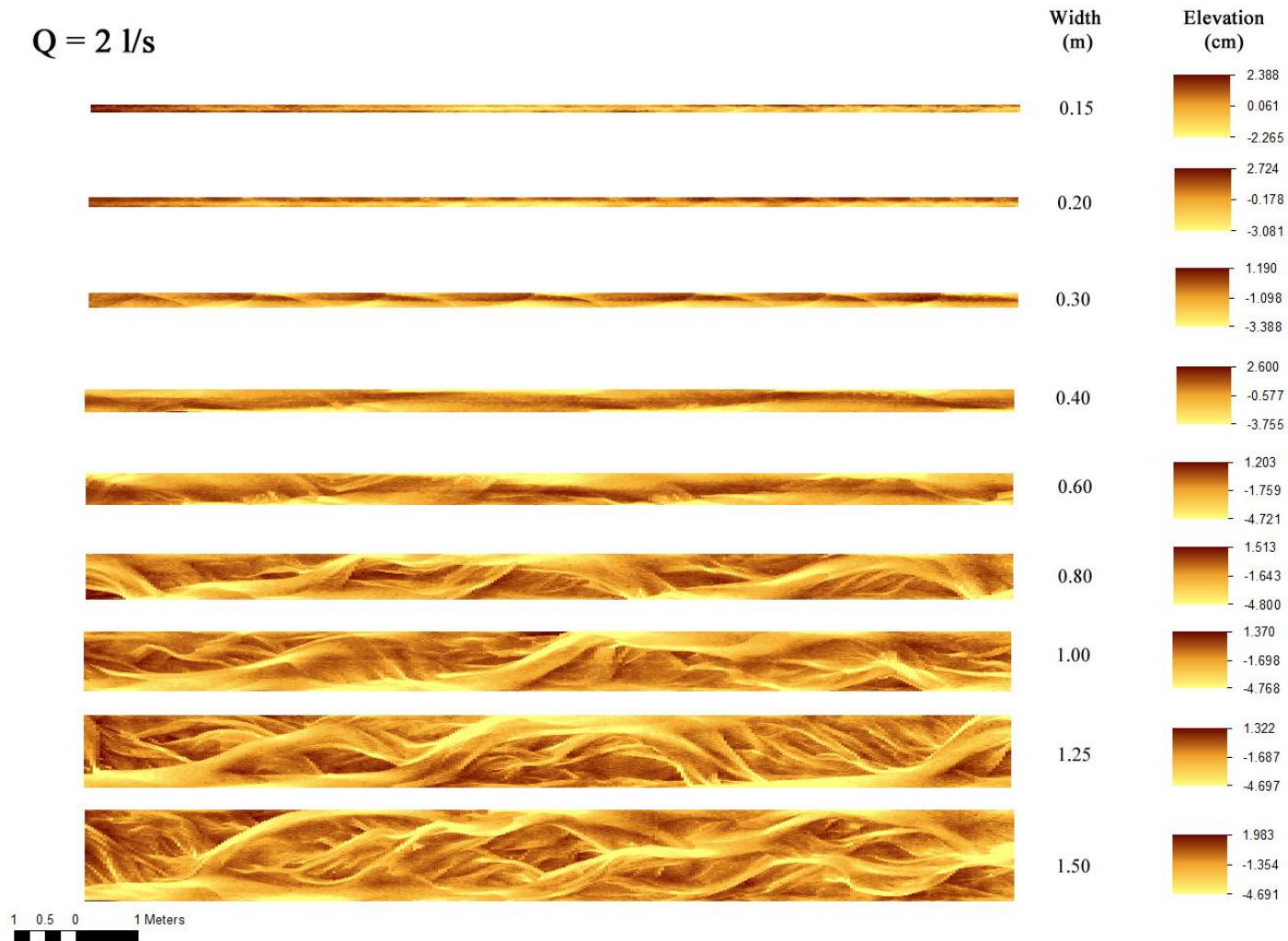


Figure 3.8 DTMs produced by a discharge of 2.0 l/s applied to different flume widths.

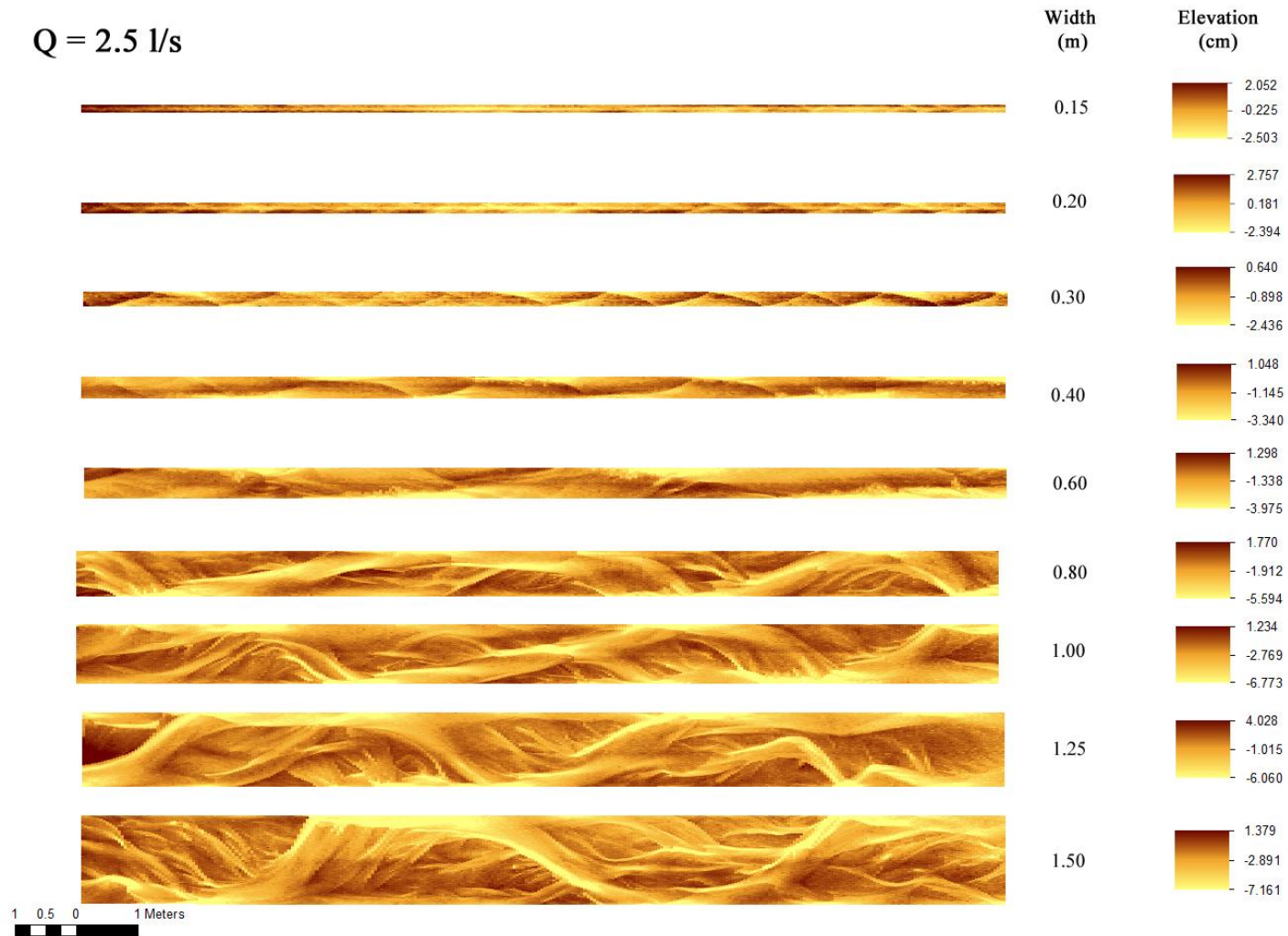


Figure 3.9 DTMs produced by a discharge of 2.5 l/s applied to different flume widths.

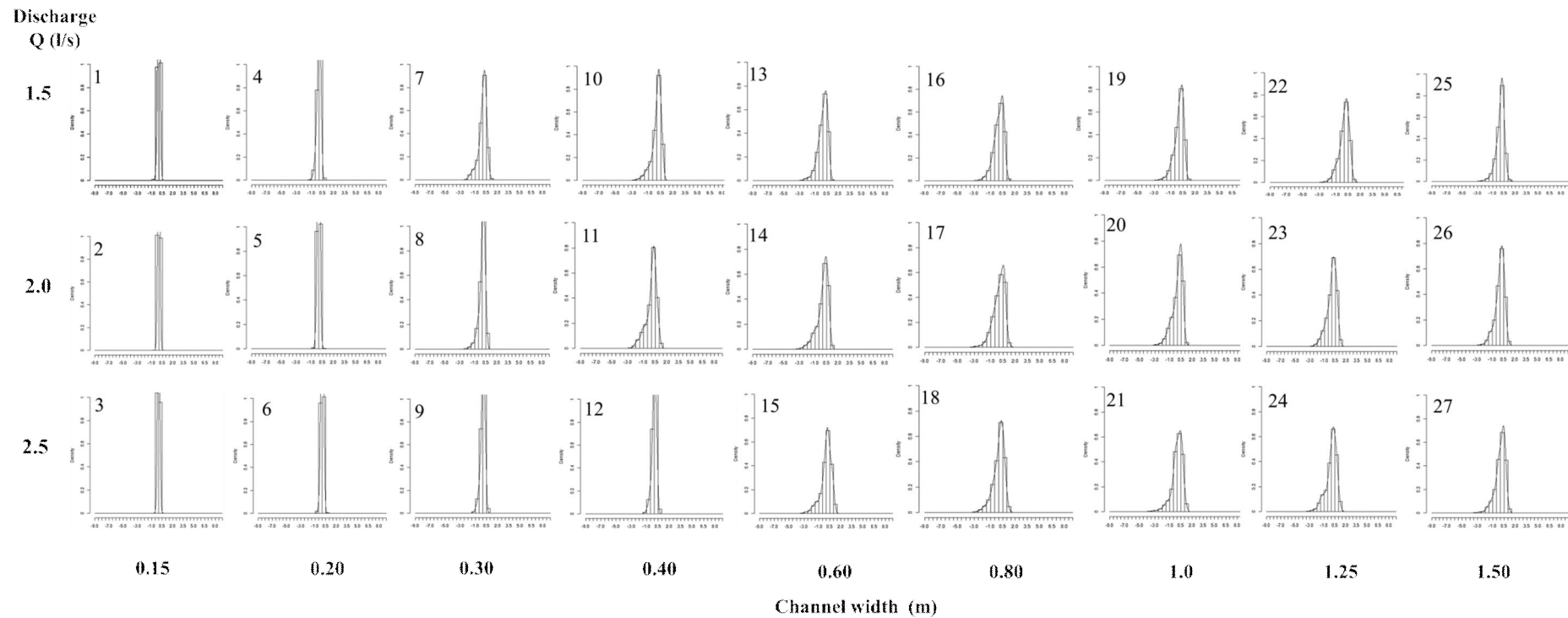


Figure 3.10 Bed elevation frequency distributions generated by different combinations of discharge (vertical) and channel width (horizontal). Each frequency distribution is labelled by run number (1 to 27) and employs an equal bin size of 0.5 on the horizontal axis with values ranging from -9 to +9. The vertical axis expresses density with a minimum value of 0 and a maximum of 1 for all of the runs.

3.3.3 Elevation Frequency Distributions

The bed elevations from these 27 DEMs can be expressed as elevation frequency distributions (Figure 3.10) from which descriptive statistics can be extracted, such as the mean, median, standard deviation, skewness and kurtosis. In the present case, because the DEMs were detrended, the mean was close to zero in all cases. However, the remaining four descriptive statistics provide useful information about the form of the bed. Comparison of median values with zero (the mean), provides an initial assessment of whether the frequency distribution has more observations greater than or less than the average elevation of the bed. The standard deviation describes how variable the bed elevation is, with small standard deviations indicative of subdued bed topography with little variation in the bed elevation, whereas a high standard deviation indicates that the elevation of the bed varies a lot. Kurtosis describes the peakedness of the distribution and so gives similar information to the standard deviation: high (positive) kurtosis indicates that many of the elevation values are similar, although there may be extreme values in the distribution tails. This suggesting a river bed with a subdued topography; low (negative) kurtosis indicates a flatter frequency distribution, suggesting an irregular river bed with much greater variability in its elevation and evenness in the frequency of different elevation values. Lastly skewness indicates the degree to which the frequency distribution is asymmetrical, with values close to 0 indicating a symmetrical distribution with balanced areas of the bed that are higher (e.g. bar tops) or lower than the average; positive skewness represents a river with relatively restricted high areas (bar tops) and extensive low areas; negative skewness represents a river with extensive high areas (bar tops) separated by relatively restricted intervening low areas. Figure 3.11 illustrates how different river beds might appear according to their skewness and kurtosis.

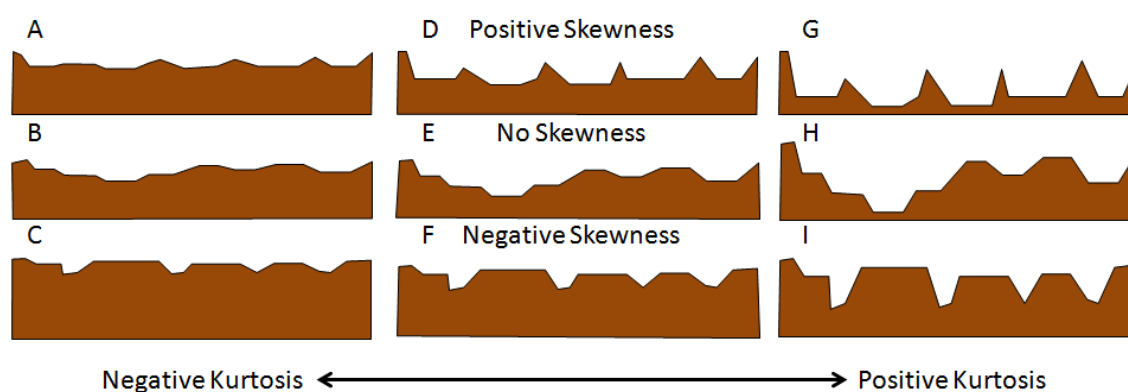


Figure 3.11 Conceptual sketches of the impact of different bed elevation kurtosis and skewness on the appearance of the cross profile of a braided river.

The observed frequency distributions (Figure 3.10) show broad trends of increasing width and skewness, and decreasing peakedness with increasing channel width, and the changes appear to occur most rapidly at lower discharges. The bed elevation frequency distribution is summarised by four descriptive statistics in Table 3.2: the median (describing central tendency of the frequency distribution), standard deviation (describing variability in the observations and thus the width of the distribution), kurtosis (describing the peakedness of the distribution), and skewness (describing the asymmetry of the distribution).

The medians of the bed elevation distributions show an increasing trend with flume width and also with discharge up to around 0.4 m width (Figure 3.12A). For widths of 0.6 m and above, there is a slightly declining trend in the median values as flume width increases, with lower values generally related to decreasing discharge, although there is considerable variability around these trends.

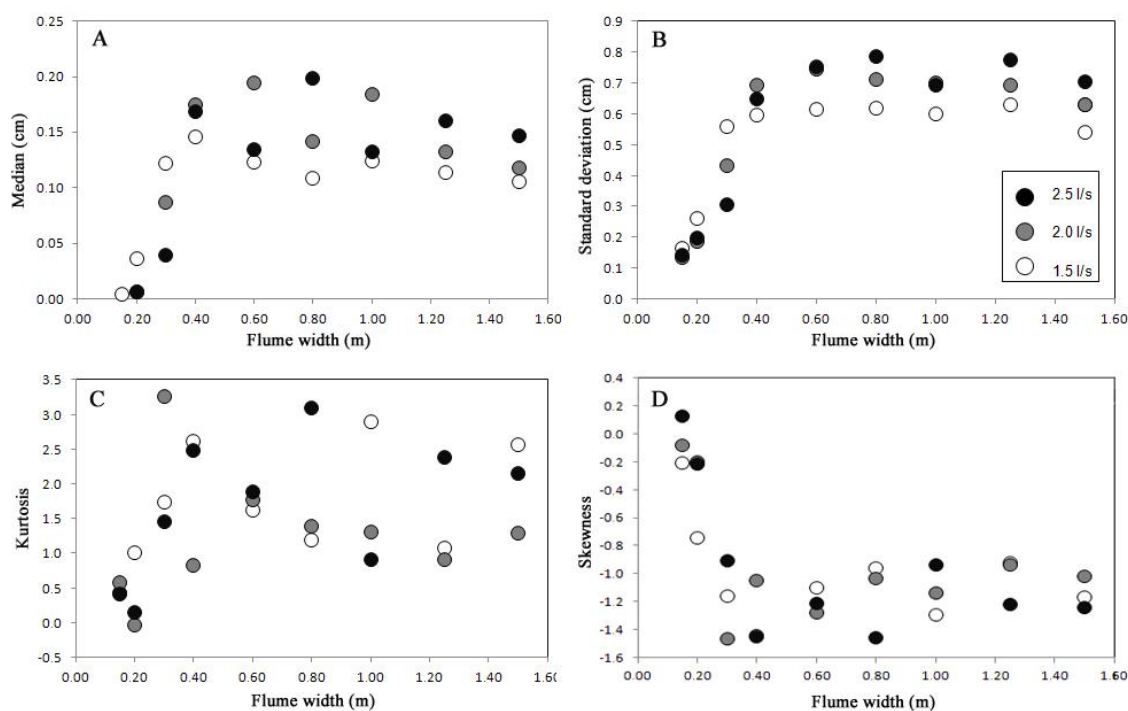


Figure 3.12 Variations in the A. median; B. standard deviation; C. kurtosis; D. skewness of the bed elevation with flume width and formative discharge.

For all three discharges, the standard deviation of the bed elevation frequency distributions (Figure 3.12B) shows a generally increasing trend with increasing flume width to a width of 0.80 m but there is no consistent trend in standard deviation with discharge for the same width. For channel widths above 0.8 m, the standard deviation

increases with discharge for the same flume width but there is no distinct change in standard deviation with increasing flume width.

Kurtosis values for the bed elevation frequency distributions (Figure 3.12C) vary widely with flume width and discharge, but they are generally positive in value, with a broad increase for flume widths of up to 0.6 m and then kurtosis declines with increasing flume width.

Skewness of the bed elevation frequency distributions (Figure 3.12D) decreases from positive to negative values with increasing channel width up to a width of 0.6 m and then remains at similar low negative values but with considerable variation between discharges for larger flume widths.

3.3.4 Associations Among Processes and Channel Size and Form

(i) *Dynamic Equilibrium in sediment transport*

In each experimental run, sediment was supplied to the flume to match the amount of sediment being transported through the given flume width by the discharge.

As previously observed from Table 3.2, the mean sediment transport rate (Q_s) and its dimensionless form (q_s) decline as flume width, wetted width and active width increase. For example, Figure 3.13 shows the relationships between Q_s and q_s and the wetted channel width. The symbols indicate widths where no mid-channel bars are present by circles and those that support mid-channel bars by triangles with darker colours indicating wider widths.

Sediment transport also varies with stream power (Figure 3.14). Q_s increases with ω across all flume widths (Figure 3.14A). When Q_s is plotted in its dimensionless form (q_s), the data tightly follow a slightly curved relationship (Figure 3.14B). This confirms that the experiments were run for long enough to reach a dynamic equilibrium in sediment transport rate that was adjusted to the discharge and channel width, and thus provides confidence that the morphological results are representative of a dynamic equilibrium condition defined by Q , Q_s and flume width.

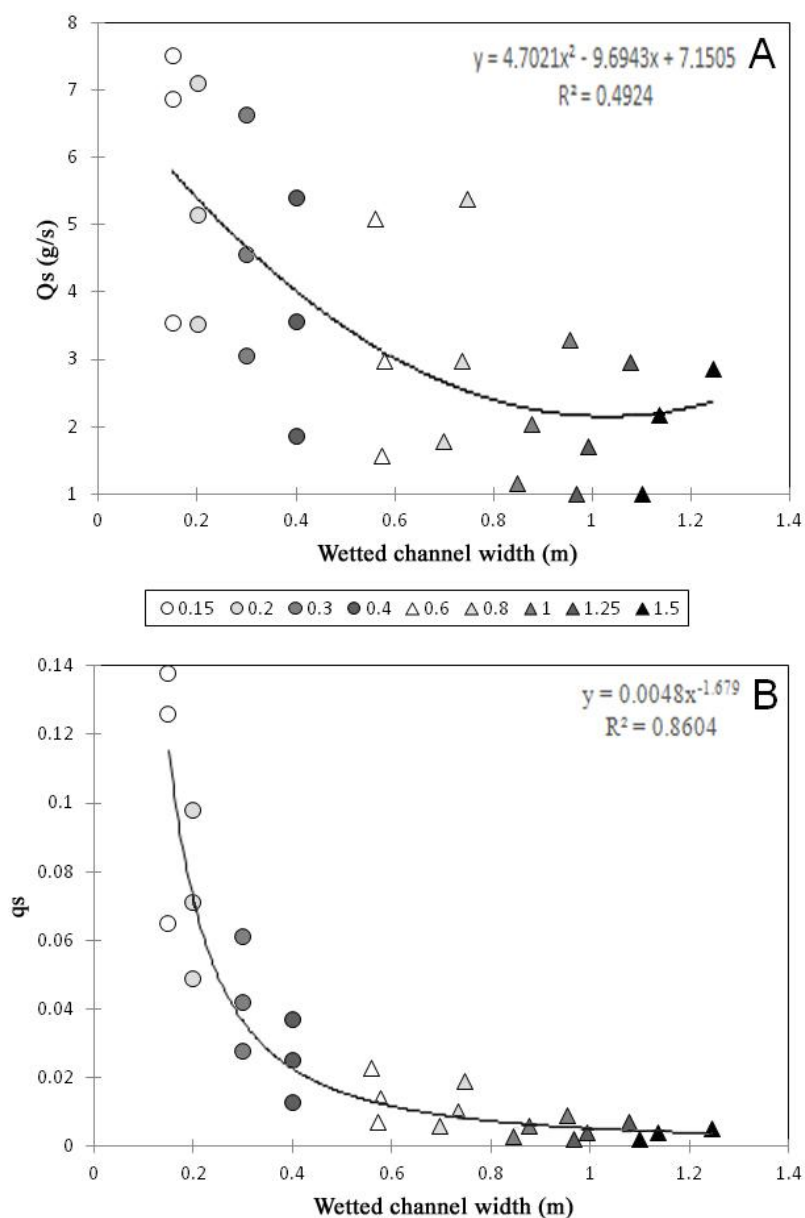


Figure 3.13 Scatter plots with indicative regression trend lines illustrating a decline in **A.** mean sediment transport rate (Q_s in g/s) and **B.** dimensionless sediment transport rate (q_s) with increasing wetted channel width. The different symbols indicate the presence (triangular markers) or absence (circular markers) of mid-channel bars, and the colours indicate different flume widths.

(ii) Wetted and active widths

Observations of the wetted and active width of each experiment provides information on the proportion of the width of flowing water (i.e. the wetted width) that is actively moving sediment (i.e. the active width) and is, therefore, actively eroding, transporting and depositing sediment to modify the channel morphology.

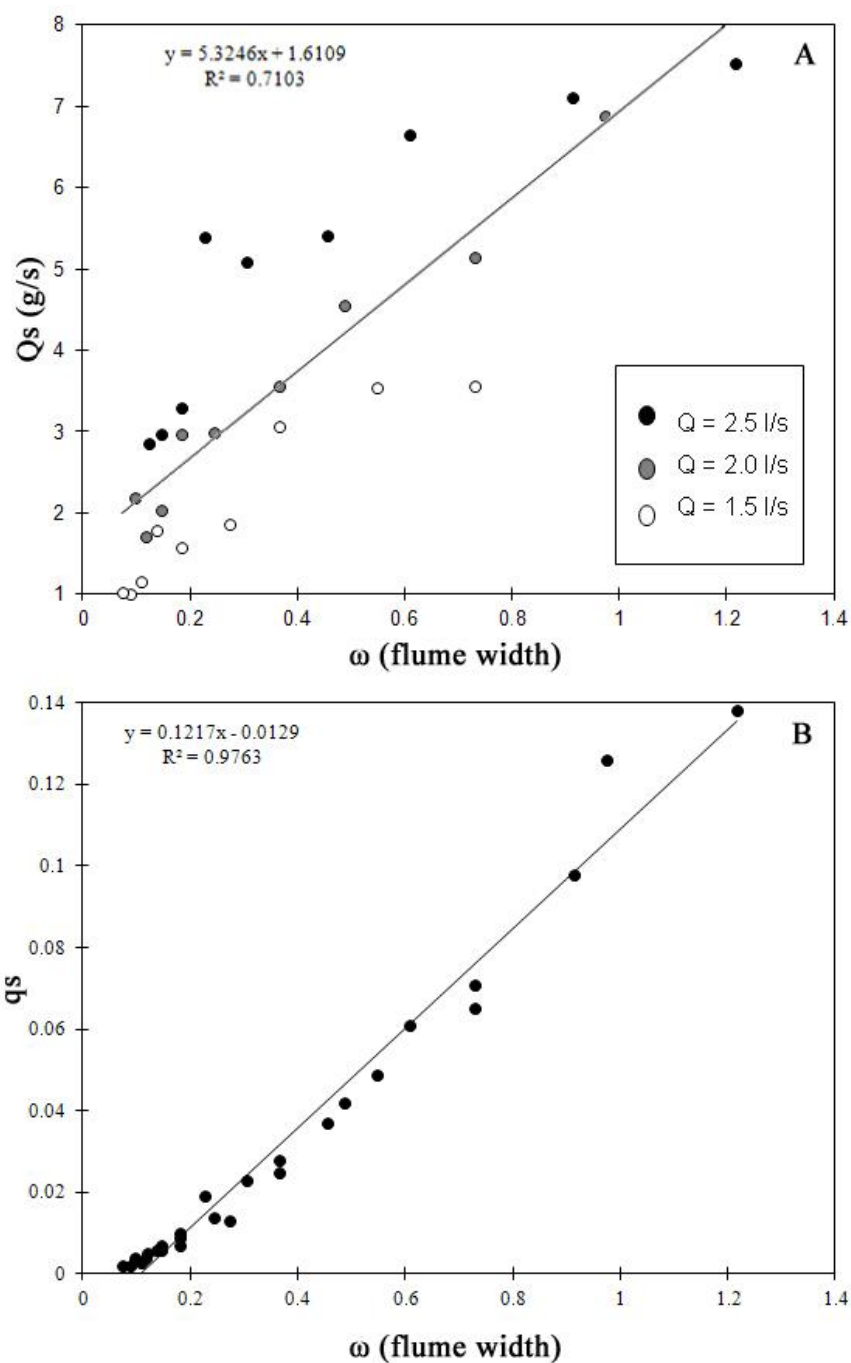


Figure 3.14 Scatter plots with indicative trend lines illustrating relationships between ω (flume width) and A. mean sediment transport rate (Q_s in g/s) and B. dimensionless sediment transport rate (q_s) defined across the 27 experimental runs.

Figure 3.15A illustrates that there is a curved relationship between the ratio of the active and wetted width and stream power, which is associated with changes in the flume width. At small channel widths (0.15 and 0.20m) stream power remains high for all experimental runs and the ratio of active to wetted channel width is equal to 1.0, with the entire width of flowing water involved in moving sediment.

As the channel width increases to 0.3 and 0.4 m, stream power decreases and there is a variable response between runs in the ratio of active to wetted width and thus the proportion of the wetted channel that is actively transporting sediment. In some runs the ratio is 1.0, indicating that the entire width is transporting sediments, but in some runs the ratio is lower, falling in a range between ca. 0.8 and 1.0. However, there is no consistent response to changes in stream power for runs with the same flume width. Once the channel exceeds 0.4 m width, the ratio of active to wetted width falls rapidly with increasing flume width, illustrating a distinct and progressive decrease in the proportion of the active channel transporting sediment.

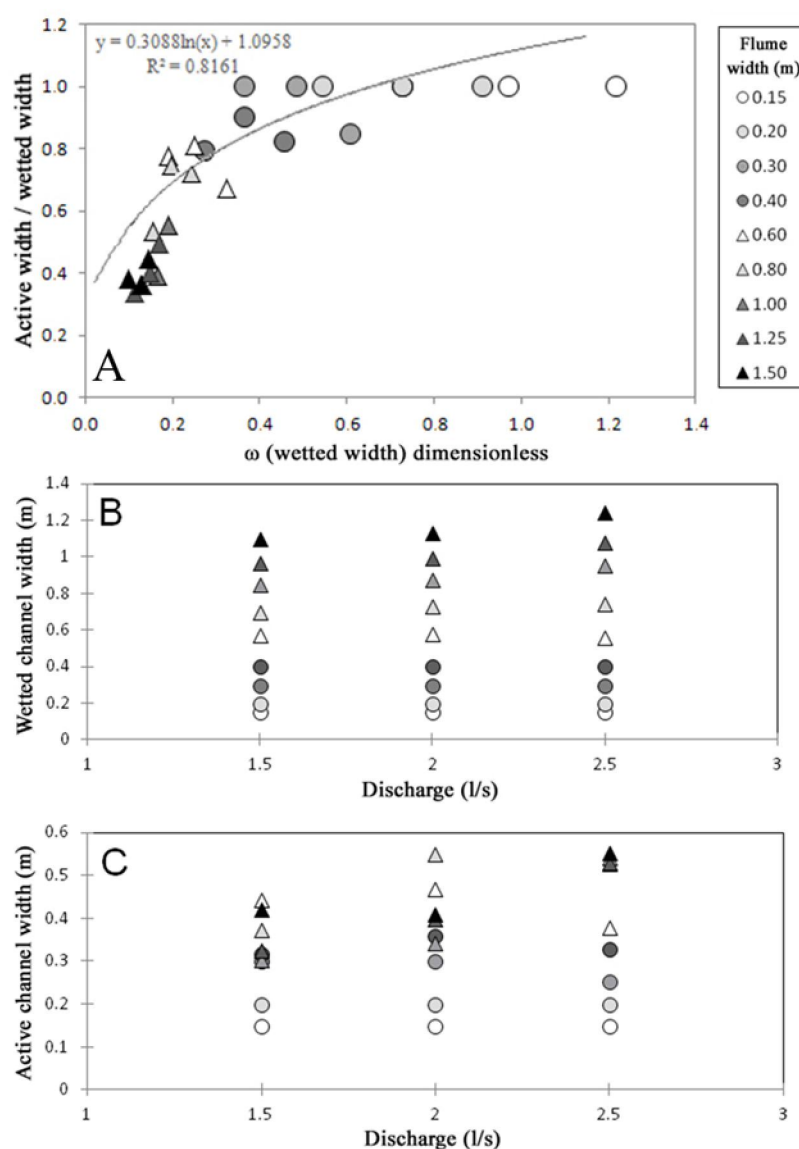


Figure 3.15 Scatter plots illustrating A) Changes in the ratio of active to wetted width as flume width with increasing ω (with trend line). B) Changes in wetted channel width with increasing discharge. C) Changes in active channel width with increasing discharge.

Figures 3.15 B and C illustrate how the wetted and active channel width change as discharge increases. At low flume widths (≤ 0.4 m), the wetted width occupies the entire flume width; at high flume widths (≥ 1.0 m) it is smaller than the flume width and shows a distinct increase with discharge; and at intermediate flume widths (0.6 and 0.8 m) the wetted width is very close to the flume width and shows no clear trend with discharge (Figure 3.15B). At very low flume widths (≤ 0.2 m), the active width occupies the entire flume width; at high flume widths (≥ 1.0 m) the active width is considerably smaller than the wetted width and shows a very distinct increase with discharge; and at intermediate flume widths (0.4 to 0.8 m) the active width is distinctly narrower than the wetted width but shows no clear trend with increasing discharge (Figure 3.15C).

(iii) Changes in channel form in response to changes in stream power and flume width

Figure 3.16 presents scatter plots illustrating how channel morphology changes across the experimental runs. The three rows of graphs represent the three measures of dimensionless stream power (flume, wetted and active channel width) and show similar patterns for each of the four properties of the channel morphology (median, standard deviation, kurtosis, skewness) but with a change in the absolute values of power as a result of the different widths used to render stream power dimensionless. However, the graphs displaying dimensionless stream power calculated from the active width show a tighter clustering of points for the highest channel widths than those displaying stream power calculated from the flume and wetted widths.

The median elevation is relatively large and similar for all runs with a flume width greater than 0.3 m, indicating that the median is consistently larger than the mean (which has been constrained to be 0.0 cm by the method of DEM analysis that was adopted). However, the median reduces and converges on zero as the flume width becomes narrower and as ω increases for any particular flume width. A similar pattern is seen in the scatter plots of standard deviation of the elevation frequency distribution, with the standard deviation showing clustered high values for flume widths greater than 0.30 m and a sequence of smaller values that decrease with reducing flume width and increasing stream power for each flume width.

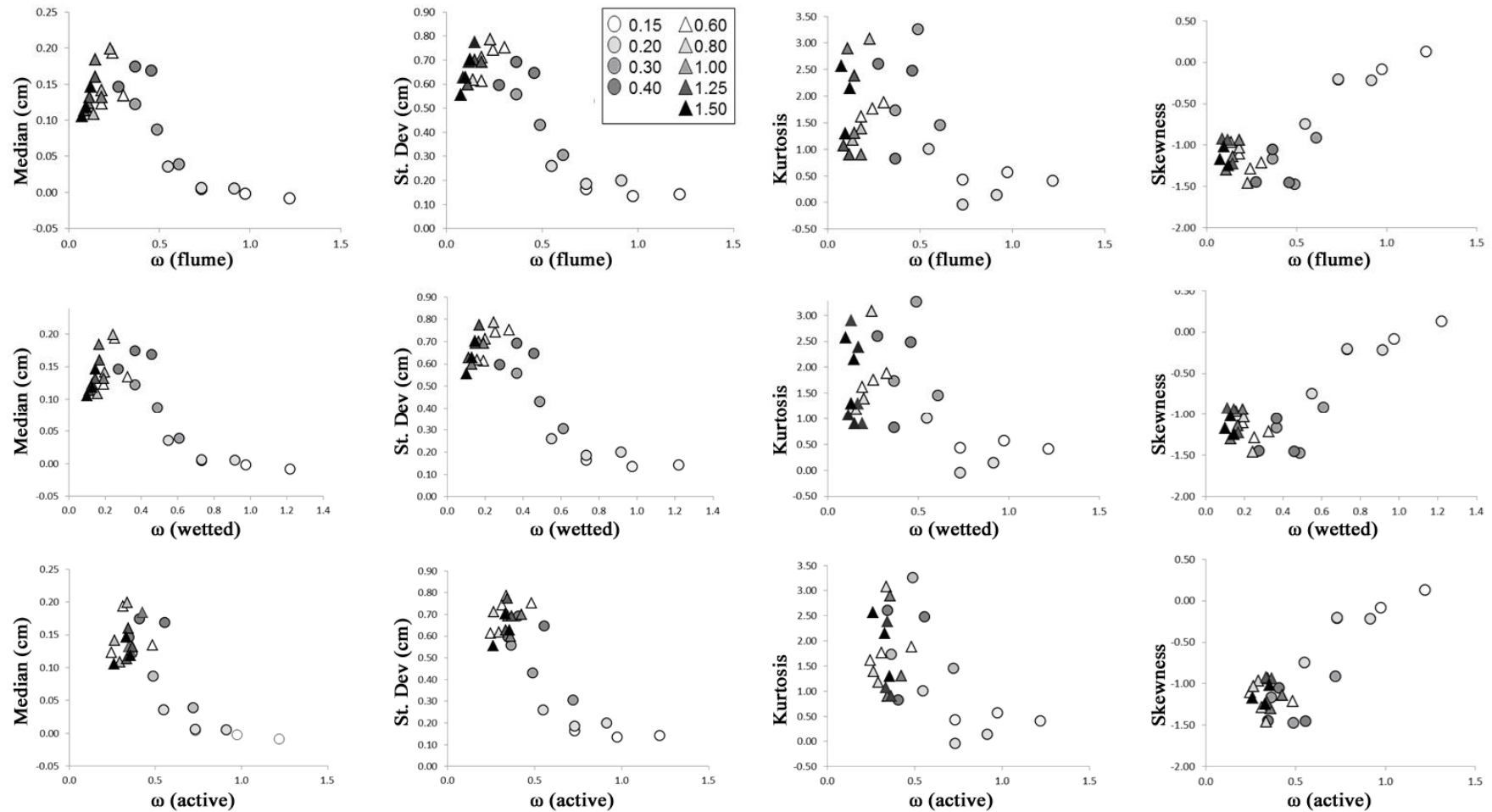


Figure 3.16 Scatter plots illustrating relationships between stream power (ω related to flume, wetted and active widths) and properties of the channel morphology (median, standard deviation, skewness and kurtosis of the elevation frequency distribution). The key explains the symbols used for runs with different flume widths).

Kurtosis describes the height and sharpness of the peak of the bed elevation frequency. Apart from the smallest channel widths (0.15 and 0.20 m), which have a kurtosis value close to zero, all bed elevation frequency distributions have positive values of kurtosis (i.e. increasingly leptokurtic or peaked), which increase with flume width, although there is enormous scatter in relation to both width and also stream power for any fixed width.

Skewness, a measure of the asymmetry of the frequency distribution, is close to zero (i.e. close to symmetrical) for a channel width of 0.15 m but then it decreases markedly for widths of 0.2 and 0.3 m until it stabilises at between -1 and ca. -1.5 for larger widths (i.e. markedly negatively skewed). There also appears to be a decrease in the value of skewness with decreasing stream power for the smaller flume widths.

When variations in the median, standard deviation, kurtosis and skewness are compared for runs of different discharge but with the same channel width, some distinct trends are revealed (Figure 3.17). For small channel widths (0.15 and 0.2 m) there is a reduction in median, standard deviation and kurtosis and an increase in skewness towards a value of 0 (symmetric distribution) with increasing discharge. For all channel widths of 0.4 m and greater, there is a trend of increasing median and standard deviation with increasing discharge, and in most cases kurtosis increases and skewness decreases. At the intervening channel width of 0.3 m there is a very strong decrease in the median and increase in the standard deviation with increasing discharge with no clear trend in skewness or kurtosis. Overall, the four parameters of the elevation frequency distribution indicate a trend from approximately normally distributed frequency distributions with skewness and kurtosis close to zero at low flume widths, particularly when combined with high stream power. This implies a relatively smooth and subdued undulating bed form with few notably high or low areas (e.g. Figure 3.11E). As stream power increases but the flume width remains small, the river bed starts to adopt a slightly negatively skewed, broader but more peaked frequency distribution, still implying a relatively smooth and subdued undulating bed but with bar tops increasing in relative importance to intervening channels and so tending towards Figure 3.11F. Once the flume width exceeds 0.3 m, all of the elevation frequency distributions show marked negative skew, and are increasingly broad but also peaked. This implies an increasingly irregular bed, with intermediate to high elevation bar tops increasing in importance relatively to lower areas (e.g. Figure 3.11I).

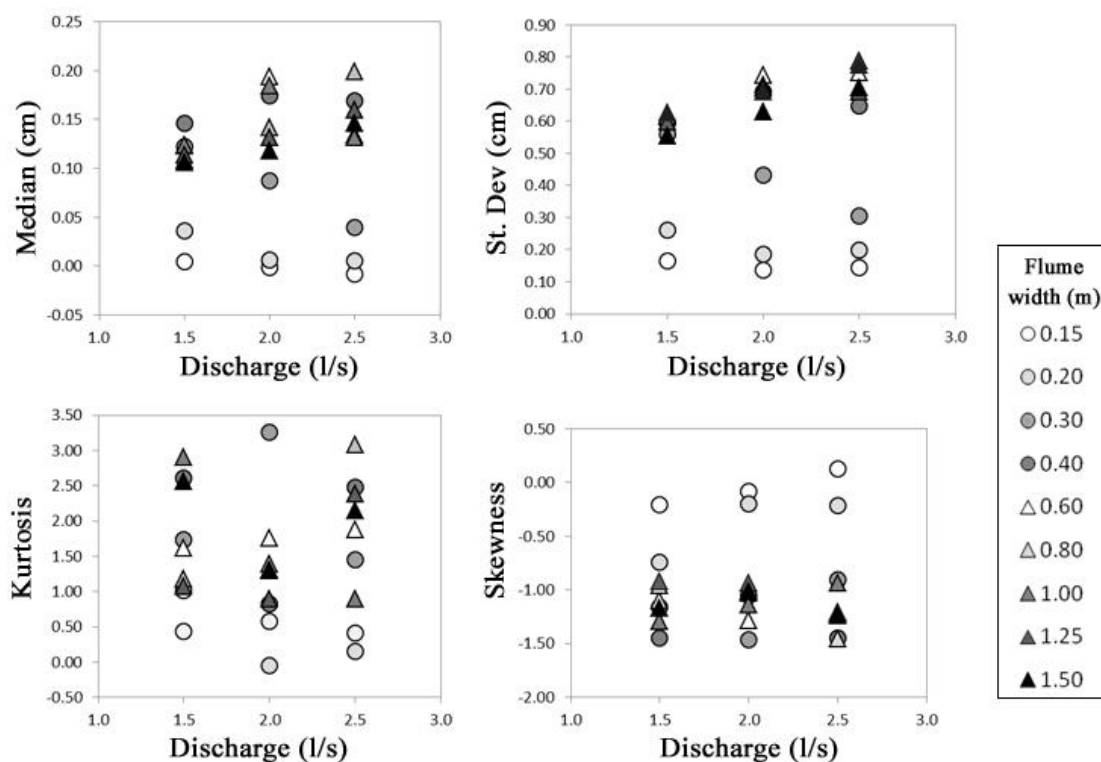


Figure 3.17 Variations in median, standard deviation, kurtosis and skewness of the bed elevation frequency distribution with changes in discharge. The key explains the symbols used for the different widths.

(iv) Channel morphology and the emergence of mid-channel bars

As discussed in section 3.3.2, mid channel bars were only observed in experimental runs of at least 0.6 m width for discharges of 1.5 and 2 l/s and they appeared at a width of 0.8 m for a discharge of 2.5 l/s. The association between the presence of mid-channel bars and the four parameters of the elevation frequency distribution are shown in Figure 3.18.

From Figure 3.18, it is apparent that channels with mid-channel bars develop (but not exclusively) in association with a median elevation greater than 0.1 cm, a standard deviation greater than 0.5 cm, a skewness less than -0.9 and an intermediate level of kurtosis.

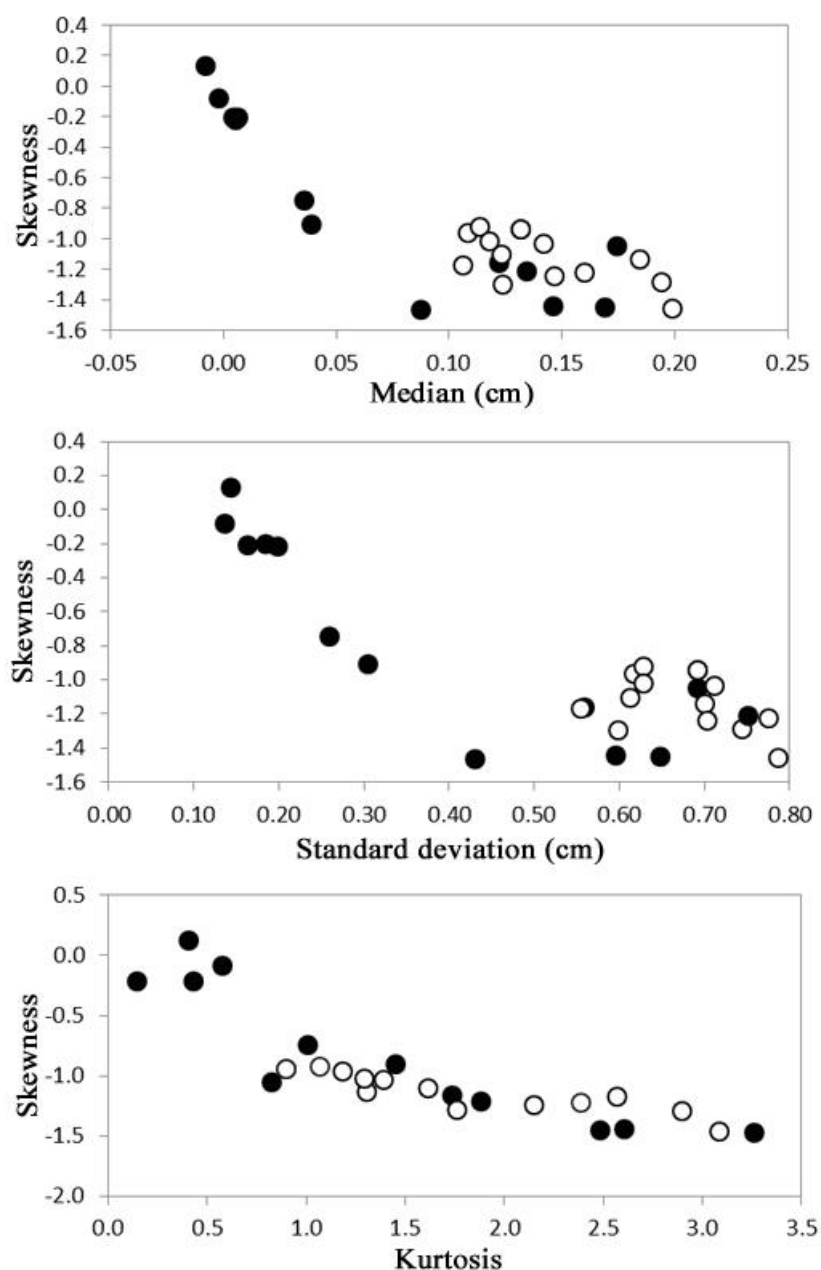


Figure 3.18 Presence of mid-channel bars in relation to the four parameters of the elevation frequency distribution (black dots are channels without mid-channel bars; white dots are channels with mid-channel bars).

(v) Repetition runs

All the results presented so far in this section exclude the repetition runs. Although there appear to be distinct trends in the data, it is important to establish that these are robust results that could be reproduced across several runs reflecting the experimental conditions of discharge and flume width that were explored. Therefore, this section compares the results on the 13 repetition runs with the initial runs under the same flume width and discharge (Table 3.3). As in previous analyses, the parameters (median,

standard deviation, kurtosis and skewness) of the bed elevation frequency distribution for each first (A) and second (B) run have been extracted. The same properties have also been extracted for the frequency distribution of the difference in bed elevation between each pair of runs (C).

The median values for the first runs (A) (range: 0.08 to 0.20; average: 0.133) and the second runs (B) (range: 0.030 and 0.152; average: 0.116) are similar. The frequency distributions of the differences in elevation between runs (C), show a very small range in the medians (-0.01 to 0.02), with an average of 0.003. Similarly, there is a significant variation in the individual standard deviations of the bed elevation frequency distributions among first runs (A) (range: 0.5 to 0.75; average: 0.629), and second runs (B) (range: 0.342 to 0.708, average: 0.595). However, the frequency distributions of the differences in elevation between runs (i.e. C) show a small range in standard deviations (0.35 to 0.65) with an average of 0.543. Kurtosis values also vary greatly among first runs (A) (range: 0.80 to 3.30; average: 1.679), and second runs (B) (range: 0.877 to 3.762; average: 2.074). However, the kurtosis of their difference (C) shows values from 1.3 to 5.65 with an average of 3.291 showing that the frequency distributions for (C) are far more peaked (compact) than either of the first and second runs. Finally, skewness shows values between -1.5 to -0.93 with an average value of -1.119 for the first runs (A), and -1.40 to -0.867 with an average value of -1.123 for the second runs (B), but the values for the difference in elevation (C) ranges from -0.75 to 0.51 with an average value of 0.032, indicating far more symmetrical distributions than for A or B.

Overall, the frequency distributions of the differences in bed elevation between runs A and B are far more compact than for the individual runs, with median values close to 0.0, low standard deviations, a peaked and symmetrical shape. This illustrates that repeat runs generate similar bed elevation frequency distributions, providing confidence that the results obtained when comparing runs under different discharges and flume widths are robust and that the trends that have been identified are genuine.

Table 3.3 Summary information on run length (hr), discharge (Q in l/s), and the parameters (median, standard deviation, kurtosis, skewness) of the bed elevation frequency distribution for runs A and B and of the frequency distribution of the difference in elevation between A and B, which is labelled C.

Run No.	Run length (hr)	Discharge Q (l/s)	Flume width (m)	Bed Elevation			
				Median (cms)	St. Dev. (cms)	Kurtosis	Skewness
7A	3.50	1.5	0.30	0.122	0.559	1.735	-1.162
7B	0.17	1.5	0.30	0.075	0.383	2.600	-1.218
7C	"	1.5	0.30	0.023	0.399	1.666	-0.350
8A	2.80	2.0	0.30	0.087	0.431	3.263	-1.468
8B	0.13	2.0	0.30	0.030	0.342	3.762	-1.142
8C	"	2.0	0.30	0.085	0.518	1.307	-0.745
10A	8.50	1.5	0.40	0.146	0.595	2.606	-1.446
10B	0.42	1.5	0.40	0.082	0.485	1.842	-1.057
10C	"	1.5	0.40	0.010	0.436	3.146	-0.143
11A	5.30	2.0	0.40	0.174	0.693	0.826	-1.051
11B	0.27	2.0	0.40	0.095	0.552	1.278	-0.982
11C	"	2.0	0.40	0.044	0.413	2.781	-0.548
13A	17.80	1.5	0.60	0.123	0.613	1.616	-1.103
13B	0.88	1.5	0.60	0.152	0.655	1.835	-1.210
13C	"	1.5	0.60	-0.011	0.524	2.463	0.390
14A	11.00	2.0	0.60	0.194	0.744	1.763	-1.285
14B	0.55	2.0	0.60	0.135	0.698	1.929	-1.185
14C	"	2.0	0.60	0.004	0.549	3.169	-0.341
16A	23.40	1.5	0.80	0.108	0.618	1.184	-0.962
16B	1.17	1.5	0.80	0.132	0.628	0.877	-0.971
16C	"	1.5	0.80	-0.038	0.559	5.609	0.289
17A	16.60	2.0	0.80	0.142	0.711	1.393	-1.032
17B	0.83	2.0	0.80	0.138	0.703	1.033	-0.867
17C	"	2.0	0.80	-0.026	0.587	3.886	0.042
19A	49.70	1.5	1.00	0.124	0.599	2.900	-1.296
19B	2.48	1.5	1.00	0.126	0.595	1.841	-1.131
19C	"	1.5	1.00	-0.012	0.602	4.343	0.304
20A	33.20	2.0	1.00	0.184	0.701	1.305	-1.137
20B	1.67	2.0	1.00	0.147	0.708	2.746	-1.400
20C	"	2.0	1.00	-0.036	0.633	4.146	0.122
22A	78.20	1.5	1.25	0.113	0.628	1.072	-0.921
22B	3.92	1.5	1.25	0.115	0.641	1.698	-1.031
22C	"	1.5	1.25	-0.008	0.547	3.321	0.507
23A	54.50	2.0	1.25	0.132	0.691	0.902	-0.940
23B	2.72	2.0	1.25	0.126	0.688	2.258	-1.108
23C	"	2.0	1.25	-0.024	0.535	2.761	0.334
25A	100.40	1.5	1.50	0.106	0.555	2.568	-1.172
25B	5.02	1.5	1.50	0.124	0.578	2.985	-1.189
25C	"	1.5	1.50	-0.012	0.596	3.414	0.069
26A	55.10	2.0	1.50	0.118	0.629	1.295	-1.019
26B	2.75	2.0	1.50	0.143	0.678	2.353	-1.234
26C	"	2.0	1.50	0.045	0.594	3.918	0.344

Discharge
Q (l/s)

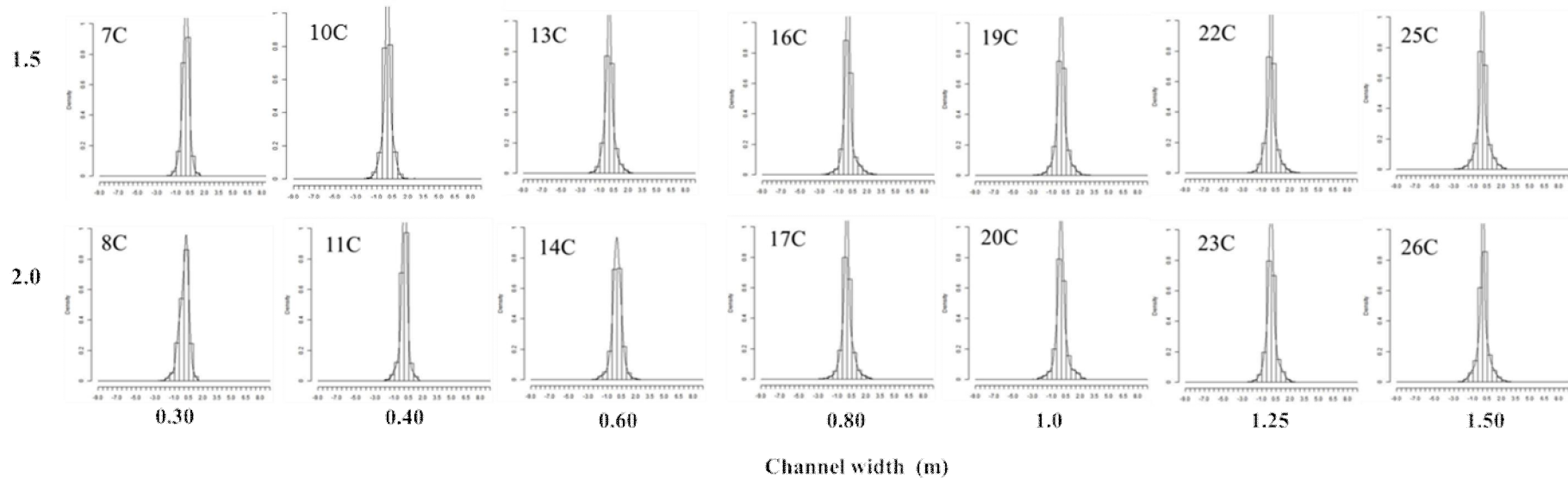


Figure 3.19 Frequency distributions of the differences in elevation between the original runs (A) and their repetition (B) organized vertically by discharge and horizontally by flume width. Each of the distributions is labelled according to the original run number with C to indicate the distribution relates to the difference in elevation between runs A and B. The individual horizontal axis for all of the figures is equally distributed in bins with a 0.5 size, with a range value from -9 to +9, while the vertical axis indicates density with a minimum value of 0 and a maximum value of 1.

3.4 DISCUSSION AND CONCLUSIONS

In section 3.1.4, four research questions were posed, which can now be answered.

3.4.1 Research Question 1: To what extent does bed morphology vary between experiments conducted with the same formative discharge and fixed maximum channel width?

There were 14 pairs of runs, where the experiment was restarted and run for a second period. All of these additional runs resulted in changes in the channel bed morphology, but the four summary statistics (median, standard deviation, skewness and kurtosis) were very similar in each pair of runs and the frequency distribution of the differences in bed elevation between the DTMs produced by each pair of runs was normally distributed with a very low standard deviation, suggesting that the changes were small and random. This suggests that the differences observed across the experiments as channel width and discharge change are robust and informative.

3.4.2 Research Question 2: To what extent does bed morphology change in response to different fixed, formative discharges / stream powers within the constraints of a fixed maximum channel width?

Small but distinct differences were observed in bed morphology in response to changes in the formative discharge or stream power for a fixed channel / flume width (Figure 3.16). These suggest that at small widths, increased discharge / stream power tends to reduce the median bed elevation as well as its standard deviation and kurtosis, suggesting a lower but more homogeneous bed. At the same time, skewness approaches zero, indicating a symmetric bed elevation frequency distribution. Thus with small channel widths, the bed appears to be lowered (scoured) and variability in elevation is reduced. However, above a width of 0.3 m, increased discharge leads to an increase in the overall bed elevation and also in its variability, suggesting increased bar accretion, with a decrease in skewness (increase in asymmetry) and thus an increase in the peakedness of the distribution. There appears to be a threshold in the response of channel morphology to increasing discharge at a flume width of 0.3 m.

3.4.3 Research Question 3: To what extent does bed morphology change in response to a fixed, formative discharge / discharge within the constraints of different fixed maximum channel widths?

Changes of bed morphology in response to flume width change were larger than those in response to discharge change. Changes in planform can be seen clearly in the DTMs displayed in Figures 3.7, 3.8 and 3.9. The same broad trend can be observed for all three discharges as the flume width increases. Up to 0.4 m flume width, a bed morphology of alternate bars can be observed with bar length increasing as width increases. For channel widths of 0.8 m and above, mid channel bars appear. Although a main channel persists with a broadly sinuous course of increasing wavelength with increasing flume width, secondary channels develop and become more numerous and complex as flume width increases. The transition between a single thread planform with alternate bars and the appearance of mid channel bars occurs at flume widths of 0.6 or 0.8 m.

These changes in planform are accompanied by changes in bed elevation frequency distribution. When the four parameters of the frequency distribution are plotted against discharge (expressed as dimensionless stream power and thus adjusted for channel size), clear trends are revealed (Figure 3.16). The single thread, alternate bar channels below 0.6 m flume width, show increases in median, standard deviation and kurtosis of bed elevation, and a decrease in skewness with increasing channel width. This indicates a trend of increasing bed elevation with a more variable, asymmetric and peaked frequency distribution. For all flume widths greater than or equal to 0.6 m, the four parameters of the elevation frequency distribution show no distinct trend with channel width, and their values are particularly similar when stream power is rendered dimensionless using the active channel width, or the width of the channel that is experiencing active sediment transport.

3.4.4 Research Question 4: To what extent does bed morphology change in response to different fixed, formative discharges within the constraints of different fixed maximum channel widths?

If we combine the responses to discharge and width changes, it is clear that bed morphology responds in quite a complex way to changes in discharge and flume width. Narrow channels respond differently from wide channels, with transitional behaviour observed at channel widths of 0.4, 0.6 and 0.7 m width depending upon the discharge applied and the response variable being considered. This transition reflects a shift from channels, where the flume width constrains both the wetted and active width (i.e. 0.15, 0.2 and 0.3 m) to those where both wetted and active width are unconstrained (0.8 m and wider).

3.4.5 Comparison of the Experimental Results with Observations and Predictions From Previous Work

The flume experiments reported in this chapter confirm and extend several relationships among processes and forms that have been established in previous work.

The sediment transport data can be compared to previous research conducted with respect to both channel width and flow energy. Warburton (1996) found a negative linear relationship between sediment discharge and initial channel width in his flume experiments. Since he also found a linear relationship between initial and final channel widths, his results can be compared with the relationship illustrated in Figure 3.13A from the present research. Figure 3.13A describes a curved relationship across a similar width range and slope to those employed by Warburton (1996), but the curve is only discernible because of the much larger data set than that of Warburton (1996) (27 compared with 8 experimental runs). A strong, curved, positive relationship was established between dimensionless mean sediment transport rate (q_s) and dimensionless unit stream power (ω (flume width)) across the entire set of runs (Figure 3.14B). This is very similar to that produced by Bertoldi et al (2009a). However, the present research considerably extends the range of values of q_s and ω for which the relationship is defined.

The research also confirms the positive associations between channel width and discharge or stream power reported in numerous previous flume studies (e.g. Ashmore, 1991, 2011; Bertoldi et al., 2009a). Nevertheless, the present research extends this previous work, by considering how the active channel develops within a wider range of fixed flume widths. Bertoldi et al. (2009a) identified slightly curved, positive relationships between active width and stream power for two separate groups of experiments conducted in different flumes. They then showed that these two data sets described a single, curved, positive relationship when the ratio of active to wetted width was plotted against dimensionless stream power. The present research has identified a positive, curved relationship when the ratio of active to wetted width was plotted against dimensionless stream power (Figure 3.15A), but in the present case, the range of values of dimensionless stream power is much larger. Moreover, the largest values of ω were achieved within narrow fixed channels, where the active width (Figure 3.15C) was close to the value of the wetted width (Figure 3.15B), which in turn occupied the entire

channel width. As a result, the upper part of the curve, between $\omega = 0.25$ and $\omega = 0.4$, extends that of Bertoldi et al. (2009a) under unconfined conditions, but above $\omega = 0.4$, the curve is defined largely by the experiments with flume widths of 0.15 and 0.2 m, where the entire width of the flume was wetted and was almost entirely active.

Table 3.4 ¹Observed BI, and estimated bar types, bar mode (m) and BI based upon ²Colombini, Seminara and Tubino (1987) and ³Crosato and Mosselman (2009) for values of their parameter b of 10 (recommended for gravel bed rivers) and 5. (M=meandering, T = transitional, B = braided)

Run	BI ¹	BI active ¹	Bar types ²	m (b=10) ³	BI (b=10) ³	Planform ³	m (b=5) ³	BI (b=5) ³	Planform ³
1	1.00	1.00	FLAT	0.4	0.7	M	0.7	0.9	M
2	1.00	1.00	FLAT	0.3	0.7	M	0.6	0.8	M
3	1.00	1.00	FLAT	0.3	0.6	M	0.6	0.8	M
4	1.00	1.00	FLAT	0.6	0.8	M	1.2	1.1	M
5	1.00	1.00	FLAT	0.5	0.8	M	1.0	1.0	M
6	1.00	1.00	FLAT	0.5	0.7	M	0.9	0.9	M
7	1.00	1.00	ALTERNATE	1.2	1.1	M	2.2	1.6	T
8	1.00	1.00	ALTERNATE	1.0	1.0	M	1.9	1.4	M
9	1.00	1.00	ALTERNATE	0.9	0.9	M	1.7	1.3	M
10	1.00	1.10	ALTERNATE	1.9	1.4	M	3.5	2.3	T
11	1.00	1.00	ALTERNATE	1.6	1.3	M	3.0	2.0	T
12	1.00	1.00	ALTERNATE	1.4	1.2	M	2.6	1.8	T
13	1.25	1.55	MULTIPLE	3.3	2.1	T	6.2	3.6	B
14	1.13	1.52	CENTRAL	2.9	2.0	T	5.5	3.2	B
15	1.10	1.09	CENTRAL	2.6	1.8	T	4.8	2.9	B
16	1.76	1.75	MULTIPLE	4.8	2.9	B	9.1	5.0	B
17	1.65	1.40	MULTIPLE	4.1	2.6	B	7.7	4.4	B
18	1.25	1.65	MULTIPLE	3.8	2.4	T	7.1	4.0	B
19	1.81	2.15	MULTIPLE	6.4	3.7	B	11.9	6.5	B
20	1.50	1.62	MULTIPLE	5.7	3.3	B	10.6	5.8	B
21	1.55	1.90	MULTIPLE	5.1	3.0	B	9.5	5.2	B
22	2.53	2.10	MULTIPLE	7.4	4.2	B	13.9	7.5	B
23	2.20	1.95	MULTIPLE	7.0	4.0	B	13.0	7.0	B
24	1.88	2.07	MULTIPLE	6.3	3.6	B	11.8	6.4	B
25	2.47	2.10	MULTIPLE	8.8	4.9	B	16.5	8.7	B
26	1.81	2.05	MULTIPLE	8.4	4.7	B	15.8	8.4	B
27	2.15	2.10	MULTIPLE	8.1	4.5	B	15.1	8.0	B

The present research has taken a three-dimensional approach to evaluating how the style of the river changes as width and discharge are evaluated. However, much previous work has evaluated or predicted such changes using simple planform measures as were described in section 3.1.2. To compare the results of the present research with other research, the braiding index and the active braiding index were extracted from the photographs taken for each experimental run. In addition, predicted bar mode (m) and associated BI values were calculated for each run using the method of Crosato and Mosselman (2009) and the style of channel was estimated using the method of Colombini, Seminara and Tubino (1987). All of these results are shown in Table 3.4.

The observed results in Table 3.4 are consistent with previous quantitative analyses of braiding intensity (e.g. Ashmore, 1991, 2009, Bertoldi et al., 2009a), which have shown an increase in braiding intensity (number of anabranches, number of links) with dimensionless stream power. Changes in bar dimensions observed in the DTMs (Figures 3.7 to 3.9) are also consistent with Ashmore's (2009) observation that 'braided channel networks ... have a characteristic length scale (or scales) related to the wavelength of the bars from which braiding develops and to the scale of the bars and confluence–bifurcation units within the braided network'. Furthermore, the variations in the observed braiding index show good correspondence with those predicted using the method of Crosato and Mosselman (2009) when their parameter B is set to 10, and the appearance of mid-channel bars in the experimental runs also corresponds with predictions from the method of Colombini et al. (1987).

3.4.6 Concluding Remarks

The reported experiments have confirmed and extended previous research by considering river width and bed responses to three experimental discharges under a constant slope and bed material size, and unrestricted bed material supply within flume channels of a range of fixed widths. Thus the experiments demonstrate morphological responses to different degrees of channel confinement. This is not only important in the context of natural channels, where confinement may result from the presence of bedrock valley walls, or the presence of highly cohesive floodplain sediments, but it also demonstrates the morphological consequences of artificial confinement of rivers that would otherwise develop a braided morphology.

Chapter 4 extends this analysis, by considering a natural channel that displays several similarities to the flume experiments but also several differences. By focusing on the lower reaches of the Tagliamento River, it is possible to investigate the morphology of reaches of different width that are subject to a similar, although highly variable, flow regime; similar, although slightly varying, slope; and high sediment availability. These provide sufficiently close natural surrogates to explore similarities between the flume results and the conditions observed in natural rivers and to consider the following research question:

In a natural river, is there any noticeable change in channel morphology as the channel width and stream power vary?

However, the morphology of the Tagliamento is also affected by vegetation, introducing an additional potential control on channel morphology. This provides an opportunity to explore a second research question:

To what extent is channel morphology affected by the presence of vegetation?

Chapter 4

Interactions Between Vegetation and Channel Morphology on a Braided River: The Lower Tagliamento River, Italy

4.1 INTRODUCTION

Chapter 3 presented results from 27 experimental runs carried out in a large laboratory flume. In these experiments, some of the controls on channel morphology that had been identified from the literature were fixed (namely, sediment size and supply, and slope) in order to investigate the influence of two particular controls: channel width (level of confinement) and discharge. The interactions between these controls produced different bed morphologies, revealing clear changes in the skewness and kurtosis of the bed elevation frequency distribution as channel width and discharge varied. There were also notable adjustments in each of the descriptive statistics of the bed elevation frequency distribution as channel width or the degree of confinement of the channel changed. In particular, there was a marked threshold in these properties as the bed morphology changed from single thread (alternate bars) to multi-thread (mid-channel bars) with increasing channel width. In this chapter, the analysis focuses on a real river, where the influence of additional factors on channel bed morphology can be explored, most importantly the impact of vegetation.

Over the last two decades, the impact of vegetation on channel morphodynamics has been increasingly recognised through field observations (e.g. McKenney et al., 1995; Gurnell et al., 2001, 2005, Corenblit et al., 2009), flume experiments (e.g. Bennett et al., 2008, Li and Millar, 2011, Tal and Paola, 2007, 2010) and modelling (e.g. Murray and Paola, 2003, Camporeale and Ridolfi, 2006, Perucca et al., 2007, Eaton and Giles, 2009, Eaton et al., 2010). Vegetation has been recognized to influence channel morphology through root reinforcement of river banks and other surfaces, and also through interactions between the vegetation canopy, flowing water and sediment transported during floods, which result in a decrease in flow velocities and trapping of mineral sediment and organic matter to aggrade the bank surface (Millar 2000, Eaton, 2006; Bennett et al., 2008; Pollen-Bankhead, et al., 2009 Pollen-Bankhead and Simon, 2009, 2010). There are two way interactions between vegetation and the fluvial processes not

only once the vegetation is established, but also in terms of the degree to which colonization can be successful and the vegetation can survive subsequent fluvial disturbances. This is observed in the evolution and destruction of vegetated landforms such as islands, scroll bars and benches (Gurnell et al., 2001, 2005; Corenblit et al., 2007, 2009; Osterkamp and Hupp, 2010). As vegetation establishment and growth is highly dependent on water availability, changes in the flow regime can have a significant impact on vegetation extent and dynamics in the river corridor (Johnson, 2000; Lytle and Merritt, 2004; Camporeale and Ridolfi, 2006; Bertoldi et al., 2009b, 2011). Extended periods of flooding or drought can lead to large changes in the vegetation cover (Amlin and Rood, 2003; Lite and Stromberg, 2005; Glenz et al., 2006; Stromberg et al., 2007; Rood et al., 2008) with potential consequences for channel morphology.

Research on vegetation – fluvial process interactions, specifically the retention and reinforcement of sediment by vegetation to build landforms such as islands that change the topography of river beds, and the flow intensities required to remove these landforms, have been hampered by a lack of appropriate data to investigate such temporally and spatially complex dynamics. In particular, study of these interactions on braided rivers has received very little research attention until recent years, probably due to the greater complexity of these dynamics in braided planforms, which are challenging to investigate using traditional methods. While, as already noted, flume and numerical modelling approaches have been informative, the acquisition of information from real rivers has required the coupling of remotely sensed data with direct field measurements. Sequences of high resolution air photographs have provided useful insights into the rate and spatial extent of vegetation dynamics (e.g. Shafroth et al., 2002; O'Connor et al., 2003; Zanoni et al., 2008, Hervouet et al., 2011), with the most recent work making use of a variety of airborne and satellite remotely-sensed data sets. Where resources are available, researchers are commissioning the capture of data sets from aircraft or are using unmanned air vehicles to capture data (e.g. Hervouet et al., 2011).

Data sets captured from satellite platforms are now widely available and are of sufficient spatial resolution to yield useful information on the plan dynamics of vegetation on larger braided rivers (e.g. Bertoldi et al., 2011a; Henshaw et al., 2013) whereas airborne lidar data sets are also becoming more accessible to researchers. These provide three-dimensional information that allows vegetation extent, height and

structure to be related to the underlying river bed topography (e.g. Bertoldi et al., 2011b). The limitation of using such data sets is the time period over which they are available, their temporal frequency and their spatial and spectral resolution. While air photo coverage often extends back to the middle of the 20th century, the longest satellite data record of consistent spatial and spectral resolution is Landsat Thematic Mapper data (1984 to present). ASTER data offers higher spatial resolution but data sets are only available from 1999. To achieve three-dimensional information, lidar data is required. This is obtained using aircraft and so data availability is spatially very variable. The spatial resolution of lidar data sets has increased rapidly as the technology has advanced.

In this chapter, the flume research reported in Chapter 3 is extended to a real river environment where human interventions are relatively small. The research makes use of airborne lidar data:

- (i) To focus on a 37 km length of braided river of relatively constant slope and bed material that is subject to the same flow regime (there are no major tributaries) but shows some variation in braid plane width and vegetation cover. This provides a natural river environment where several of the key factors influencing channel dynamics are relatively uniform.
- (ii) To adopt a similar methodology to that applied to the flume experiments to characterise bed morphology using lidar data.
- (iii) To additionally characterise vegetation properties from the lidar data.
- (iv) To explore associations between vegetation and braid plain morphology.

This research adopts the methodology developed by Bertoldi et al. (2011b) and applies it to a different and longer length of the Tagliamento river by analysing lidar data captured on a different date.

4.2 THE STUDY SITE

The braided, gravel-bed Tagliamento river is located in the Friuli Venezia Giulia region of Italy. It rises in the Italian Alps and flows for approximately 170 km to the Adriatic Sea, draining a catchment area of approximately 2580 km². It is considered to be one of the last morphologically intact rivers in Europe (Tockner et al., 2003) since, with the

exception of its most downstream part, its corridor is mainly unconfined by embankments and bordered by riparian woodland.

The analysis presented in this chapter, focuses upon a 37 km section of the lower Tagliamento, extending downstream from 46° 11' 0.83''N, 12° 57' 24.71''E (close to the town of Pinzano) through a continuously braided section until the river passes through a transitional section into a meandering section at 45° 05' 37.87''N, 12° 58' 32.16''E (close to the town of Madrisio). Since only small tributaries join the river within this section, the entire 37 km of river is subject to essentially the same flood regime. However, downwelling and upwelling to / from the alluvial aquifer generates significant changes in baseflow along the river, with the central part often drying out completely in mid-summer. Riparian woodland, dominated by poplar trees (*Populus nigra*) is present along the entire 37 km section. Trees actively colonise the braid plain giving rise to the formation of a dynamic mosaic of islands (Gurnell et al., 2001)

4.3 METHODS

As reviewed in section 4.1, vegetation colonisation of the bar surfaces of braided rivers is accompanied by sediment retention, bar surface aggradation and root-reinforcement of the aggrading surface. As a result, a morphological response is expected in association with vegetation colonisation, with increasing surface aggradation and the formation of island landforms in vegetated areas as the vegetation persists and grows. Therefore, bar surface elevation is anticipated to increase with the height and age of the riparian tree species that colonise the river bars of the Tagliamento River. Therefore, the methods described below investigate the morphology of the river bed (4.3.1) and also the extent and height (surrogate for age and biomass) of vegetation (4.3.2) in order to investigate the degree to which any sediment retention and aggradation effect of vegetation may have affected the overall morphology of the river bed.

4.3.1 Extraction and Analysis of a Digital Elevation Model of the River Bed

An airborne lidar survey of approximately 37 km of the Tagliamento river (the study section) was conducted between 9 and 13 January 2001, at a point density of approximately 1.02 m², by the Autorita di Bacino dei fiumi dell'Alto Adriatico. No information is available concerning the vertical accuracy of this survey. However, published estimates of the accuracy of elevations derived from a scanner of similar vintage, operating at a similar elevation (ca. 1200m) with similar point density (2m) in

comparison with ground measurements from a total station have been found to be less than 20 cm (root mean square error) on flat surfaces and around 25 cm over forests (Hodgson and Bresnahan (2004). The 24 data files covering the active corridor included measurements that extended at least 4 km laterally from the river banks.

These data were converted and imported into the free software FUSION (developed by the US Department of Agriculture, Forest Service, Remote Sensing Applications Center, downloadable from <http://www.fs.fed.us/eng/rsac/>). The data in the imported point cloud was then filtered using the 'ground filter' command in order to identify points that are at the ground surface and differentiate them from points located on the surface of the vegetation and other protruding surfaces. This command uses the Krauss & Pfeifer (1998) filtering technique, where points are more likely to be classified as vegetation if they protrude from other points in the surrounding point cloud. Hollaus et al. (2006) found that this filtering method works well on ground surfaces that are reasonably flat (not characterised by steep slopes) and where the vegetation is sufficiently sparse for > 25% of points to reach the ground surface. Given the relatively flat nature of the river bed (relative relief < 5m) and the early spring date of the survey (before significant leaf development on the woodland canopy), these criteria are comfortably met in the present application. Following the filtering procedure, a 4 m by 4 m pixel digital elevation model (DEM) of the bare ground was created from each of the raw lidar files using the 'grid surface create' command. All of the files were then converted to ASCII format and imported into ArcGIS 10 using the conversion tool option "ASCII to Raster", and a single raster file was created using the "mosaic to new raster" option in ArcGIS 10 (selected mosaic operator was "last" and mosaic colour map mode was "first") to create a single DEM.

Using a neighbourhood statistics tool within ArcGIS 10, a provisional land surface slope was calculated and was subtracted from the DEM in order to identify the edges of the main channel and its planform. A polygon shape file was then created to delimit the area enclosed by the main channel and this was used as a mask to extract the area of the active river channel and create a new raster DEM of the channel bed alone for morphological analysis.

To facilitate analysis of different parts of the 37km long river bed, it was divided into 1 km long reaches. The choice of 1km length reaches, and the location of the most

upstream reach in the present analysis, followed previous work on the Tagliamento by Bertoldi et al. (2011), where lidar data from 2005 had been analysed. It was initially hoped that comparison of data for the two dates might yield an interesting comparison of channel morphology following 4 years of vegetation colonisation. Unfortunately, the short length and laterally confined location of the area of overlap of the two surveys, prevented any useful comparison of vegetation development between the two dates. First a central axis (line) was constructed along the entire 37 km river bed and perpendicular lines to this central axis were constructed at 1 km intervals to create individual polygon shape files for every 1 km reach. The resultant polygon shape files were used to define, extract and export the relevant elevation data and co-ordinates as a 'txt' file to Excel, where it was saved in 'csv' format.

Once the DEM data for each 1 km reach had been exported into Excel, it was detrended to remove the downstream slope, so that the local relative elevation could be examined. A code was written in R to analyse the data within each 'csv' file as a matrix. Each ground matrix was de-trended by calculating the average elevation of each cross-channel line in the grid and then subtracting the average from each of the individual elevations in that line to create a new detrended matrix.

A relative frequency histogram (vertical axis ranging from 0 to 1; horizontal axis displaying a fixed 0.1 m bin size) and set of descriptive statistics were extracted (mean, median, standard deviation, skewness, kurtosis, upper and lower quartile) from the elevation data within the detrended grid for each 1 km reach.

4.3.2 Extraction and Analysis of a Vegetation Canopy Surface Model

The canopy surface model (CSM) was calculated using the ground-filtered file (i.e. with the ground elevation as a reference surface) in the 'canopy model' command within FUSION. Vegetation height and spatial distribution was evaluated within spatial units defined by a 12 m by 12 m grid in order to give a sufficient sample of vegetation points to make a reliable assessment. These data points were analysed to identify the proportion indicating 1) an unvegetated / open gravel surface: all points less than or equal to 1m above the estimated ground surface level; 2) vegetation taller than 1 m: all points greater than 1 m above the estimated ground surface; 3) vegetation taller than 5 m: all points greater than 5 m above the estimated ground surface; and 4) vegetation taller than 10 m: all points greater than 10 m above the estimated ground surface. The

above analyses resulted in 4 files which indicated the proportion (0 to 100 %) of points within each of the elevation ranges inside the 12 x 12 grid units that were then expressed in 4 files of 4 m by 4 m pixel size to match the previously produced DEM. The files were exported in ASCII format and were imported into ArcGIS 10 using the 'ASCII to raster' conversion tool, where they were mosaiced into four different canopy surface model (CSM) rasters for the four different height classes. Finally the active channel area was extracted by using the previously-produced active channel polygon shape files.

Within ArcGIS 10 each of the three Canopy Surface Models representing the presence of vegetation of different heights height (i.e. >1 m, >5 m, and >10 m) was reclassified to filter out spurious values, by using the rule that the 'true' presence of vegetation required at least a 5% cover value. Hence, everything with a cover below 5 % was considered non-vegetated and was coded with a value of '0' and everything with a cover above 5% was coded with a value of '1'. To produce an unvegetated or bare gravel raster, the "vegetation >1m" raster was reclassified so that values of 0 to 5 % were coded with a value of "1" and others with a value of '0'. Using the 'raster calculator' the CSM for vegetation >10 m was subtracted from the CSM for vegetation >5 m to obtain all the vegetation in a 5 to 10 m height range, similarly the CSM for vegetation >5 m was subtracted from the CSM for vegetation >1m in order to obtain the vegetation in a 1 to 5 m height. Using the reach polygons previously created for each of the 37 1 km reaches, the reclassified rasters were subdivided into 1 km reaches and then using the 'attribute table', the amount of vegetated pixels within each 1 km reach was counted in each of the selected categories.

Lastly, for comparison with other research on braided rivers, some planform indices were extracted. First, using the reclassified raster for vegetation >1 m (i.e. vegetation present) and extracting each of the data for each of the 37 reaches with the previously used polygons, the channel centre line was superimposed on the vegetation distribution for each reach and 10 cross sections were placed at 90 degrees to the centre line every 50 metres. The averaged total channel width was then calculated. The average vegetated, non-vegetated and total channel width was calculated for each 1 km reach using these transects. Second, the braiding index (BI) was calculated using the only image in Google Earth that covered the entire 37 km section. Each of the 1 km reaches was investigated in this image (dated 25th June 2008). Using 50 m spaced transects

constructed perpendicular to the channel centre line, the number of ‘flowing channels’ was counted along each transect and then these estimates were averaged to give an estimate of BI for each 1 km reach.

4.4 RESULTS

4.4.1 Description of the Detrended DEM Data for the 36 1km Reaches

During analysis of the DEM data for the 37 km section of the Tagliamento, it became apparent that rail and road bridge construction at ponte Tagliamento (45°57'47.08"N, 12°54'14.38"E) had such a major effect on one of the 1 km reaches, that its morphology could not usefully contribute to an analysis of ‘natural’ braid morphology, and so this reach was excluded from further analysis. This left 36 reaches which, on the basis of their planform and confinement by mountains, were assigned to four descriptive categories: confined braided, braided, transitional and meandering. The term confined braided was only applied when both edges of the braid plain were confined by mountains or terraces. The detrended DEMs for each 1 km reach are illustrated in Figures 4.1 and 4.2 and the relative frequency histograms of bed elevation for these reaches are presented in Figures 4.3 to 4.6.

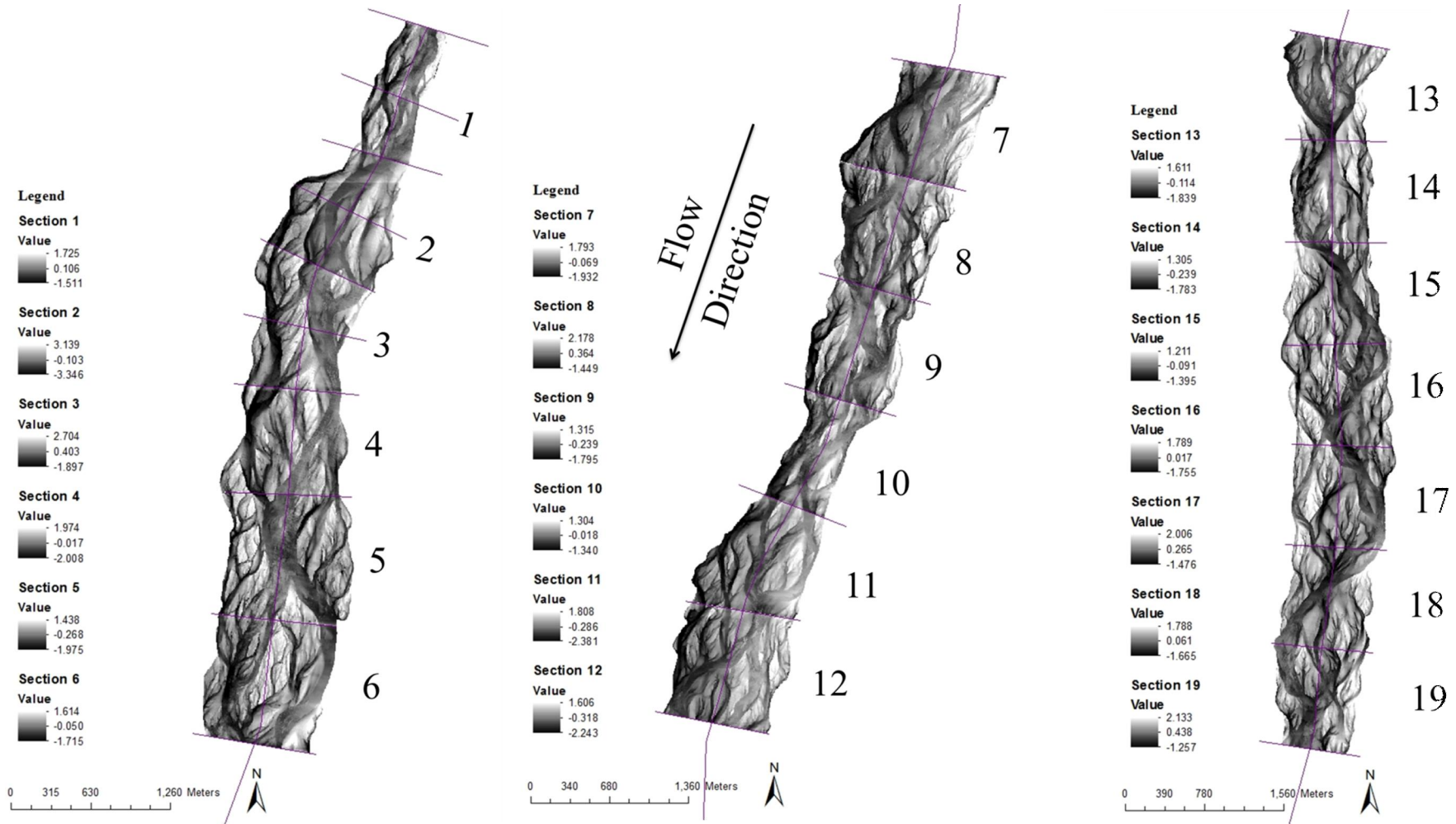


Figure 4.1 Detrended DEMs for 1 km reaches 1 to 19. Note that length scales vary slightly between the three images.

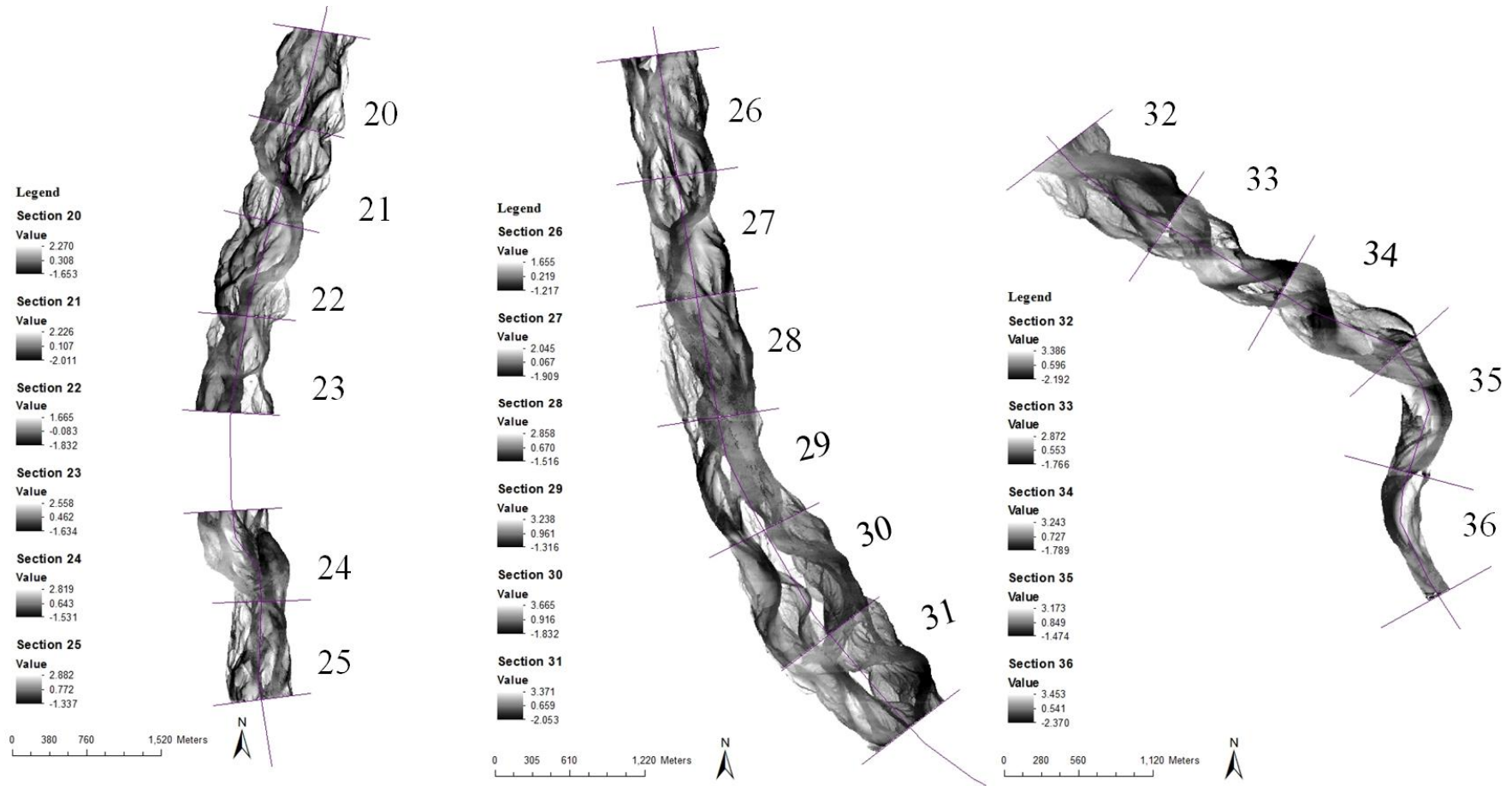


Figure 4.2 Detrended DEMs for 1 km reaches 20 to 36. Note that length scales vary slightly between the three images.

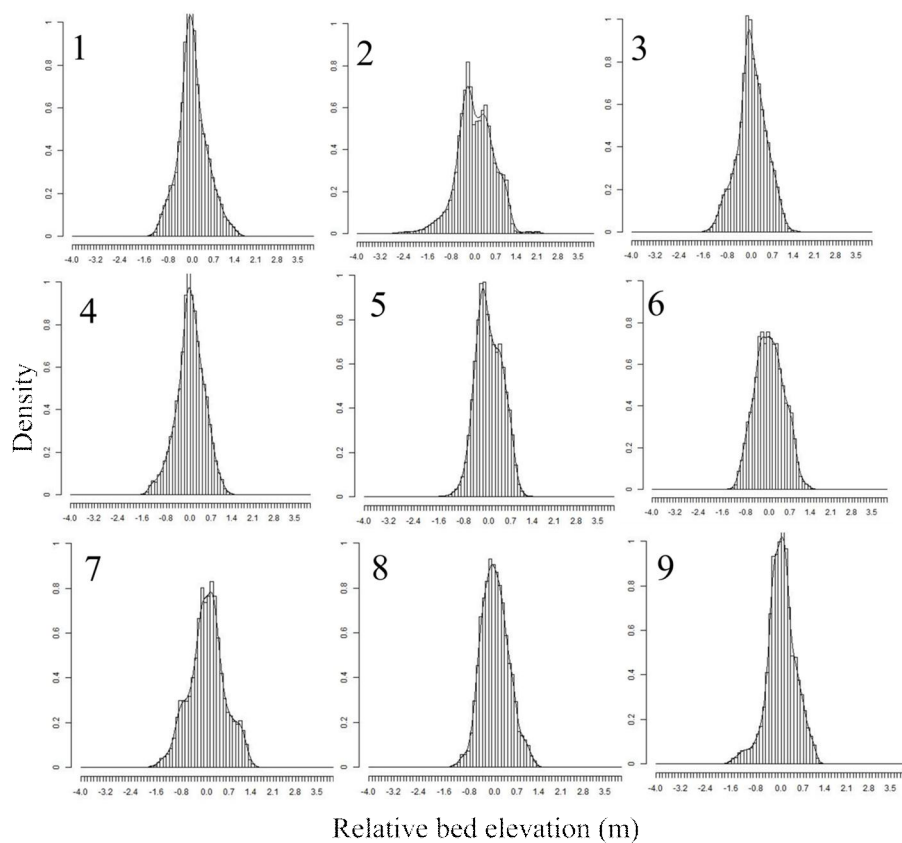


Figure 4.3 Relative elevation frequency distributions for 1 km reaches 1 to 9.

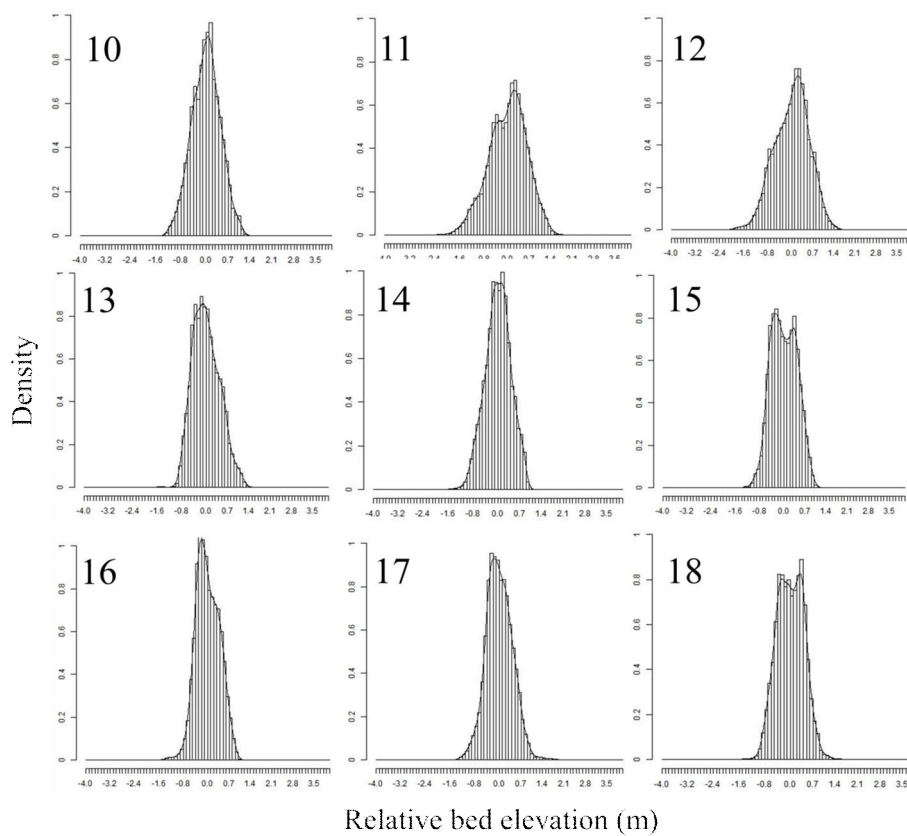


Figure 4.4 Relative elevation frequency distributions for 1 km reaches 10 to 18.

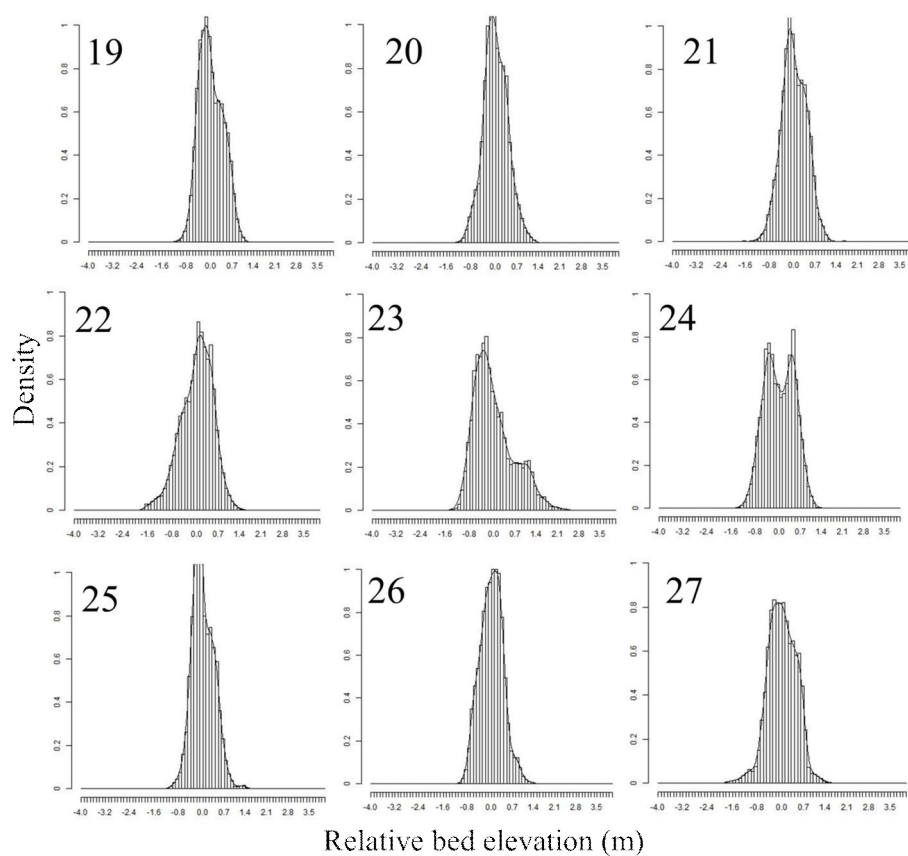


Figure 4.5 Relative elevation frequency distributions for 1 km reaches 19 to 27.

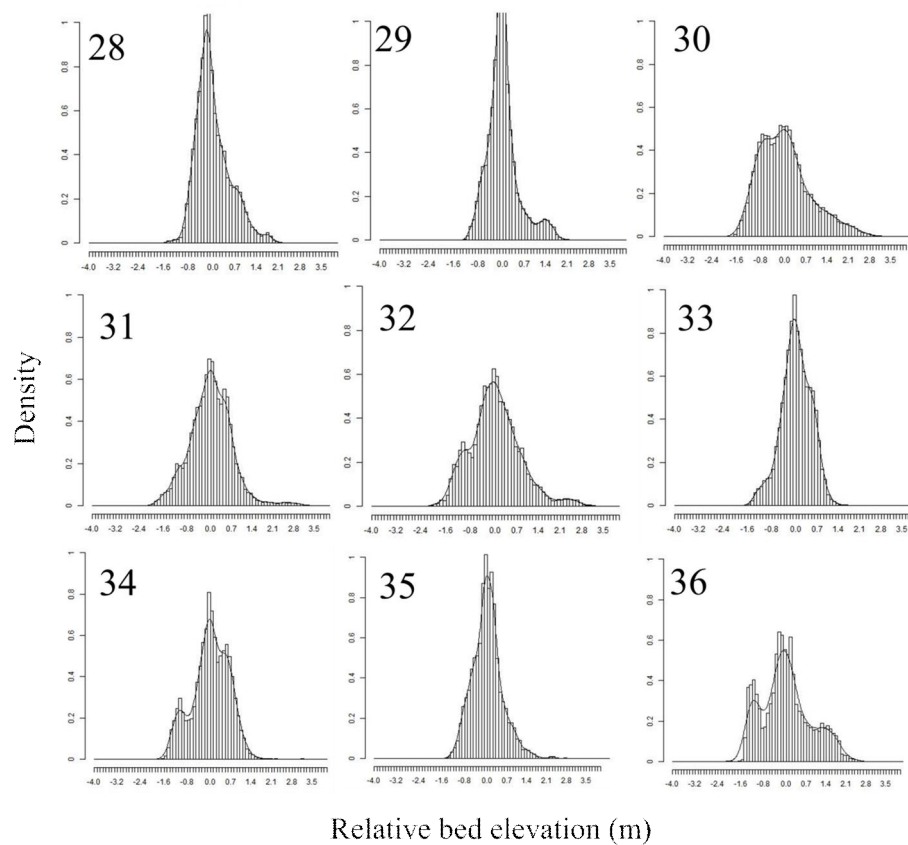


Figure 4.6 Relative elevation frequency distributions for 1 km reaches 28 to 36.

Table 4.1 Description of the shape of the frequency histograms in Figures 4.3 to 4.6 according to five types (where specified, L and R refer to the location of the ‘bump’ or secondary peak on the left or right side of the histogram).

Reach	Single peak	Single peak, secondary 'bump'	Single peak, small secondary peak	Two peaks of similar magnitude	One main peak, two secondary peaks
1	√				
2				√	
3	√				
4	√				
5		√ R			
6		√ R			
7		√ L & R			
8	√				
9	√				
10	√				
11			√ L		
12		√ L			
13		√ R			
14	√				
15				√	
16		√ R			
17	√				
18				√	
19		√ R			
20		√ R			
21		√ R			
22		√ L			
23		√ R			
24				√	
25		√ R			
26	√				
27		√ R			
28		√ R			
29			√ R		
30				√	
31			√ R		
32			√ L		
33		√ R			
34					√
35		√ L			
36					√

A visual inspection of the frequency histograms shows that, although they are all dominated by a broadly unimodal form, similar to that of the experimental channels reported in Chapter 3, there are quite wide variations in their detailed shape. In addition, some of the distributions show secondary features, which were not observed in the experimental channels, allowing five main shapes of frequency distribution to be identified (Table 4.1). First and most prominent are single peaked, symmetrical histograms with the peak frequency at or very close to 0.0 m. The second shape is similar to the first but with a small secondary ‘bump’ on one side of the distribution (in Table 4.1, the side of the peak affected by the bump is indicated as L or R for the left or right side). The third shape shows a main peak with a small secondary peak (in Table 4.1, the side of the peak affected by the small secondary peak is indicated as L or R for the left or right side). The fourth shape shows two close peaks of similar magnitude. The last, fifth shape shows one major peak and two smaller ones.

The most common types of frequency histogram shape are single peaked with (n=16) and without (n=9) a ‘bump’ (Table 4.1). Where a ‘bump’ or small secondary peak (n=4) is present, it occurs mainly on the right side of the histogram (n=16 out of 20). Five histograms have a bump or small secondary peak on the left side of the histogram, and one of these has a bump on both sides. With the exception of reach 2, double (n=5) and multiple secondary (n=2) peaked histograms occur from reach 15 downstream. Such peaks or bumps represent particular elevation ranges that are strongly represented in the bed topography. Where they occur on the right side of the distribution, they represent extended elevated areas, which in geomorphological terms could be major bench or terrace-type forms within the braided channel, probably reflecting past areas of river bed left isolated by bed incision. Where they occur on the left side of the distribution, their geomorphological explanation could be the presence of one or more braid threads with beds that are relatively higher than the majority of braid threads, perhaps indicating side channels that are only occupied when flows are elevated. In either case, the peaks and bumps most probably indicate channel adjustments in response to changes in fluvial processes such as the occurrence of extreme flow events or changes in the sediment supply / transport regime. Therefore, they represent deviations from the dynamic equilibrium conditions that were imposed during the flume experiments described in Chapter 3.

Further descriptive statistics extracted from the bed elevation frequency data for each of the 1 km reaches (1 to 36) are provided in table 4.2. These show a wide range across the 36 reaches, reflecting to some extent the variations in the shape of the elevation frequency distributions described above. Indeed, there is considerable variability in the descriptive statistics. Median elevation ranges from -0.161 to $+0.060$ m, standard deviation from 0.360 to 0.867 m, lower quartile from -0.644 to -0.243 m, and upper quartile from $+0.169$ to $+0.473$ m. These can be compared with the total elevation range within the data for each reaches which ranges from 2.607 to 6.486 m. As already noted from a visual inspection of Figures 4.3 to 4.6, the shape of the elevation distributions vary considerably, and this is reflected in kurtosis values ranging from -0.733 to $+2.256$ and skewness values ranging from -0.417 to $+1.108$. Thus, the full range of bed elevation shapes, reflecting different combinations of skewness and kurtosis, is present as was illustrated in the schematic diagrams of Figure 3.11.

In addition to the increasing occurrence of secondary peaks from reach 15 downstream, these other properties of the morphology of the river bed also appear to show trends along the downstream sequence of the 36 reaches that were analysed (Figure 4.7), with the standard deviation decreasing gradually to around reach 25 and then sharply increasing; skewness varying widely, but showing generally lower values between reaches 1 and 22 than between reaches 23 and 36; kurtosis decreasing gradually to around reach 25 and then increasing sharply to reach 36; and the range in elevation decreasing from reach 1 to 10 and increasing from reach 15 to 36. Referring to Figure 3.11, the bed elevation distributions in reaches 1 to 20 are approximately symmetrical but with a downstream trend from slightly positive to slightly negative kurtosis and slightly negative to near zero skewness, demonstrating a gradual transition from a profile tending towards Figure 3.11F to one tending towards Figure 3.11B. Downstream to reaches 28 to 30, both skewness and kurtosis increase sharply, indicating a transition towards a profile similar to Figure 3.11G. Further downstream to reach 35, both properties decline back to values close to zero, indicating a transition towards a profile similar to Figure 3.11E. The June 2008 values of BI (Table 4.2), are highly variable within the braided reaches, but the section between reach 22 and 30 (where the bed profile transitions from Figure 3.11E to H) has generally low BI values (<3), reflecting a zone of low water stage associated with gradual recovery of groundwater levels from their typically lowest summer values around reach 20 (Gurnell and Petts, 2006).

Table 4.2 Descriptive statistics of the bed morphology of thirty-six 1 km reaches of the Tagliamento river based on the analysis of lidar data from early spring 2001.

Reach number	Width (m)	Slope (m/m)	Planform Type	Parameters of the Bed Elevation Frequency Distribution						Vegetation cover				Braiding Index
				Median (m)	Standard deviation (m)	Kurtosis	Skewness	Lower quartile (m)	Upper quartile (m)	% taller than 10m	% taller than 5m	% taller than 1m	% no vegetation	
1	400.984	0.004	Confined Braided	-0.037	0.481	0.320	0.264	-0.280	0.278	0.000	1.592	15.613	84.387	5.1
2	612.568	0.003	Braided	-0.018	0.636	1.111	-0.332	-0.379	0.423	0.201	1.084	13.981	86.019	7.0
3	810.242	0.003	Braided	-0.014	0.490	0.076	-0.104	-0.279	0.319	0.000	0.803	8.373	91.627	4.3
4	804.738	0.003	Braided	0.006	0.467	0.262	-0.259	-0.264	0.305	0.020	0.565	7.865	92.135	3.5
5	952.385	0.004	Braided	-0.035	0.425	-0.245	0.011	-0.301	0.323	0.018	0.768	12.065	87.935	3.2
6	945.753	0.004	Braided	-0.012	0.488	-0.501	0.071	-0.348	0.345	0.133	2.000	16.628	83.372	6.3
7	795.706	0.004	Braided	0.010	0.566	-0.077	-0.035	-0.344	0.334	0.090	0.934	5.699	94.301	6.3
8	916.756	0.003	Braided	-0.025	0.434	0.002	0.230	-0.307	0.279	0.103	1.782	9.159	90.841	5.6
9	701.783	0.003	Braided	0.001	0.453	0.845	-0.334	-0.258	0.264	0.093	1.372	7.596	92.404	5.1
10	485.82	0.003	Braided	0.013	0.445	-0.252	-0.046	-0.316	0.302	0.338	1.744	4.693	95.307	5.3
11	712	0.003	Braided	0.060	0.613	-0.110	-0.304	-0.409	0.430	0.040	0.707	7.226	92.774	4.7
12	947.809	0.003	Braided	0.055	0.568	-0.211	-0.257	-0.399	0.396	0.121	0.467	4.804	95.196	2.5
13	837.485	0.003	Braided	-0.040	0.442	-0.258	0.333	-0.338	0.306	0.118	0.438	3.165	96.835	1.5
14	752.589	0.004	Braided	0.011	0.410	-0.143	-0.183	-0.264	0.277	0.056	0.685	2.740	97.260	4.7
15	769.8	0.004	Braided	-0.016	0.421	-0.709	0.041	-0.333	0.335	0.028	0.315	3.221	96.779	6.7
16	1005.376	0.004	Braided	-0.034	0.383	-0.208	0.047	-0.279	0.287	0.000	0.051	3.762	96.238	6.9
17	949.805	0.004	Braided	-0.024	0.422	0.407	0.225	-0.290	0.279	0.002	0.325	10.574	89.426	3.9
18	791.788	0.004	Braided	-0.002	0.417	-0.337	0.026	-0.316	0.320	0.000	0.031	3.761	96.239	3.3
19	826.125	0.003	Braided	-0.049	0.392	-0.435	0.278	-0.298	0.296	0.000	0.114	3.412	96.588	3.0
20	712.768	0.004	Braided	-0.023	0.392	0.119	0.127	-0.260	0.267	0.000	0.021	1.879	98.121	2.8
21	793.296	0.004	Braided	-0.024	0.412	0.095	0.010	-0.275	0.302	0.006	0.148	2.890	97.110	3.3
22	703.097	0.003	Braided	0.053	0.518	0.076	-0.417	-0.343	0.378	0.016	0.660	9.245	90.755	1.7

Table 4.2 continued.

Reach number	Width (m)	Slope (m/m)	Planform Type	Parameters of the Bed Elevation Frequency Distribution					Vegetation cover				Braiding Index	
				Median (m)	Standard deviation (m)	Kurtosis	Skewness	Lower quartile (m)	Upper quartile (m)	% taller than 10m	% taller than 5m	% taller than 1m		% no vegetation
23	619.594	0.003	Braided	-0.161	0.654	0.112	0.814	-0.489	0.356	0.309	3.542	21.892	78.108	2.6
24	701.988	0.004	Braided	-0.012	0.490	-0.733	0.006	-0.391	0.409	0.044	0.835	6.817	93.183	2.1
25	570.253	0.003	Braided	-0.054	0.360	0.716	0.434	-0.243	0.249	0.000	0.162	2.434	97.566	6.1
26	625.403	0.003	Braided	0.008	0.381	-0.044	0.152	-0.264	0.258	0.000	0.392	5.196	94.804	2.8
27	551.27	0.003	Braided	-0.008	0.456	0.341	-0.172	-0.312	0.337	0.203	0.909	5.490	94.510	2.9
28	677.062	0.002	Braided	-0.120	0.556	0.898	0.892	-0.372	0.298	0.146	3.511	27.244	72.756	2.8
29	577.669	0.002	Braided	-0.050	0.515	2.256	1.108	-0.285	0.169	0.536	5.839	18.368	81.632	2.9
30	806.242	0.002	Braided	-0.102	0.853	0.410	0.779	-0.644	0.441	2.364	12.848	31.539	68.461	2.9
31	881.413	0.003	Braided	-0.004	0.720	1.659	0.475	-0.447	0.438	2.442	8.272	22.377	77.623	3.6
32	630.426	0.003	Braided	-0.044	0.818	0.759	0.567	-0.511	0.458	1.107	9.204	23.069	76.931	3.0
33	464.754	0.003	Transitional	-0.006	0.497	0.294	-0.202	-0.300	0.351	1.588	7.581	13.466	86.534	2.6
34	465.487	0.003	Transitional	0.019	0.637	0.023	-0.149	-0.372	0.473	7.876	16.720	25.983	74.017	2.5
35	332.086	0.002	Meandering	-0.017	0.533	1.512	0.599	-0.342	0.268	0.728	1.957	9.592	90.408	2.0
36	277.641	0.002	Meandering	-0.080	0.867	-0.344	0.411	-0.588	0.480	5.499	9.228	20.312	79.688	1.3

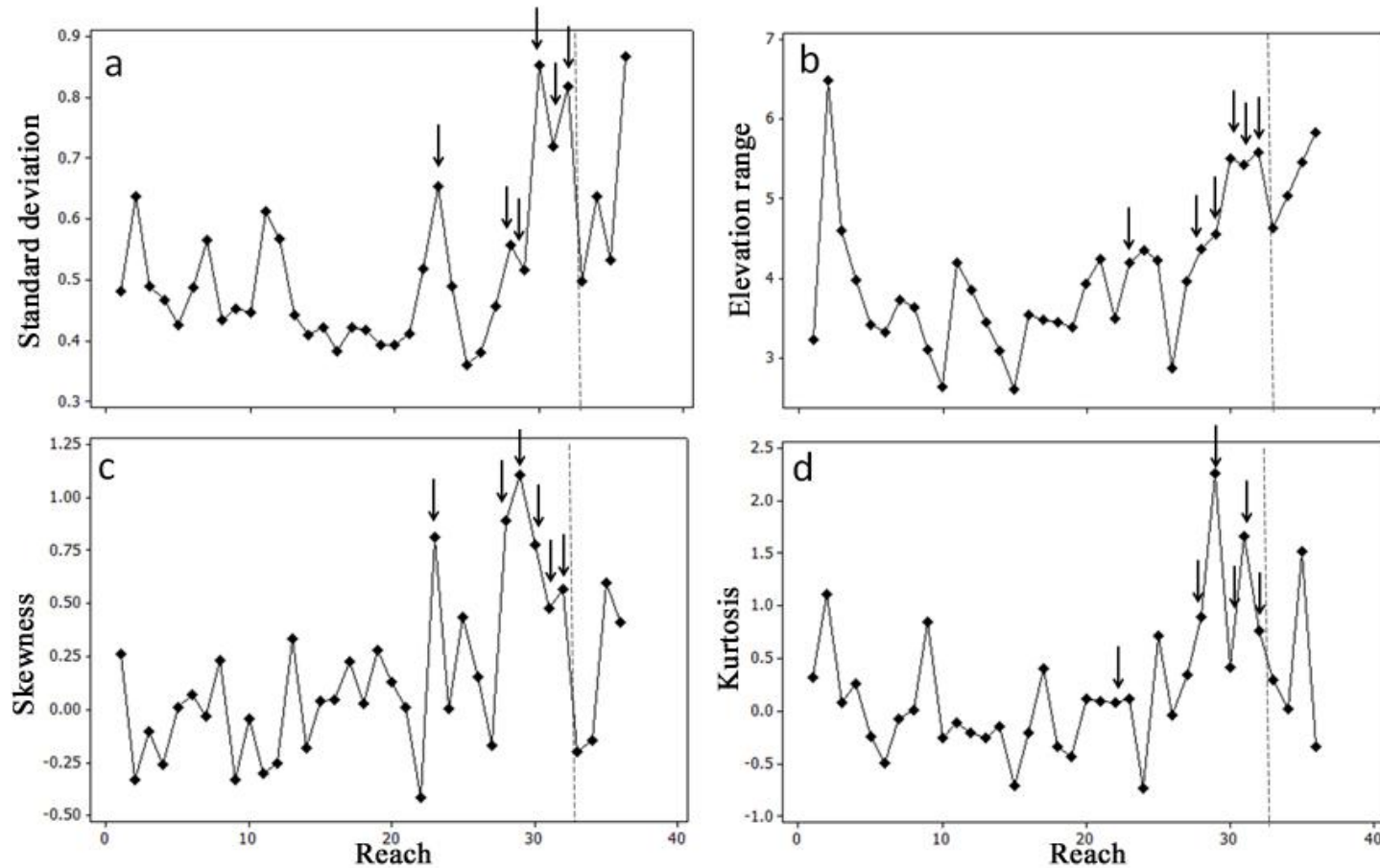


Figure 4.7 Changes in a: standard deviation (m), b: elevation range (m), c: skewness and d: kurtosis from reach 1 downstream to reach 36. The dashed line denotes the downstream limit of the braided reaches (reach 1 to reach 32). The arrows indicate reaches 23, 28, 29, 30, 31, 32, which are discussed later in section 4.4.2.

4.4.2 Relationships Among Bed Morphological Properties Across the 1 km Reaches

Correlations among the main morphological variables across all 36 reaches are presented in Table 4.3. To link with the flume experiments of Chapter 3, the channel width was included in the analysis as well as several properties of the bed elevation frequency distribution (median elevation, standard deviation, skewness, kurtosis, and elevation range).

Table 4.3 Product moment correlations among channel width and properties of the bed elevation frequency distribution (median elevation, standard deviation, skewness, kurtosis, and elevation range) across the 36 1km reaches and the 34 braided reaches (emboldened correlations are statistically significant ($p < 0.05$), italicised correlations are not statistically significant).

	Channel width	Median elevation	Standard deviation	Skewness	Kurtosis
All reaches (n=36)					
Median elevation	<i>0.135</i>				
Standard deviation	<i>-0.289</i>	<i>-0.279</i>			
Skewness	<i>-0.169</i>	-0.783	0.324		
Kurtosis	<i>-0.278</i>	<i>-0.183</i>	<i>0.256</i>	0.466	
Elevation range	-0.357	<i>-0.269</i>	0.749	<i>0.294</i>	0.516
Braided reaches (n=32)					
Median elevation	<i>0.138</i>				
Standard deviation	<i>-0.081</i>	<i>-0.241</i>			
Skewness	<i>-0.156</i>	-0.800	0.338		
Kurtosis	<i>-0.311</i>	<i>-0.239</i>	0.391	0.466	
Elevation range	<i>-0.079</i>	<i>-0.278</i>	0.731	<i>0.289</i>	0.586

Despite the small sample size of only 36 reaches, correlations between skewness and each of median elevation, standard deviation and kurtosis are all statistically significant. However channel width is only significantly correlated with the range in elevation of the bed, which is also significantly correlated with the standard deviation and kurtosis. This may suggest that there was insufficient range in width to show a strong correlation with bed morphology, particularly as only two of the reaches could be strictly described as single thread. When only braided reaches are considered (Table 4.3) all of the correlations strengthen apart from those with channel width. The latter would be

expected as the range in channel widths has been reduced even further by removing the four meandering and transitional reaches from the data set.

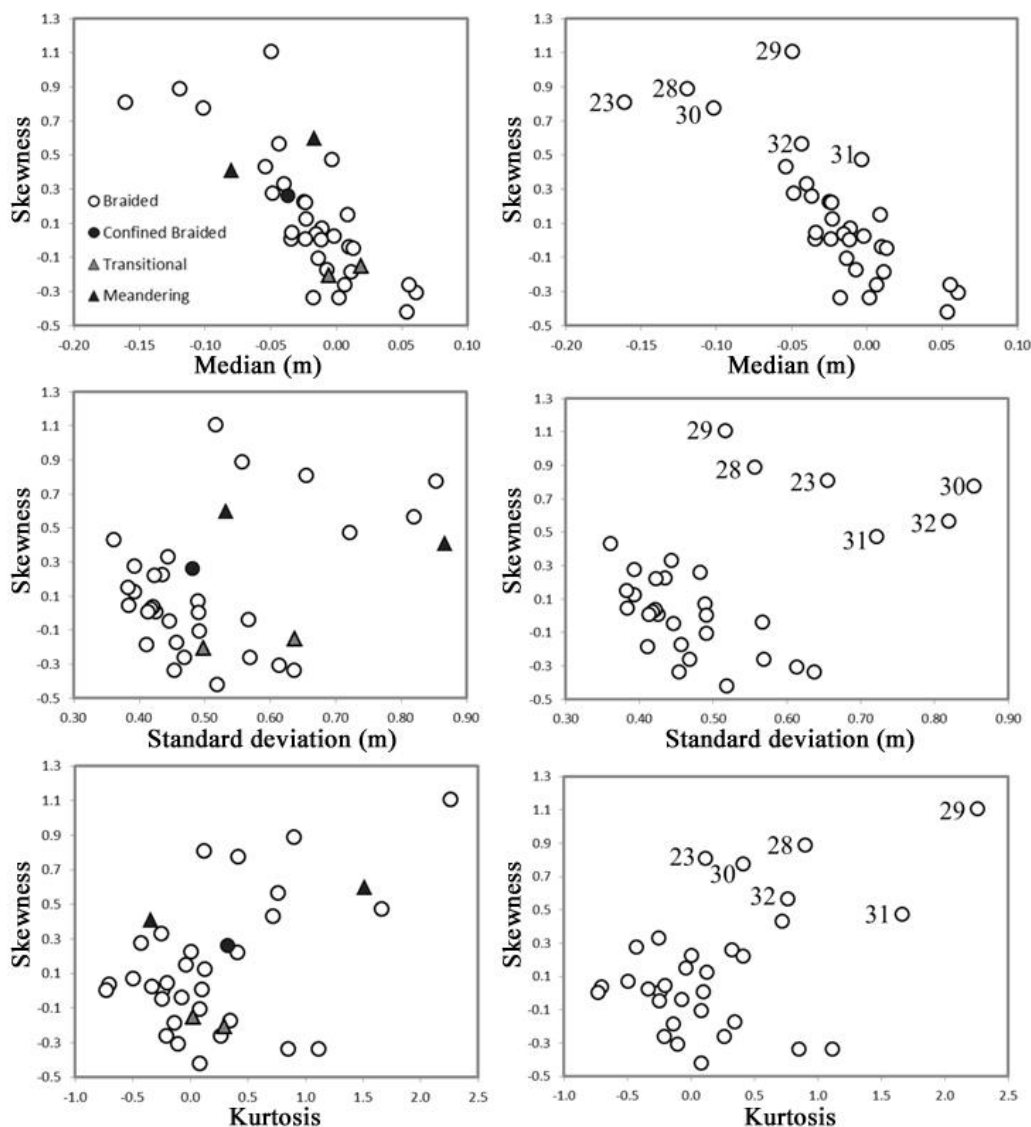


Figure 4.8 Scatter plots of skewness of the bed elevation frequency distribution against the median (m), standard deviation (m), and kurtosis. Left: scatter plots include all 1 km reaches; Right: scatter plots for braided reaches only, with outlier reaches indicated by their reach number.

The significant correlations among the other morphological properties require a more detailed examination, in particular the summary properties of distribution shape (median, standard deviation, skewness and kurtosis). In Figure 4.8 scatter plots illustrate relationships between skewness of the bed elevation frequency distribution and the median, standard deviation, and kurtosis. The three plots on the left show data from all reaches, whereas the three plots on the right show data only for unconfined braided reaches. The broad patterns are similar for all reaches and for only the braided reaches, showing negative associations between skewness and both the median and standard deviation of the bed frequency distribution, and a positive association between skewness and kurtosis, with a few notable outliers among the most downstream braided reaches (23, 28, 29, 30, 31, 32). The standard deviation, skewness and kurtosis of these outlier reaches all seem to be generally higher than other reaches. This is confirmed by the arrows locating these reaches in Figure 4.7. Furthermore, the significant positive association between skewness and kurtosis of the braided reaches disappears when the outlier reaches are excluded ($r = 0.083$, $p = 0.679$).

4.4.3 Relationships Between Vegetation and Bed Morphological Properties Across the 1 km Reaches

Table 4.4 summarises the correlations between vegetation and morphological properties of all reaches and only the braided reaches. The correlations tend to be positive between all measures of vegetation presence (% taller than 1 m, % taller than 5 m, % taller than 10 m) and the standard deviation, kurtosis and skewness of the bed elevation distribution and negative between all measures of vegetation presence and the median. Correlations between all four morphology parameters and % unvegetated is the exact inverse of the correlations with % taller than 1 m, since this is the threshold used to indicate the presence of a vegetation cover. All correlations become stronger when only braided reaches are considered, and all correlations apart from one are statistically significant.

Figures 4.9 and 4.10 plot the four vegetation cover variables (unvegetated, % vegetation > 1 m, % vegetation > 5 m, % vegetation > 10 m) against the median and standard deviation of the bed elevation frequency distribution for all 1 km reaches (Figure 4.9) and for braided reaches only (confined and unconfined, Figure 4.10). Reaches 23, 28, 29, 30, 31, and 32, which appeared as outliers in the scatter plots of Figure 4.8, are indicated on the scatter plots of Figure 4.10.

Table 4.4 Product moment correlation coefficients between channel bed morphological and vegetation variables for all reaches and only braided reaches (emboldened correlations are statistically significant ($p < 0.05$), italicised correlations are not statistically significant).

	Median	Standard deviation	Kurtosis	Skewness
All reaches (n=36)				
% taller than 10 m	<i>-0.065</i>	0.576	<i>0.045</i>	<i>0.116</i>
% taller than 5 m	<i>-0.236</i>	0.713	<i>0.257</i>	0.350
% taller than 1m	-0.510	0.762	0.408	0.504
% unvegetated	0.510	-0.762	-0.408	-0.504
Braided reaches (n=32)				
% taller than 10 m	<i>-0.233</i>	0.735	0.443	0.445
% taller than 5 m	-0.413	0.793	0.499	0.619
% taller than 1m	-0.579	0.768	0.526	0.595
% unvegetated	0.579	-0.768	-0.526	-0.595

The two meandering reaches appear as outliers on plots a, b, e and f in Figure 4.9, indicating that their percentage cover of taller vegetation (> 5m and > 10 m) is higher than would be expected for the median and standard deviation of their bed elevation frequency distribution. However, plots c, d, g and h show fairly clear associations between vegetation cover and the median and standard deviation of the bed elevation frequency distribution for all reaches and there are statistically significant correlations with the standard deviation (+/-0.762) and median (+/-0.510).

When only the braided reaches are considered, the strength of the associations between vegetation and morphology variables strengthens (Table 4.4, Figure 4.10). However, plots a, b, e, f (Figure 4.10) illustrate that the outlier reaches identified in Figure 4.9, show higher proportions of more mature vegetation (> 5m, > 10m) than the other reaches, and this is particularly notable for reaches 30, 31 and 32, which are located immediately upstream of the transitional (33 and 34) and meandering (35 and 36) reaches.

Figures 4.11 and 4.12 plot the four vegetation cover variables (unvegetated, %vegetation > 1m, %vegetation > 5m, % vegetation > 10m) against the kurtosis and

skewness of the bed elevation frequency distribution for all 1 km reaches (Figure 4.11) and for braided reaches only (Figure 4.12). Reaches 23, 28, 29, 30, 31, and 32, which appeared as outliers on the plots in Figure 4.9 are indicated on the scatter plots of Figure 4.12.

When the four vegetation cover variables are plotted against the kurtosis and skewness of the bed elevation frequency distribution (Figure 4.11), the meandering reaches once again stand out as having a higher more mature vegetation cover ($> 5\text{m}$, $> 10\text{m}$, Figure 4.11 a, b, e, f) than might be expected for their morphology in comparison with other reaches. Several braided reaches plot in the same area of these scatter plots as the meandering reaches, and when the braided reaches are plotted alone (Figure 4.12), these braided reaches with more mature vegetation are identified as reaches 30, 31 and 32.

Overall, while some reaches appear as outliers when the two measures of taller (more mature vegetation) are considered, when the proportion vegetated or unvegetated are used as measures of vegetation, the braided reaches show a strong association with morphological properties, particularly with standard deviation (Figure 4.9 c and d) and skewness (Figure 4.11 g and h) of the bed elevation frequency distribution.

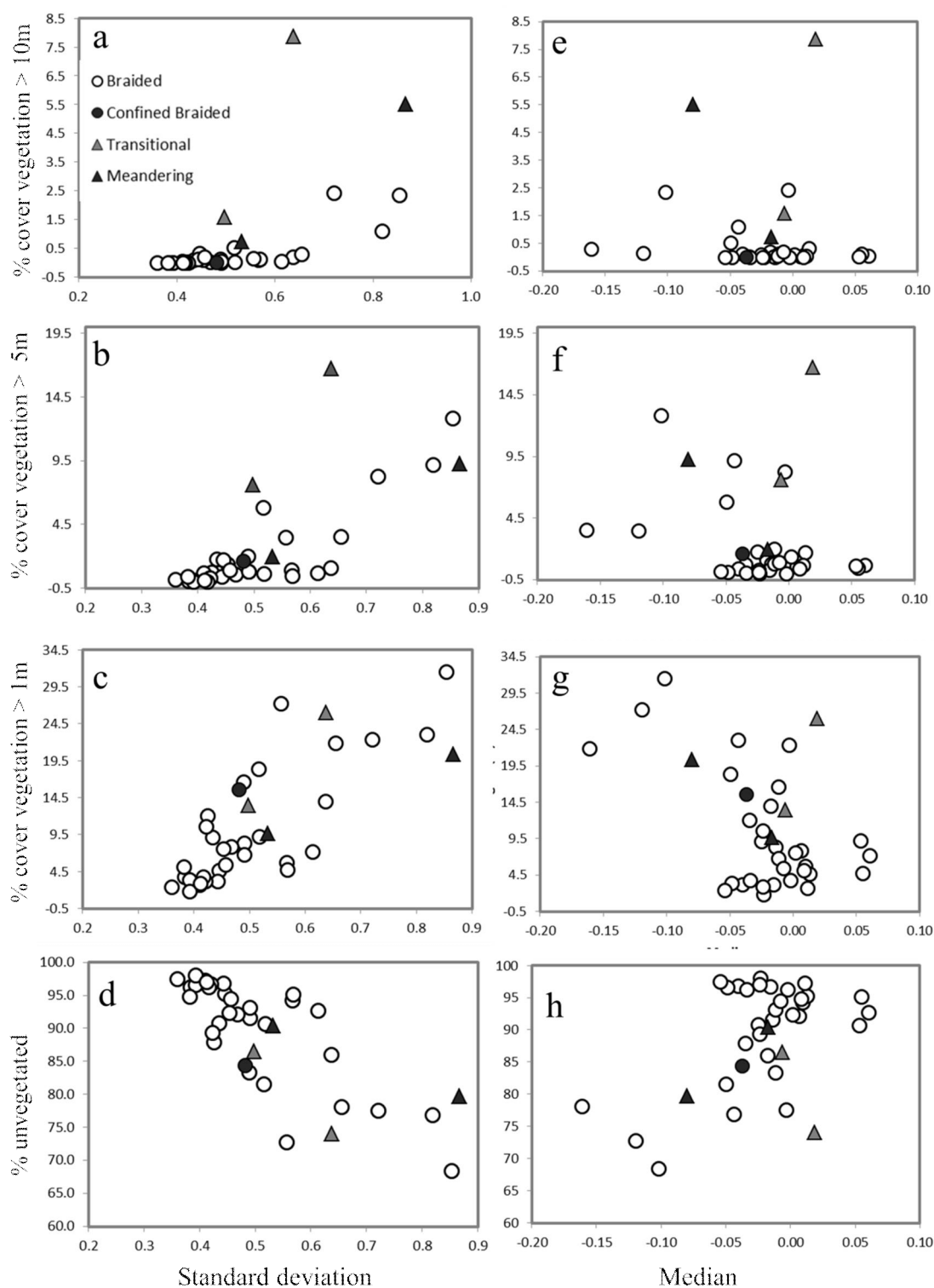


Figure 4.9 Scatter plots of vegetation cover variables (unvegetated, %vegetation > 1m, %vegetation > 5m, % vegetation > 10m) against the standard deviation (a to d) and the median (e to h) of the bed elevation frequency distribution for all 1 km reaches.

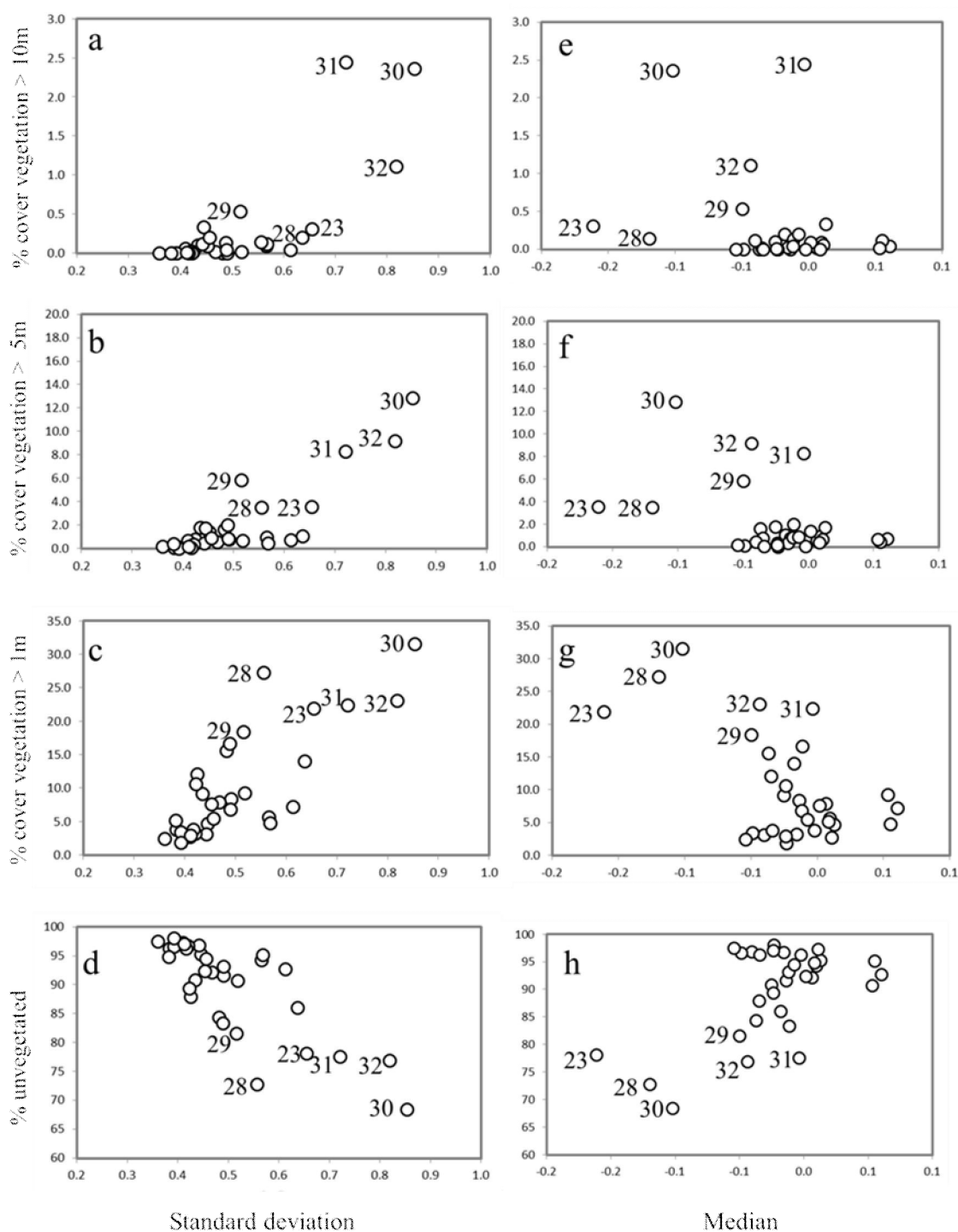


Figure 4.10 Scatter plots of vegetation cover variables (unvegetated, %vegetation > 1m, %vegetation > 5m, % vegetation > 10m) against the standard deviation (a to d) and the median (e to h) of the bed elevation frequency distribution for braided reaches only.

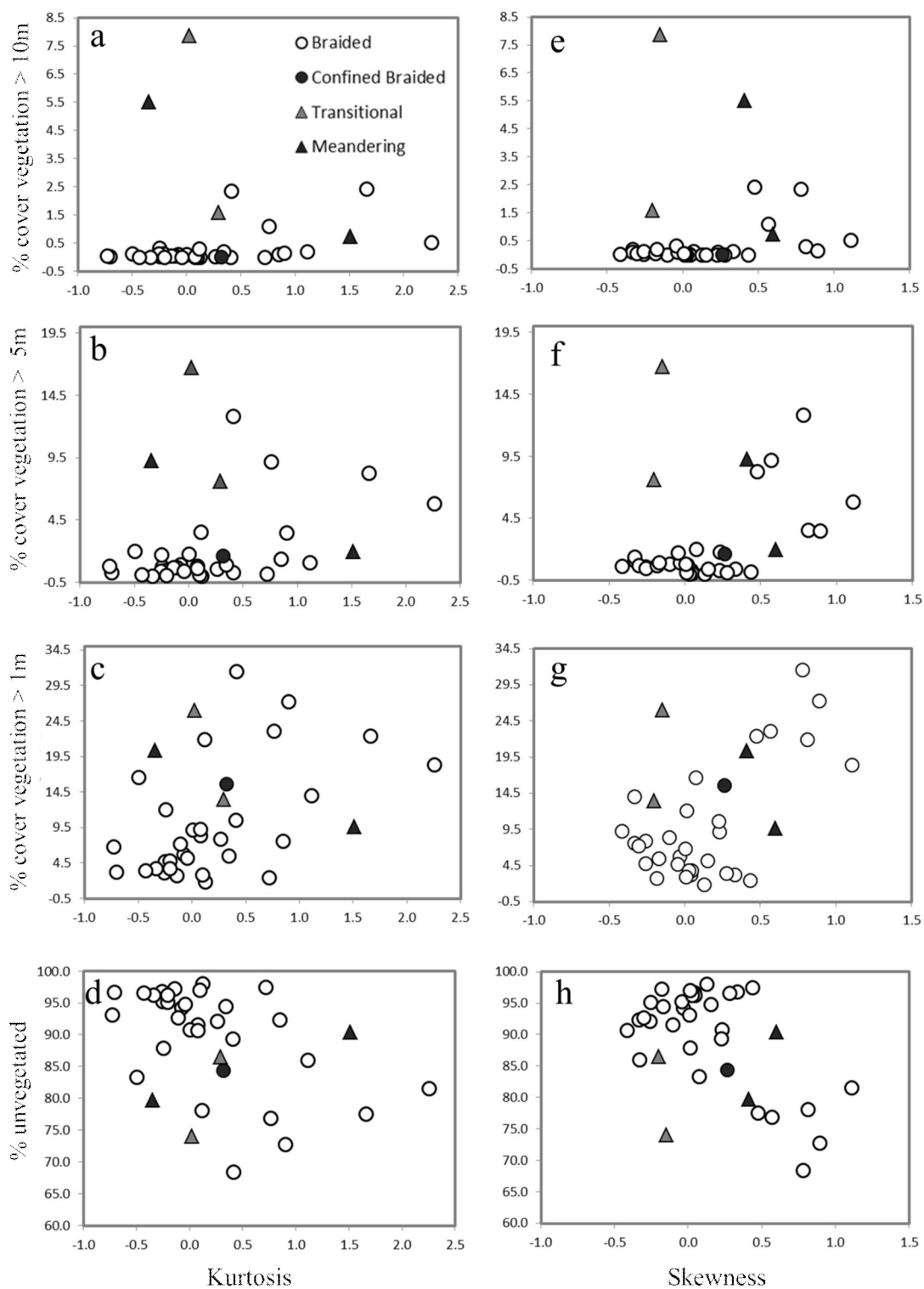


Figure 4.11 Scatter plots of vegetation cover variables (unvegetated, %vegetation > 1m, %vegetation > 5m, % vegetation > 10m) against the kurtosis (a to d) and the skewness (e to h) of the bed elevation frequency distribution for all 1 km reaches.

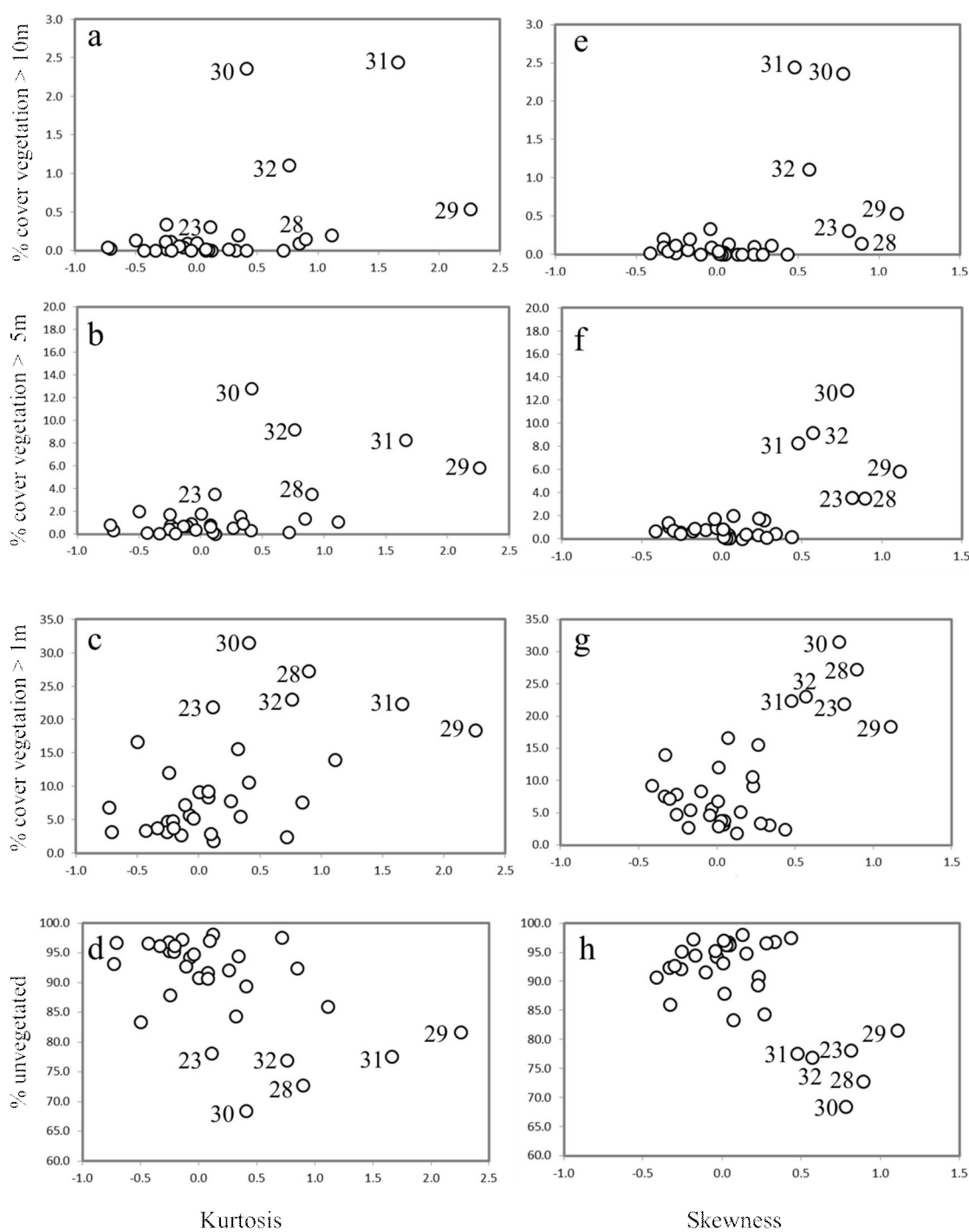


Figure 4.12 Scatter plots of vegetation cover variables (% unvegetated, %vegetation > 1m, %vegetation > 5m, % vegetation > 10m) against the kurtosis (a to d) and the skewness (e to h) of the bed elevation frequency distribution for braided reaches only.

The downstream pattern of the four vegetation cover variables from reach 1 to reach 36 are illustrated in Figure 4.13. The Figure shows a gradual downstream decrease in the percentage of the braid plain that is vegetated to around reach 20, after which the vegetated area varies greatly but generally increases sharply through the remaining braided reaches (21 to reach 32) and then remains high through the transitional and meandering reaches (33 to 36). This broad pattern is maintained for the percentage of the braid plane under vegetation taller than 5m, although the percentage cover between reaches 1 to around reach 20 is much lower than the downstream reaches. The cover of vegetation taller than 10 m is negligible downstream to reach 28, where it starts to increase, with the highest percentages found in the transitional and meandering reaches.

Figures 4.14 and 4.15 show maps of the vegetation distribution on the braid plain in comparison with the DTM for selected reaches. Figure 4.14 shows nine reaches in the upstream part of the study area (downstream to reach 22). In general, vegetation is patchy, with many small areas indicative of pioneer and small building islands (Gurnell et al., 2001). These patches appear in groups on higher bar surfaces, and in reaches 8, 11 and 22, the patches have aggregated to form larger areas of vegetation containing some taller areas of trees. Figure 4.15 shows nine reaches all located downstream of reach 22. Although numerous small patches of vegetation are present, in these downstream reaches there are sizeable areas of continuous vegetation taller than 5m and containing discrete patches taller than 10 m. These extended areas of vegetation are particularly noticeable in reaches 23, 28, 29, 30, 31, 32 and 36. Reach 36 shows a discrete patch of tall vegetation located on the inside of the bend of this meandering reach and coincident with the highest area of a point bar on the DTM. The growth of vegetation on point bars in association with meander migration appears to explain the taller vegetated areas in the transitional and meandering reaches (33 to 36). The other reaches with discrete patches of > 5 m and > 10 m vegetation are braided reaches, and the vegetated areas are on the highest parts of the braid plain and form major established islands.

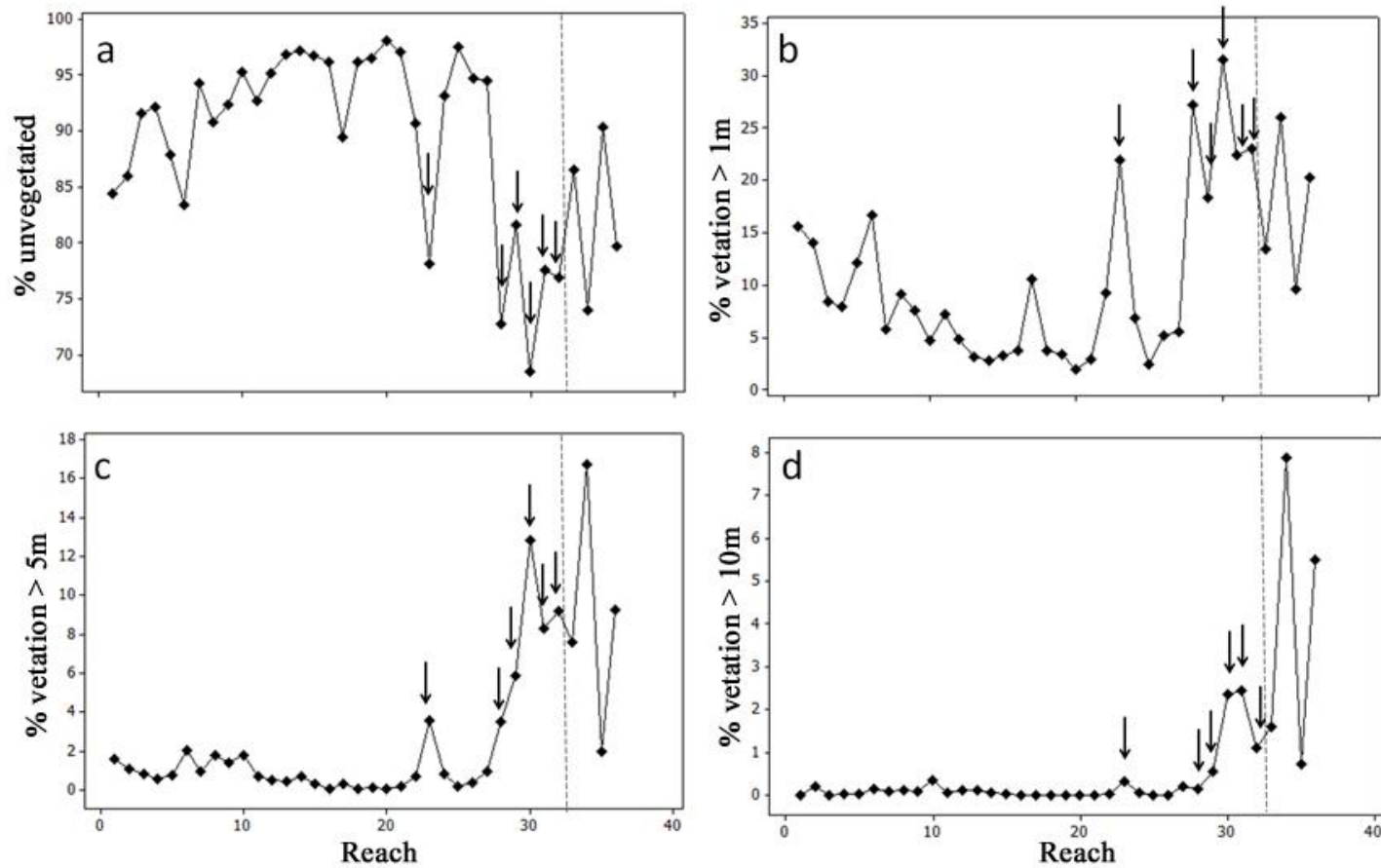


Figure 4.13 Changes in the cover of vegetation across the braid plain (a: % unvegetated, b: % vegetated, c: % with vegetation taller than 5 m; d: % with vegetation taller than 10 m) from reach 1 downstream to reach 36. The dashed lines denotes the downstream limit of the braided reaches (reach 1 to reach 32). The arrows indicate reaches 23, 28, 29, 30, 31, 32.

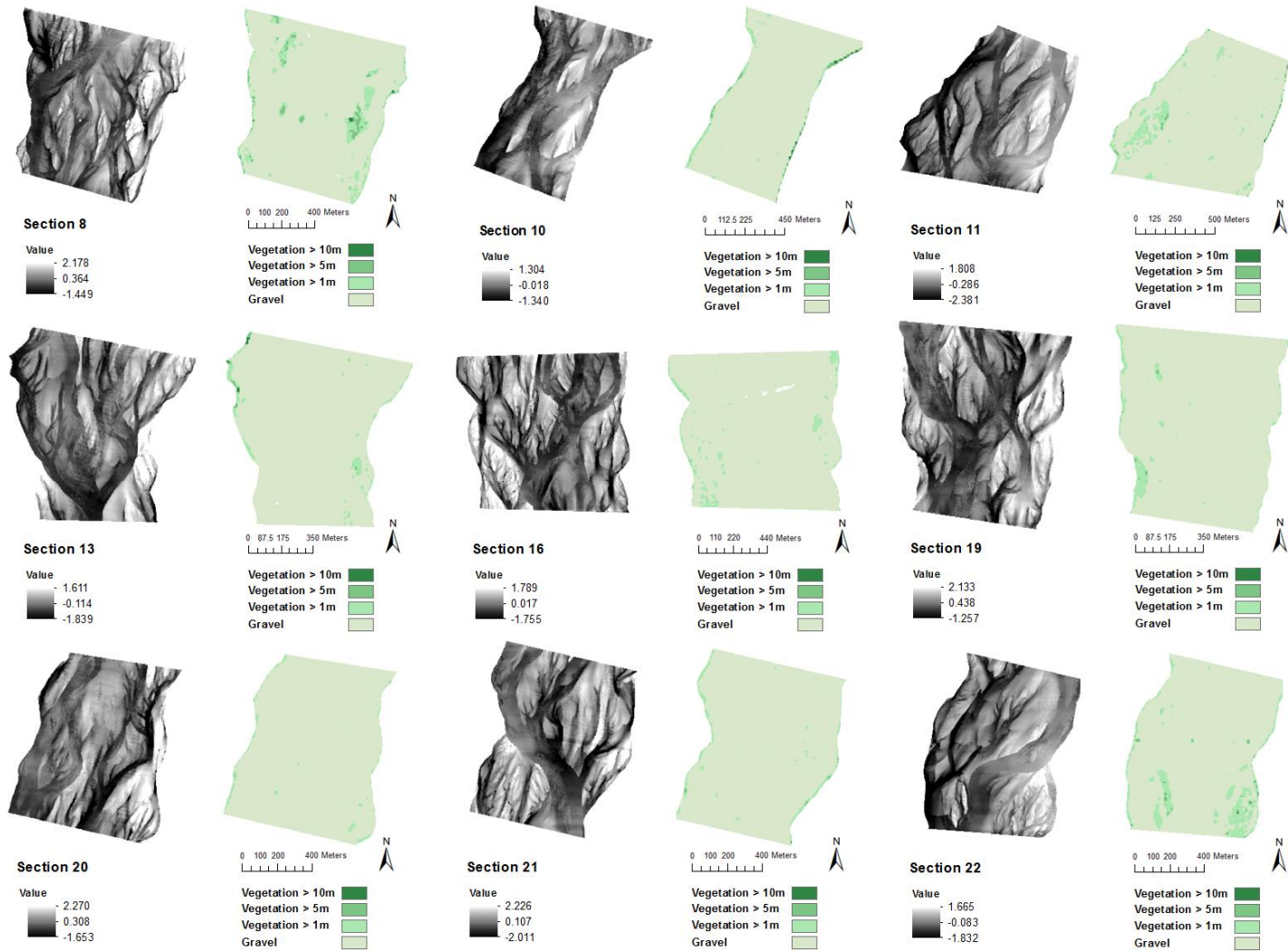


Figure 4.14 DTM and vegetation cover maps for nine of the 1 km reaches upstream of reach 23.

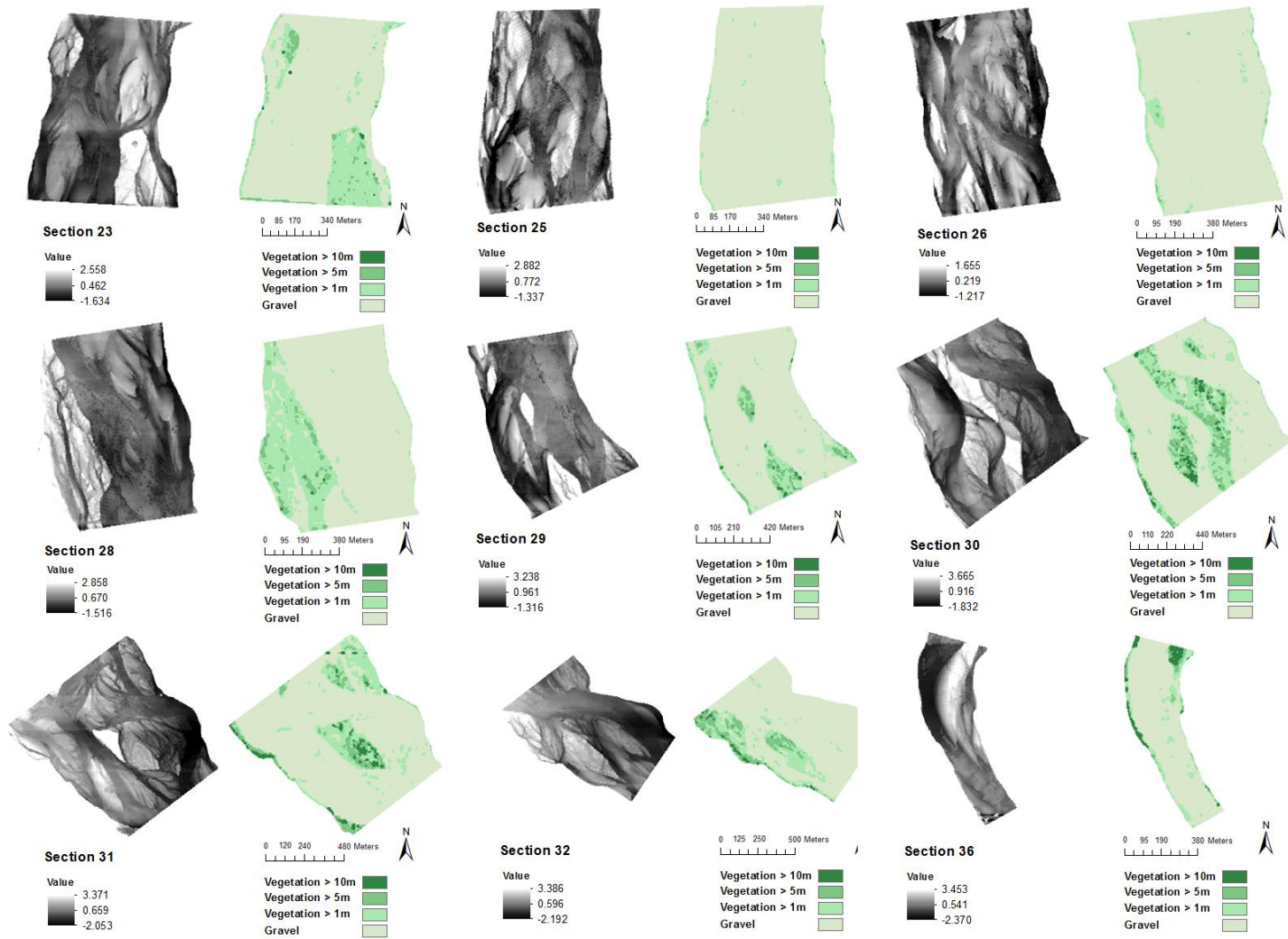


Figure 4.15 DTM and vegetation cover maps for nine of the 1 km reaches downstream of reach 22.

Figures 4.16 and 4.17 provide further topographic information on braided reaches 23, 28, 29, 30, 31 and 32, which show more extensive patches of taller vegetation than the other braided reaches. The cross profiles for each reach illustrate that these more mature vegetated patches are located on the highest areas of the braid plain and usually show sharp boundaries with the remainder of the braid plain. For example in reach 23, the main vegetated areas are crossed on the left side (right bank) of transects 1 and 2 and on the right side of transects 4, 5 and 6. In each case distinct tabular structures are found, which are elevated 1.5 m above the surrounding braid plain surface. In reach 28, there is an area of the braid plane along the left (right bank) of the reach that is elevated approximately 1.5 m above the rest of the braid plane. In reach 29, two central islands support distinct areas of taller vegetation and have surfaces approximately 1.5 m above the braid plane (transects 3 and 4 for a smaller upstream island and transect 6 for the downstream island). Similarly two heavily vegetated areas in reach 30 correspond to tabular island surfaces elevated approximately 2.5 m and 2 m above the surrounding braid plane. The small patch of taller vegetation in reach 31 is located on a tabular area that protrudes up to 2.5 m above the rest of the braid plane, whereas in reach 32 there is an elevated area on the left side (right bank) of the channel that is less tabular than the features in the other reaches, but is elevated some 1.5 metres above the rest of the channel bed.

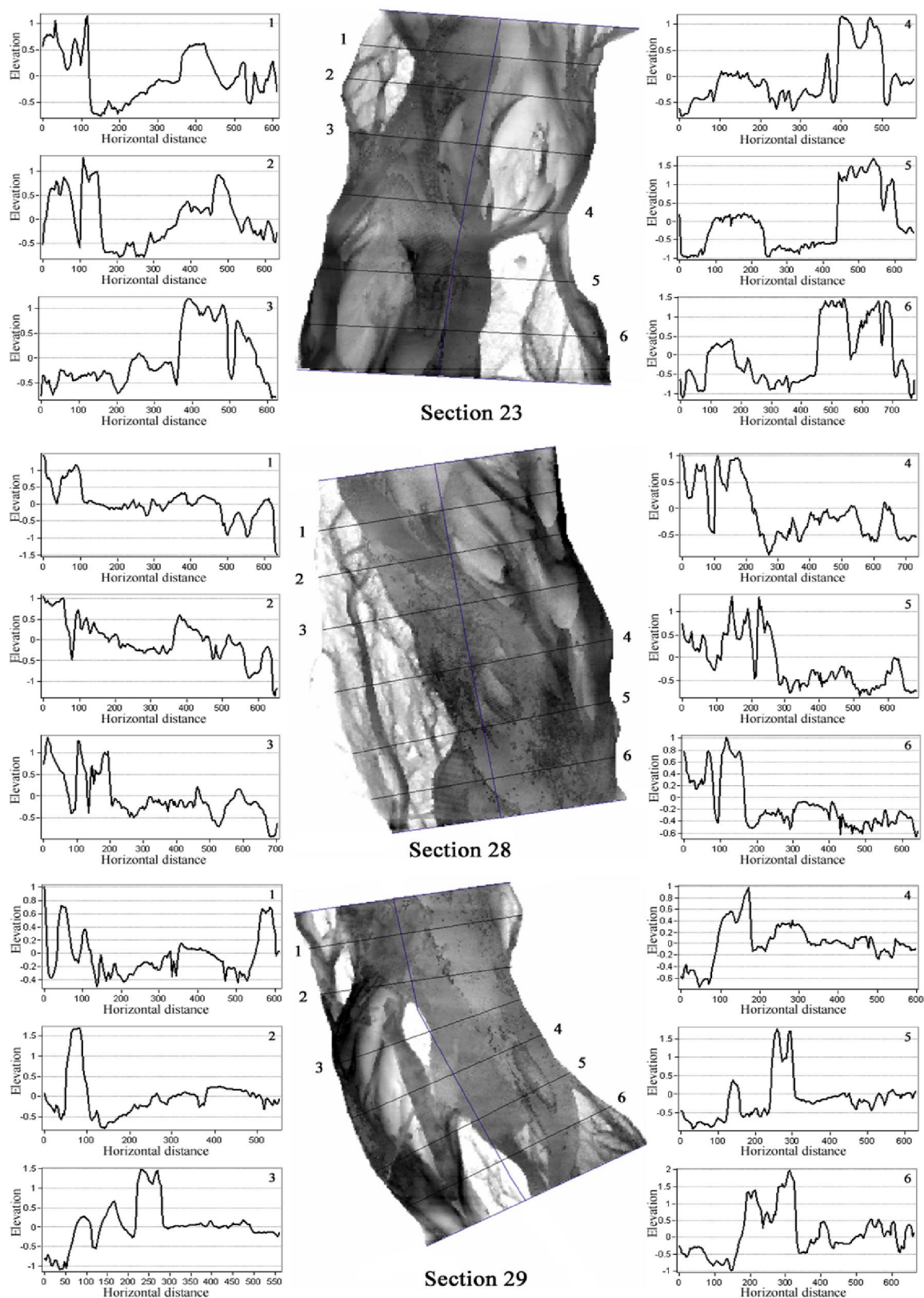


Figure 4.16 DTM and cross profiles for reaches 23, 28 and 29 (note differences in the scales of the cross-sectional profiles).

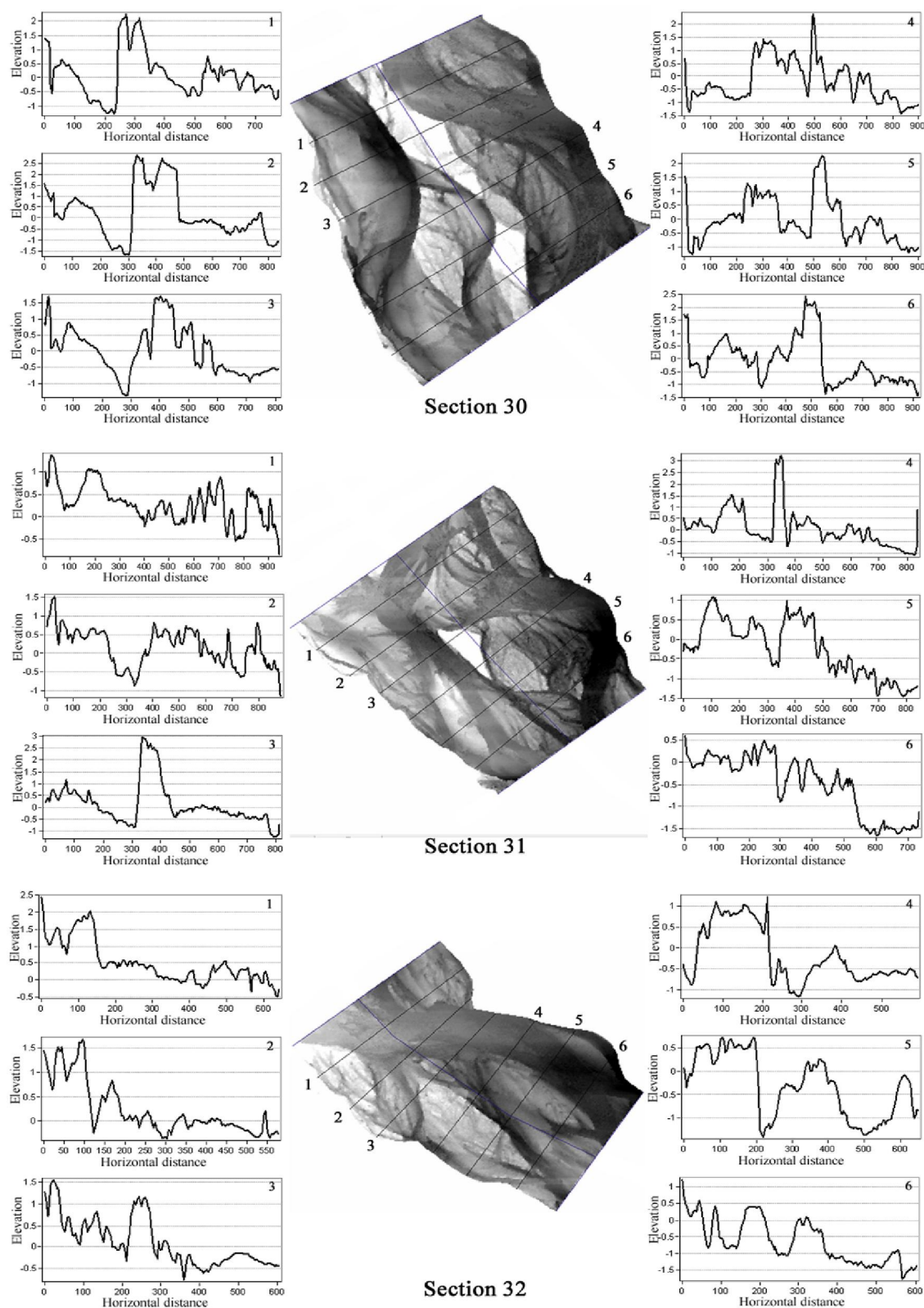


Figure 4.17 DTM and cross profiles for reaches 30, 31 and 32 (note differences in the scales of the cross-sectional profiles).

4.5 DISCUSSION AND CONCLUSIONS

4.5.1 River Bed Topography

Analysis of bed elevation frequency distributions from a lidar survey of 36 1km reaches of the middle-lower Tagliamento river has revealed five basic forms, of which two (single, symmetrical peak, single peak with a ‘bump’) are particularly common. Where a ‘bump’ or secondary peak is observed, this is almost always observed on the right side of the elevation frequency distribution, indicating a locally more extensive area of an elevation band that is higher than the median elevation. In many reaches, these elevation bands are typically located between 1 and 1.5 m higher than the elevation of the main peak of the distribution.

There was insufficient variation in the widths of the channels investigated on the Tagliamento to explore associations between bed morphology and channel width for comparison with the analyses in Chapter 3. However, summary statistics extracted from the elevation frequency distributions show statistically significant correlations among the median, standard deviation, skewness and kurtosis which strengthen when only braided reaches are considered. Figure 4.18 compares scatter plots between skewness and median, standard deviation, and kurtosis of the bed elevation frequency distribution for the 36 Tagliamento reaches and the 27 experiment channel morphologies presented in Chapter 3. Although the ranges in the axes are completely different, if one compares the distributions of the unconfined braided reaches on the left plots with those of the bed morphologies with mid-channel bars on the right plots (both represented by white circles), similar trends are apparent in the upper two pairs of plots, particularly when the outlier braided reaches are excluded from the Tagliamento data set. However, the Tagliamento braided reaches show a much greater variability in their skewness than the experimental reaches, even when the outliers are excluded. Of course the comparison is not robust because of the completely different scales of the two data sets; the inherent variability among the Tagliamento reaches in slope, particle size, and probably sediment supply; and the very small length to width ratios of the Tagliamento reaches in comparison with the experimental channels. An additional factor that may influence the form of the Tagliamento reaches is vegetation (see 4.5.2).

There are also distinct downstream patterns in the standard deviation, skewness, kurtosis and elevation range of the bed elevation frequency distributions. Although there is local reach-to-reach variability, the middle reaches (5-22) generally show the

lowest combined values of all four variables, the upstream reaches (1-4) showing a higher elevation range and kurtosis than most of the middle reaches and the lower reaches (23-36) showing generally higher values of all four variables than the middle and upstream reaches.

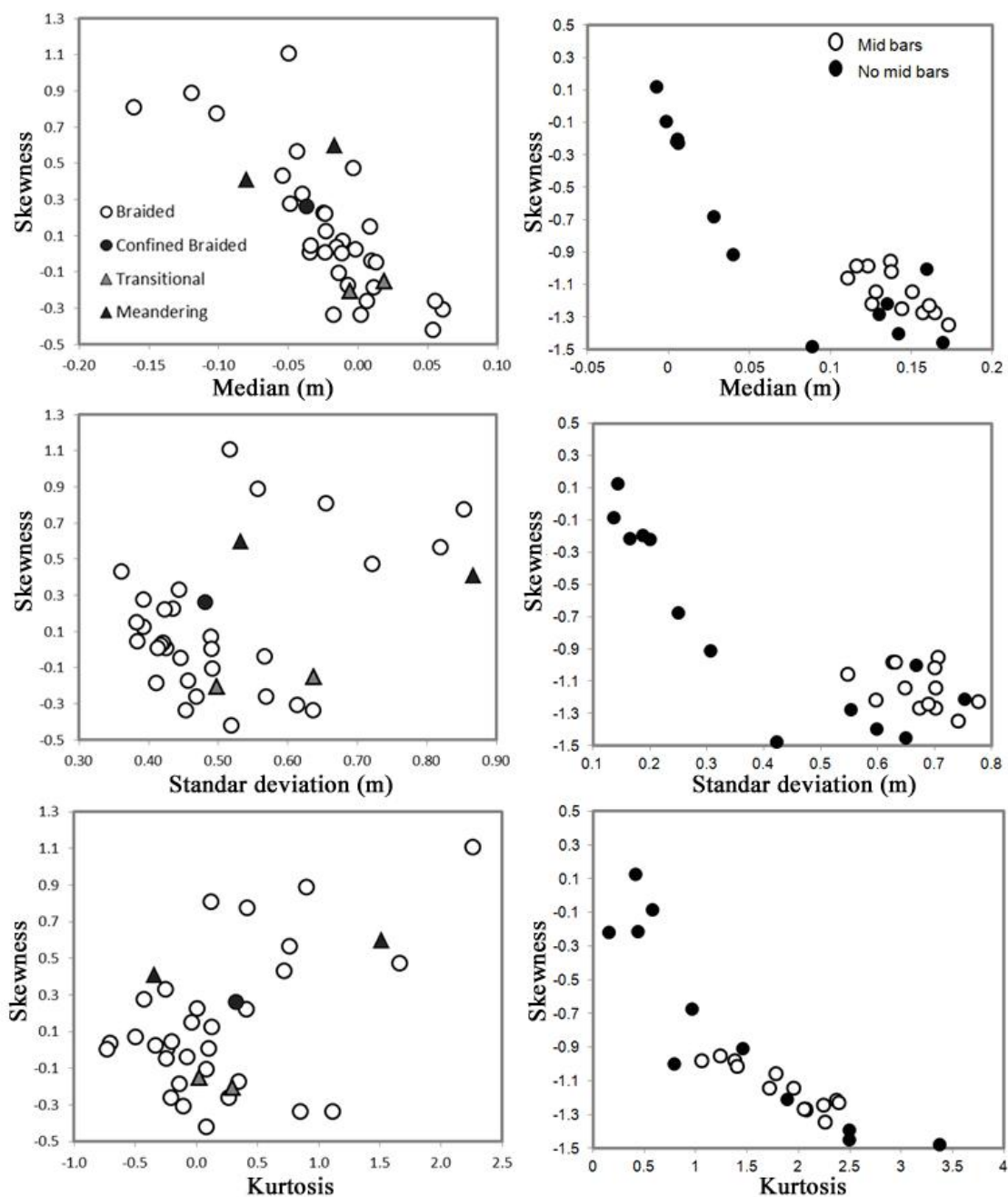


Figure 4.18 Scatter plots for the 36 Tagliamento reaches (left) and the 27 flume experiments (right) illustrating relationships between skewness and the median, standard deviation and kurtosis of the bed elevation frequency distribution.

4.5.2 Associations Between Bed Topography and Vegetation

Properties of the vegetation cover were also extracted from lidar data.

Strong correlations were identified between % unvegetated, % vegetated and taller than 1m, % vegetated and taller than 5 m, and % vegetated and taller than 10 m, and the median, standard deviation, skewness and kurtosis of the bed elevation frequency distribution. When only the braided reaches are considered all of the correlations apart from that between the median of the bed elevation frequency distribution and % vegetated taller than 10 m are statistically significant. These vegetation – morphology correlations (Table 4.4) are all stronger than correlations among the morphological properties of the reaches (Table 4.3) whether all 36 reaches or just the 32 braided reaches are considered.

As with the bed morphology, there are also distinct downstream variations in the vegetation indices (Figure 4.13). The middle reaches (7-22) show the lowest vegetation cover. The upper reaches (1-6) show a higher cover of vegetation (taller than 1m) than the middle reaches, although the cover shows a declining trend downstream through these six reaches. The downstream reaches (23 to 36) show the highest cover of all three vegetation heights (taller than 1 m, taller than 5 m, taller than 10 m), with a generally increasing cover of all three from reach 23 downstream to reach 36. Therefore, both morphology and vegetation cover show broadly similar downstream trends, but those for vegetation cover are more marked and show clearer transitions than those for the morphological variables. This association between vegetation and morphology has been explained by Gurnell (2014) to be associated with the rate of vegetation growth, which varies with groundwater levels in the alluvial aquifer. There is down-welling and then up-welling of groundwater through the 36 studied reaches, often leading to the river drying up in mid-summer in the most central reaches of the study area. Therefore, the downstream trends in both morphology and vegetation cover may reflect the vigour of the vegetation and thus its potential to influence the morphology of the braid plain.

Overall the vegetation is shorter and sparser than that observed by Bertoldi et al. (2011a) but this may be explained by several factors:

1. The lidar data used in the present analysis was collected in April 2001, which is only a few months after the largest flood on the Tagliamento since 1980, which

occurred on 7 November 2000. This bank full event would have removed much of the vegetation that was present in the braid plain. There was no significant flood between the April 2001 lidar survey that is analysed here and the May 2005 lidar survey that was analysed by Bertoldi et al., (2011a), giving over four years of uninterrupted vegetation growth by the time of the latter lidar survey.

2. The lidar data used in the present analysis was obtained earlier in the year than the 2005 survey. This difference in the month of survey is critical, since it is the period of the year when foliage starts to appear on the riparian trees. As a result, the point cloud of the 2001 lidar survey is far less likely to intercept vegetated surfaces than that of the 2005 survey.
3. Although lidar surveys vary in the density of their point cloud, providing a further possible explanation for differences in the representation of the vegetation canopy, there was very little difference in point cloud density between the 2001 and 2005 surveys.

Correspondence between vegetation and morphology is also likely to be weaker in 2001 because the large flood only five winter months before the lidar survey would not only have removed much of the vegetation cover but it would also have reshaped the braid plane. By 2005 vegetation cover would be taller, uprooted trees and pioneer islands left after the 2001 flood would have had time to develop and accumulate fine sediment from flow pulse and wind storm events (Gurnell et al., 2008), whereas those islands that survived the flood would also have had time for their vegetation cover and morphology to start to recover.

In summary, the present research has shown similar associations between bed morphology and vegetation to those revealed by Bertoldi et al. (2011a) but, for the reasons given above, the associations are not as strong. Nevertheless, the topographic signature of vegetation is present. Furthermore, the 'bumps' and secondary peaks observed between 1 and 1.5 m above the median elevation on many of the bed elevation frequency distributions (section 4.5.1) are probably part of that topographic signature, since island surfaces gradually aggrade until their surfaces are 2 m or more above the gravel bar surfaces when they are fully developed.

4.5.3 Outlier Reaches

In the downstream reaches, the areas occupied by taller vegetation (taller than 5 m, taller than 10 m) are clearly defined and surrounded by continuous areas of vegetation taller than 1 m, suggesting that they mark distinct islands within the braid plain, whereas elsewhere in these downstream reaches and across much of the other reaches, the vegetation is predominantly short (taller than 1m) and patchy, suggesting that it represents pioneer and building islands (Gurnell et al., 2001).

One notable feature of these large patches of taller vegetation (Figure 4.15) in the downstream reaches is that they are associated with particularly high areas that rise abruptly from the braid plain (Figure 4.16). These areas of higher elevation undoubtedly gave the taller vegetation some protection from the November 2000 flood, allowing it to survive and be observed in the January 2001 lidar data. Although these vegetated areas may simply be established island surfaces, channel incision has been observed in the lower reaches of the Tagliamento to a depth of approximately 1 m (Ziliani and Surian, 2012). This is believed to be mainly the consequence of gravel mining from the river bed. It is possible that many of the larger patches of taller vegetation revealed in Figure 4.16, which are often 2m above the adjacent level of the braid plain are at least partly associated with elevated areas that have been isolated by this bed incision, combined with prolonged surface aggradation associated with this taller (and older) riparian woodland cover. However, more detailed research incorporating field observations is needed to investigate this issue.

Chapter 5

Braiding, Anastomosing and Sinuosity Indices: a Comparison Among Reaches of Six European Braided Rivers

5.1 INTRODUCTION

Following from the detailed three-dimensional analysis of the Tagliamento River presented in Chapter 4, this chapter considers several European braided rivers and compares their physical properties.

Lidar data was not available for the investigated rivers apart from the Tagliamento, and so information was assembled largely from high resolution images to make the comparison. Google Earth was the main data source because it provides elevation data as well as aerial images, and often provides images for several dates for the same site. However, aerial photographs were also used for one river to give a longer time series of images for analysis. These data sets were complemented where possible by flow records and information on bed material calibre.

As a result of this reliance on planform information, comparisons among rivers and dates used more traditional indices of braiding complexity such as the braiding index, to replace the three-dimensional comparisons based on the elevation frequency distribution, which were used in Chapters 3 and 4.

The aims of this chapter are:

- (i) To identify some naturally braiding rivers across Europe that span a range of biogeographical conditions and thus are subject to different riparian vegetation as well as having different size, gradient and flow.
- (ii) To extract from aerial imagery and other data sources, a set of physical properties of reaches of these rivers to represent the core physical controls and braiding responses of the selected rivers across space (several river reaches) and through time (images of different date).

- (iii) To investigate variations in braiding response across the rivers and at different dates in order to identify how they vary and whether riparian vegetation appears to be a significant control on their behaviour.

5.2 MATERIALS AND METHODS

5.2.1 Selection of Rivers and Images

A selection of six transitional to braided rivers were identified for investigation (Table 5.1). In addition to the Tagliamento, which provides a link with chapter 4, five other rivers were identified that showed stark differences in riparian vegetation and for which discharge data could be obtained to support estimation of stream power. This meant that the selection was to some extent opportunistic, and, given more time to search and conduct analyses, a larger sample of rivers would have been identified to increase both the coverage and replication of riparian vegetation types, as well as other factors, including gradient, discharge and sediment supply/calibre characteristics. On this basis, the following analysis should be treated as exploratory.

Table 5.1 The six rivers selected for study, their location, the number of reaches selected and the number of years for which data were available for analysis.

River Number	River	Country	No. reaches	Years	Location	
					Latitude	Longitude
1	Feshie	UK	9	10	57° 0'36.97"N	3°54'21.16"W
2	Coquet	UK	2	1	55°18'59.08"N	2° 3'50.09"W
3	Liza	UK	1	1	54°30'42.21"N	3°19'53.43"W
4	Bialka	Poland	5	1	49°20'42.13"N	20° 7'52.66"E
5	Val Roseg	Switzerland	4	1	46°25'26.21"N	9°51'39.01"E
6	Tagliamento	Italy				
	Middle reaches		8	7	46°10'40.31"N	12°57'24.93"E
	Headwater reaches		4	1	46°23'09.65"N	12°39'21.09"E

The Tagliamento was separated for analysis into two areas, the middle reaches, where the riparian woodland is affected by a warm, moist Mediterranean climate, and is dominated by Black Poplar (*Populus nigra*) and the Alpine headwaters, which are dominated by Grey Alder (*Alnus incana*) and Hoary Willow (*Salix eleagnos*). The Val Roseg is a pro-glacial river located high above the tree line in the Alps in Switzerland, and its riparian vegetation is sparse, comprising low alpine herbs and grasses. The Bialka River in Poland is bordered by coniferous forest. All of these rivers are braided. The remaining three rivers are located in the UK, and have riparian zones that are covered by moorland with few trees. While the Feshie is a braided river, the analysed

reaches of the Coquet and Liza are wandering rather than braided. Inclusion of these three UK rivers was based on advice from Environment Agency personnel.

Each of the study rivers were subdivided into 1 km long reaches for analysis. Freely available images of these rivers were identified in Google Earth and were analysed using the tools available in Google Earth Pro. All available images within Google Earth were inspected. For every reach, all cloud-free images that provided complete coverage from a single date (i.e. no mosaicing within the reach) were selected for analysis. In the case of the Feshie, a sequence of seven historical photographs (1946 to 2005) were available for a single reach, and so these were analysed in addition to images from Google Earth.

5.2.2 Extraction of Information From Images

Table 5.2 summarises the reach properties extracted from aerial images.

Each reach was defined on every image by a polygon. A centre line was drawn along each river using the “path” option of the measuring tool. The limits of the 1 km reaches were then set on this line with the “place mark” tool. These place marks were used to ensure that the same reach was analysed in every selected image, although the centre line was adjusted between images to follow the river planform at the time of the image. Using the measurement tool, individual polygons were then drawn around each reach on every selected image to enclose the active channel at the time of the image. In a few cases, the outer limit of the active channel could be interpreted in two different ways (e.g. Figure 5.1), and so a second polygon was also defined (labelled “Opt.2” in Table 5.2). From these polygons, the area and perimeter of the active channel was calculated.

The slope of each reach on each image was calculated using the following formula:

$$S = \frac{(y1 - y2)}{x}$$

where S is the slope, y1 is the elevation on the centre line at the upstream end of the reach, y2 is the elevation on the centre line at the downstream end of the reach and x is the length of the centre line between between y1 and y2.

Channel width was determined by measuring the width of the active channel at 10 cross sections equally spaced at 50 m intervals along each reach, and at the same time, information was extracted for the following indices:

- i) The Braided index (B_i) was the reach average number of wetted channels found in each of the 10 cross sections.
- ii) The Anabranching index (A_i , A_{i2}) was the reach average number of the active channels separated by vegetated islands in the 10 cross sections. Although only mature vegetation was included in estimates of the anabranching index, two different indices allowed for islands with a completely closed canopy and islands where vegetation showed gaps in the canopy. A_i (island a in Figure 5.2) was calculated using only islands with a mature closed canopy, whereas A_{i2} (islands a and b in Figure 5.2) included islands comprised of a closed canopy or a combination of closed and partly open canopy.
- iii) The Sinuosity index (S_i) was calculated for the main braid channel by dividing the main channel length by the straight line distance between its start and end points.

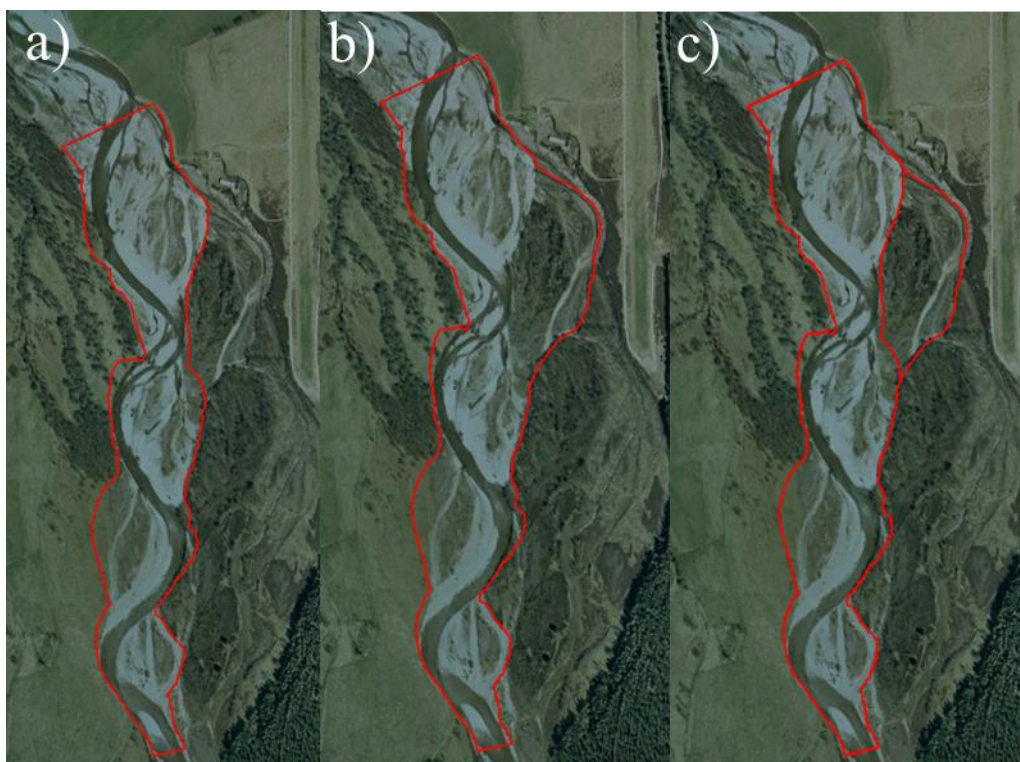


Figure 5.1 Reach 2 of the Feshie River near Feshiebridge, a) shows a first interpretation of the active channel, b) shows a second possible interpretation of the active channel, referred to as “option 2”, and c) shows the difference between the two interpretations of the active channel.

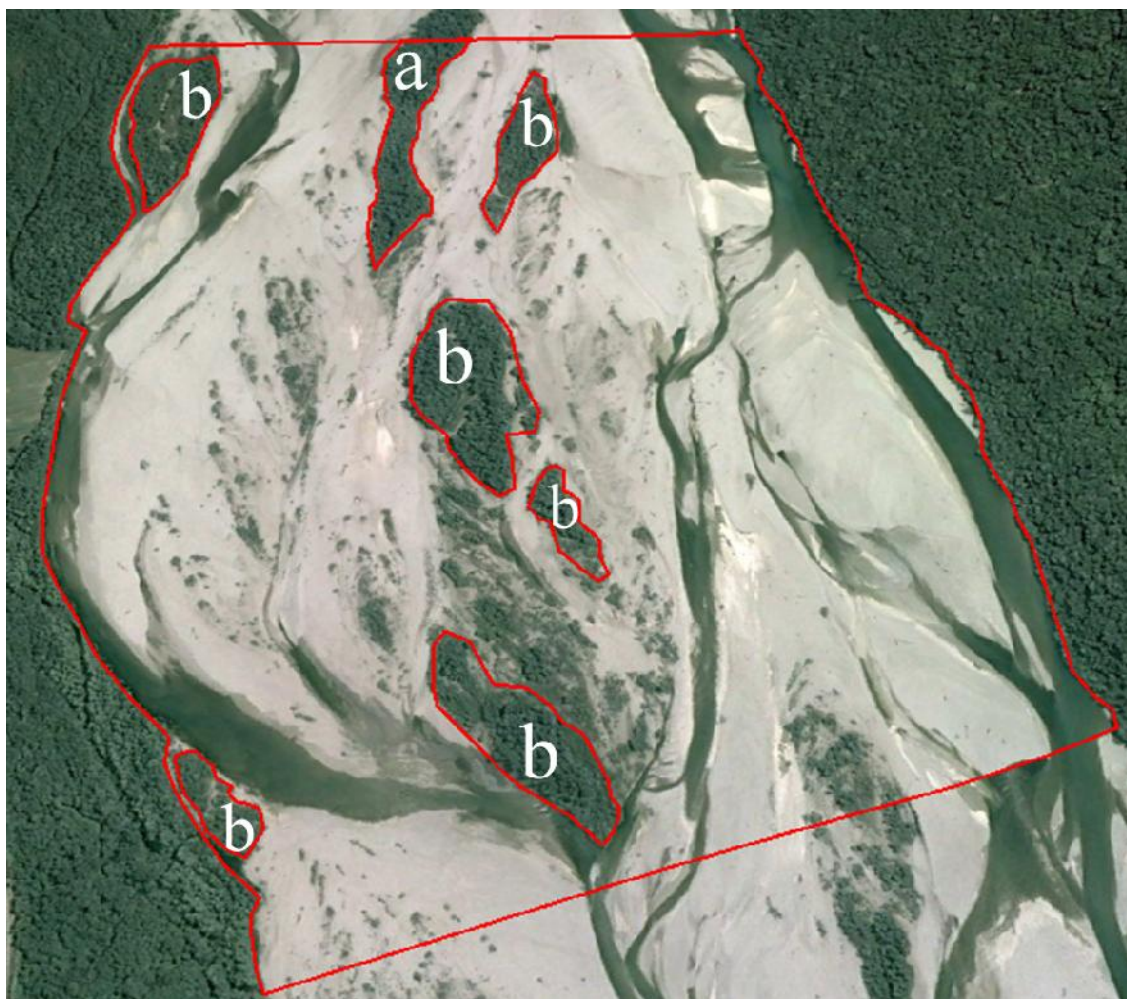


Figure 5.2 In order to illustrate the process followed to determine vegetated islands when measuring the Anabranching index (A_i) the Tagliamento river section 9 is shown a) Island consists of closed canopy vegetation b) Islands consist of a combination of closed canopy vegetation plus some adjacent discrete sparse vegetation areas.

The seven historical images obtained for the Feshie river for the years 1946, 1955, 1964, 1989, 1993, 1997, 2000, and 2005 were analysed in Arc GIS 10. A shape file was created in the Arc Catalog for each individual year in order to separate the active channel and then a central transect line was drawn. The B_i , A_i , and S_i indices and the channel width were estimated for each image (as described above for the Google Earth images).

Table 5.2 Information extracted from satellite and aerial images for the study rivers, river reaches and dates.

River name	Reach	Image Year	Bi	Ai	Ai2	Si	Slope	Width (m)	Perimeter (m)	Area (m ²)
Bialka	1	2012	1.7	1.3	1.3	1.10	0.015	65	2225	69335
Bialka	2	2012	2.1	1.1	1.1	1.12	0.015	70	2292	69931
Bialka	3	2012	1.4	1.6	1.6	1.13	0.015	88	2378	104445
Bialka	4	2012	2.6	1.7	2.1	1.13	0.015	94	2199	74131
Bialka	5	2012	1.6	1	1	1.10	0.015	55	2180	53854
Coquet	1	2009	1.9	1	1	1.30	0.004	58	2202	45715
Coquet	2	2009	2	1.3	1.3	1.23	0.004	91	2315	80311
Feshie	1	2000	2.1	1.8	1.9	1.14	0.002	109		
Feshie	2	1946	3.3	1.8	1.9	1.33	0.002	150		
Feshie	2	1955	1.7	2.5	2.5	1.13	0.002	146		
Feshie	2	1964	2.4	2.3	2.3	1.18	0.002	153		
Feshie	2	1989	1.8	1.2	1.3	1.16	0.002	102		
Feshie	2	1993	3.4	1.3	1.3	1.20	0.002	143		
Feshie	2	1997	4.7	1.7	1.9	1.11	0.002	148		
Feshie	2	2000	2.7	2.1	2.1	1.06	0.002	115		
Feshie	2	2005	3.8	1.3	1.3	1.02	0.002	143		
Feshie	3	2000	2.8	1.2	1.2	1.13	0.002	71		
Feshie	4	2005	2.1	1	1	1.19	0.006	50	2217	77205
Feshie	4	2011	1.7	1	1.1	1.26	0.008	49	2233	79632
Feshie	5	2006	2.3	1	1	1.22	0.010	128	2310	116902
Feshie	5	2011	2.2	1	1.9	1.20	0.008	136	2407	122719
Feshie	6	2006	1.4	1	1	1.11	0.010	65	2344	67130
Feshie	6	2011	1.2	1	1.6	1.22	0.008	70	2517	126364
Feshie	7	2006	1.9	1.3	1.4	1.19	0.010	70	2376	60795
Feshie	7	2011	2.4	1.5	1.7	1.28	0.008	137	2268	93180
Feshie	8	2005	3.8	1	1	1.11	0.002	151	2345	113972
Feshie	9	2005	3.3	1	1	1.14	0.012	150	2429	128872

Table 5.2 continued.

River name	Reach	Image Year	Bi	Ai	Ai2	Si	Slope	Width (m)	Perimeter (m)	Area (m ²)
Liza (Ennerdale Lake)	1	2008	1.9	1.2	1.2	1.22	0.012	40	2344	49466
Tagliamento Middle	5	2003	2.3	1	1	1.06	0.003	281	2694	319315
Tagliamento Middle	5	2005	5	1	1	1.09	0.003	366	2719	324217
Tagliamento Middle	5	2011	4.6	1	1.3	1.16	0.003	364	2783	328173
Tagliamento Middle	6	2003	1.7	1	1	1.04	0.003	179	2778	257313
Tagliamento Middle	6	2003	1.7	1	1	1.06	0.003	177	2974	267569
Tagliamento Middle	6	2005	2.4	1	1	1.09	0.003	178	2941	262150
Tagliamento Middle	6	2011	1.8	1	1	1.11	0.003	168	2792	256677
Tagliamento Middle	7	2003	1.6	1	1.6	1.08	0.003	668	3295	645242
Tagliamento Middle	7	2005	1.6	1.4	1.4	1.32	0.003	643	3324	650269
Tagliamento Middle	7	2011	3	1	1.6	1.25	0.003	676	3347	655293
Tagliamento Middle	8	2003	1.2	1	1.2	1.16	0.001	550	3322	586167
Tagliamento Middle	8	2005	1.2	1	1.2	1.05	0.003	573	3386	614157
Tagliamento Middle	8	2008	3.2	1.2	1.2	1.28	0.003	579	3288	597030
Tagliamento Middle	8	2011	3.6	1	1	1.05	0.003	619	3408	640000
Tagliamento Middle	1	2002	2.6	1	1	1.15	0.001	770	3801	838295
Tagliamento Middle	1	2003	1.5	1	1	1.13	0.001	772	3860	858505
Tagliamento Middle	1	2005	2.8	1	1	1.45	0.003	787	3924	869439
Tagliamento Middle	1	2011	2.6	1	1.2	1.47	0.003	815	3950	886247
Tagliamento Middle	1	2012	3.6	1.6	3.3	1.08	0.001	827	3944	892900
Tagliamento Middle	2	2002	4.4	1.7	2.2	1.27	0.001	786	3549	716294
Tagliamento Middle	2	2002	4.4	1.7	2.2	1.27	0.001	786	3511	710648
Tagliamento Middle	2	2005	4.8	1.8	2	1.23	0.003	818	3640	762632
Tagliamento Middle	2	2011	5.3	1.4	1.4	1.30	0.003	842	3718	784231
Tagliamento Middle	2	2012	4.4	2.8	3	1.31	0.001	843	3667	774141
Tagliamento Middle	3	2002	3.4	1.4	1.4	1.08	0.001	545	3193	572767

Table 5.2 continued.

River name	Reach	Image Year	Bi	Ai	Ai2	Si	Slope	Width (m)	Perimeter (m)	Area (m ²)
Tagliamento Middle	3	2003	3.6	1.4	1.4	1.10	0.001	542	3140	563440
Tagliamento Middle	3	2005	4.2	1.5	1.5	1.12	0.003	550	3205	569244
Tagliamento Middle	3	2012	3.8	1.5	1.5	1.24	0.001	551	3114	565116
Tagliamento Middle	4	2002	4.9	2.7	2.7	1.10	0.001	688	3416	703030
Tagliamento Middle	4	2002	5.1	2.7	2.7	1.11	0.002	673	3354	679470
Tagliamento Middle	4	2003	2.9	2.7	2.7	1.00	0.001	681	3362	703707
Tagliamento Middle	4	2005	4.1	2.6	2.6	1.00	0.003	692	3385	706077
Tagliamento Middle	4	2011	3.6	2.5	2.9	1.03	0.003	687	3426	684254
Tagliamento Middle	4	2012	3.4	2.3	2.3	1.05	0.001	656	3349	685939
Tagliamento Headwaters	1	2003	1.5	1.7	1.8	1.09	0.010	130	2397	126769
Tagliamento Headwaters	2	2003	1.7	1.6	1.7	1.16	0.010	121	2516	148212
Tagliamento Headwaters	3	2003	2.1	1.3	1.3	1.13	0.010	170	2761	184560
Tagliamento Headwaters	4	2003	2.7	1.4	1.6	1.09	0.010	178	2505	163789
Val Roseg	1	2010	2.5	1	1	1.15	0.034	66	2279	47064
Val Roseg	2	2010	2.1	1	1	1.15	0.034	70	2677	196241
Val Roseg	3	2010	8.8	5.6	5.6	1.17	0.034	222	2748	176150
Val Roseg	4	2010	2.7	1.2	1.2	1.10	0.034	63	1555	44964
Opt. 2 reaches										
River name	Reach	Image Year	Bi	Ai	Ai2	Si	Slope	Width (m)	Perimeter (m)	Area (m ²)
Feshie	8	2005	4.2	1	1	1.13	0.002	225	2530	156634
Feshie	6	2006	2.3	1	1	1.22	0.01	65	2310	116902
Feshie	5	2011	2.2	1.6	1.6	1.19	0.008	178	2470	148653
Feshie	7	2011	1.5	1.1	1.7	1.28	0.008	149	2277	123901
Bialka	4	2012	3	2.4	3	1.13	0.015	121	2186	87034

5.2.3 Discharge, Bed Material and Stream Power

Wherever possible, discharge records were obtained from a gauging station close to the analysed reaches of each river. Daily average flow records were used and the Q_2 , Q_5 and Q_{10} flows were estimated using the annual maximum series fitted to an EV1 (Gumbel) distribution using an online calculator (available at <http://ponce.sdsu.edu/onlinegumbel.php>).

For the Tagliamento River, Q_2 , Q_5 and Q_{10} values of 1100, 1600 and 2150 m³/s were used. These were estimated from records at Venzone, which is close to the reaches studied in the middle of the river. Since within the part of the catchment upstream of Venzone the average discharge has been shown to be related to catchment area raised to the power 0.955 (Mosetti, 1983), these estimates of Q_2 , Q_5 and Q_{10} were scaled by catchment area to give 1133, 1648, 2215 m³/s, respectively, for the middle reaches and 117, 170, 229 m³/s, respectively, for the headwater reaches.

Bed material calibre data was available for some of the reaches, and so wherever possible an estimate of d_{50} (median grain size) was extracted. However, the quality of this data was highly variable and generally poor.

Using the three discharge and bed material estimates, three stream power indices were estimated for each of the Q_2 , Q_5 and Q_{10} events

1. Total stream power was calculated for the Q_2 , Q_5 and Q_{10} events for each reach and time using the formula:

$$\omega^* = \rho g Q S$$

where ω^* is the stream power, ρ is the water density, g is the acceleration due to gravity, Q is the discharge, and S is the slope.

2. Unit stream power was calculated for the Q_2 , Q_5 and Q_{10} events for each reach and time using the formula:

$$\omega^{**} = \frac{\rho g Q S}{w}$$

where ω^{**} is the stream power, ρ is the water density, g is the acceleration due to gravity, Q is the discharge, S is the slope, and w is the width of the channel.

3. Dimensionless stream power was calculated for the Q₂, Q₅ and Q₁₀ events for each reach and time using the formula:

$$\omega^{***} = \frac{Q \cdot S}{w \cdot \sqrt{g \left(\frac{\rho_s - \rho_w}{\rho_w} \right) d_{50}^3}}$$

Where ω^{***} is dimensionless stream power, Q is the water discharge, w is the channel width, g is gravity, ρ_s is the sediment density, ρ_w is the water density, and d_{50} is the median grain size.

The discharge, d_{50} and stream power estimates for the studied reaches are listed in Table 5.3.

Table 5.3 Discharge, d_{50} and stream power estimates for the studied reaches.

River name	Reach	Image Year	d_{50} (mm)	Q2	Q5	Q10	Total Stream Power			Unit Stream Power			Dimensionless Stream Power		
							ω^* Q2	ω^* Q5	ω^* Q10	ω^{**} Q2	ω^{**} Q5	ω^{**} Q10	ω^{***} Q2	ω^{***} Q5	ω^{***} Q10
Bialka	1	2012		69	108	134	10153	15892	19718	156	244	302			
Bialka	2	2012		69	108	134	10153	15892	19718	145	226	281			
Bialka	3	2012		69	108	134	10153	15892	19718	115	181	224			
Bialka	4	2012		69	108	134	10153	15892	19718	109	170	211			
Bialka	5	2012		69	108	134	10153	15892	19718	183	287	356			
Coquet	1	2009													
Coquet	2	2009													
Feshie	1	2000	140	198	237	2747	3885	4650	25	36	43	0	0.081	0.097	0.029
Feshie	2	1946	140	198	237	2747	3885	4650	18	26	31	0	0.059	0.070	0.070
Feshie	2	1955	140	198	237	2747	3885	4650	19	27	32	0	0.060	0.072	0.072
Feshie	2	1964	140	198	237	2747	3885	4650	18	25	30	0	0.057	0.069	0.069
Feshie	2	1989	140	198	237	2747	3885	4650	27	38	46	0	0.086	0.103	0.103
Feshie	2	1993	140	198	237	2747	3885	4650	19	27	33	0	0.062	0.074	0.074
Feshie	2	1997	140	198	237	2747	3885	4650	19	26	31	0	0.060	0.071	0.071
Feshie	2	2000	140	198	237	2747	3885	4650	24	34	41	0	0.077	0.092	0.097
Feshie	2	2005	140	198	237	2747	3885	4650	19	27	33	0	0.062	0.074	0.173
Feshie	3	2000	140	198	237	2747	3885	4650	39	55	66	0	0.125	0.149	0.092
Feshie	4	2005	62	83	97	3649	4885	5709	73	98	115	0	0.222	0.260	0.074
Feshie	4	2011	62	83	97	4866	6514	7613	98	132	154	0	0.299	0.349	0.149
Feshie	5	2006	62	83	97	6082	8142	9516	48	64	75	0	0.145	0.169	0.260
Feshie	5	2011	62	83	97	4866	6514	7613	36	48	56	0	0.108	0.127	0.349
Feshie	6	2006	62	83	97	6082	8142	9516	93	124	145	0	0.282	0.330	0.330
Feshie	6	2011	62	83	97	4866	6514	7613	69	93	109	0	0.210	0.246	0.127
Feshie	7	2006	62	83	97	6082	8142	9516	87	116	136	0	0.263	0.307	0.330
Feshie	7	2011	62	83	97	4866	6514	7613	36	48	56	0	0.108	0.126	0.246
Feshie	8	2005	62	83	97	1216	1628	1903	8	11	13	0	0.024	0.029	0.307
Feshie	9	2005	62	83	97	7299	9771	11419	49	65	76	0	0.148	0.173	0.126

Table 5.3 continued.

River name	Reach	Image Year	d ₅₀ (mm)	Q2	Q5	Q10	Total Stream Power			Unit Stream Power			Dimensionless Stream Power			
							ω^* Q2	ω^* Q5	ω^* Q10	ω^{**} Q2	ω^{**} Q5	ω^{**} Q10	ω^{***} Q2	ω^{***} Q5	ω^{***} Q10	
Liza (Ennerdale Lake)	1	2008														
Tagliamento Middle	5	2003	62	1133	1648	2215	33344	48501	65187	119	173	232	0.195	0.284	0.381	
Tagliamento Middle	5	2005	62	1133	1648	2215	33344	48501	65187	91	132	178	0.149	0.217	0.292	
Tagliamento Middle	5	2011	62	1133	1648	2215	33344	48501	65187	92	133	179	0.150	0.219	0.294	
Tagliamento Middle	6	2003	62	1133	1648	2215	33344	48501	65187	186	271	364	0.306	0.445	0.598	
Tagliamento Middle	6	2003	62	1133	1648	2215	66688	97001	130375	377	548	737	0.618	0.899	1.209	
Tagliamento Middle	6	2005	62	1133	1648	2215	33344	48501	65187	187	273	366	0.307	0.447	0.601	
Tagliamento Middle	6	2011	62	1133	1648	2215	33344	48501	65187	198	288	387	0.325	0.473	0.636	
Tagliamento Middle	7	2003	62	1133	1648	2215	33344	48501	65187	50	73	98	0.082	0.119	0.160	
Tagliamento Middle	7	2005	62	1133	1648	2215	33344	48501	65187	52	75	101	0.085	0.124	0.166	
Tagliamento Middle	7	2011	62	1133	1648	2215	33344	48501	65187	49	72	96	0.081	0.118	0.158	
Tagliamento Middle	8	2003	62	1133	1648	2215	11115	16167	21729	20	29	40	0.033	0.048	0.065	
Tagliamento Middle	8	2005	62	1133	1648	2215	33344	48501	65187	58	85	114	0.096	0.139	0.187	
Tagliamento Middle	8	2008	62	1133	1648	2215	33344	48501	65187	58	84	113	0.095	0.138	0.185	
Tagliamento Middle	8	2011	62	1133	1648	2215	33344	48501	65187	54	78	105	0.088	0.129	0.173	
Tagliamento Middle	1	2002	48	1133	1648	2215	11115	16167	21729	14	21	28	0.035	0.051	0.068	
Tagliamento Middle	1	2003	48	1133	1648	2215	11115	16167	21729	14	21	28	0.035	0.050	0.068	
Tagliamento Middle	1	2005	48	1133	1648	2215	33344	48501	65187	42	62	83	0.102	0.148	0.200	
Tagliamento Middle	1	2011	48	1133	1648	2215	33344	48501	65187	41	59	80	0.099	0.143	0.193	
Tagliamento Middle	1	2012	48	1133	1648	2215	11115	16167	21729	13	20	26	0.032	0.047	0.063	
Tagliamento Middle	2	2002	48	1133	1648	2215	11115	16167	21729	14	21	28	0.034	0.050	0.067	
Tagliamento Middle	2	2002	48	1133	1648	2215	11115	16167	21729	14	21	28	0.034	0.050	0.067	
Tagliamento Middle	2	2005	48	1133	1648	2215	33344	48501	65187	41	59	80	0.098	0.143	0.192	
Tagliamento Middle	2	2011	48	1133	1648	2215	33344	48501	65187	40	58	77	0.095	0.139	0.187	
Tagliamento Middle	2	2012	48	1133	1648	2215	11115	16167	21729	13	19	26	0.032	0.046	0.062	
Tagliamento Middle	3	2002	48	1133	1648	2215	11115	16167	21729	20	30	40	0.049	0.071	0.096	

Table 5.3 continued.

River name	Reach	Image Year	d ₅₀ (mm)	Q2	Q5	Q10	Total Stream Power			Unit Stream Power			Dimensionless Stream Power		
							ω^* Q2	ω^* Q5	ω^* Q10	ω^{**} Q2	ω^{**} Q5	ω^{**} Q10	ω^{***} Q2	ω^{***} Q5	ω^{***} Q10
Tagliamento Middle	3	2003	48	1133	1648	2215	11115	16167	21729	20	30	40	0.049	0.072	0.097
Tagliamento Middle	3	2005	48	1133	1648	2215	33344	48501	65187	61	88	119	0.146	0.213	0.286
Tagliamento Middle	3	2012	48	1133	1648	2215	11115	16167	21729	20	29	39	0.049	0.071	0.095
Tagliamento Middle	4	2002	48	1133	1648	2215	11115	16167	21729	16	23	32	0.039	0.057	0.076
Tagliamento Middle	4	2002	48	1133	1648	2215	22229	32334	43458	33	48	65	0.080	0.116	0.156
Tagliamento Middle	4	2003	48	1133	1648	2215	11115	16167	21729	16	24	32	0.039	0.057	0.077
Tagliamento Middle	4	2005	48	1133	1648	2215	33344	48501	65187	48	70	94	0.116	0.169	0.227
Tagliamento Middle	4	2011	48	1133	1648	2215	33344	48501	65187	49	71	95	0.117	0.170	0.229
Tagliamento Middle	4	2012	48	1133	1648	2215	11115	16167	21729	17	25	33	0.041	0.059	0.080
Tagliamento Headwaters	1	2003	90	117	170	229	11478	16677	22465	88	129	173	0.083	0.121	0.163
Tagliamento Headwaters	2	2003	90	117	170	229	11478	16677	22465	95	138	186	0.089	0.129	0.174
Tagliamento Headwaters	3	2003	90	117	170	229	11478	16677	22465	68	98	132	0.063	0.092	0.124
Tagliamento Headwaters	4	2003	90	117	170	229	11478	16677	22465	65	94	126	0.061	0.088	0.119
Val Roseg	1	2010		26	37	45	8672	12341	15009	131	186	226			
Val Roseg	2	2010		26	37	45	8672	12341	15009	124	177	215			
Val Roseg	3	2010		26	37	45	8672	12341	15009	39	56	68			
Val Roseg	4	2010		26	37	45	8672	12341	15009	138	196	238			
Opt. 2 reaches															
River name	Reach	Image Year	d ₅₀ (mm)	Q2	Q5	Q10	Total Stream Power			Unit Stream Power			Dimensionless Stream Power		
							ω^* Q2	ω^* Q5	ω^* Q10	ω^{**} Q2	ω^{**} Q5	ω^{**} Q10	ω^{***} Q2	ω^{***} Q5	ω^{***} Q10
Feshie	8	2005	50	62	83	97	1216	1628	1903	5	7	8	0.012	0.016	0.019
Feshie	6	2006	50	62	83	97	6082	8142	9516	48	64	75	0.108	0.145	0.169
Feshie	5	2011	50	62	83	97	4866	6514	7613	27	37	43	0.062	0.083	0.097
Feshie	7	2011	50	62	83	97	4866	6514	7613	33	44	51	0.074	0.099	0.116
Bialka	4	2012		69	108	134	10153	15892	19718	84	131	163			

5.2.4 Data Analysis

Through the above analyses, values of four planform variables (B_i , A_i , A_{i2} , S_i), four reach dimensions (average channel width, slope, active channel area and perimeter length), median bed material grain size (d_{50}), and twelve flow-related variables (discharge, total stream power, unit stream power, dimensionless stream power, each related to the Q_2 , Q_5 and Q_{10} return period floods) were estimated for the reach and date combinations (Tables 5.2 and 5.3). However, there were missing values for some of these variables, whereas others had poor accuracy. Therefore, the first stage in data analysis was to establish which combination of variables was the most promising for investigating associations between the four planform variables and their likely controls.

A second stage was to produce scatter plots to provide a preliminary assessment of the associations between the four planform variables and channel width (a measure of 'size' that is usually associated with discharge and for which there were estimates for all reaches and times) and stream power, within and between rivers.

Lastly, Principal Components Analysis was used to investigate multivariate associations between the four planform variables and subsets of likely controlling variables.

5.3 RESULTS

5.3.1 Options 1 and 2

Five reaches were subject to an analysis under Option 2 in addition to Option 1. Four of these were on the Feshie and one on the Bialka. Table 5.4 summarises the values for the four indices of planform and the active channel width derived from using the two options on these five reaches. The use of Option 2 results in very significant increases in the active width of the channel as a result of incorporating significant areas of well vegetated land within the 'active channel' in order to incorporate side/distributary channels into the 'braided' channel. This major increase in width leads to a very significant reduction in estimates of unit and dimensionless stream power. The effect on the four planform indices varies. In general, there are small increases in A_i and A_{i2} and small decreases in S_i with larger increases in B_i . Since only five channels required consideration of Option 2, with fairly small adjustments in the planform indices but significant consequences for unit and dimensionless stream power estimates, Option 2 estimates were excluded from further analysis. This exclusion can also be justified on

geomorphic grounds, since the excluded islands were large and defined by a relatively small outer channel, suggesting that they are probably relict features that are close to merging with the floodplain or are simply areas of the floodplain defined by minor avulsion channels at high flow. In this way, the analysed data set focused on a restricted but probably more appropriate meaning of the term ‘active channel width’.

Table 5.4 Planform indices and active channel widths derived from applying options 1 and 2 to five river reaches.

River	Reach	Year	Bi	Ai	Ai2	Si	Width (m)
Feshie Opt. 1	8	2006	1.9	1.3	1.4	1.19	70
Feshie Opt. 2	8	2006	4.2	1	1	1.13	225
Feshie Opt. 1	6	2006	1.4	1	1	1.11	65
Feshie Opt. 2	6	2006	2.3	1	1	1.22	128
Feshie Opt. 1	5	2011	1.7	1	1.1	1.26	49
Feshie Opt. 2	5	2011	2.2	1.6	1.6	1.19	178
Feshie Opt. 1	7	2011	1.2	1	1.6	1.22	70
Feshie Opt. 2	7	2011	1.5	1.1	1.7	1.28	149
Bialka Opt. 1	4	2012	2.6	1.7	2.1	1.13	94
Bialka Opt. 2	4	2012	3	2.4	3	1.13	121

5.3.2 Selecting Informative Variables

Of the variables with potential to explain the four indices of planform (Bi, Ai, Ai2, Si), all reaches and dates had values of slope and active channel width. Since both active channel area and perimeter were very highly correlated ($p < 0.0001$) with width (0.904, 0.997, respectively) and had some missing values (for the seven historical photographs of the Feshie, Table 5.2), area and perimeter were not included in any further analysis. All of the channels were located in narrow valleys and so were to some extent confined by the valley sides. In some cases (e.g. Tagliamento), terraces also provided a degree of confinement. Estimates of discharge (Q_2 , Q_5 , Q_{10}) were also not available for two of the UK rivers (Coquet, Liza, Table 5.3). However, this only affected a single image for three reaches, otherwise the data set was complete. As a result, total stream power and unit stream power could be estimated for virtually all reaches for all three discharges. The estimation of dimensionless stream power was further restricted by lack of information on d_{50} , and also by the poor quality of some of the d_{50} estimates. Correlations among the different estimates of stream power were investigated to identify their information content (Table 5.5).

Table 5.5 Correlations among different stream power indices (ω^* is total stream power, ω^{} is unitstream power and ω^{***} is dimensionless stream power; Q_2 , Q_5 , and Q_{10} refer to the discharges for which the three different stream power indices are estimated).**

	ω^* (Q_2)	ω^{**} (Q_2)	ω^{***} (Q_2)		ω^* (Q_2)	ω^* (Q_5)	ω^* (Q_{10})
ω^* (Q_2)	1	0.372	0.338	ω^* (Q_2)	1	1.000	0.999
ω^{**} (Q_2)	0.372	1	0.937	ω^* (Q_5)	1.000	1	1.000
ω^{***} (Q_2)	0.338	0.937	1	ω^* (Q_{10})	0.999	1.000	1

	ω^* (Q_5)	ω^{**} (Q_5)	ω^{***} (Q_5)		ω^{**} (Q_2)	ω^{**} (Q_5)	ω^{**} (Q_{10})
ω^* (Q_5)	1	0.389	0.365	ω^{**} (Q_2)	1	0.999	0.992
ω^{**} (Q_5)	0.389	1	0.940	ω^{**} (Q_5)	0.999	1	0.997
ω^{***} (Q_5)	0.365	0.940	1	ω^{**} (Q_{10})	0.992	0.997	1

	ω^* (Q_{10})	ω^{**} (Q_{10})	ω^{***} (Q_{10})		ω^{***} (Q_2)	ω^{***} (Q_5)	ω^{***} (Q_{10})
ω^* (Q_{10})	1	0.416	0.410	ω^{***} (Q_2)	1	0.998	0.985
ω^{**} (Q_{10})	0.416	1	0.945	ω^{***} (Q_5)	0.998	1	0.994
ω^{***} (Q_{10})	0.410	0.945	1	ω^{***} (Q_{10})	0.985	0.994	1

The left column of Table 5.5 shows correlations among the three unit stream power indices for Q_2 (top), Q_5 (middle) and Q_{10} (bottom). From these correlation matrices, it is clear that the correlation between unit stream power and dimensionless stream power is very high ($p < 0.0001$) for all three discharge estimates (0.937, 0.940, 0.945, respectively). Given the missing values and poor quality of the d_{50} data set, which is included in the estimation of dimensionless stream power, it was decided to omit this variable from further analysis. The right column of Table 5.5 shows correlations among the three estimates of total (top), unit (middle) and dimensionless stream power (bottom) for the three discharge estimates (Q_2 , Q_5 , and Q_{10}). In all cases the correlations are extremely high, suggesting that estimates based on any one of the three discharges provide similar information. Therefore, analysis proceeded using indices based on Q_{10} alone.

Therefore analysis proceeded using the following variables: B_i , S_i , A_i , A_{i2} , slope, active channel width, Q_{10} and total and unit stream power estimated from Q_{10} .

5.3.3 Associations Among Variables within a Single River

Multi-date aerial images were available for two rivers, the Feshie and the middle reaches of the Tagliamento. These data sets were explored to assess the level of variance in the four indices of planform among the image dates for each investigated reach.

Eight reaches were considered in the middle Tagliamento, which displayed widely varying active channel widths. This resulted from differential confinement of the channel by mountains or terraces and ranged from narrow reaches close to the Pinzano gorge to very wide, semi-confined, reaches downstream and upstream of the gorge. Figure 5.3 shows scatter plots of active channel width plotted against the four indices of planform and unit stream power estimated for the Q_2 and Q_{10} flows, with data from a single reach but at different dates represented by the same symbol.

The plots representing the two measures of unit stream power (Figures 5.3 E and F) confirm that there is no significant change in the pattern of the data points whichever unit stream power value is used (i.e. for Q_2 , Q_5 or Q_{10}). This further supports the use of stream power values for only one flow (Q_{10}) in all subsequent analyses. Since the same discharge is used in all of the computations, the vertical shifts in the plotting position for some reaches in Figures 5.3 E and F represent changes in channel width and/or slope estimated from different images, but there is a clear overall reduction in unit stream power with increasing channel width across the reaches and images of different date.

All of the planform indices show an increase in their maximum values with increasing channel width, although this is most marked for the two anabranching indices (A_i , A_{i2}). Furthermore, although there are variations in the plotting position for each reach across the sampled image dates, this variation is relatively small, particularly for S_i , A_i and A_{i2} , which are not significantly affected by flow stage. Even B_i , which is affected by flow stage at the time of the image, shows relatively small variance for any individual reach. These results give confidence in the analysis of a mix of reaches and image dates.

Figure 5.4 shows scatter plots for the river Feshie of the four planform indices against the active channel width. The Feshie shows greater variance in each of the indices than the Tagliamento, with a similar range in planform index values for a group of much narrower reaches than those of the Tagliamento. One reach (dark grey diamonds) has

values extracted from images dating from 1946 to 2005, a period over which the river has changed greatly. The planform indices and channel width are presented as time series for this reach in Figure 5.5, illustrating variability in Bi, Si, Ai, and Ai2 that largely reflects changes in channel width and also shows an apparently declining trend in Ai, Ai2 and width through time reflecting lateral encroachment of the vegetated floodplain.

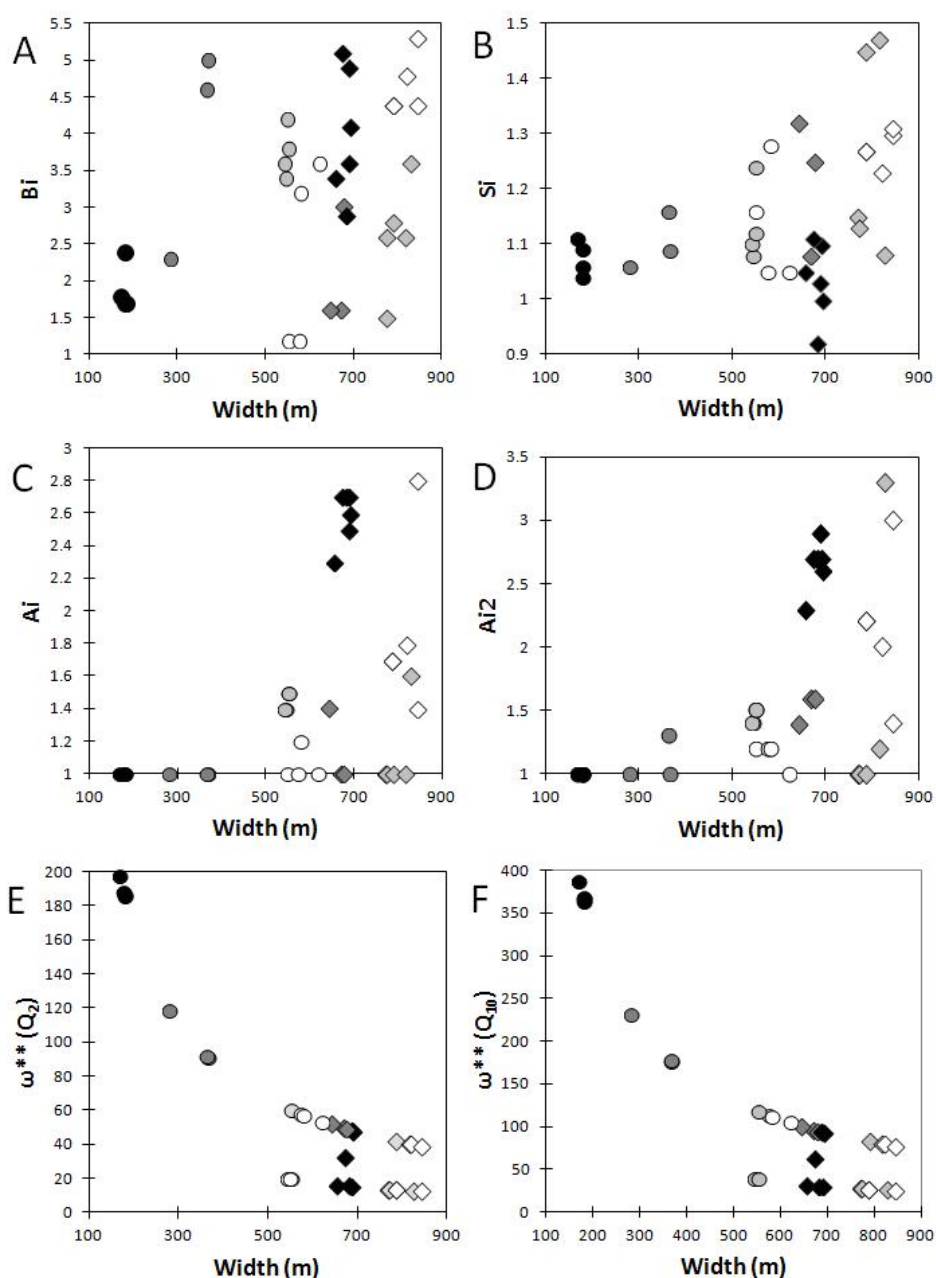


Figure 5.3 Four indices of planform (A. Bi; B. Si; C. Ai; D. Ai2) and unit stream power for Q_2 (E) and Q_{10} (F) plotted against active channel width for the Tagliamento middle reaches. Each symbol represents a different reach, with all image dates marked using the same symbol for the reach.

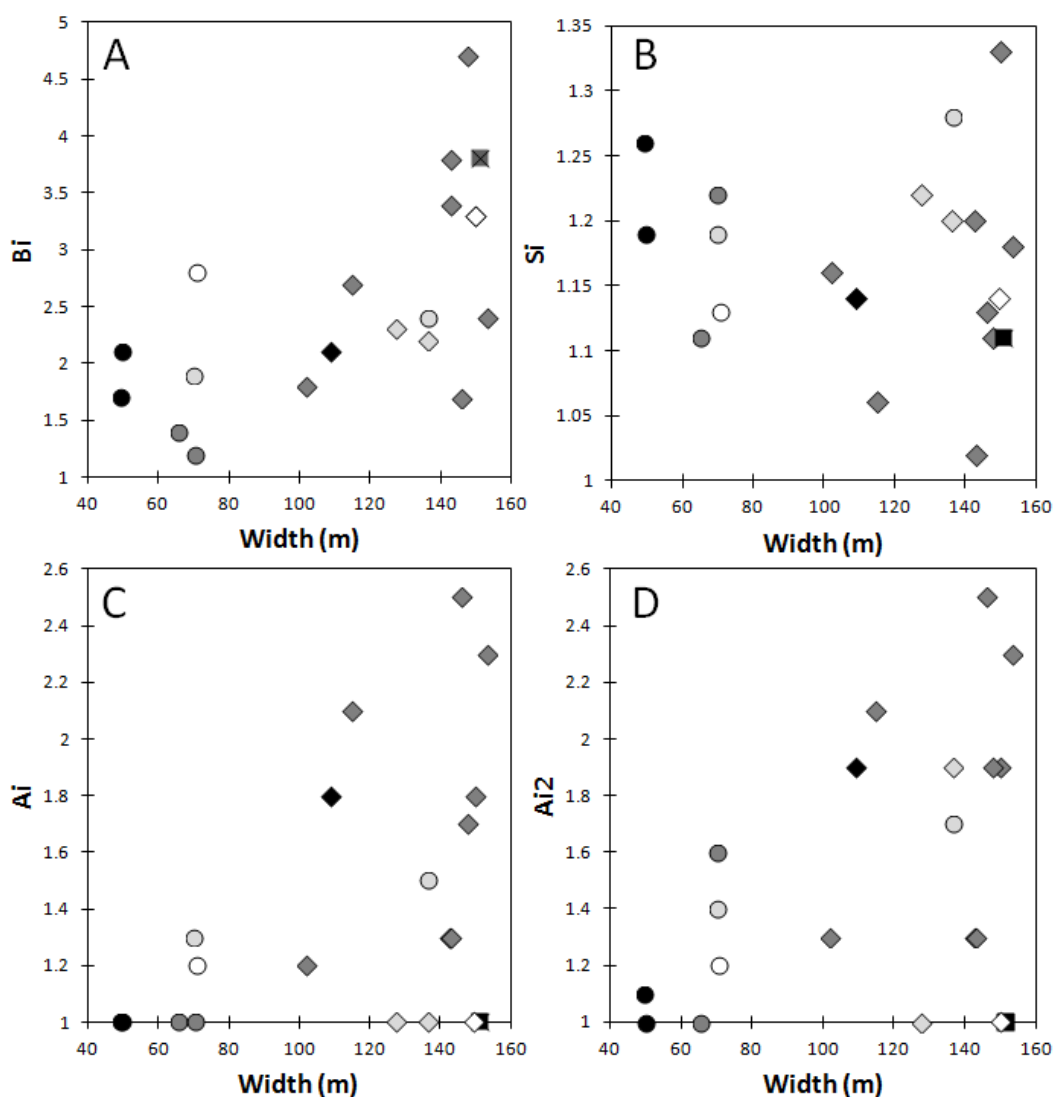


Figure 5.4 Four indices of planform (A. Bi; B. Si; C. Ai; D. Ai2) plotted against active channel width for the river Feshie reaches. Each symbol represents a different reach, with all image dates marked using the same symbol for the reach.

Thus, it appears that at least some of the variability in Ai, Ai2 and probably Si reflect genuine changes in reach morphology through time, whereas there is additional variability in Bi as a result of differences in flow at the times when the images were collected. The following analyses of the entire data set from 6 rivers cannot make allowance for flow stage variations because in many cases only one image is available. However, the above analyses suggest that comparisons of Ai, Ai2 and Si are more likely to represent true differences in the morphology between reaches than Bi.

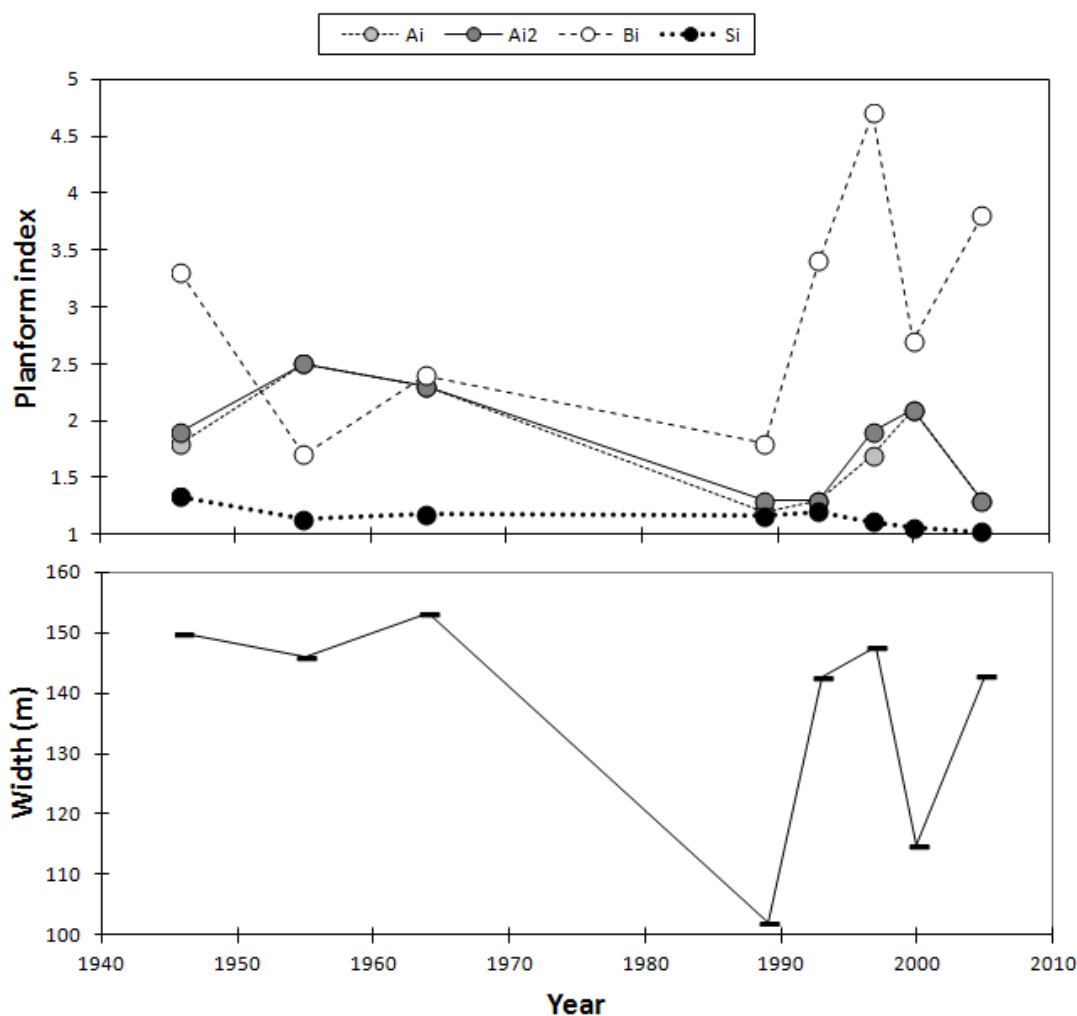


Figure 5.5 Time series plots of Bi, Si, Ai, Ai2 for one reach of the river Feshie.

5.3.4 Associations Among Planform, Channel Dimension and Stream Power Variables Across Six European Braided Rivers

Figure 5.6A shows unit stream power plotted against channel width, with the expected decline in unit stream power with increasing channel width and with higher unit stream power in relation to channel width for the Tagliamento middle reaches (black circle) in comparison with the Tagliamento headwaters (dark grey circle), Bialka (dark grey diamond), Val Roseg (white diamonds), which in turn show higher stream power for the same width than the Feshie (white circle). The colours of the symbols represent woodland vegetation with relatively vigorous growth (black), other woodland vegetation (grey), vegetation with few trees (white).

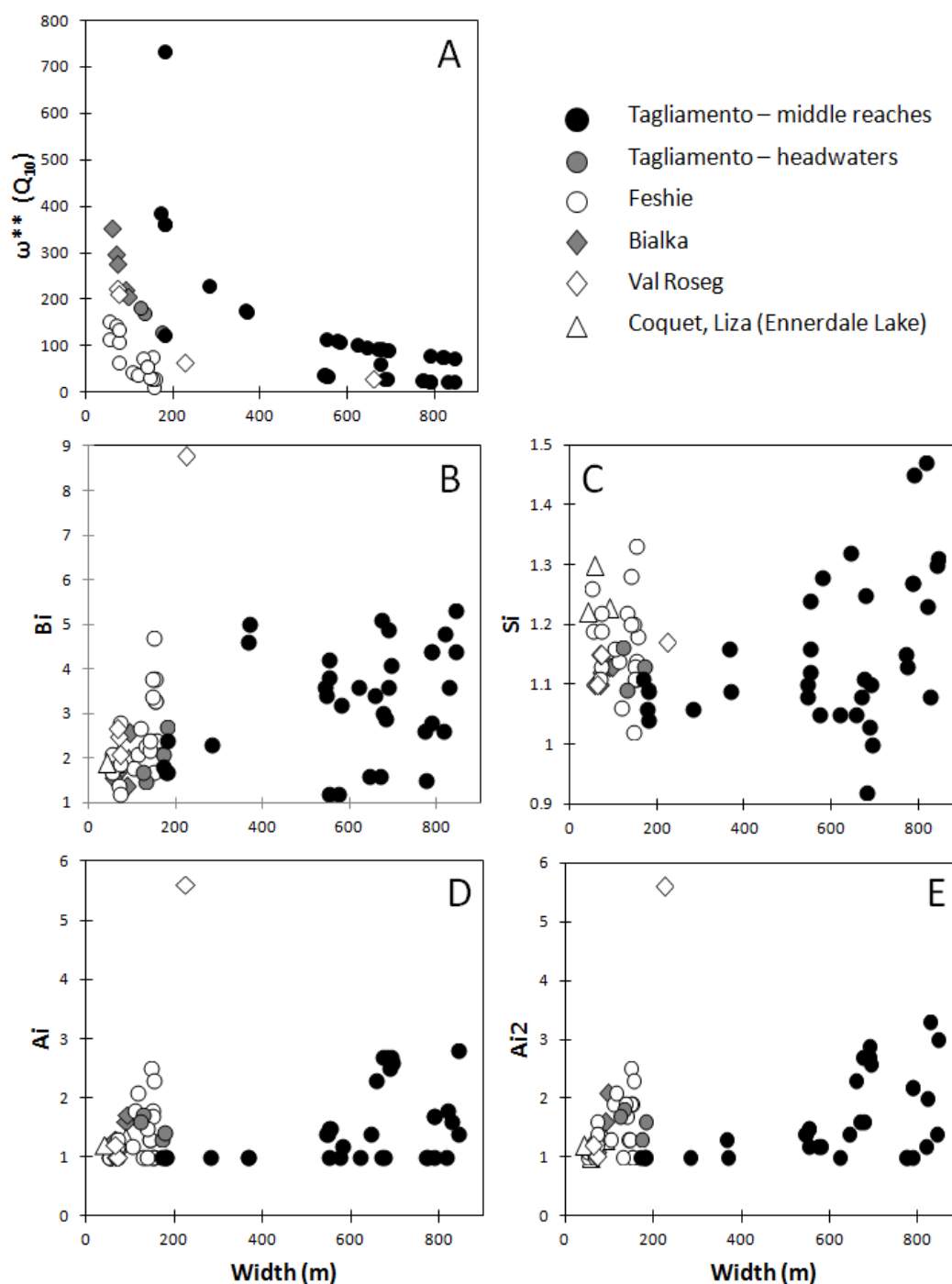


Figure 5.6 Scatter plots of A. unit stream power; B. B_i ; C S_i ; D A_i ; E A_{i2} plotted against active channel width (the colours of the symbols represent woodland vegetation with vigorous growth (black), other woodland vegetation (grey), vegetation with few trees (white)).

Figure 5.6 shows scatter plots of the four planform indices plotted against channel width. Because of the very wide channel widths (and values of total stream power – not illustrated) the plots in Figure 5.6 show little discrimination between rivers apart from the Tagliamento middle reaches. However, one reach of the Val Roseg shows

anomalously high values of B_i , A_i and A_{i2} , reflecting the width of this reach, which allows numerous braid channels to develop during the summer high flows of the image and also allows the alpine vegetation between these channels to survive from year to year relatively undisturbed. The width of this reach is probably more a reflection of past glacial processes than any self-forming channel related to the current flow regime.

Figure 5.7 shows log-log scatter plots of the four planform indices plotted against unit stream power. Unit stream power expresses total stream power per unit width of channel, and so it removes some of the contrasts between the relatively wide Tagliamento middle reaches and the other rivers. The log-log plot also allows the data set to be viewed in a more integrated way and reveals a gradual reduction in the maximum values of S_i , A_i and A_{i2} (Figure 5.7 B, C, D) with increasing unit stream power. A similar decreasing trend may be present in the B_i plot (Figure 5.7A) but it is less clear.

In order to explore gradients in the data set that might indicate the most important controls on the four planform indices, groups of variables were subjected to Principal Components Analysis (PCA). The first PCA was conducted on the four planform indices, slope and channel width (Table 5.6). The first two PCs had eigenvalues greater than 1 and, therefore explained more of the variance than any of the original variables, and jointly explained almost 69% of the variance in the data set. Judging from the variable loadings on the first two PCs, PC1 describes a gradient of increasing B_i , A_i and A_{i2} , whereas PC2 describes a gradient of increasing slope and decreasing channel width. A scatter plot of the reach scores on the two PCs (Figure 5.8A) shows that the different rivers are separated along PC2 and show different ranges along PC1 according to the range in values of three planform indices within each individual river. This suggests that little of the variation in B_i , A_i and A_{i2} is explained by slope or channel width across this 6 river data set.

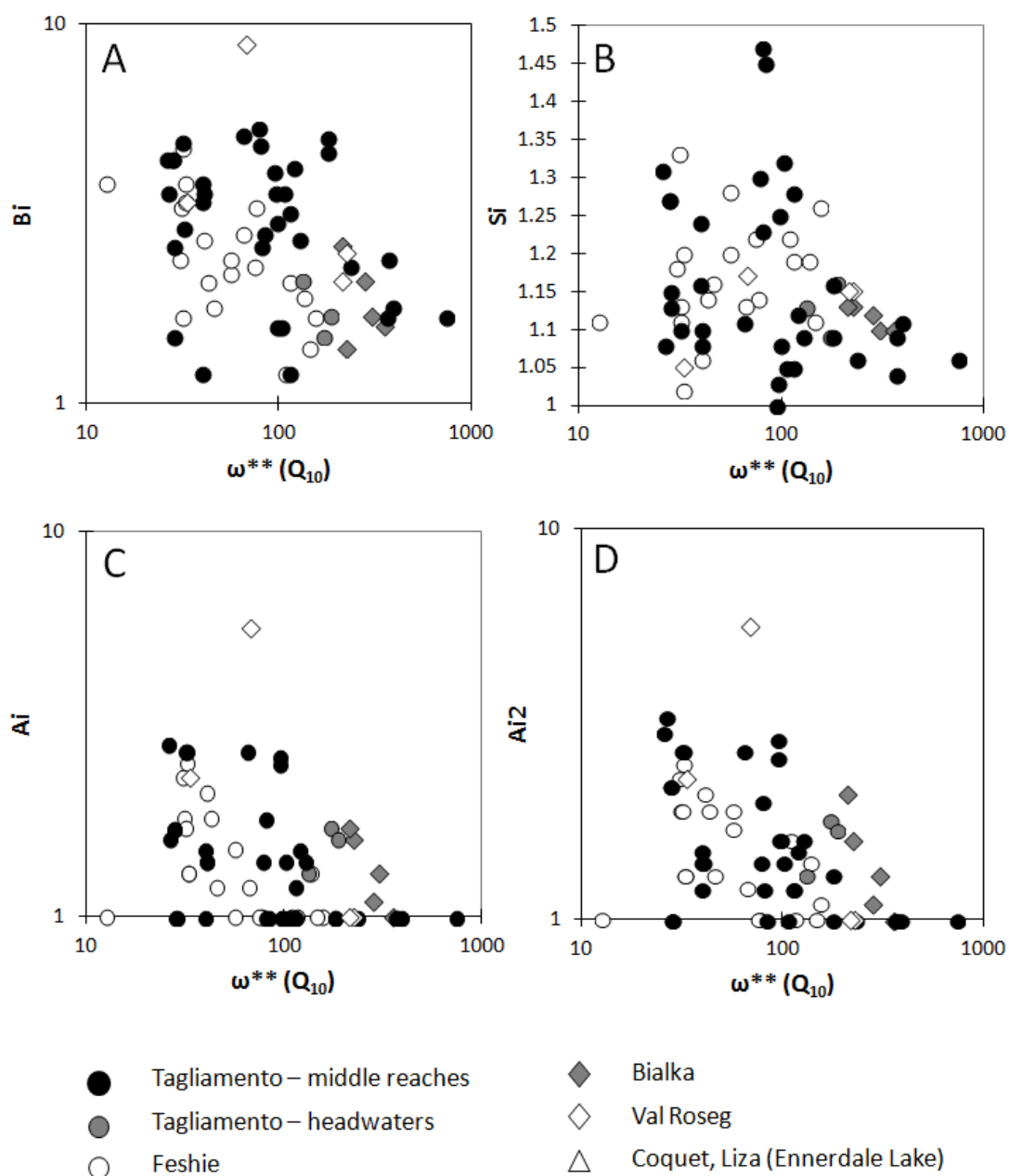


Figure 5.7 Scatter plots of A. B_i ; B. S_i ; C. A_i ; D. A_{i2} plotted against active channel width (the colours of the symbols represent woodland vegetation with vigorous growth (black), other woodland vegetation (grey), vegetation with few trees (white)).

Table 5.6 Eigenvalues, variability explained and variable loadings on the first four PCs of a PCA on Bi, Si, Ai, Ai2, slope, and channel width (all loadings >0.7 are emboldened).

	PC1	PC2	PC3	PC4
Eigenvalue	2.617	1.497	0.981	0.484
Variability (%)	43.624	24.955	16.355	8.059
Cumulative %	43.624	68.579	84.934	92.993
Loadings	PC1	PC2	PC3	PC4
Bi	0.825	-0.071	0.135	0.382
Ai	0.917	0.272	-0.006	-0.234
Ai2	0.926	0.191	-0.007	-0.251
Si	-0.062	-0.397	0.896	-0.188
Slope	-0.041	0.820	0.397	0.328
Width	0.482	-0.743	-0.057	0.276

Table 5.7 Eigenvalues, variability explained and variable loadings on the first four PCs of a PCA on Bi, Si, Ai, Ai2, slope, channel width and Q₁₀ (all loadings >0.7 are emboldened).

	PC1	PC2	PC3	PC4
Eigenvalue	2.757	2.110	1.028	0.553
Variability (%)	39.380	30.143	14.685	7.896
Cumulative %	39.380	69.522	84.208	92.103
Loadings	PC1	PC2	PC3	PC4
Bi	0.781	-0.260	0.149	0.227
Ai	0.741	-0.609	-0.053	-0.165
Ai2	0.773	-0.547	-0.031	-0.195
Si	0.047	0.207	0.963	-0.146
Slope	-0.316	-0.703	0.207	0.566
Width	0.741	0.573	0.082	0.179
Q ₁₀	0.591	0.711	-0.157	0.250

A second PCA introduced Q₁₀ as an additional variable (Table 5.7). The first three PCs had eigenvalues greater than 1 and jointly explained almost 85% of the variance in the data set. However, PC3 only describes a gradient in Si that is independent of the other variables. Judging from the variable loadings on the first two PCs, PC1 describes a gradient of increasing Bi, Ai, Ai2 and channel width, whereas PC2 describes a gradient of increasing Q₁₀ and decreasing slope, it also has quite a strong negative loading on Ai. A scatter plot of the reach scores on the two PCs (Figure 5.8B) shows that the different rivers are separated along a diagonal across the plot that follows the vectors for

decreasing slope and increasing Q_{10} and channel width, and each river is aligned along the vectors of increasing B_i , A_i and A_{i2} . This suggests that little of the variation in B_i , A_i and A_{i2} is explained by slope or channel width across this 6 river data set.

Since width, slope and Q_{10} all contribute to the estimation of unit stream power, a final PCA substituted unit stream power for slope, width and Q_{10} (Table 5.8). The first two PCs had eigenvalues greater than 1 and jointly explained almost 77% of the variance in the data set. Judging from the variable loadings on the first two PCs, PC1 describes a gradient of increasing B_i , A_i , A_{i2} and a weak decrease in unit stream power, whereas PC2 describes a gradient of increasing S_i and a weak decrease in unit stream power. A scatter plot of the reach scores on the two PCs (Figure 5.8C) shows that there is no longer separation between the rivers on the plot, but there is a general trend of increasing B_i , A_i and A_{i2} with decreasing unit stream power, with a slight tendency within the Tagliamento middle reaches for an increase in S_i with decreasing unit stream power.

Table 5.8 Eigenvalues, variability explained and variable loadings on the first four PCs of a PCA on B_i , S_i , A_i , A_{i2} , slope, channel width and Q_{10} (all loadings >0.7 are emboldened).

	PC1	PC2	PC3	PC4
Eigenvalue	2.653	1.193	0.637	0.455
Variability (%)	53.064	23.868	12.745	9.094
Cumulative %	53.064	76.932	89.678	98.772
Loadings	PC1	PC2	PC3	PC4
B_i	0.801	0.067	0.201	0.560
A_i	0.927	-0.222	0.113	-0.219
A_{i2}	0.930	-0.168	0.074	-0.266
S_i	0.009	0.893	0.423	-0.151
$\omega^{**} Q_{10}$	-0.536	-0.560	0.632	-0.006

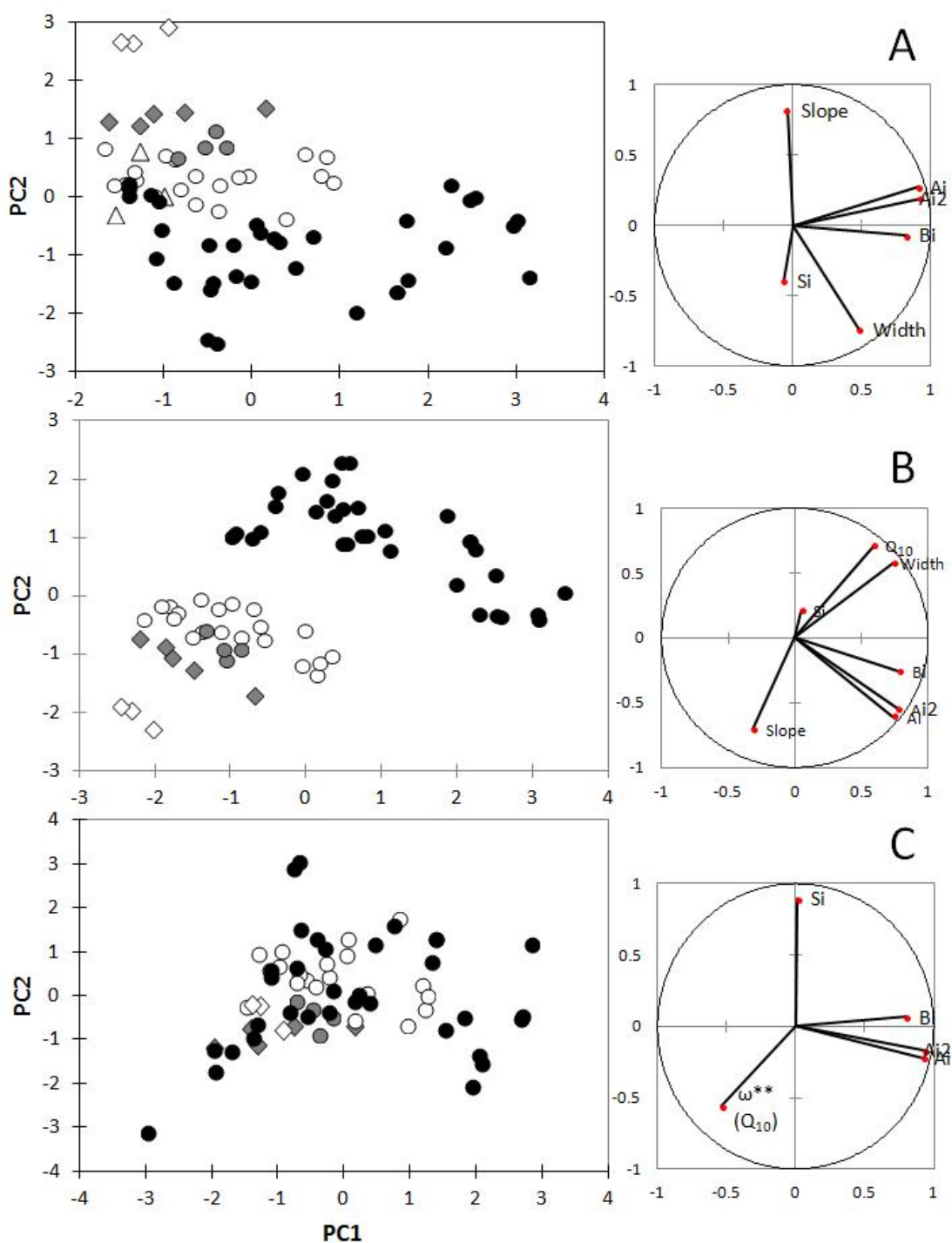


Figure 5.8 (Left graphs) Scatter plots showing reach scores on the first two PCs of three different PCAs. (Right graphs) Vectors illustrating the loadings of the variables included in the PCA on the first two PCs.

5.4 DISCUSSION AND CONCLUSIONS

A range of planform, reach dimension, bed material grain size, and flow-related variables were extracted from aerial imagery (Google Earth and air photographs), flow gauging station records and other sources that provided information on bed material. This information was extracted for 70 reach - image date combinations for six European rivers. For five reaches, a second option (including major side channels) was used to define a further set of values of the planform and geometric variables.

This data set was then investigated to define a core set of variables, emphasising the completeness of the variable estimates across all investigated reaches, the reliability/accuracy of the variable estimates, and the information content of the variables (one variable was selected when a group were very strongly inter-correlated). The core set of variables selected for analysis were B_i , S_i , A_i , A_{i2} , slope, active channel width, Q_{10} and total and unit stream power estimated from Q_{10} . Since only five channels required consideration of Option 2, with resultingly small adjustments in the planform indices but significant consequences for unit and dimensionless stream power estimates, Option 2 estimates were also excluded from further analysis.

The rivers Feshie and Tagliamento (middle reaches) had data sets incorporating repeat measurements of the same reach at different dates, and so the information for these two rivers was investigated to assess the within-reach variability of the measured variables as well as any broad trends in the four planform indices in relation to channel width and unit stream power.

The Tagliamento data set incorporated a wide range in channel width and unit stream power estimates, and revealed relatively small within-reach variations in B_i , S_i , A_i , A_{i2} , width, and unit stream power among different image dates in relation to the overall variability in the data set. There was a clear inverse relationship between unit stream power and channel width, which mainly reflects different levels of confinement (from completely to partly confined), since there are no significant tributary confluences influencing discharge among the investigated reaches, and there are only small differences in channel gradient.changes. The four planform indices showed an increase in their maximum value with increasing channel width and thus decreasing unit stream power (Figure 5.3), in part indicating a response to changing confinement similar to that observed in the laboratory experiments (Chapter 3). In particular, the maximum values

of Si, Ai, Ai2 showed a marked increase once the channel width exceeded 500 m, indicating that on this large river, such a channel width is necessary to allow vegetation to establish to maturity on bar tops to form islands in association with the potential for the main braid channel to develop a sinuous course. This increase in all four planform indices with increasing channel width and decreasing stream power supports the previous findings in chapters 3 and 4. The relatively small variability in Bi, Si, Ai, Ai2 and channel width between images in part reflects the relatively small time period represented by the analysed images. All information was extracted from Google Earth, with image dates spanning the period 2002 to 2012.

For the Feshie, the planform indices Bi, Ai and Ai2 also showed increasing maximum values with increasing channel width. However, within-reach variability was greater than that observed for the Tagliamento (Figure 5.4). This can partly be explained by the smaller range in width displayed on the Feshie, where the investigated reaches are quite tightly confined by adjacent hillslopes, with restricted space for the development of floodplain 'pockets'. More importantly, most of the variability is observed within one reach, where air photos spanning six decades (1946 to 2005) were analysed. A more detailed investigation of the data for this reach (Figure 5.5), showed considerable correspondence in the temporal patterns of the four planform indices and channel width and there also appeared to be an underlying trend of decreasing Ai, Ai2 and width over the 60 years, suggesting that the variability reflects true changes in the river's morphology over that period. A potential explanation of these temporal changes is that there were few floods during the 1970s in Scotland, whereas more recently, and particularly since 1989, flooding has been more frequent. Such variations allow floodplain pockets to fluctuate in their presence and width, with a corresponding change in braid plain width and in the space available for braid threads and islands to develop.

These analyses of the Feshie and Tagliamento (middle reaches) data sets suggest that pooling data from different dates across the six rivers is most likely to reveal genuine variations in their morphology across space and time, although the stage-dependence of Bi, may introduce additional variance that is not attributable to morphological change.

Analysis of the entire data set confirmed an inverse relationship between unit stream power and channel width across all of the studied rivers (Figure 5.6 A). Since unit stream power incorporates channel width, it implicitly provides an indication of channel

confinement by valley side slopes, terraces or vegetated floodplain pockets in the studied confined / semi-confined reaches. Nevertheless, three parallel curved relationships were defined rather than a single curve. The Tagliamento middle reaches plotted above the Tagliamento headwaters, Bialka, and Val Roseg, which in turn plotted above the Feshie. The bounding vegetation on these rivers varies with relatively vigorously growing riparian trees in the warm moist climate of the middle Tagliamento, less vigorously growing riparian trees in the cooler climates of the Tagliamento headwaters and the Bialka, and riparian vegetation essentially without trees in the high mountain environment of the Val Roseg, and the heavily grazed moorland of the Feshie. Therefore, the shift in the curved relationship between unit stream power and channel width could be interpreted as reflecting a change in the erosion resistance (relative bank strength) of the channel margins: the Tagliamento middle reaches show the highest unit stream power for any channel width, with intermediate values for the Tagliamento headwaters, Bialka and Val Roseg, and the lowest values for the Feshie. This supports the model proposed by Eaton et al. (2010), which includes relative bank strength (incorporating vegetation) as well as stream power (slope and dimensionless discharge) as the primary determinants of channel pattern. However, a larger data set incorporating more rivers would be needed to confirm this suggestion, particularly given the different approach used to estimate discharge values for the two Tagliamento sites in comparison with the other rivers.

A major problem faced in integrating data from the six rivers is the enormous differences in their size, discharge, slope and probably bed material calibre (although note the problems encountered in obtaining data for bed material). Dimensionless stream power would have provided the most effective way of scaling the data for these differences, but because of the poor quality of the bed material data, unit stream power was used instead, which at least standardises the data for slope and channel width / confinement. Broad trends of decreasing maximum B_i , S_i , A_i and A_{i2} were observed with increasing unit stream power across the entire data set, with no apparent differences displayed by any of the six rivers (Figure 5.7). Therefore, the different response of the Tagliamento middle reaches to unit stream power for any given width is not reflected in the response of the planform indices. Principal Components Analysis applied to the four planform indices, unit stream power, and its component variables (slope, width, Q_{10}) (Figure 5.8), further confirm the differences in scale (slope, width, Q_{10}) of the selected rivers. When these differences are removed by expressing them in

the form of unit stream power, all four planform indices show an increase in their maximum values with decreasing unit stream power across the entire 6 river data set. This suggests a common response of planform indices across the different rivers, once the differences in slope and width / confinement are accounted for.

Despite the wide variability in river size and in all of the investigated variables within and between rivers and river reaches, some general trends emerge from the analyses presented in this chapter. A larger data set is required before these trends can be verified, but the main preliminary conclusions are as follows:

- The analysis of aerial images (mainly from Google Earth) and other data sets has provided a data set that has revealed trends that are geomorphologically interpretable.
- Where information is available for a single reach spanning several decades, longer and shorter term fluctuations can be identified that confirm the importance of such historical analyses for identifying trajectories of braided river adjustment including planform change (e.g. Comiti et al., 2011; Ziliani and Surian, 2012), and also indicate how planform indices adjust in parallel with channel width in relatively confined situations as floodplain pockets are removed or vary in size in response to erosive floods and riparian extension under colonising riparian vegetation.
- Within individual rivers, increases in the maximum value of B_i , S_i , A_i and A_{i2} have been observed with increasing channel width (or decreasing confinement).
 - Within the middle reaches of the Tagliamento, this is associated with essentially the same discharge record since there are no major tributary confluences between the investigated reaches, justifying the use of a single gauged flow record. Therefore, the analyses of this data set can be compared with the outcomes of flume experiments reported in chapter 3, where channels of different width as a result of different levels of confinement were subjected to the same selected discharges. However, since B_i values are adversely affected by flow stage, the A_i and A_{i2} indices provide more robust indicators of the presence of (stable) bars. Both of these indices show a clear increase in their maximum value and variability with increasing channel width. The increase in variability, probably reflects differences in the growth performance of riparian trees

in the different reaches of the river (Bertoldi et al., 2011 a, b), since each reach is represented by a tight cluster of points in the scatter plots (Figure 5.3).

- Within the Feshie, flow variability among reaches and through time provide greater scatter in the plots relating planform indices to channel width. Thus the Feshie may support previous observations on the impact of river flow events and intervening vegetation colonisation on braid channel width and complexity (e.g. Henshaw et al., 2013), but a more detailed analysis is required to confirm this.
- The association among discharge, slope, width and discharge across the entire data set revealed two PCs describing weak gradients of increasing B_i , A_i and A_i^2 with decreasing slope and with increasing discharge and width (Figure 5.8B), confirming much of the research reviewed in the introduction to chapter 3. However, the enormous differences in the size of the investigated rivers, led to the plotting positions of river reaches being arranged along a diagonal across the PC1-PC2 plot which was essentially independent of (at right angles to) the vectors describing the loadings of B_i , A_i and A_i^2 on the two PCs. Nevertheless, when these controlling variables were combined into a single index (unit stream power), gradients of increasing S_i , B_i , A_i and A_i^2 with decreasing unit stream power were revealed and all reaches from all rivers plotted in the same broad area of the PC1-PC2 plot (Figure 5.8C).
- The only clear differentiation among the rivers that could be attributable to contrasts in riparian vegetation appeared when unit stream power was plotted against channel width (Figure 5.6 A). Although this may be an artifact of the way that discharge indices were calculated or of the particular rivers that were selected, the three apparently different curved relationships displayed in the plot could be attributed to the erosion resistance of the banks associated with different types of riparian vegetation, as suggested by Millar (2000). This requires further investigation, including assembly of a larger set of rivers and reaches, a more robust set of d_{50} measurements to estimate dimensionless stream power, and a careful consideration of how 'relative bank strength' can be estimated. Such an enhanced data set could be used to explore and confirm the analyses presented by Eaton et al. (2010) who proposed an interaction among dimensionless discharge, slope and relative bank strength in defining transitions from braided through anabranching to single thread rivers.

Chapter 6

Summary, Implications, Future Research, and Conclusions

6.1 INTRODUCTION

This thesis has been concerned with braided rivers and their transition to single-thread forms. Following a brief review of the literature on alluvial river channel styles and the braid-meander transition, Chapter 2 concluded with the following research questions:

1. What are the influences of variations in discharge and river confinement on river style and bed morphology?
2. What is the influence of vegetation on braided and transitional river morphology?
3. Does the type and extent of vegetation influence / co-vary with braided river planform?

Each of these questions was investigated in turn in chapters 3, 4 and 5. This chapter summarises the results of the research reported in these three chapters and some of its limitations (section 6.2), discusses the potential for future research (section 6.3), and then considers the potential applications of the research for river management and restoration (section 6.4).

6.2 SUMMARY OF RESEARCH FINDINGS AND SOME LIMITATIONS

6.2.1 Research Question 1: What are the influences of variations in discharge and river confinement on river style and bed morphology?

Chapter 3 reported on 27 flume experiments that investigated the impact of channel confinement (nine fixed maximum channel widths were explored: 0.15, 0.2, 0.3, 0.4, 0.6, 0.8, 1.0, 1.25, 1.5 m) and discharge (three fixed discharges: 1.5, 2.0, 2.5 l/s) on channel morphology. In all of these experiments the 25 m long by 2.9 m wide flume retained a constant slope (0.010), was filled with well-sorted sand with a typical grain size of 1 mm, and sediment input to the flume was maintained to balance sediment output from the flume. Morphological outcomes of the experiments were judged using four parameters of the bed elevation frequency distribution (median, standard deviation,

skewness and kurtosis); wetted and active channel width; total and active Bi (braiding index) and visual descriptions of the planform. Formative processes were represented by discharge and dimensionless stream power calculated for the flume fixed width, wetted width and active channel width, and also by the mean and dimensionless sediment transport rate.

The repetition runs showed little change in the four parameters of the bed elevation frequency distribution, giving confidence that any changes in bed morphology were a true response to changes in channel confinement or discharge.

Changes of bed morphology in response to flume width change were larger than those in response to discharge change. Up to a 0.4 m flume width, a bed morphology of alternate bars was observed and bar length increased as width increased. For channel widths of 0.8 m and above, mid channel bars appeared. Although a main channel persisted with a broadly sinuous course of increasing wavelength with increasing flume width, secondary channels developed and became more numerous and complex as flume width increased. The transition between a single thread planform with alternate bars and the appearance of mid channel bars occurred at flume widths of 0.6 or 0.8 m. These changes in planform were accompanied by changes in bed elevation frequency distribution. The single thread, alternate bar channels that formed below 0.6 m flume width, showed increases in median, standard deviation and kurtosis of bed elevation, and a decrease in skewness with increasing channel width. This indicates a trend of increasing bed elevation with a more variable, asymmetric and peaked frequency distribution. For all flume widths greater than or equal to 0.6 m, the four parameters of the elevation frequency distribution show no distinct trend with channel width, and their values are particularly similar when stream power is rendered dimensionless using the active channel width, or the width of the channel that is experiencing active sediment transport.

Small but distinct differences were observed in bed morphology in response to changes in the formative discharge. At small widths, increased discharge tended to reduce the median bed elevation as well as its standard deviation and kurtosis, suggesting a lower but more homogeneous bed. At the same time, skewness approached zero, indicating a symmetric bed elevation frequency distribution. Thus with small channel widths, the bed appears to be lowered (scoured) and variability in elevation is reduced. However,

above a width of 0.3 m, increased discharge leads to an increase in the overall bed elevation and also in its variability, suggesting increased bar accretion, with a decrease in skewness (increase in asymmetry) and thus an increase in the peakedness of the distribution.

Contribution and limitations:

The flume experiments reported in this thesis extend previous flume work. They confirm the positive associations between channel width and discharge or stream power reported in numerous previous flume studies (e.g. Ashmore, 1991, 2011; Bertoldi et al., 2009a), but more importantly, they extend this work by considering how the active channel develops within a wider range of fixed flume widths. Bertoldi et al. (2009a) identified slightly curved, positive relationships between active width and stream power for two separate groups of experiments conducted in different flumes, which described a single, curved, positive relationship when the ratio of active to wetted width was plotted against dimensionless stream power. The present research identified a positive, curved relationship when the ratio of active to wetted width was plotted against dimensionless stream power, and in the present case, the range of values of dimensionless stream power was much larger. The largest values of ω were achieved within narrow fixed channels, where the active width was close to the value of the wetted width, which in turn occupied the entire channel width. As a result, the upper part of the curve extends that of Bertoldi et al. (2009a) which only reflected unconfined conditions.

In terms of bed morphology, the analysis of summary statistics describing the bed frequency distribution, allow morphological changes to be represented as trajectories across the conceptual diagram presented as Figure 3.11. Thus, Figure 6.1 illustrates a transition from a relatively featureless bed in the the narrowest flume widths, when combined with the highest discharge. This transforms into a more complex, higher relief bed as discharge increases. However, the most complex channels arise when flume width increases further. As flume widths increases above 0.3 m, the relative relief of the bed also progressively increases, with an increasing tendency of bar tops to dominate the cross profile relative to intervening braid channels.

The experiments throw light on the transition from single-thread to braided channels and, in the context of river management, illustrate the morphological consequences of confining braided rivers. The huge increase in stream power results in single thread

channels with lowered, morphologically simple beds, even when sediment supply is not limited. Such environments lack morphological complexity and suffer high shear stresses changing a diverse braided channel into a simplified and hostile river environment from an ecological perspective (e.g. Figure 6.1).

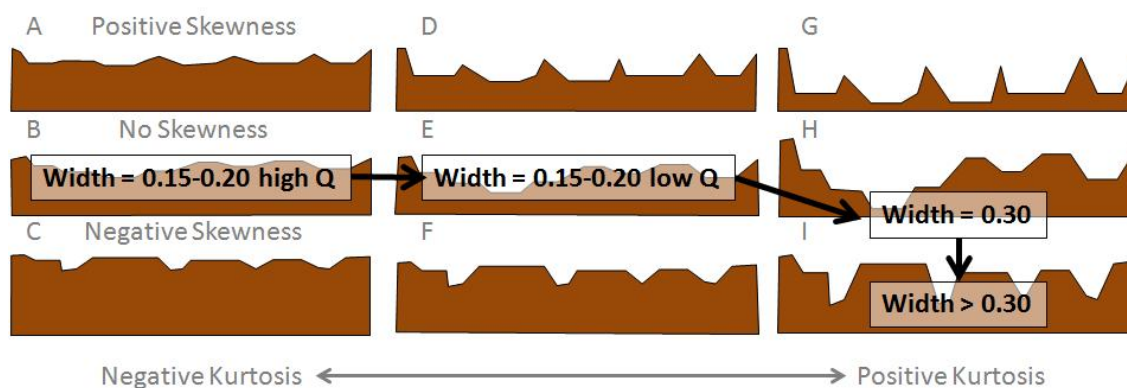


Figure 6.1 Schematic changes in the bed cross profile, associated with shifts in skewness and kurtosis, as discharge and unit stream power decrease and flume width increases.

6.2.2 Research Question 2: What is the influence of vegetation on braided and transitional river morphology?

The role of riparian vegetation in river morphology was explored through analysis of a lidar survey of 36 1 km length reaches of the middle-lower Tagliamento river, Italy. This part of the Tagliamento was selected partly because of the availability of lidar data but also because the vigour of the riparian vegetation is known to vary from reach to reach in response to variations in moisture availability (Gurnell, 2014). Lidar data provides the ability to extract a DEM for the studied reaches and thus to perform a similar analysis of the bed elevation frequency distribution to that performed in relation to the flume experiments of Chapter 3. Lidar data also provides information from which properties of the vegetation cover can be extracted. Unfortunately, the lidar survey was conducted only a few months after the largest flood in three decades, which would undoubtedly have removed much of the riparian vegetation from the active channel, and it was conducted in January before foliage had appeared on the deciduous trees that grow along the river, reducing the ability of the lidar to interact with the tree canopy.

In terms of bed morphology, there was insufficient variation in the widths of the channels investigated on the Tagliamento to explore associations between bed morphology and channel width for comparison with the analyses in Chapter 3. Summary statistics extracted from the elevation frequency distributions showed statistically significant correlations among the median, standard deviation, skewness and kurtosis of the reach bed elevation frequency distributions. The correlations strengthened when only braided reaches were considered, but the Tagliamento braided reaches showed a much greater variability in their skewness than the experimental reaches of Chapter 3. There were also distinct downstream patterns in the standard deviation, skewness, kurtosis and elevation range of the bed elevation frequency distributions of the 36 reaches: the middle reaches (5-20) generally showed the lowest combined values of all four variables, the upstream reaches (1-4) showed a higher elevation range and kurtosis than most of the middle reaches and the lower reaches (23-36) showed generally higher values of all four variables than the middle and upstream reaches. The broad changes in skewness and kurtosis are overlain on Figure 3.11 to produce Figure 6.2. This Figure highlights how shifts in the skewness and kurtosis of the bed elevation frequency distribution describe river bed cross profile changes. The cross profiles are reasonably complex in the upstream reaches and then decline to their lowest complexity around reach 20, where vegetation extent is lowest, reflecting the deeper groundwater levels in the alluvial aquifer and thus poor vegetation development in this part of the river (Gurnell and Petts, 2006). Downstream from reach 20, complexity increases again, initially with the development of relatively narrow bar tops / islands in comparison with the braid channel widths, but the bar tops / islands then progressively widen at the expense of the intervening braid channels in a downstream direction.

In terms of associations between vegetation and bed morphology, strong correlations were identified between all measures of vegetation cover and the median, standard deviation, skewness and kurtosis of the bed elevation frequency distribution. When only the braided reaches were considered all of the correlations apart from that between the median of the bed elevation frequency distribution and % vegetated taller than 10 m were statistically significant. These vegetation – morphology correlations were all stronger than correlations among the morphological properties of the reaches, suggesting an association (causal relationship?) between vegetation and river bed morphology. There were also distinct downstream variations in the measures of

vegetation cover: the middle reaches (7-22) showed the lowest vegetation cover; the upper reaches (1-6) showed a higher cover of vegetation than the middle reaches, and the downstream reaches (23 to 36) showed the highest cover, including the highest cover of trees taller than 10 m. Overall, morphology and vegetation cover showed broadly similar downstream trends through the 36 reaches, suggesting that vegetation and morphology interact and are both controlled by hydrological processes (floods, groundwater levels).

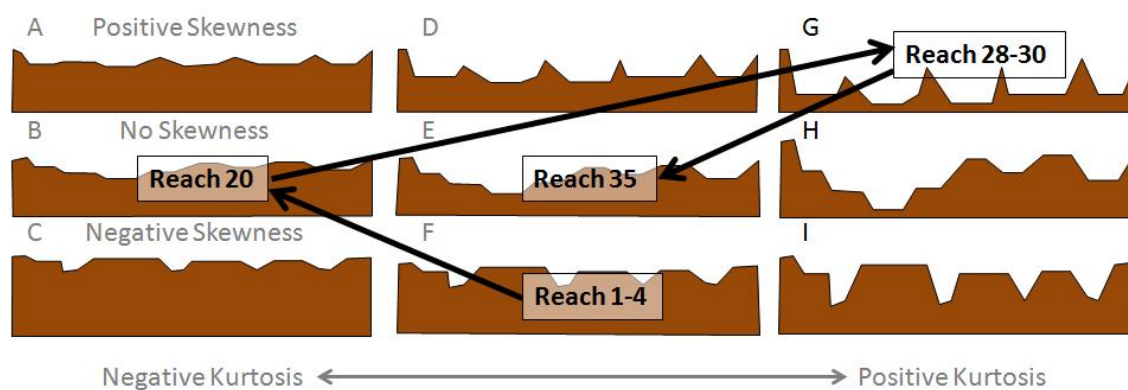


Figure 6.2 Schematic downstream changes in the bed cross profile, indicated by skewness and kurtosis of the bed elevation frequency distribution, along the 36km length of the Tagliamento River.

In the downstream reaches, the areas occupied by taller vegetation (taller than 5 m and 10 m) are clearly defined and are associated with particularly high areas that rise abruptly from the braid plain (Figure 6.3). Although these vegetated areas may simply be established island surfaces, channel incision has been observed in the lower reaches of the Tagliamento to a depth of approximately 1 m (Ziliani and Surian, 2012), and so it is possible that many of the larger patches of taller vegetation, which are often 2m above the adjacent level of the braid plain are associated with elevated areas that have been isolated by this bed incision. These features appear to be associated with distinct secondary bumps or peaks on the bed elevation frequency distribution.

Contribution and limitations:

Although lidar data were only available for a single date, and this date was a few months after a very large flood, associations existed between vegetation and bed morphology, particularly within the braided reaches. This confirms the ‘topographic signature of vegetation’ identified by Bertoldi et al. (2011a) from lidar data obtained on

a different date, when vegetation cover was better developed, and for another part of the Tagliamento River. The new contributions of the present research are that:

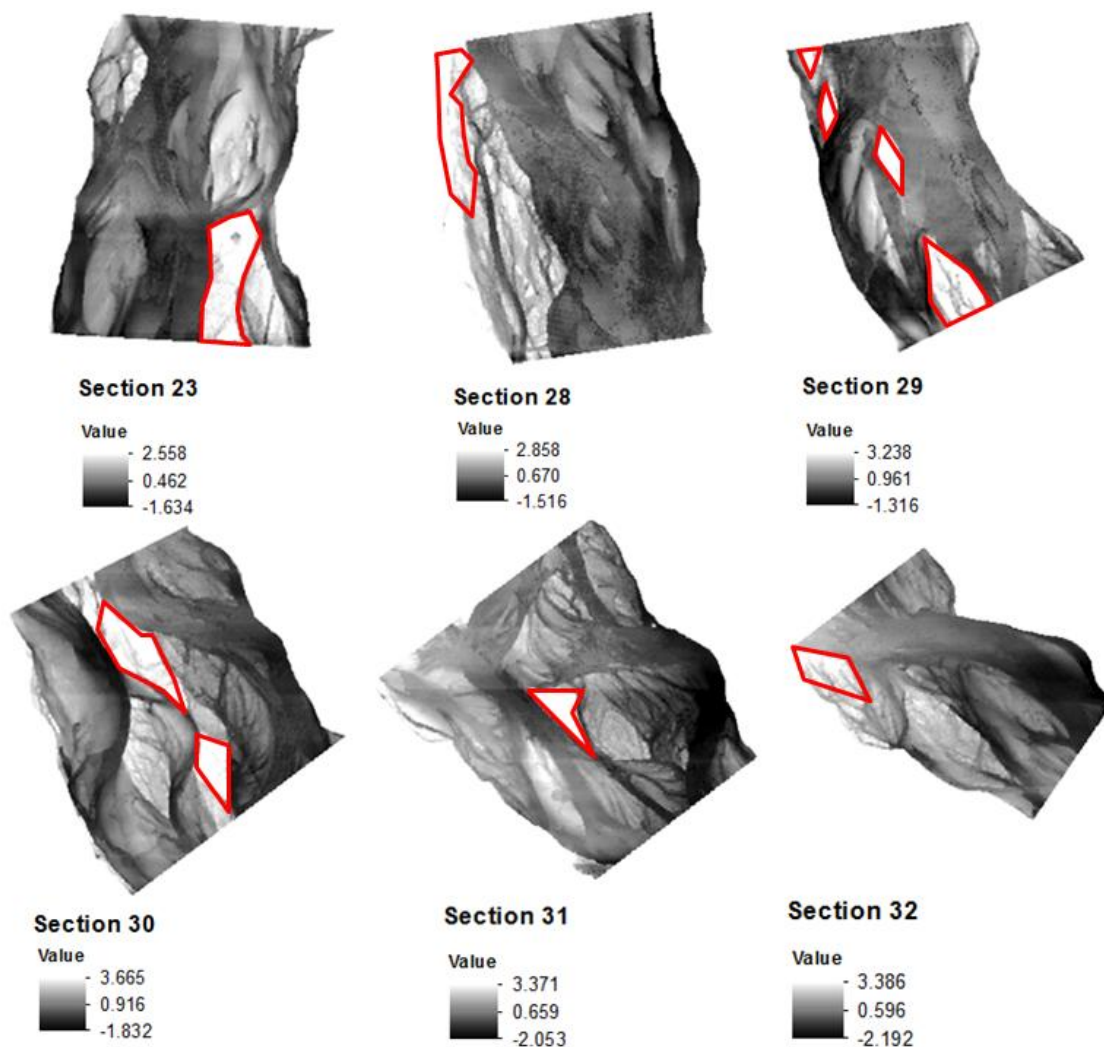


Figure 6.3 Distinct elevated areas (red polygons) within reaches 23, 28-32 that are represented as bumps and secondary peaks on the bed elevation frequency distribution, support mature riparian vegetation and may represent areas of the braid plain isolated by bed incision.

- (i) The topographic signature of vegetation appears to persist despite the occurrence of a very large flood immediately prior to the lidar survey;
- (ii) The topographic signature changes along the river in this 36 km section, and changes in bed morphology parallel changes in vegetation cover, which both map onto the growth rate of the dominant riparian tree species, *Populus nigra*, as measured by Gurnell (2014).

Unfortunately, because of the availability of only a single lidar survey and its limitations for vegetation assessment due to its timing in early spring and after a major

flood, only simple associations can be identified. Multi-date lidar observations gathered during the summer, when foliage is fully developed, are essential if vegetation-morphology interactions are to be tracked in sufficient detail and the processes driving that interaction are to be inferred more reliably.

6.2.3 Research Question 3: Does the type and extent of vegetation influence / covary with braided river planform?

Having established a link between vegetation and braid plain morphology in chapter 4, a sample of European braided and transitional river reaches with different riparian vegetation were selected for analysis to assess whether differences in their morphology could, in part, be attributed to vegetation. Six rivers were selected from the UK, Poland, Switzerland and Italy. These included a glacier-fed braided river (Val Roseg, Switzerland) located above the tree line; a braided (Feshie) and two transitional (Coquet, Liza) UK rivers surrounded by moorland with minimal tree cover; two braided rivers (Bialka, Poland and the headwaters of the Tagliamento, Italy) which, because of their altitude and latitude, are bordered by relatively slow-growing riparian woodland; and a low-lying, river located in southern Europe (middle reaches of the Tagliamento, Italy), where riparian trees grow vigorously if they are not short of water.

Each river was subdivided into 1 km long reaches and information was extracted from one or more aerial images (mainly from Google Earth) to describe the channel planform (width, braiding index (Bi), anastomosing index (Ai, Ai2), and sinuosity (Si) of the main channel) and gradient. In addition flow records were analysed to estimate total and unit stream power associated with the 2, 5 and 10 year flow events.

Analysis of the entire data set revealed an inverse relationship between unit stream power and channel width across all of the studied rivers, and three parallel curved relationships were defined. The Tagliamento middle reaches plotted above the Tagliamento headwaters, Bialka, and Val Roseg, which in turn plotted above the Feshie. Since the bounding vegetation on these rivers varies, the shift in the curved relationship between unit stream power and channel width could be interpreted as reflecting a change in the erosion resistance (relative bank strength) of the channel margins: the Tagliamento middle reaches show the highest unit stream power for any channel width, with intermediate values for the Tagliamento headwaters, Bialka and Val Roseg, and the

lowest values for the Feshie. However, a larger data set incorporating more rivers would be needed to confirm this suggestion.

A major problem faced in integrating data from the six rivers was the enormous differences in their size, discharge, slope and probably bed material (although it was not possible to obtain reliable bed material calibre estimates). Dimensionless stream power would have provided the most effective way of scaling the data to account for these differences, but because of the poor quality of the bed material data, unit stream power had to be used instead.

Broad trends of decreasing maximum B_i , S_i , A_i and A_{i2} were observed with increasing unit stream power across the entire data set, with no apparent differences displayed among any of the six rivers. Therefore, the different response of the Tagliamento middle reaches to unit stream power for any given width is not reflected in the response of the planform indices. Principal Components Analyses applied to the four planform indices, unit stream power, and its component variables (slope, width, Q_{10}), further confirmed the differences in scale (slope, width, Q_{10}) of the selected rivers. When these differences were removed by expressing slope, width, and Q_{10} in the form of unit stream power in the PCA, differences between the rivers were removed and all four planform indices showed an increase in their maximum values with decreasing unit stream power across the entire 6 river data set.

Contribution and limitations:

Despite the wide variability in river size and in all of the investigated variables within and between rivers and river reaches, some general trends emerged from the analyses presented in chapter 5, but a far larger data set is required before these trends can be verified.

Therefore, the contribution of the research in Chapter 5 was to reveal:

- (i) differences in the relationship between unit stream power and channel width that may relate to 'bank strength'.
- (ii) differences in the morphological indices (B_i , A_i , A_{i2} , S_i) through time within individual reaches that may contribute to tracking trajectories of channel change reflecting long term adjustments in the interactions between flow, sediment transport and vegetation growth.

- (iii) broad associations between the morphological indices (B_i , A_i , A_{i2} , S_i) and unit stream power that are common to all of the investigated rivers.

However, the small sample of rivers investigated and the lack of information on bed material calibre limited the analytical results and made it difficult to assess whether the type and extent of vegetation influenced / co-varied with braided river planform, which was the initial aim of the research.

6.3 FUTURE RESEARCH

Although each of chapters 3 to 5 has made a clear research contribution, the expected links between these contributions were not as strong as was initially hoped. In particular, (i) the focus on transitions between braided and single thread channels, which was clearly addressed in the flume experiments of Chapter 3, was not developed as greatly as anticipated in subsequent chapters and (ii) although associations were found between vegetation and channel morphology, insufficient information was assembled in Chapters 4 and 5 to investigate the underlying processes driving this association.

The limited focus on transitional rivers partly reflects the fact that within the European river context of Chapters 4 and 5, transitional and single thread reaches are often heavily influenced by human modifications, making it difficult to obtain a large enough data set of naturally-functioning rivers of these types. In addition, in the context of Chapter 4, insufficient lidar data was available for single thread and transitional reaches to be fully examined. The insufficiently detailed evaluation of the impact of vegetation on river bed morphology also reflects lack of data, but in this case it is a function of time limitations in identifying suitable river reaches and data sources and then in processing the data for those additional reaches and data sources. Both of these shortcomings could be addressed in future research that extends all three of the research elements reported in Chapters 3 to 5.

In relation to the flume experiments of Chapter 3, additional work incorporating different flume slopes, calibres of bed material, discharges (fixed and variable) and sediment supply would be extremely time consuming but also informative in developing a general model of transitions between single thread and braided morphologies. However, perhaps the most relevant research to the broad theme of this thesis would be

to retain the tested flume conditions of slope, bed material, width and discharge but to introduce vegetation. Although there are many published flume experiments that consider the impact of vegetation on river planform and bed morphology, which generally indicate a simplification of planform with the introduction of vegetation and a shift from multi-thread towards single thread forms (e.g. Braudrick et al., 2009; Jang and Shimizu, 2007; Li and Millar, 2010; Tal and Paola, 2007, 2010), there has been no research which has considered this topic in the context of different degrees of channel width confinement. Such research would be interesting from both scientific and river management viewpoints.

In relation to the analysis of airborne lidar data, as illustrated in Chapter 4, real advances in understanding vegetation - channel morphology interactions could be achieved if analysis could be extended to annual lidar surveys collected at the same time of year (summer) over at least a decade, and calibrated using field measurements. The research by Bertoldi et al. (2011a) illustrates the power of coupling field observations with lidar data. If multiple lidar surveys were available, changes in morphology could be precisely linked with the occurrence of floods and changes in vegetation extent, height and biomass through time, and the vegetation properties could be quantified and verified using field observations. In this way the timing of vegetation and morphological change could be tracked, hopefully confirming the way in which vegetation appears to lead to sediment retention and morphological change in braided rivers (Gurnell et al., 2001; Gurnell and Petts, 2006; Bertoldi et al., 2011b).

Coupled with the above, if the repeat lidar surveys were extended into transitional and single thread reaches, a better understanding of the role of vegetation at these transitions could be achieved. Historical analyses of information extracted from air photographs have revealed temporal transitions in river planform that appear to be coupled with vegetation development (e.g. Zanoni et al., 2008), but shorter term coverage with lidar data could reveal precisely how vegetated landforms develop in transitional reaches and so would provide evidence of how transitions in planform from multi-thread to transitional might be achieved. This would once again be of both scientific and river management interest

Finally, in relation to the multiple river research reported in Chapter 5, the analysis of a rather small sample of reaches and images showed considerable promise. However, if a

much larger data set could be assembled, preferably including information on bed material size, a more integrated analysis could be achieved following that proposed by Eaton et al. (2010). Their analysis incorporates dimensionless formative discharge, slope, and relative bank strength into a three dimensional model describing thresholds between single thread, anabranching and braided rivers. They use data from other previously-published studies to test the model, but a more robust test would be achieved with a large purpose-collected data set. If the model could be supported, it would provide not only an important scientific finding but it would be a useful tool for river managers, enabling them to understand why particular channel types are present or to design channels to restore river function.

6.4 RELEVANCE OF RESEARCH TO RIVER MANAGEMENT

The relevance of each of the research elements and their possible future development to river management is mentioned in section 6.3. In this section these comments are synthesised and extended to indicate how the research could be used by river managers.

Within Europe, the Water Framework Directive (WFD; European Commission, 2000) requires that rivers are managed to achieve good ecological status. It also highlights the importance of the hydrology, morphology and dynamics of river channels and their floodplains (abbreviated to ‘hydromorphology’ in EU documents) as crucial supporting elements in achieving understanding of river ecosystem functioning, and identifying appropriate management actions. In essence, hydromorphology as it relates to the diversity, dynamics and functioning of physical habitats, is a crucial component of river ecosystems (Newson and Large, 2006; Vaughan et al., 2009).

Braided rivers, particularly those with a gravel bed, are the most complex and dynamic type of river morphology (Church, 2006), and also offer particularly high hydrological, water quality and temperature diversity (Arscott et al., 2001) as a result of complex surface-groundwater downwelling and upwelling pathways (Malard et al., 2000). They are also the most endangered river type within Europe as a result of centuries of river engineering (e.g. Petts et al., 1989). Therefore, the protection and reinstatement of braided rivers is an important aim for river managers, which nevertheless needs to be achieved against the demands and pressures placed upon rivers by humans.

The present research has illustrated the morphological consequences of confining braided rivers (Chapter 3); the role of vegetation in contributing to the morphological complexity of braided rivers (Chapter 4); and has pointed to the potential role of riparian vegetation in constraining the relationship between stream power and width of braided rivers (Chapter 5). Outputs of all of these research elements have the potential to contribute to improved management concepts and tools.

The research in Chapter 3 has demonstrated how river confinement leads to a simplification of river bed morphology, the reduction in size of many bed features and the disappearance of others. In any particular river reach, this reduction in the diversity, size and 'roughness' of bedforms is accompanied by an increase in unit stream power (the narrowed channel has to accommodate the same discharge). This increase in stream power and associated flow velocities result in a reduction in the size and area of hydraulic 'refugia' within the channel and an increase in the proportion of the bed that becomes active and unstable. All of these changes are demonstrated in the experiments reported in chapter 3. When translated into the context of a real river subject to confinement, the changes represent an increasingly hostile environment for the biota, whether the focus is on fish, invertebrates or plants. Therefore, the research implicitly projects the *management concept*, that artificial confinement of rivers should be kept to a minimum, in order to retain as a diverse a range of physical habitats and hydraulic refugia as is feasible within the constraints imposed by human requirements and activities. It also underpins the *management concept* that by manipulating channel width, a range of particular, sustainable habitat mosaics and dynamics are induced that do not require any artificial creation through other human interventions.

Although strategies in river restoration and flood protection increasingly reflect the above-stated concept that an increase in river width is needed to improve bed morphological complexity and ecological quality (e.g. Rohde et al., 2004, 2005; Jähnig et al., 2009; Weber et al., 2009), few studies have provided detailed quantitative information on the effect of different width constraints on river bed form. This research has provided this quantitative information and has proposed an innovative approach to defining channel bed complexity by extracting summary parameters of the bed elevation frequency distribution. Importantly, with airborne laser scanning becoming increasingly affordable and the resulting data sets becoming more accessible, the possibility of defining braided river bed form in great detail is becoming a realistic aim for river

managers. As a result, the outputs produced here (e.g. Figure 6.1) that link the style of bed topography to, for example, the skewness and kurtosis of the bed elevation distribution, becomes a realistic *management tool* for assessing pre- and post-project bed form and for designing the width of channels based on expectations of the outcomes for bed form.

Chapters 4 and 5 extend the work of chapter 3 by including consideration of vegetation. In particular, Chapter 4 illustrates an association between vegetation and river bed morphology, supporting the previous suggestion by Bertoldi et al. (2011a) that the former imposes a topographic signature on the latter. As with chapter 3, the analysis of bed topography using lidar data is feasible for managers, and has the potential for devising a *management tool* along the lines of Figure 6.2. However in this case, analysis of a greater range of island braided rivers is needed, as is analysis of the same rivers at different vegetation colonisation and growth stages following disturbing floods (e.g. Bertoldi et al., 2011b, Henshaw et al., 2012). If this research were performed, it should be possible to use properties of the bed elevation frequency distribution (range, standard deviation, skewness and kurtosis), to summarise the form of the currently active bed and its potential adjustments under vegetation development and destruction whether by natural processes or human interventions (planting, pruning), and also under changes in gradient and width induced by management actions. Furthermore, instabilities in the channel bed form have been shown to be effectively isolated by the bed elevation frequency distribution, providing useful indicators for managers of issues such as incision, which may need to be considered in the design of management actions. A crucial point is that lidar data gathered for management purposes should not be preprocessed to ‘get rid of the vegetation’ (and other surface features), as is currently the case with most data sets gathered for the UK Environment Agency, since vegetation and morphology need to be jointly quantified to gain a full insight into river functioning.

Lastly, Chapter 5, although only an exploratory analysis that requires further development, has illustrated the potential for a further management tool. River width is determined mainly by fluvial processes, and is manipulated through management activities to suit human and/or environmental needs. The initial results from Chapter 5 indicate that freely developed riparian vegetation may also influence channel width, allowing also for different styles of river to evolve as riparian vegetation changes. This

concept underpins the model proposed by Eaton et al. (2010), and the concept's management implications have been demonstrated in some field situations, where 'floodplain unravelling' (i.e. a change from a meandering to braided planform) has occurred as a consequence of overgrazing of floodplain / riparian vegetation (e.g. Smith, 2004). Developing a larger data set to feed into the analysis of Chapter 4 could lead to the development of a *management tool* similar to that of Eaton et al. (2010) but simpler so that it would be more readily applicable by managers.

In conclusion, this thesis has gone a considerable distance in developing scientific understanding of interactions between fluvial processes, confinement, vegetation and morphology in braided and transitional rivers that underpins some simple management concepts and tools. Some of these tools could be applied now with great effect, whilst others need some refinement or improvement before they can be fully adopted by river managers.

References

- ALABYAN, A. M. & CHALOV, R. S. 1998. Types of river channel patterns and their natural controls. *Earth Surface Processes and Landforms*, 23, 467-474.
- AMLIN, N. M. & ROOD, S. B. 2003. Drought stress and recovery of riparian cottonwoods due to water table alteration along Willow Creek, Alberta. *Trees*, 17, 351-358.
- ARSCOTT, D. B., TOCKNER, K., & WARD, J. V. 2001. Thermal heterogeneity along a braided floodplain river (Tagliamento River, northeastern Italy). *Canadian Journal of Fisheries and Aquatic Sciences* 58(12), 2359--2373.
- ASHMORE, P. 1990. Channel morphology and bed load pulses in braided, gravel-bed streams. *Geografiska Annaler. Series A. Physical Geography*, 37-52.
- ASHMORE, P. 2009. Intensity and characteristic length of braided channel patterns This paper is one of a selection of papers in this Special Issue in honour of Professor M. Selim Yalin (1925-2007). *Canadian Journal of Civil Engineering*, 36, 1656-1666.
- ASHMORE, P. 2013. Morphology and dynamics of braided rivers. In: John F. Shroder (Editor-in-chief), Wohl, E. (Volume Editor). *Treatise on Geomorphology*, Vol 9, Fluvial Geomorphology, San Diego: Academic Press; 2013. p. 289-312.
- ASHMORE, P., BERTOLDI, W. & TOBIAS GARDNER, J. 2011. Active width of gravel-bed braided rivers. *Earth Surface Processes and Landforms*, 36, 1510-1521.
- ASHMORE, P. E. 1982. Laboratory modelling of gravel braided stream morphology. *Earth Surface Processes and Landforms*, 7, 201-225.
- ASHMORE, P. E. 1991. How do gravel-bed rivers braid? *Canadian Journal of Earth Sciences*, 28, 326-341.
- BEECHIE, T. J., LIERMANN, M., POLLOCK, M. M., BAKER, S. & DAVIES, J. 2006. Channel pattern and river-floodplain dynamics in forested mountain river systems. *Geomorphology*, 78, 124-141.
- BEGIN, Z. 1981. The relationship between flow-shear stress and stream pattern. *Journal of Hydrology*, 52, 307-319.
- BENNETT, S. J., WU, W., ALONSO, C. V. & WANG, S. S. 2008. Modeling fluvial response to in-stream woody vegetation: implications for stream corridor restoration. *Earth Surface Processes and Landforms*, 33, 890-909.
- BERTOLDI, W., ASHMORE, P. & TUBINO, M. 2009a. A method for estimating the mean bed load flux in braided rivers. *Geomorphology*, 103, 330-340.
- BERTOLDI, W., DRAKE, N. & GURNELL, A. 2011b. Interactions between river flows and colonizing vegetation on a braided river: exploring spatial and temporal dynamics in riparian vegetation cover using satellite data. *Earth Surface Processes and Landforms*, 36, 1474-1486.
- BERTOLDI, W., GURNELL, A. & DRAKE, N. 2011a. The topographic signature of vegetation development along a braided river: results of a combined analysis of airborne lidar, color air photographs, and ground measurements. *Water Resources Research*, 47.
- BERTOLDI, W., ZANONI, L. & TUBINO, M. 2009b. Planform dynamics of braided streams. *Earth Surface Processes and Landforms*, 34, 547-557.
- BRAUDRICK, C. A., DIETRICH, W. E., LEVERICH, G. T. & SKLAR, L. S. 2009. Experimental evidence for the conditions necessary to sustain meandering in coarse-bedded rivers. *Proceedings of the National Academy of Sciences*, 106, 16936-16941.

- BRAY, D. I. 1973. Regime relations for Alberta gravel-bed rivers. *Proceedings of the 7th Canadian Hydrology Symposium*.
- BRAY, D. I. 1982. Regime equations for gravel-bed rivers In: HEY, R. D., BATHURST, J. C. & THORNE, C. R. (eds.) *Gravel-bed Rivers: Fluvial processes, Engineering and Management*. Chichester: Wiley.
- BRICE, J. 1960. Index for description of channel braiding. *Geological Society of America Bulletin*, 71, 1833.
- BRICE, J. C. 1964. *Channel patterns and terraces of the Loup Rivers in Nebraska*, US Government Printing Office.
- BRIDGE, J. S. 1993. The interaction between channel geometry, water flow, sediment transport and deposition in braided rivers. *Geological Society, London, Special Publications*, 75, 13-71.
- BRIERLEY, G. J. & FRYIRS, K. A. 2008. *Geomorphology and river management: applications of the river styles framework*, John Wiley & Sons.
- CALLANDER, R. 1969. Instability and river channels. *Journal of Fluid Mechanics*, 36, 465-480.
- CAMPOREALE, C. & RIDOLFI, L. 2006. Riparian vegetation distribution induced by river flow variability: A stochastic approach. *Water resources research*, 42.
- CARLING, P., JANSEN, J. & MESHKOVA, L. 2013. Multichannel rivers: their definition and classification. *Earth Surface Processes and Landforms*, 39, 26-37.
- CARSON, M. 1984a. The meandering-braided river threshold: a reappraisal. *Journal of Hydrology*, 73, 315-334.
- CARSON, M. A. 1984b. Observations on the Meandering-Braided River Transition, the Canterbury Plains, New Zealand: Part One. *New Zealand Geographer*, 40, 12-19.
- CARTER JOHNSON, W. 2000. Tree recruitment and survival in rivers: influence of hydrological processes. *Hydrological Processes*, 14, 3051-3074.
- CHARLTON, R. 2007. *Fundamentals of fluvial geomorphology*, Routledge.
- CHEW, L. & ASHMORE, P. E. 2001. Channel adjustment and a test of rational regime theory in a proglacial braided stream. *Geomorphology*, 37, 43-63.
- CHURCH, M. 1992. Channel morphology and typology. *The rivers handbook*, 1, 126-143.
- CHURCH, M. 2002. Geomorphic thresholds in riverine landscapes. *Freshwater Biology*, 47, 541-557.
- CHURCH, M. 2006. Bed material transport and the morphology of alluvial river channels. *Annu. Rev. Earth Planet. Sci.*, 34, 325-354.
- COLOMBINI, M., SEMINARA, G. & TUBINO, M. 1987. Finite-amplitude alternate bars. *Journal of Fluid Mechanics*, 181, 213-232.
- COMITI, F., DA CANAL, M., SURIAN, N., MAO, L., PICCO, L. & LENZI, M. 2011. Channel adjustments and vegetation cover dynamics in a large gravel bed river over the last 200years. *Geomorphology*, 125, 147-159.
- CORENBLIT, D., STEIGER, J., GURNELL, A. & TABACCHI, E. 2007. Darwinian origin of landforms. *Earth Surface Processes and Landforms*, 32, 2070-2073.
- CORENBLIT, D., STEIGER, J., GURNELL, A. M., TABACCHI, E. & ROQUES, L. 2009. Control of sediment dynamics by vegetation as a key function driving biogeomorphic succession within fluvial corridors. *Earth Surface Processes and Landforms*, 34, 1790-1810.
- CROSATO, A. & MOSSELMAN, E. 2009. Simple physics-based predictor for the number of river bars and the transition between meandering and braiding. *Water Resources Research*, 45.
- DADE, W. 2000. Grain size, sediment transport and alluvial channel pattern. *Geomorphology*, 35, 119-126.

- DAVIS, W. M. 1899. The geographical cycle. *The Geographical Journal*, 14, 481-504.
- DESLOGES, J. R. & CHURCH, M. A. 1989. Wandering gravel-bed rivers. *The Canadian Geographer/Le Géographe canadien*, 33, 360-364.
- EATON, B., MILLAR, R. G. & DAVIDSON, S. 2010. Channel patterns: braided, anabranching, and single-thread. *Geomorphology*, 120, 353-364.
- EATON, B. C. 2006. Bank stability analysis for regime models of vegetated gravel bed rivers. *Earth Surface Processes and Landforms*, 31, 1438-1444.
- EATON, B. C. & GILES, T. R. 2009. Assessing the effect of vegetation-related bank strength on channel morphology and stability in gravel-bed streams using numerical models. *Earth Surface Processes and Landforms*, 34, 712-724.
- EGOZI, R. & ASHMORE, P. 2008. Defining and measuring braiding intensity. *Earth Surface Processes and Landforms*, 33, 2121-2138.
- EGOZI, R. & ASHMORE, P. 2009. Experimental analysis of braided channel pattern response to increased discharge. *Journal of Geophysical Research: Earth Surface (2003–2012)*, 114.
- EUROPEAN COMMISSION, 2000. Directive 2000/60/EC of the European Parliament and of the Council of 23 October 2000 Establishing a Framework for Community Action in the Field of Water Policy. Official Journal L 327, 22/12/2000, Brussels, Belgium, 73 pp.
- FERGUSON, R. 1984. The threshold between meandering and braiding. *Channels and channel control structures*. Springer.
- FERGUSON, R. 1987. Hydraulic and sedimentary controls of channel pattern. *River channels: environment and process*, 129-158.
- FERGUSON, R. 1993. Understanding braiding processes in gravel-bed rivers: progress and unsolved problems. *Geological Society, London, Special Publications*, 75, 73-87.
- FRIEND, P. & SINHA, R. 1993. Braiding and meandering parameters. *Geological Society, London, Special Publications*, 75, 105-111.
- GERMANOSKI, D. & SCHUMM, S. 1993. Changes in braided river morphology resulting from aggradation and degradation. *The Journal of Geology*, 451-466.
- GLENZ, C., SCHLAEPFER, R., IORGULESCU, I. & KIENAST, F. 2006. Flooding tolerance of Central European tree and shrub species. *Forest Ecology and Management*, 235, 1-13.
- GRAN, K. & PAOLA, C. 2001. Riparian vegetation controls on braided stream dynamics. *Water Resources Research*, 37, 3275-3283.
- GRIFFIN, E. R. & SMITH, J. D. 2004. Floodplain stabilization by woody riparian vegetation during an extreme flood. *Riparian Vegetation and Fluvial Geomorphology*, 221-236.
- GURNELL, A. 2014. Plants as river system engineers. *Earth Surface Processes and Landforms*, 39, 4-25.
- GURNELL, A. & PETTS, G. 2006. Trees as riparian engineers: the Tagliamento River, Italy. *Earth Surface Processes and Landforms*, 31, 1558-1574.
- GURNELL, A., SURIAN, N. & ZANONI, L. 2009. Multi-thread river channels: A perspective on changing European alpine river systems. *Aquatic sciences*, 71, 253-265.
- GURNELL, A., THOMPSON, K., GOODSON, J. & MOGGRIDGE, H. 2008. Propagule deposition along river margins: linking hydrology and ecology. *Journal of Ecology*, 96, 553-565.
- GURNELL, A., TOCKNER, K., EDWARDS, P. & PETTS, G. 2005. Effects of deposited wood on biocomplexity of river corridors. *Frontiers in Ecology and the Environment*, 3, 377-382.

- GURNELL, A. M., PETTS, G. E., HANNAH, D. M., SMITH, B. P., EDWARDS, P. J., KOLLMANN, J., WARD, J. V. & TOCKNER, K. 2001. Riparian vegetation and island formation along the gravel-bed Fiume Tagliamento, Italy. *Earth Surface Processes and Landforms*, 26, 31-62.
- HABERSACK, H. 2001. Radio-tracking gravel particles in a large braided river in New Zealand: A field test of the stochastic theory of bed load transport proposed by Einstein. *Hydrological Processes*, 15, 377-391.
- HANSEN, E. 1967. The formation of meanders as a stability problem. *Basic Res. Prog. Rep.*, 13, 9-13.
- HENDERSON, F. M. 1963. Stability of alluvial channels. *Transactions of the American Society of Civil Engineers*, 128, 657-686.
- HENSHAW, A. J., GURNELL, A. M., BERTOLDI, W. & DRAKE, N. A. 2013. An assessment of the degree to which Landsat TM data can support the assessment of fluvial dynamics, as revealed by changes in vegetation extent and channel position, along a large river. *Geomorphology*, 202, 74-85.
- HERVOUET, A., DUNFORD, R., PIÉGAY, H., BELLETTI, B. & TRÉMÉLO, M.-L. 2011. Analysis of post-flood recruitment patterns in braided-channel rivers at multiple scales based on an image series collected by unmanned aerial vehicles, ultra-light aerial vehicles, and satellites. *GIScience & Remote Sensing*, 48, 50-73.
- HEY, R. D. & THORNE, C. R. 1986. Stable channels with mobile gravel beds. *Journal of Hydraulic Engineering*, 112, 671-689.
- HOLLAUS, M., WAGNER, W., EBERHÖFER, C. & KAREL, W. 2006. Accuracy of large-scale canopy heights derived from LiDAR data under operational constraints in a complex alpine environment. *ISPRS Journal of Photogrammetry and Remote Sensing*, 60, 323-338.
- HONG, L. B. & DAVIES, T. 1979. A study of stream braiding. *Geological Society of America Bulletin*, 90, 1839-1859.
- HODGSON, M.E. & BRESNAHAN, P. 2004. *Photogrammetric Engineering and Remote Sensing*, March 2004, 331-339
- HOWARD, A. D., KEETCH, M. E. & VINCENT, C. L. 1970. Topological and geometrical properties of braided streams. *Water Resources Research*, 6, 1674-1688.
- JACKSON, J. 1834. Hints on the subject of geographical arrangement and nomenclature. *Journal of the Royal Geographical Society of London*, 4, 72-88.
- JÄHNIG, S.C., BRUNZEL, S., GACEK, S., LORENZ, A. W. & HERING, D. 2009. Effects of re-braiding measures on hydromorphology, floodplain vegetation, ground beetles and benthic invertebrates in mountain rivers, *Journal of Applied Ecology*, 46, 406-416.
- JANG, C.-L. & SHIMIZU, Y. 2007. Vegetation effects on the morphological behavior of alluvial channels. *Journal of Hydraulic Research*, 45, 763-772.
- JEROLMACK, D. J. & MOHRIG, D. 2007. Conditions for branching in depositional rivers. *Geology*, 35, 463-466.
- KELLERHALS, R. 1982. Effect of river regulation on channel stability. *Gravel-bed rivers*, 685-715.
- KELLERHALS, R., BRAY, D. I. & CHURCH, M. 1976. Classification and analysis of river processes. *Journal of the Hydraulics Division*, 102, 813-829.
- KLEINHANS, M. G. 2010. Sorting out river channel patterns. *Progress in Physical Geography*, 34, 287-326.
- KLEINHANS, M. G. & VAN DEN BERG, J. H. 2011. River channel and bar patterns explained and predicted by an empirical and a physics-based method. *Earth Surface Processes and Landforms*, 36, 721-738.

- KNIGHTON, A. D. & NANSON, C. G. 1993. Anastomosis and the continuum of channel pattern. *Earth Surface Processes and Landforms*, 18, 613-625.
- KRAUS, K. & PFEIFER, N. 1998. Determination of terrain models in wooded areas with airborne laser scanner data. *ISPRS Journal of Photogrammetry and remote Sensing*, 53, 193-203.
- LANE, E. W. 1955. Design of stable channels. *Transactions of the American Society of Civil Engineers*, 120, 1234-1260.
- LANE, E. W. 1957. *A study of the shape of channels formed by natural streams flowing in erodible material*, US Army Engineer Division, Missouri River.
- LANE, S. 2006. Approaching the system-scale understanding of braided river behaviour. In: SAMBROOK-SMITH, G., BEST, J.L., BRISTOW, C.S., PETTS, G. (ed.) *Braided Rivers*. Oxford: Blackwell Publishers.
- LEOPOLD, L. B. & WOLMAN, M. G. 1957. *River channel patterns: braided, meandering, and straight*, US Government Printing Office Washington, DC.
- LEOPOLD, L. B., WOLMAN, M. G. & MILLER, P. 1964. *Fluvial processes in geomorphology*. San Francisco: WH Freeman.
- LEWIN, J. & BREWER, P. A. 2001. Predicting channel patterns. *Geomorphology*, 40, 329-339.
- LI, S. & MILLAR, R. 2011. A two-dimensional morphodynamic model of gravel-bed river with floodplain vegetation. *Earth Surface Processes and Landforms*, 36, 190-202.
- LITE, S. & STROMBERG, J. 2005. Surface water and ground-water thresholds for maintaining *Populus Salix* forests, San Pedro River, Arizona. *Biological Conservation*, 125, 153-167.
- LOKHTIN, V. 1897. About a Mechanism of River Channel. *Voprosy gidrotekhniki svobodnykh rek*, 23-59.
- LYTLE, D. A. & MERRITT, D. M. 2004. Hydrologic regimes and riparian forests: a structured population model for cottonwood. *Ecology*, 85, 2493-2503.
- MALAVOI, J., GAUTIER, J. & BRAVARD, J. 2002. Free space for rivers: A geodynamical concept for sustainable management of the water resources. *River Flow 2002*, 507-514.
- MALARD, F., TOCKNER, K., & WARD, J.V. 2000. Physico-chemical heterogeneity in a glacial riverscape. *Landscape Ecology* 15, 679-695.
- MARTIN, Y. & CHURCH, M. 1995. Bed-material transport estimated from channel surveys: Vedder River, British Columbia. *Earth Surface Processes and Landforms*, 20, 347-361.
- MARTIN, Y. & HAM, D. 2005. Testing bedload transport formulae using morphologic transport estimates and field data: lower Fraser River, British Columbia. *Earth Surface Processes and Landforms*, 30, 1265-1282.
- MCKENNEY, R., JACOBSON, R. B. & WERTHEIMER, R. C. 1995. Woody vegetation and channel morphogenesis in low-gradient, gravel-bed streams in the Ozark Plateaus, Missouri and Arkansas. *Geomorphology*, 13, 175-198.
- MCLEAN, S., WOLFE, S. & NELSON, J. 1999. Predicting boundary shear stress and sediment transport over bed forms. *Journal of Hydraulic Engineering*, 125, 725-736.
- MIALL, A. D. 1977. A review of the braided-river depositional environment. *Earth-Science Reviews*, 13, 1-62.
- MILLAR, R. G. 2000. Influence of bank vegetation on alluvial channel patterns. *Water Resources Research*, 36, 1109-1118.
- MILLAR, R. G. 2005. Theoretical regime equations for mobile gravel-bed rivers with stable banks. *Geomorphology*, 64, 207-220.

- MOLLARD, J. 1973. Air photo interpretation of fluvial features. *Fluvial Processes and Sedimentation. Research Council of Canada*, 341-380.
- MOSLEY, M. P. 1982. Analysis of the effect of changing discharge on channel morphology and instream uses in a braided river, Ohau River, New Zealand. *Water resources research*, 18, 800-812.
- MOSLEY, M. P. 1983. Response of braided rivers to changing discharge. *Journal of Hydrology*, 22.
- MOSELNAN, E., TUBINO, M. & ZOLEZZI, G. The overdeepening theory in river morphodynamics: Two decades of shifting interpretations. *River Flow*, 2006. 1175-1181.
- MURRAY, A. B. & PAOLA, C. 1994. A cellular model of braided rivers. *Nature*, 371, 54-57.
- MURRAY, A. B. & PAOLA, C. 2003. Modelling the effect of vegetation on channel pattern in bedload rivers. *Earth Surface Processes and Landforms*, 28, 131-143.
- NANSON, G. C. & KNIGHTON, A. D. 1996. Anabranching rivers: their cause, character and classification. *Earth surface processes and landforms*, 21, 217-239.
- NEWSON, M. D., LARGE, A. R. G. 2006. 'Natural' rivers, 'hydromorphological quality' and river restoration: a challenging new agenda for applied fluvial geomorphology. *Earth Surface Processes and Landforms* 31, 1606–1624.
- O'CONNOR, J. E., JONES, M. A. & HALUSKA, T. L. 2003. Flood plain and channel dynamics of the Quinault and Queets Rivers, Washington, USA. *Geomorphology*, 51, 31-59.
- OLESEN, K. 1984. Alternate bars in and meandering of alluvial rivers. in *River Meandering*, edited by C. M. Elliott, pp. 873 – 884, *Am. Soc. of Civ. Eng., New York*.
- OSTERKAMP, W. 1978. Gradient, discharge, and particle-size relations of alluvial channels in Kansas, with observations on braiding. *American Journal of Science*, 278, 1253-1268.
- OSTERKAMP, W. & HUPP, C. 2010. Fluvial processes and vegetation—glimpses of the past, the present, and perhaps the future. *Geomorphology*, 116, 274-285.
- PAOLA, C. 2001. Modelling stream braiding over a range of scales. *Gravel Bed Rivers V*, 11-46.
- PARKER, G. 1976. On the cause and characteristic scales of meandering and braiding in rivers. *Journal of Fluid Mechanics*, 76, 457-480.
- PERUCCA, E., CAMPOREALE, C. & RIDOLFI, L. 2007. Significance of the riparian vegetation dynamics on meandering river morphodynamics. *Water Resources Research*, 43.
- PETTS, G. E., MOLLER, H., ROUX, A. L. 1989. *Historical change of large alluvial rivers: Western Europe*. Wiley, Chichester, 355pp.
- PIEGAY, H., ALBER, A., SLATER, L. & BOURDIN, L. 2009. Census and typology of braided rivers in the French Alps. *Aquatic Sciences*, 71, 371-388.
- POLLEN-BANKHEAD, N. & SIMON, A. 2010. Hydrologic and hydraulic effects of riparian root networks on streambank stability: Is mechanical root-reinforcement the whole story? *Geomorphology*, 116, 353-362.
- POLLEN-BANKHEAD, N., SIMON, A., JAEGER, K. & WOHL, E. 2009. Destabilization of streambanks by removal of invasive species in Canyon de Chelly National Monument, Arizona. *Geomorphology*, 103, 363-374.
- POLLEN-BANKHEAD, N. & SIMON, A. 2009. Enhanced application of root-reinforcement algorithms for bank-stability modeling. *Earth Surface Processes and Landforms*, 34, 471-480.

- RICHARDS, K. S. 1982. Rivers: Form and Process in Alluvial Channels. *London, Routledge*.
- ROBERTSON-RINTOUL, M. & RICHARDS, K. 1993. Braided-channel pattern and palaeohydrology using an index of total sinuosity. *Geological Society, London, Special Publications*, 75, 113-118.
- ROHDE, S., SCHÜTZ, M., KIENAST, K., & ENGELMAIER, P. 2005. River widening: an approach to restoring riparian habitats and plant species, *River Research and Management*, 21, 1075-1094.
- ROOD, S. B., PAN, J., GILL, K. M., FRANKS, C. G., SAMUELSON, G. M. & SHEPHERD, A. 2008. Declining summer flows of Rocky Mountain rivers: Changing seasonal hydrology and probable impacts on floodplain forests. *Journal of Hydrology*, 349, 397-410.
- ROSGEN, D. L. 1994. A classification of natural rivers. *Catena*, 22, 169-199.
- RUST, B. R. 1977. A classification of alluvial channel systems.
- SCHUMM, S.A. 1963. Sinuosity of alluvial rivers on the Great Plains. *Geological Society of America Bulletin*, 74, 1089-1100.
- SCHUMM, S. A. 1963. *Tentative classification of alluvial river channels*. USGS Circular 477, 10pp.
- SCHUMM, S. A. 1985. Patterns of alluvial rivers. *Annual Review of Earth and Planetary Sciences*, 13, 5.
- SCHUMM, S. A. 1981. Evolution and response of the fluvial system, sedimentologic implications. *The Society of Economic Paleontologists and Mineralogists Special Publication* 31, 19-29.
- SEMINARA, G. & TUBINO, M. 1989. Alternate bars and meandering. *River meandering*, 267-320.
- SHAFROTH, P. B., STROMBERG, J. C. & PATTEN, D. T. 2002. Riparian vegetation response to altered disturbance and stress regimes. *Ecological Applications*, 12, 107-123.
- SMITH, J. D. 2004. The role of riparian shrubs in preventing floodplain unraveling along the Clark Fork of the Columbia River in the Deer Lodge Valley, Montana. *Riparian Vegetation and Fluvial Geomorphology*, 71-85.
- SMITH, L. C., ISACKS, B. L., BLOOM, A. L. & MURRAY, A. B. 1996. Estimation of discharge from three braided rivers using synthetic aperture radar satellite imagery: Potential application to ungaged basins. *Water Resources Research*, 32, 2021-2034.
- SMITH, S. D., WELLINGTON, A. B., NACHLINGER, J. L. & FOX, C. A. 1991. Functional responses of riparian vegetation to streamflow diversion in the eastern Sierra Nevada. *Ecological Applications*, 89-97.
- STROMBERG, J. C., LITE, S. J., MARLER, R., PARADZICK, C., SHAFROTH, P. B., SHORROCK, D., WHITE, J. M. & WHITE, M. S. 2007. Altered stream-flow regimes and invasive plant species: the Tamarix case. *Global Ecology and Biogeography*, 16, 381-393.
- STRUIKSMA, N., OLESEN, K., FLOKSTRA, C. & DE VRIEND, H. 1985. Bed deformation in curved alluvial channels. *Journal of Hydraulic Research*, 23, 57-79.
- SURIAN, N. 1999. Channel changes due to river regulation: the case of the Piave River, Italy. *Earth Surface Processes and Landforms*, 24, 1135-1151.
- TAL, M., GRAN, K., MURRAY, A. B., PAOLA, C. & HICKS, D. M. 2004. Riparian vegetation as a primary control on channel characteristics in multi-thread rivers. *Riparian Vegetation and Fluvial Geomorphology, Water Sci. Appl. Ser.*, 8, 43-58.

- TAL, M. & PAOLA, C. 2007. Dynamic single-thread channels maintained by the interaction of flow and vegetation. *Geology*, 35, 347-350.
- TAL, M. & PAOLA, C. 2010. Effects of vegetation on channel morphodynamics: results and insights from laboratory experiments. *Earth Surface Processes and Landforms*, 35, 1014-1028.
- TOCKNER, K., PAETZOLD, A., KARAU, U., CLARET, C. & ZETTEL, J. 2006. Ecology of braided rivers. *Special Publication-International Association Of Sedimentologists*, 36, 339.
- TOCKNER, K., WARD, J. V., ARSCOTT, D. B., EDWARDS, P. J., KOLLMANN, J., GURNELL, A. M., PETTS, G. E. & MAIOLINI, B. 2003. The Tagliamento River: a model ecosystem of European importance. *Aquatic Sciences*, 65, 239-253.
- TOFFOLON, M. & CROSATO, A. 2007. Developing macroscale indicators for estuarine morphology: The case of the Scheldt estuary. *Journal of Coastal Research*, 195-212.
- VAN DEN BERG, J. H. 1995. Prediction of alluvial channel pattern of perennial rivers. *Geomorphology*, 12, 259-279.
- VAN DER NAT, D., SCHMIDT, A. P., TOCKNER, K., EDWARDS, P. J. & WARD, J. 2002. Inundation dynamics in braided floodplains: Tagliamento River, NORTHEAST ITALY. *ECOSYSTEMS*, 5, 0636-0647.
- VAUGHAN, I. P., DIAMOND, M., GURNELL, A. M., HALL, K. A., JENKINS, A., MILNER, N. J., NAYLOR, L. A., SEAR, D. A., WOODWARD, G., ORMEROD, S. J., 2009. Integrating ecology with hydromorphology: a priority for river science and management. *Aquatic Conservation: Marine and Freshwater Ecosystems* 19, 113–125.
- WARBURTON, J. 1996. Active braidplain width, bed load transport and channel morphology in a model braided river. *Journal of Hydrology New Zealand*, 35, 259-286.
- WEBER, C., SCHAGER, E.V.A. & PETER, A. 2009., Habitat diversity and fish assemblage structure in local river widenings: a case study on a swiss river, *River Research and Applications*, 701, 687-701.
- ZANONI, L., GURNELL, A., DRAKE, N. & SURIAN, N. 2008. Island dynamics in a braided river from analysis of historical maps and air photographs. *River Research and Applications*, 24, 1141-1159.
- ZILIANI, L. & SURIAN, N. 2012. Evolutionary trajectory of channel morphology and controlling factors in a large gravel-bed river. *Geomorphology*, 173, 104-117.